PACIFIC EARTHQUAKE ENGINEERING RESEARCH CENTER

Pacific Earthquake Engineering Research Center Highway Demonstration Project

Anne Kiremidjian
Stanford University

James Moore
Yue Yue Fan
University of Southern California

Nesrin Basoz
St. Paul Fire and Marine Insurance
Concord, California

Ozgur Yazali
Meredith Williams
Stanford University

PEER 2006/02
APRIL 2006

Pacific Earthquake Engineering Research Center Highway Demonstration Project

Anne Kiremidjian
Department of Civil and Environmental Engineering
Stanford University

James Moore
Department of Civil and Environmental Engineering
University of Southern California

Yue Yue Fan
Department of Civil and Environmental Engineering
University of Southern California

Nesrin Basoz
St. Paul Fire and Marine Insurance
Concord, California

Ozgur Yazali
Department of Management Science and Engineering
Stanford University

Meredith Williams
GIS Consultant
Stanford University

PEER Report 2006/02
Pacific Earthquake Engineering Research Center
College of Engineering
University of California, Berkeley

April 2006

ABSTRACT

A method for earthquake risk assessment of transportation network systems is presented that considers loss from damage to bridges and from opportunity costs from trips forgone due to increased traffic congestion. Earthquake hazards include ground shaking, landslides, and liquefaction. Transportation network analysis models are developed with fixed and variable travel demand assumptions. The method is applied to five counties in the San Francisco Bay Area. Four scenario earthquakes are defined: moment magnitude 7.0 and 7.5 events on the Hayward fault, and 7.5 and 8.0 events on the San Andreas fault.

For the four scenario earthquakes, losses from bridge damage due to ground shaking are estimated in millions as \$77, \$283, \$285, and \$634 million, respectively. These values increase to \$475 million, \$1.09 billion, \$970 million, and \$1.5 billion, respectively, when all hazards are considered with liquefaction as the main contributor to the increase. A retrofit analysis shows that a 20% increase in ground-shaking capacity uniformly for all bridges results in approximately 25% decrease in the loss. The opportunity costs for a two-hour peak A.M. traffic are estimated as \$6M for commuter and \$280M for freight traffic. Comparisons to the Loma Prieta 1989 earthquake were inconclusive.

An emergency traffic-routing algorithm, T-RoutER, is developed to demonstrate post-event travel paths. A key feature of T-RoutER is that it identifies available multiple origin-destination (O-D) pairs that are critical for emergency response.

ACKNOWLEDGMENTS

This work was supported primarily by the Earthquake Engineering Research Centers Program of the National Science Foundation, under award number EEC-9701568 through the Pacific Earthquake Engineering Research Center (PEER). Any opinions, findings, and conclusions or recommendations expressed in this material are those of the author(s) and do not necessarily reflect those of the National Science Foundation.

This project was supported by the Pacific Earthquake Engineering Research Center (PEER) through Grants UC-Berkeley/SA3487-1 and UC-Berkeley/SA2401B-6. The authors express their gratitude to PEER for their continued support.

Several individuals at the California Department of Transportation (Caltrans) provided guidance and data through the development of this project. We are indebted to Drs. Cliff Roblee and Zhongren Wang for their strong support, numerous suggestions, and the wealth of data that they made available to our team. Evan Evans, Mark Yashinsky, Mandy Chu, and other individuals at Caltrans also reached out and provided guidance on bridge inspection, operations, and design procedures. We are also grateful to the Metropolitan Transportation Commission of the San Francisco Bay Area, who provided the network connectivity and operations data. TeleAtlas Corporation provided the street level data used in the emergency response software E-Router.

Several students worked on the project either as part of their research or as summer interns. Kelly Burnell, Abigail Baca, Mark Audigier, and Ayshe Hortacsu were students at Stanford while working on the project. Elizabeth Gordon served as a summer undergraduate PEER scholar working with the team, and collected valuable demographic data. Renee Lee, current doctoral student, revised the final manuscript. We thank every one of them for their dedication to the project.

CONTENTS

ABSTRACT .... **iii**

ACKNOWLEGMENTS .... **iv**

TABLE OF CONTENTS .... **v**

LIST OF FIGURES .... **ix**

LIST OF TABLES .... **xiii**

1 INTRODUCTION **1**

1.1 Background 1

1.2 Objectives and Scope 4

1.3 Report Organization 5

2 METHODOLOGY FOR SEISMIC RISK ASSESSMENT **7**

2.1 Risk Assessment of Transportation Network Components 10

2.1.1 Seismic Hazard Assessment 11

2.1.1.1 Ground Motion and Ground Effects 11

2.1.2 Vulnerability of Transportation Network Components 15

2.1.3 Physical Loss Assessment from Damage to Bridges 19

2.1.4 A "What-If" Retrofit Analysis 20

2.2 Transportation Network Risk Analysis Method 20

2.2.1 Traffic Assignment Model 21

2.2.1.1 Fixed-Demand Assignment 21

2.2.1.2 Variable-Demand Assignment 24

2.2.2 Freight Demand 28

2.2.2.1 Trip Generation 30

2.2.2.2 Data Verification 34

2.2.2.3 Trip Distribution 35

2.2.2.4 Comparison with MTC Freight O-D Estimates 35

2.2.2.5 Limitations of the Freight Demand Model 37

2.2.2.6 Economic Value of Freight Trips 38

3 APPLICATION TO THE SAN FRANCISCO BAY AREA **41**

3.1 Databases and Characterization of Bridges 43

3.2 Seismic Hazard of San Francisco Bay Area 51

3.3 Vulnerability Assessment of Bridges 56
3.3.1 Results of Retrofit Analysis 63
3.4 Highway Network Characteristics 65
3.5 Performance Assessment of Network System 68
3.5.1 Summary of the Application 68
3.5.2 Pre-Processing Data Inputs 68
3.5.2.1 Auto-Merge of Bridges and Links 68
3.5.2.2 Obtaining Two-Hour Morning Peak Travel Demand 69
3.5.3 Damage States and Loss of Functionality 71
3.5.4 Selected Scenarios 72
3.5.5 Fixed-Demand Results 73
3.5.6 Variable-Demand Model Application 78
3.5.6.1 Estimating Parameters for Distance Decay Function 79
3.5.6.2 Results from Variable-Demand Assignment Model 82
3.5.7 Opportunity Costs 92
3.5.8 Extensions 93
3.5.8.1 Relationship between Bridge Damage Status and Functionality 93
3.5.8.2 Time Period To Be Modeled 94
3.6 Loss Estimation 95
3.6.1 Direct Loss Estimation 95
3.6.2 Results of Retrofit Analysis 96
3.7 Loma Prieta (1989) Earthquake 98
4 EMERGENCY RESPONSE NETWORK ANALYSIS WITHIN GIS 105
4.1 Background and Problem Definition 105
4.2 Network Analysis in GIS — Methodology 106
4.2.1 Defining Fundamental Properties of the Highway Network System in GIS 107
4.2.2 Analyzing the Highway Network in GIS — Shortest Path 108
4.2.3 T-RoutER — Traffic Routing for Emergency Response 109
4.2.3.1 Components of T-RoutER — Data and Software 109
4.2.4 Application in GIS — Automation and Customization 112
4.2.5 Steps for Using T-RoutER: 113

4.2.6 Connecting the Bridge Database and the Highway Network 115
4.3 Emergency Response Scenario 118
4.3.1 Case Study Area 118
4.3.2 T-RoutER in Action 119
4.3.2.1 Input 119
4.3.2.2 Pre-Event Analyses 123
4.3.2.3 Earthquake Event Simulation 127
4.3.2.4 Post-Event Routing 129
5 CONCLUSION 135
5.1 Network Component Systems Seismic Risk Assessment 135
6 EXTENSIONS 145
6.1 Key Outstanding Issues 145
6.2 Decision Support for Highway Systems 146
6.2.1 Network Design Problem 147
6.2.1.1 Deterministic Network Design 147
6.2.1.2 The Special Implications of Demand Shifts: Quantifying Welfare Losses 149
6.2.1.3 Stochastic Network Design 153
6.2.2 Role of Heuristics 154
6.2.3 Accounting for Activity Shifts 154
REFERENCES 159
APPENDIX A: EXPECTED DISPLACEMENT FACTOR FOR LANDSLIDE ANALYSIS 167
APPENDIX B: DEFINITIONS OF DAMAGE STATES 169
APPENDIX C: *PGA* DISTRIBUTIONS BY SCENARIO EVENT AND BY COUNTY 171
APPENDIX D: *PGD* DISTRIBUTIONS BY HAZARD CATEGORY BY SCENARIO AND BY COUNTY 173
APPENDIX E: EXPECTED DAMAGE-STATE DISTRIBUTIONS BY COUNTY AND SCENARIO EVENT (NO RETROFIT CASE Γ = 0%) 177
APPENDIX F: EXPECTED DAMAGE-STATE DISTRIBUTIONS BY SCENARIO EVENT AND BY RETROFIT CATEGORY 179

LIST OF FIGURES

Fig. 1.1 Examples of damage to bridges in the Loma Prieta 1989 earthquake (from H.G. Wilshire, U.S. Geological Survey) 2
Fig. 1.2 Collapse of an 18-section viaduct of the January 17, 1995, Great Hanshin-Awaji, Japan, earthquake (from Ghasemi et al., 1996) 3
Fig. 1.3 Examples of (a) liquefaction and (b) landslide damage in the October 17, 1989, Loma Prieta, California, earthquake. 4
Fig. 2.1 Risk-assessment methodology for highway network systems 8
Fig. 2.2 User equilibrium transportation flows given fixed travel demand in a network damaged by an earthquake 22
Fig. 2.3 User equilibrium transportation flows given variable travel demand in a network damaged by an earthquake 25
Fig. 2.4 Summary of the freight origin–destination estimation model 29
Fig. 2.5 Seaports 31
Fig. 2.6 Airports 32
Fig. 2.7 Rail yards 32
Fig. 2.8 Highway entry and exit points 33
Fig. 3.1 Counties and major faults and scenario events in the San Francisco Bay Area 42
Fig. 3.2 Distribution of bridges by design category in five counties 44
Fig. 3.3 Local soil conditions according to NEHRP site classes 48
Fig. 3.4 Liquefaction potential for the five counties and bridge locations 49
Fig. 3.5 Landslide potential for the five counties and bridge locations 50
Fig. 3.6 Number of bridges by *PGD* and ground failure category for the scenario SA8.0 55
Fig. 3.7 Ground motion contours and distribution of pre-retrofitted bridges by estimated damage state category for HW7.0 and HW7.5 scenarios 60
Fig. 3.8 Ground motion contours and distribution of pre-retrofitted bridges by estimated damage state category for SA7.5 and HW8.0 scenarios 61
Fig. 3.9 Number of bridges by standard normal statistic (Z) level and damage calculation case for scenario SA8.0 and damage state 5 63
Fig. 3.10 San Francisco Bay Area traffic analysis zones (TAZ) 66
Fig. 3.11 MTC San Francisco Bay Area highway network 67

Fig. 3.12 Caltrans district 4 bridges 67
Fig. 3.13 Evaluating the benefits of bridge retrofits based on the impact of an earthquake on the Bay Area transportation network 70
Fig. 3.14 Bridge Damage state vs. residual traffic capacity: risk-tolerant and risk-averse bridge closure policies 71
Fig. 3.15 Distribution of damage to Caltrans district 4 bridges resulting from scenario events 73
Fig. 3.16 Distribution of damage to Caltrans district 4 bridges resulting from the magnitude 6.9 Loma Prieta event on the San Andreas fault 74
Fig. 3.17 Resultant link closures by earthquake scenario: bridge closure criterion 1 74
Fig. 3.18 Magnitude 6.9 Loma Prieta event on the San Andreas fault 75
Fig. 3.19 Damaged bridges in scenario Hayward 7.5 75
Fig. 3.20 Observed and estimated trip rates as a function of travel time for the San Francisco Bay Area 79
Fig. 3.21 Final procedure for obtaining coefficients in the travel demand function 83
Fig. 3.22 Traffic increases on some local streets in Scenario HW751, variable travel demand 84
Fig. 3.23 Traffic reductions on freeway links and some local streets in Scenario HW751, variable travel demand 85
Fig. 3.24 Cumulative distribution of post-earthquake volume/capacity ratios: a comparison of fixed and variable travel demand estimates 87
Fig. 3.25 Proportionate differences in trip production estimates, variable vs. fixed-demand models 89
Fig. 3.26 Proportionate differences in trip attraction estimates, variable vs. fixed-demand models 90
Fig. 3.27 Bridge damage state vs. expected residual traffic capacity 94
Fig. 3.28 Loma Prieta 1989 earthquake rupture zone, ground motion contours, and damaged bridges in the study area 100
Fig. 3.29 Bridge locations by estimated damage state when only ground shaking is considered 102
Fig. 3.30 Bridge locations by estimated damage state and when ground shaking, liquefaction, and landslide hazards are considered together 103

Fig. 4.1 Road network database maintained by State DOTs (GIS-T, 2002) 107
Fig. 4.2 A generic description of highway network in GIS 108
Fig. 4.3 Customized ArcView application UI 112
Fig. 4.4 Points do not align with the street segments from the TeleAtlas highway database. 116
Fig. 4.5 Damage ratio for the default building inventory in Alameda County.....................119
Fig. 4.6 Highway network data for the San Francisco Bay Area 120
Fig. 4.7 Highway network overlaid with the state and local bridge inventory.....................121
Fig. 4.8 Location of Alameda County hospitals and critical facilities with state and local bridges 122
Fig. 4.9 Load inventory open file window...123
Fig. 4.10 Routing pull-down menu 124
Fig. 4.11 Pop-up window for loading the highway network to be analyzed 124
Fig. 4.12 Pop-up window for origin theme selection 124
Fig. 4.13 Pop-up window for selecting cost unit for the path calculations............................125
Fig. 4.14 Pre-event routes among selected origins and destinations. 126
Fig. 4.15 Load ground-shaking map theme 127
Fig. 4.16 State and local bridges overlaid on ground shaking (*PGA*) from a magnitude 7 event on the Hayward fault...128
Fig. 4.17 State bridges damaged from a magnitude 7 event on the Hayward fault................129
Fig. 4.18 Information dialog box after updating the network due to bridge closures 130
Fig. 4.19 Pre- and post-event routes between two selected origin – destination pairs (fastest path) 131
Fig. 4.20 Close-up view of the pre- and post-event routes between two selected origin – destination pairs...131
Fig. 4.21 Close-up view of the pre- and post-event routes between two selected origin – destination pairs...132
Fig. 4.22 Pre- and post-event routes between two selected origin – destination pairs (shortest path) 132
Fig. 6.1 The total cost of pre-event travel...150
Fig. 6.2 The total benefits of pre-event travel...151
Fig. 6.3 The net benefits of pre-event travel—consumer surplus..151

Fig. 6.4 Reductions in the net benefits of travel on a network damaged by an earthquake....152
Fig. 6.5 Simultaneous changes in transportation demand and supply in a region damaged by an earthquake....156

LIST OF TABLES

Table 2.1 Average shear-wave velocities used in Equation 2.6. 12

Table 2.2 Site classification for attenuation function (from Boore et al., 1993) 13

Table 2.3 Liquefaction susceptibility categories 14

Table 2.4 Critical accelerations (a_c) in g for landslide susceptibility categories 15

Table 2.5 Damage states and corresponding failure mechanisms from Basoz and Mander (1999) 16

Table 2.6 Case definitions for damage state calculations 18

Table 2.7 Repair cost ratio, RCR_j^t, used in the calculations 19

Table 2.8 Comparison between aggregate estimated employment and actual number of jobs (millions jobs/year) 34

Table 2.9 Summary of the MTC 1998 freight O-D data (trips/day) 35

Table 2.10 Intra-zonal freight trip distribution by number of truck axles (trips/day) 36

Table 2.11 Truck trip proportion of total vehicle (person + freight) trips (PCEs/day): Comparison of MTC and PEER estimates 36

Table 2.12 Summary of truck volumes in Caltrans District 4 (1997 trips) 38

Table 2.13 PCEs by truck size (number of axles) 39

Table 2.14 The distribution of trucks and PCEs by sector 39

Table 3.1 Rupture lengths for different scenario events 42

Table 3.2 Number of bridges by category and county 45

Table 3.3 Number of bridges by structural type and county 45

Table 3.4 Number of bridges by design criteria and county 47

Table 3.5 Number of bridge sites by soil, liquefaction susceptibility, and landslide susceptibility, and county 51

Table 3.6 Number of bridge sites by *PGA* category and scenario event from Boore et al. (1997) attenuation function and NEHRP (2000) site classification 52

Table 3.7 Number of bridge sites by *PGA* category, scenario event, and county 53

Table 3.8 Number of bridge sites by *PGD* category and scenario event 53

Table 3.9 Number of bridge sites by *PGD* category, two scenario events, and county 54

Table 3.10 Number of bridge sites by *PGD* category and ground failure category for the SA8.0 scenario event 55

Table 3.11 Number of bridges by expected damage state and damage case 6 (see Table 2.6), applying Boore et al. (1997) attenuation function and NEHRP (2000) site classification. (All bridges are in pre-retrofitted state.) 56

Table 3.12 Number of bridge sites by damage state category and scenario event from Boore et al. (1994) attenuation function. (All bridges are in pre-retrofitted state.) 57

Table 3.13 Number of pre-retrofitted bridges by expected damage state and by hazard case for scenario SA8.0 58

Table 3.14 Number of bridges by standard normal statistic and damage estimates for damage state 5 and scenario SA8.0 62

Table 3.15 The distribution of expected damage states for the scenario SA8.0 for hazard cases 1 and 4 64

Table 3.16 Free-flow speed, and capacity$_b$ by facility and area types$_c$ 65

Table 3.17 Study case reference list 72

Table 3.18 Summary of volume-capacity ratios by facility type given fixed travel demand 76

Table 3.19 Post-earthquake share of oversaturated ($v/c > 1$) links given fixed travel demand 77

Table 3.20 Summary of total vehicle hours by link type, fixed travel demand (hours) 78

Table 3.21 Summary of total trips assigned to the network in a 2-hour period given variable travel demand and two different bridge closure criteria 82

Table 3.22 Summary of volume-capacity ratio by link type, scenario, and bridge closure criterion given variable travel demand 86

Table 3.23 Post-earthquake share of oversaturated ($v/c > 1$) links given variable travel demand 87

Table 3.24 Summary of total vehicle hours of travel by link type, variable travel demand model 91

Table 3.25 Delay and opportunity cost in two earthquake scenarios, two-hour A.M. peak period 93

Table 3.26 Repair cost per unit area for NBI bridge classes 95

Table 3.27 Expected total repair cost by hazard and cost categories for the four scenario events (costs are in \$x1000) 96

Table 3.28 Expected total repair costs by hazard case and by retrofit category for the scenario event SA8.0 (cost in \$x1000) 97

Table 3.29 Number of bridges by estimated damage state and actual damage state category for the Loma Prieta 1989 earthquake 99
Table 3.30 Loss estimates of Loma Prieta (1989) earthquake by hazard case and by repair cost category....................101
Table 4.1 TeleAtlas database — attributes used for routing 110
Table 4.2 Attributes used in matching Caltrans point bridge data to TeleAtlas line data......117
Table 4.3 Abbreviations used in TeleAtlas Database....................118
Table 4.4 TeleAtlas functional roadway classes 122
Table 4.5 Travel time between selected origins and destinations — pre-earthquake 126
Table 4.6 Pre-event and post-event travel times for different origin-destination pairs..........133
Table 5.1 Estimated losses ($x1000) for ground-shaking hazard only, liquefaction hazard only, and for ground shaking, liquefaction, and landslide hazards combined* 138
Table 5.2 Estimated losses for different repair costs for ground shaking and all hazards for the San Andreas scenario 8.0 earthquake (SA8.0)*. (Estimates in $x1000) 139
Table 5.3 Loss estimates ($x1000) for the San Andreas 8.0 (SA8.0) scenario earthquake for increased bridge capacity*....................140
Table 5.4 Comparison of reported and estimated damage for the Loma Prieta 1989 earthquake* 140
Table 5.5 Post-earthquake share of oversaturated (v/c > 1) links given fixed travel demand 141
Table 5.6 Summary of total vehicle hours by link type, fixed travel demand (hours)...........142
Table 5.7 Summary of v/c-ratios given for variable travel demand and two different bridge closure criteria....................142
Table 5.8 Summary of total vehicle hours of travel by link type, variable travel demand model....................143
Table 5.9 Delay and opportunity cost in two earthquake scenarios, two-hour A.M. peak period 144

1 Introduction

1.1 BACKGROUND

Recent earthquakes have caused significant damage to bridges, roadways, tunnels, and road embankments, resulting in traffic delays or significant traffic rerouting. For example, "more than 80 bridges suffered major damage, 10 needed temporary supports, and 10 were closed due to major structural damage" (EERI, 1990) after the October 17, 1989, Loma Prieta earthquake in California (Fig. 1.1). The failure of one span of the San Francisco–Oakland Bay Bridge after the same earthquake required that traffic be rerouted through adjacent bridges across the bay. Freight traffic rerouted through the southern bay significantly extended travel length and time and resulted in additional economic losses. Similarly, the January 17, 1994, Northridge, California, earthquake caused minor damage to 85 bridges, moderate damage to 94 bridges, major damage to 47 bridges, and the collapse of six bridges (Basoz and Kiremidjian, 1997). After these events the transportation network was briefly disrupted, whereas after 1995 Hanshin-Awaji earthquake (Fig. 1.2) in Kobe, Japan, major traffic congestion in the Kobe-Osaka area lasted for more than six months. Additionally, this traffic congestion seriously hampered emergency response and may have been a contributing factor in the spread of fires in Kobe. Two other recent events, the Chi-Chi, Taiwan, earthquake of September 21, 1999, and the Koceli, Turkey, earthquake of August 17, 1999, also serve as reminders that most seismic regions in the world are still highly vulnerable to seismic events.

(a) Failure of the span of the San Francisco–Oakland Bridge (C.E. Meyer, U.S. Geological Survey)

(b) Collapsed sections of the Cypress viaduct of Interstate Highway 880. (H.G. Wilshire, U.S. Geological Survey)

Fig. 1.1 Examples of damage to bridges in the Loma Prieta 1989 earthquake (from H.G. Wilshire, U.S. Geological Survey)

In order to provide design basis for new bridges and retrofit strategies of existing bridges, it is necessary to develop a risk-based strategy. The Pacific Earthquake Engineering Center has developed such risk-based strategy through the performance-based earthquake engineering framework (PBEE). PBEE was initially formulated for the design of buildings. However, the framework is general enough to be extended to transportation and other lifeline systems. In this report, the PBEE framework is extended to network systems with a focus on transportation systems.

Transportation networks are spatially distributed systems whereby components of the system are exposed to different ground motions in the same earthquake event. Consideration of the spatial dependence of individual components, connectivity, and flow through the network are key factors in the development of an earthquake risk-assessment model for such systems that form the basis of PBEE. The ground effects that various components of the system are subjected to include ground shaking, vertical displacements due to settlement, and horizontal displacements due to lateral spreading and sliding (Fig. 1.3). Bridges are key components of transportation systems and are particularly susceptible to liquefaction and landslides, as they are located over streams and rivers with piers situated over sandy saturated deposits; or these components may be over canyons with high slopes, resulting in slope instability. Thus, it is important to integrate each site effect into the overall earthquake risk of a transportation system.

Fig. 1.2 Collapse of an 18-section viaduct of the January 17, 1995, Great Hanshin-Awaji, Japan, earthquake (from Ghasemi et al., 1996)

Transportation network risk-assessment methods require not only evaluation of the component performance but also estimation of overall system performance. Most recently, Basoz and Kiremidjian (1996) and Werner et al. (2000) considered the problem of transportation network systems subjected to earthquake events. In both of these publications, the risk to the transportation system is computed from the direct damage to major components such as bridges and the connectivity between a predefined origin-destination (O-D) set. Basoz and Kiremidjian (1996) also consider the time delay and use the information for retrofit prioritization strategies. The current software HAZUS (1999) for regional loss estimation developed by the National Institute for Building Standards (NIBS) for the Federal Emergency Management Agency (FEMA) considers only the direct loss to bridges in the highway transportation network. The connectivity and traffic delay problems resulting from damage to components of the system are not presently included in that software. Chang et al. (2000) propose a simple risk measure for transportation systems to represent the effectiveness of retrofit strategies by considering the difference in costs associated with travel times before and after retrofitting.

	
(a) Differential settlement due to liquefaction-caused cracking of paved road on Paul's Island. (S.D. Ellen, U.S. Geological Survey)	(b) Landslide debris blocks both eastbound lanes of Highway 17 near Summit Road. Foreground material is damaged lane separators. (C.E. Meyer, U.S. Geological Survey)

Fig. 1.1 Examples of (a) liquefaction and (b) landslide damage in the October 17, 1989, Loma Prieta, California, earthquake

1.2 OBJECTIVES AND SCOPE

A general methodology for seismic risk assessment of transportation systems is postulated to enable scenario-event analysis. Risk to transportation network systems in this formulation is defined as the expected annual loss from physical damage to components of the system and from functional loss due to reduced capacity or efficiency of the system’s operation. Thus, detailed formulations are presented for component-based loss estimation and transportation network analysis under reduced efficiency. In addition, prototype emergency response software is developed to illustrate the potential use of Geographic Information Systems for emergency response traffic routing. A key advantage of the prototype software is that it considers traffic routing from multiple origins to multiple destinations given the closure of damaged links. A limitation of the software is that it assumes a constant traffic demand and may not be representative of congestions that may occur due to the inefficiency of the system after a large earthquake event.

The scenario-based methodology is applied to the San Francisco Bay region in order to illustrate the utility of the method. Network component and traffic flow data are gathered for nine counties in the region. To make the application more manageable, only five counties are considered in the study. The seismic hazard analysis is limited to ground shaking, liquefaction, and landslides. Differential fault displacement due to fault rupture across a network component is not included because no damage functions for this hazard are available at the present time. In all the analyses, bridges are considered in their pre-retrofitted state. Fragility functions for retrofitted bridges were not available at the time this research was being conducted; however, a “what-if” analysis is performed assuming an increase in the seismic resistance of bridges to reflect possible retrofitting or upgrades. These analyses can provide useful information on the benefit of retrofitting.

Damage and physical loss estimates are also obtained using the methodology under the 1989 Loma Prieta earthquake scenario. The results from the analysis are compared to observed physical damage. It is recognized that a single event cannot provide information for validation purposes but nevertheless can provide realistic assessments of losses.

1.3 REPORT ORGANIZATION

Chapter 2 presents the general risk-assessment methodology for highway transportation systems. The performance-based earthquake engineering (PBEE) formulation is developed for scenario event analysis. The network analysis methods are discussed in Section 2.2. The application of the network system risk analysis is presented in Chapter 3. The application to the Loma Prieta earthquake scenario is also included in this chapter (Section 3.7). Chapter 4 summarizes the transportation emergency response software that was developed as part of this study. The conclusions from this investigation are discussed in Chapter 5. Key outstanding issues that still remain for further research and studies are discussed in Chapter 6.

2 Methodology for Seismic Risk Assessment

In general, seismic risk analysis consists of three major components: (1) seismic hazard estimation, (2) vulnerability assessment, and (3) consequence analysis. The approach presented in this report follows the Pacific Earthquake Engineering Research Center (PEER) performance-based earthquake engineering (PBEE) formulation. Figure 2.1 summarizes the components of the PBEE risk-assessment methodology as it is cast within a Geographic Information System (GIS) framework.

A fundamental difference between the single-building PBEE and transportation network system PBEE is that the components of such systems are spatially distributed; thus they are exposed to different ground effects from the same earthquake event. The ground effects include ground shaking, ground settlement and lateral spreading due to liquefaction, and sliding due to landslides. In addition, bridges and roadbeds are likely to cross faults. Fault displacements along the rupture zone of a fault can also contribute to severe damage or collapse of structures at these locations. Therefore, the hazard from ground shaking, liquefaction, landslides, and differential fault displacement denoted as *IM* needs to be evaluated at all components of the transportation network. Thus, in characterizing the hazard exposure of the network system, the spatial distribution of various hazards needs to be integrated. GIS provides a suitable tool for managing and integrating the spatially distributed hazard information as demonstrated in Chapter 3 of this report.

In order to evaluate the vulnerability of the transportation network system, two types of databases need to be compiled. These include (1) an inventory of bridges, tunnels, and road links and (2) a network connectivity and traffic flow database. The number of components in such a system is very large, making it computationally prohibitive to perform component-specific analysis for each bridge, tunnel, and road segment. Thus, transportation network components are classified into major engineering categories, for which generic damage functions, hereafter referred to as *fragility functions*, need to be generated. Fragility functions describe the probability of a component being in or exceeding a particular damage state as a function of a hazard parameter. The results of seismic hazard analysis and the information about component fragilities are integrated to evaluate the damage, *DM*, to network components.

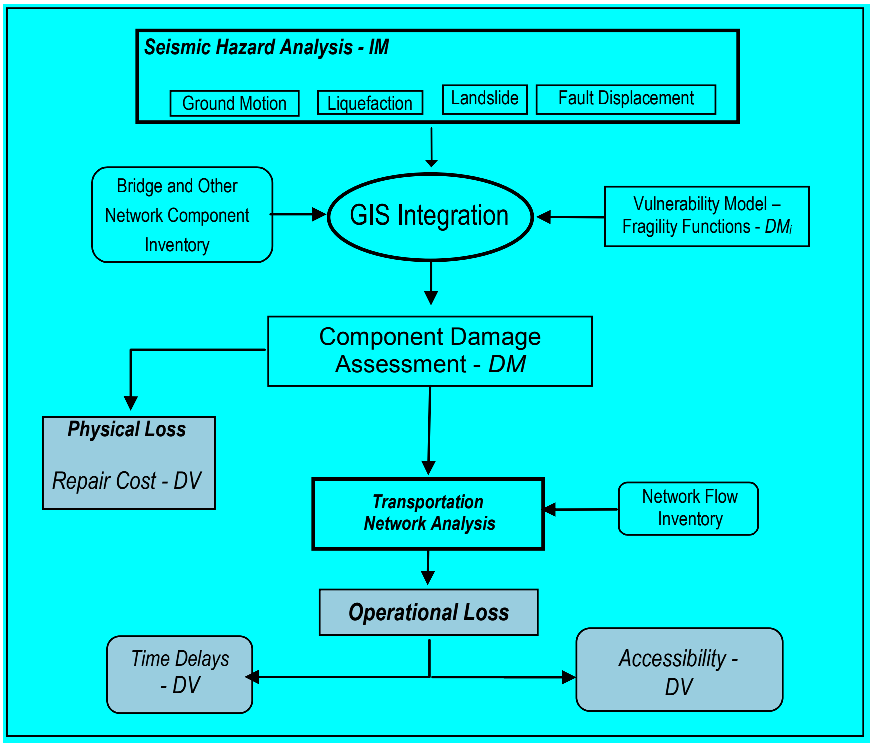

Fig. 2.1 Risk-assessment methodology for highway network systems

The economic loss from damage to the transportation system is due to physical damage and to diminished functional capacity, represented by the decision variable, *DV*, in the PBEE equation. *Physical loss is* the cost of repair or replacement of damaged components needed to bring the system back to its original functionality. *Operational loss* is due to the reduced capacity of the network resulting in inefficiencies of commuter and freight traffic. The inefficiencies are measured in terms of time delays of the traffic due to closure of key components of the system such as bridges, or due to reduced flow capacities of the roads (either from imposed lower speed limits or closure of a number of available traffic lanes). In principle, time delays and/or an excessive travel path can be related to monetary loss. The time over which the system remains inefficient also needs to be estimated in order to compute the total operational losses of the system.

Two types of analyses can be performed to estimate the *physical* and *operational* losses. These include scenario and complete probabilistic analysis. Both formulations are presented in the next sections; however, the emphasis is on the scenario analysis.

Equation (2.1) describes the expected loss from *physical* damage and loss of functionality of the system (or *operational loss*) when subjected to a severe earthquake, denoted by $E[Loss|Q_i]$, where $E[.]$ is expectation and Q_i is the scenario event. For a given earthquake event Q_i, the expected loss from the system is given as follows:

$$E[Loss \mid Q_i] = \int_0^1 l(D \mid Q_i) f_D(d \mid Q_i) dd + \int_0^1 l(t \mid D, Q_i) f_D(d \mid Q_i) dd \tag{2.1}$$

where

$l(D \mid Q_i)$ = cost of repair of individual components of the system at damage D due to an event Q_i, where the damage is $0 \leq D \leq 1.0$,

$f_D(d \mid Q_i)$ = probability density of damage D due to an event Q_i,

$l(t \mid D, Q_i)$ = costs associated with time delays due to detours of route closures or reduced capacity for event Q_i causing damage D.

The annualized risk of loss for the transportation system from all possible events Q_i that may affect the system, occurring with rates ν_i, is:

$$\begin{aligned} E[Loss] &= \sum_{allevents} E[Loss \mid Q_i]\nu_i \\ &= \sum_{allevents} \nu_i \left\{ \int_0^1 l(D \mid Q_i) f_D(d \mid Q_i) dd + \int_0^1 l(t \mid D, Q_i) f_D(d \mid Q_i) dd \right\} \end{aligned} \tag{2.2}$$

The damage functions $l(D \mid Q_i)$ in Equations (2.1) and (2.2) include losses due to damage from ground shaking and ground deformations such as those due to liquefaction, landslides, and differential fault displacements. For a given event Q_i, losses due to time delays arise from delays in commuter and freight traffic. The time delays result from closure of particular routes because of excessive damage to key components, such as bridges, or due to reduced flow capacity, due to minor or moderate damage. At moderate damage states, lower speed limit or closure of traffic lanes may be imposed to reduce the traffic flow, resulting in increased travel times.

2.1 RISK ASSESSMENT OF TRANSPORTATION NETWORK COMPONENTS

In this section the method for estimating *physical loss* from damage to components is presented. Thus, only the first integral in Equations (2.1) and (2.2) is considered. Expanding this integral to take into account ground shaking, liquefaction, landslides, and fault rupture, the equations become:

$$
\begin{aligned}
E[Loss \mid Q_i] &= I_A \int_D \int_A l(D \mid A, Q_i) f_D(d \mid A, Q_i) f_A(a \mid Q_i)\, da\, dd \\
&+ I_L \int_D \int_{S_H} l(D \mid S_H, Q_i) f_D(d \mid S_H, Q_i) f_{S_H}(s_H \mid Q_i)\, ds_H\, dd \\
&+ I_L \int_D \int_{S_V} l(D \mid S_V, Q_i) f_D(d \mid S_V, Q_i) f_{S_V}(s_V \mid Q_i)\, ds_V\, dd
\end{aligned}
\tag{2.3}
$$

where,

$$
I_A = \begin{cases} 1 & \text{if there is no liquefaction, or landslides, or fault rupture at a site} \\ 0 & \text{if there is liquefaction or landslide or fault rupture at a site} \end{cases}
\tag{2.4}
$$

$$
I_L = \begin{cases} 1 & \text{if there is liquefaction or landslides orfault rupture at a site} \\ 0 & \text{if there is no liquefaction or landslide or fault rupture at a site} \end{cases}
\tag{2.5}
$$

A = ground motion severity and can represent either peak ground acceleration or response spectral acceleration, or another appropriate parameter;

S_H = horizontal ground displacement due to either liquefaction or landslides or to differential fault displacement in the horizontal direction

S_V = vertical ground displacement due to liquefaction, landslides, or differential fault displacement in the vertical direction.

In this formulation it is assumed that liquefaction, landslides, or differential fault displacement from fault rupture occur at a site, but none occur simultaneously. Similarly, ground shaking alone is preempted if any one of the following occurs: liquefaction, landslide, or fault displacement.

2.1.1 Seismic Hazard Assessment

The seismic hazard, *IM*, at a network component site can be expressed in terms of peak ground acceleration, *PGA*, spectral acceleration, $S_a(T, \xi)$ as a function of the fundamental period of vibration of the structural system T and its damping ξ, and expected permanent ground deformation, *PGD*.

2.1.1.1 Ground Motion and Ground Effects

Computation of the earthquake demand at the site due to a given earthquake event, Q_i, is fundamental to hazard assessment. Of the four site hazards identified earlier in this chapter, only three major ones are considered in the study: (1) ground shaking, (2) liquefaction, and (3) landslide. Differential fault displacement due to surface fault rupture is not included at the present time because bridge fragility functions for fault rupture are not available. The general formulation, however, would follow in a way similar to that for landslide and liquefaction analyses.

In the study, the ground-shaking demand, *IM*, at the site is characterized by the following three parameters: (1) *peak ground acceleration, PGA*, (2) s*pectral accelerations* for a period of 0.3, $S_a(0.3)$, and (3) s*pectral accelerations* for a period of 1.0 seconds, $S_a(1.0)$ as dictated by the availability of fragility functions. The ground-shaking demand is a function of the magnitude of the earthquake, the distance from the source to the site, and the local soil conditions. Ground motion attenuation functions provide the relationship between these earthquake parameters. In this study, the attenuation function of Boore et al. (1997) is used, but the formulation is general and can accommodate any ground motion attenuation function. The Boore at al. (1997) attenuation function is given in Equation (2.6):

$$\ln Y = b_1 + b_2(M-6) + b_3(M-6)^2 + b_5 \ln r + b_V \ln \frac{V_S}{V_A} \tag{2.6}$$

where

$r = \sqrt{r_{jb}^2 + h^2}$.

M = earthquake magnitude

Y = ground-shaking parameter (PGA, $S_a(0.3)$, or $S_a(1.0)$ at 5% damping)

r_{jb} = the shortest distance from site to the surface projection of the rupture zone of the scenario earthquake

V_s = the average shear-wave velocity used for site amplification. The National Earthquake Hazard Reduction Program, NEHRP, soil classification scheme is used for the local soil characterization and Boore et al. (1997) recommends the use of average shear velocity values listed in NEHRP for these site classes.

b_1 = regression coefficient that depends on the type of fault of faulting (e.g., strike-slip, dip-slip, normal or reverse).

B_2, b_3, b_5, b_V, V_A = regression coefficient

All three accelerations are defined in terms of *acceleration of gravity*, g.

Table 2.1 Average shear-wave velocities used in Equation (2.6)

NEHRP Site Class	Average shear velocity
B	1070
C	520
D	250
E	180 *

* Used in this study but not listed in Boore et al. (1997)

The analysis presented in this report was first performed with the Boore et al. (1993) attenuation function. Thus, for completeness the Boore et al. (1993) attenuation function used is given in Equation (2.7), and damage state estimates and soil site classifications used for that analysis are presented in Section 3.1 of this report.

$$\begin{aligned}\log_{10}(SD) &= B_{SA} + a_{SS} \cdot G_{SS} + a_{RS} \cdot G_{RS} + b(M-6) + c(M-6)^2 + d(\sqrt{r^2 + h^2}) \\ &+ e[\log_{10}(\sqrt{r^2 + h^2})] + f(2.881 - \log_{10} V_B)\end{aligned} \tag{2.7}$$

where

M = earthquake moment magnitude

SD = mean of seismic demand (PGA or S_a in units of g)

r = horizontal distance (km) from the site to the closest point on the surface projection of fault rupture

B_{SA} = a factor converting S_v (cm/s) to S_a (g)

a_{SS} , a_{RS} = coefficients for strike-slip and reverse-slip faults, respectively, as given in HAZUS99 Technical Manual, Table 4.4

G_{SS}, G_{RS} = fault type flags: G_{ss} = 1 for strike-slip faults, 0 otherwise; G_{RS} =1 for reverse-slip/thrust faults, 0 otherwise

b,c,d,e,f = coefficients provided in HAZUS99 Technical Manual, Table 4.4

h = value of a "fictitious" depth determined by regression methods and which varies by period

V_B = effective shear-wave velocity for rock sites as listed in HAZUS99, Table 4.4

Table 2.2 Site classification for attenuation function (from Boore et al., 1993)

NEHRP Site Class	Average shear velocity in upper 30 m
A	> 750 m/s
B	360 – 750 m/s
C	180 – 360 m/s

The ground failure hazards considered in this study include liquefaction and landslide. The formulation presented in this section follows that given in HAZUS (1999). Ground failure potential at the bridge site is measured in terms of *expected permanent ground displacement* (*PGD*), which is calculated considering the local ground-shaking demand at the site in terms of *PGA*.

It is assumed that the combined hazard due to ground failure at the site is the maximum of the liquefaction and landslide hazards at the bridge site. Equation (2.8) expresses this relationship as follows:

$$PGD = Maximum\{PGD^{liq}, PGD^{land}\} \tag{2.8}$$

where PGD^{liq} and PGD^{land} are the expected permanent ground displacements at the site due to liquefaction and landslide, respectively.

The liquefaction analysis is based on the approach of Youd and Perkins (1978). A liquefaction susceptibility category from Table 2.3 below is assigned to the site based on the local soil conditions.

Table 2.3 Liquefaction susceptibility categories

Susceptibility Category	**VH**	**H**	**M**	**L**	**VL**	**WATER**
Definition	very high	high	moderate	low	very low	water

Two different consequences of liquefaction are taken into account: (1) lateral spreading, and (2) ground settlement. The combined effect of these two is assumed to be the maximum of their individual *PGD* given as follows:

$$PGD^{liq} = Maximum\{PGD^{LS}, PGD^{GS}\} \tag{2.9}$$

where PGD^{LS} and PGD^{GS} are the expected permanent ground displacements at the site due to *lateral spreading* and *ground settlement,* respectively. It is assumed that the expected displacement due to lateral spreading for a normalized ground-shaking level cannot be higher than 100 inches.

The landslide analysis is based on the work of Wilson and Keefer (1985). Similar to the liquefaction analysis, the local soil conditions are assigned to one of the 11 landslide susceptibility categories listed in Table 2.4. Based on the *PGA* value estimated for the site, expected displacement due to landslide PGD^{land} is calculated as in Equation (2.9):

$$PGD^{land} = \mathrm{E}[DF \mid a_c / a_{is}] \cdot a_{is} \cdot n \tag{2.10}$$

where

$E[DF|a_c/a_{is}]$ = expected displacement factor for a given ratio of the critical acceleration (a_c) and the induced acceleration (a_{is}), and

n = number of cycles of the earthquake for a given moment magnitude of M.

The critical acceleration for a particular landslide susceptibility category can be interpreted as the minimum amount of *PGA* that can initiate a landslide at a site in that category (see Table 2.4 for the critical accelerations). *PGA* is used as the induced acceleration, a_{is}.

Table 2.4 Critical accelerations (a_c) in g for landslide susceptibility categories

Susceptibility Category	**None**	**I**	**II**	**III**	**IV**	**V**	**VI**	**VII**	**VIII**	**IX**	**X**
Critical Acceleration	N/A*	0.60	0.50	0.40	0.35	0.30	0.25	0.20	0.15	0.10	0.05

*: N/A stands for not applicable

The function used to calculate the expected displacement factor is given only graphically HAZUS (1999). This function is approximated from the original figure (Fig. 4.16 of HAZUS) with discrete points, and a new empirical function defined from those points is used in the current study. The points used in the study are listed in 0 for reference.

2.1.2 Vulnerability of Transportation Network Components

In this report, the vulnerability of only bridges is considered. As described earlier, bridge vulnerability is expressed in terms of a fragility function. Fragility functions are defined as the probability that the bridge system will be in or will exceed a damage state for different levels of ground shaking or ground deformation. This definition is the first step in defining the damage states for bridges.

Several damage state definitions have been used in earlier studies and in prior damage assessments after major earthquake events. The earthquake damage of a bridge is categorized into five different damage states. Table 2.5 provides definitions for these five damage states and summarizes the corresponding failure mechanisms as proposed by Basoz and Mander (1999):

Table 2.5 Damage states and corresponding failure mechanisms from Basoz and Mander (1999)

Damage State	Definition	Failure Mechanism
1	None	First yield
2	Slight	Cracking
3	Moderate	Bond, abutment back wall collapse
4	Extensive	Pier concrete failure
5	Complete	Deck unseating, pier collapse

Equation (2.11) defines the general form of a damage function for the bridge (for simplicity of notation, the index denoting the individual bridges are ignored):

$$Pr\left\{D^k \geq j\right\} = \boldsymbol{1} - \boldsymbol{\Phi}_j^k\left(x^k\right) \tag{2.11}$$

where

D^k = damage state of the bridge due to hazard k ($k = S$ - ground shaking, F – ground failure);

P{ $D^k \geq j$} = probability of D^k being in damage state j or higher (j = 1, 2, 3, 4, 5);

$\Phi_j^k(\cdot)$ = cumulative distribution function of a normal random variable with mean $\ln\alpha_j^k$ and standard deviation β^k (i.e., N($\ln\alpha_j^k$,($\beta^k)^2$);

x^k = the earthquake intensity measure demand, IM, at the site of the bridge due to hazard k. For $k=1$ it corresponds to the spectral acceleration with a period of 1.0 second, S_a(1.0), for calculating the damage due to ground shaking, and for $k=2$ it is expected peak ground deformation, *PGD*, for damage due to ground failure calculations.

α_j^k = *modified median value* of the earthquake demand; it is the measure of central tendency characterizing the damage functions. The median value α_j^k is calculated based on the median values of earthquake demand provided by the spectral acceleration S_a(1.0) for ground shaking, and peak ground deformation *PGD* for ground failure. The modification is based on the structural characteristics of the bridge.

β^k = dispersion of the distribution equal to 0.4 for ground shaking, and 0.2 for ground failure damage for all bridge classes.

Fragility functions are needed for all the bridges in a network system. With the large number of bridges present in a transportation system, it is not computationally feasible to evaluate a damage function for each individual bridge. Thus, bridges are categorized according to a classification scheme based on the structural characteristics, such as the construction year, material used, span continuity, number of columns, number of bents, etc.

It is assumed that all five damage states can be observed due to ground shaking but that only damage states 1, 4, and 5 can be observed due to ground failure. In other words, a bridge cannot be in damage states 2 or 3 if ground failure is the only type of seismic hazard considered for that bridge site. This constraint on the ground failure damage calculations implies that the same median value is used for damage states 2, 3, and 4 (i.e., $\alpha_2^F = \alpha_3^F = \alpha_4^F$).

The modification of the median values aims to incorporate the effects of several other structural properties of the bridges on damage distributions. The modification for ground shaking depends on the *angle of skewness* and *number of spans* of the bridge, and the damage state j considered for the calculation. The angle of skewness is defined as the angle between the centerline of a pier and a line normal to the roadway centerline. The modification for ground failure depends on the *angle of skewness*, *bridge length*, *number of spans*, and *maximum span width* of the bridge.

In the course of this study it is observed that these modifications may result in inconsistencies in the damage functions. For example, a modified median value for damage state 3 can be less than the same parameter for damage state 2, which implies a negative probability of being in damage state 3. HAZUS (1999) does not provide an explicit normalization technique to handle this problem. However, Basoz and Mander (1999) use an implicit assumption that solves this problem. Their assumption states that the modified median values for any damage state cannot be less than the modified median values of the lower damage states. For the above example, the modified median value for damage state 3 is assigned the same value of damage state 2 (i.e., if $\alpha_3^k < \alpha_2^k$, then assign $\alpha_3^k \leftarrow \alpha_2^k$; the same holds for higher damage states). Therefore, the probability of the structure being in damage state 2 becomes zero. Although it is not easy to measure the effects of this assumption, one obvious impact is on the damage state distributions. With this assumption, the damage state distributions tend to be stochastically larger than if another normalization procedure were used.

Equations (2.1) and (2.2) require P_j^k, the probability of being in damage state j (j=1,…,5) due to earthquake hazard k (S for ground shaking, and F for ground failure). P_j^k is calculated according to Equation (2.12) below.

$$P_j^k = \Pr\{D^k \geq j\} - \Pr\{D^k \geq j+1\}, \text{ for j = 1,2,3,4} \tag{2.12}$$

and

$$P_5^k = \Pr\{D^k \geq 5\} = \Pr\{D^k = 5\} \tag{2.13}$$

For ground deformation P_2^F and P_3^F are both zero.

The combined damage state distribution of the bridge is found using the principle of independent events in probability theory. Equation (2.14) summarizes this operation:

$$P_j^C = P_j^S + P_j^F - \left(P_j^S \cdot P_j^F\right) \tag{2.14}$$

Using the damage probability P_j^k, the expected damage state of the bridge is calculated as given by Equation (2.15) below (for $k = S, F, C$):

$$\mathrm{E}\left[D^k\right] = \sum_{j=1}^{5} j \times P_j^k \tag{2.15}$$

where S = ground shaking, F = ground failure, and C = a combination of ground shaking and ground failure.

In order to study the effects of the different hazard components on the damage estimates, six hazard combinations are identified and listed in Table 2.6 referred to as "hazard cases." In Chapter 3, the results are presented for the various cases listed in this table.

Table 2.6 Case definitions for damage state calculations

Hazard Case	Definition
1	ground shaking only
2	liquefaction only
3	landslide only
4	ground shaking and liquefaction
5	ground shaking and landslide
6	ground shaking, liquefaction, and landslide

2.1.3 Physical Loss Assessment from Damage to Bridges

The expected loss from a bridge due to earthquake hazard k is simply the weighted average of the direct costs of repair for the five damage states. The weights are the probability of being in each damage state (i.e., P_j^k).

The *repair cost* of the bridge in a particular damage state is defined as the estimated cost of repairing (or replacing) the structure such that it can start operating with full performance after the repair. It is reasonable to assume that the repair cost increases according to the damaged functional area of the bridge.

Since different damage states imply different rates of damage on the structure, a *repair cost ratio* is introduced as a measure of this effect. Based on the work of Basoz and Mander (1999) three different cost ratio categories are used in this study (*best mean*, *minimum*, and *maximum*), which provide a range of loss estimates. Equation (2.16) below is used to calculate the loss of the bridge due to hazard k for a cost category t (best mean, minimum, and maximum).

$$\mathrm{E}[Loss^t] = \sum_{j=1}^{5} P_j^k \cdot RCR_j^t \cdot Cost \cdot Area \tag{2.16}$$

where,

RCR_j^t = repair cost ratio for damage state j and cost category t.

Cost = the per unit area cost of repair for the bridge class of the bridge, and

Area = surface area of the bridge, which is the product of bridge width and length.

The repair cost ratios used for loss calculations are listed in Table 2.7. Since damage state 1 corresponds to no damage, there is no loss of functionality due to that damage state.

Table 2.7 Repair cost ratio, RCR_j^t, used in the calculations

<table>
<tr><th>Damage State</th><th colspan="2">Best Mean</th><th>Minimum</th><th>Maximum</th></tr>
<tr><td>slight</td><td>0.03</td><td></td><td>0.01</td><td>0.03</td></tr>
<tr><td>moderate</td><td>0.08</td><td></td><td>0.02</td><td>0.15</td></tr>
<tr><td>extensive</td><td>0.25</td><td></td><td>0.10</td><td>0.40</td></tr>
<tr><td rowspan="2">complete</td><td>1.00</td><td>if $x < 3$ †</td><td rowspan="2">0.30</td><td rowspan="2">1.00</td></tr>
<tr><td>2/n</td><td>if $x \geq 3$ †</td></tr>
</table>

† x - number of spans of the bridge

The repair cost ratio for the *best mean* cost category and damage state 5 is evaluated in a different manner than the other cases due to the following assumption. Basoz and Mander (1999) assume that the most common failure mechanism is the unseating of at most two spans; thus they propose that bridges with high numbers of spans be handled according to the modifications in Table 2.7. An important point to note is that this modification may result in inconsistencies when the number of spans is 5 or higher. For example, if the number of spans of the bridge is 5, then the repair cost ratio for damage state 5 is 0.20. In contrast, that ratio for damage state 4 is 0.25.

2.1.4 A "What-If" Retrofit Analysis

In an effort to reduce the risk of damage and failure of bridges, the California Department of Transportation (Caltrans) has been retrofitting and seismically upgrading bridges in the state under a federally and state-funded programs. In order to obtain an estimate of the benefits of this program, a simple approach is considered for retrofitted bridge risk assessment. A more rigorous analysis is not possible at this time because fragility functions for retrofitted bridges were not available at the time this study was conducted. In order to obtain a simple estimate of the expected loss reduction and thus risk reduction from retrofitting, the fragility functions of Basoz and Mander (1999) are *modified by shifting the median value* α_j^k with a γ percentage value to a higher damage state. The implication of this assumption is that the bridge ground motion capacity will increase by γ% due to retrofitting. Based on this assumption, the analyses can be repeated, replacing the modified median value α_j^k by the retrofitted median value $\bar{a}_j^k$ for different γ values, where

$$\bar{a}_j^k = a_j^k\,(1+\gamma) \tag{2.17}$$

2.2 TRANSPORTATION NETWORK RISK ANALYSIS METHOD

In addition to the replacement and repair costs of damage to the individual network components described in the previous sections, earthquake damage results in loss of functionality of the system. This results in an increase in travel times and in a reduction in trip making. Change in demand for or in the functionality of any transportation link may affect the level of service available for other links. Research must be conducted on a network basis to study the impact of individual damage on the entire study area. Earthquake losses due to travel time increases may be evaluated by examining the difference in performance between baseline conditions and performance in an earthquake scenario (Cho et al., 2000).

A transportation network can be represented conceptually by a set of nodes and links that connect these nodes. A transportation study area is normally divided into a number of traffic analysis zones (TAZs) based on population, employment, and land-use patterns. These zones are represented mathematically as centroid nodes, which are connected to the street network via virtual links. Trips originating from or destined for a travel analysis zone are routed through the network over the shortest, most congested paths. Travelers compete for access to the shortest paths, and predicted network performance is generally modeled as a short-term economic equilibrium. Path costs are endogenous in this context because time has value, and link travel times are affected by link volumes when links are subject to congestion (Sheffi, 1985).

2.2.1 Traffic Assignment Model

The overarching behavioral assumption in modeling network flows is that each user chooses the route that the user perceives to be the best. This satisfies Wardop's user optimality principle, i.e., that no user can improve travel time by changing routes (Wardop, 1952). Two types of equilibrium traffic assignment models are applied here. These are a conventional, fixed-demand model, and a novel variable-demand model. These two models are discussed and compared in the following sections with respect to the algorithmic and practical aspects. The application of such models in the San Francisco Bay Area subject to earthquakes provides a better understanding of the importance of applying a variable-demand model under extreme situations.

2.2.1.1 Fixed-Demand Assignment

The user equilibrium model is a standard transportation analysis model. The model assumes that the trip rate (origin-destination requirement) between every origin-destination (O-D) pair is known and fixed. When a fixed, defined set of origin-destination requirements greatly exceeds the network capacity, the standard model predicts unrealistic (oversaturated) link volumes in excess of physical capacity.

If a transportation system loses capacity due to an earthquake, the congestion level would necessarily increase given fixed O-D requirements. This relationship is depicted in Figure 2.2. Network capacity is reduced from S_1 to S_2, while the demand stays at level D_1. The travel cost would increase from P_1 to P_2 accordingly.

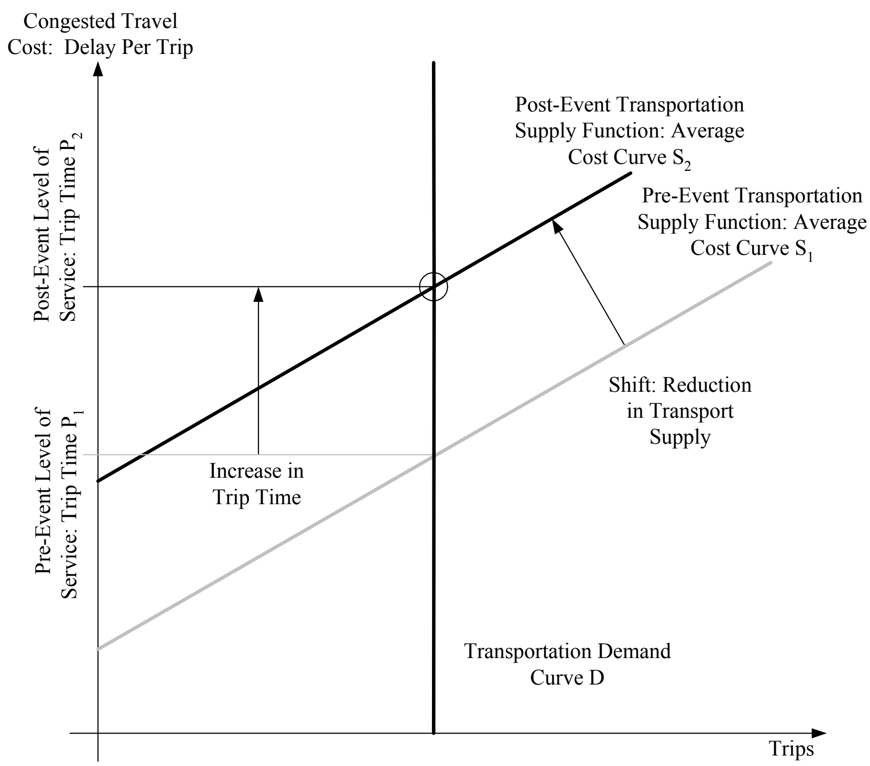

Fig. 2.2 User equilibrium transportation flows given fixed travel demand in a network damaged by an earthquake

In a fixed-demand model, total demand for travel between an origin-destination pair does not vary with minimum travel cost between these nodes. Route selection is a function of cost, but the propensity to travel is not. Link travel costs are functions of the volume on each link. Trips are assigned to shortest paths so that the total cost, *Z*, perceived by an individual is a minimum. This problem can be formulated as following a linear program,

$$\min Z = \sum_a \int_0^{x_a} t_a(w)dw \tag{2.18}$$

subject to

$$\sum_{k} f_k^{rs} = q_{rs} \tag{2.19}$$

$$x_a = \sum_{rs}\sum_{k} f_k^{rs} \cdot \delta_{a,k}^{rs} \tag{2.20}$$

$$0 \le x_a \le c_a \tag{2.21}$$

$$q_{rs} \ge 0 \tag{2.22}$$

where

x_a = traffic volume on link *a,*

c_a = capacity of link *a*,

q_{rs} = demand from origin node *r* to destination node *s*,

f_k^{rs} = flow on path *k* connecting O-D pair *r-s*,

$\delta_{a,k}^{rs}$ = binomial index, 1 if link *a* is on path *k* between O-D pair *r-s*, 0 otherwise,

$v_{a,k}^{rs}$ = volume on link *a* that belongs to path *k* between O-D pair *r-s*, and

$t_a(w)$ = volume-delay function on link *a*.

This is a conceptual formulation requiring complete enumeration of network paths, which is not a tractable approach. The problem is conventionally treated as an equivalent nonlinear program that includes only link flow variables. The numerical solution to this equivalent problem is obtained relatively efficiently via the Frank-Wolfe algorithm, implemented here by a commercial software product (INRO, 1998). A summary of the solution procedure is given as follows.

- Step 0. Initialization.
  Set link volume x_a^n as 0 for all links when $n = 0$. Run all-or-nothing trip assignment given link cost $t_a^0 = t_a(0)$.
- Step 1. Update link cost.
  Set $t_a^n = t_a(x_a^n)$ for all links.
- Step 2. Update link volume.
  Compute the shortest path, *m*, between each O-D pair *r-s* based on link travel time t_a^n. Obtain link volume y^k by an all-or-nothing assignment.
- Step 3. Determine the best direction of search *l*.
  Solve the following system for *l*.

$$\min Z(l) = \sum_a \int_0^{x_a + l(y_a^n - x_a^n)} t_a(w)dw\,, \tag{2.23}$$

subject to $0 \le l \le 1$.

- Step 4. Flow update.

$$x_a^{n+1} = x_a^n + l(y_a^n - x_a^n)\,. \tag{2.24}$$

- Step 5: Convergence test.

If

$$|\, z^n - z^{n-1} \,| \le \varepsilon\,, \tag{2.25}$$

terminate. Otherwise, set $n = n+1$ and go to step 1.

2.2.1.2 Variable-Demand Assignment

More realistically, trip rates are influenced by the level of service on the network. For example, as the congestion level increases, drivers may change their travel modes, shift the time of travel, change the destination, or even cancel trips. These effects are most often minor in conventional transportation engineering applications and thus are usually ignored. But following a major earthquake, the congestion level would greatly increase because of reductions in network capacity. The increased congestion level would then induce a reduction in travel demand. Figure 2.2 shows this relationship. Before an earthquake occurs, the transportation system supplies service along curve S_1, and equilibrium travel of d_1 uses the system at average cost of P_1. After an earthquake affects the network, the transportation supply function drops to S_2, and demand responds to the change in level of service by reducing d_2, at average cost of P_2'. P_2' in Figure 2.2 is lower than the value P_2 in Figure 2.2 (Cho et al., 2003).

This effect can be accounted for by a function explaining how trip rates are influenced by travel time. To proceed, the trip rate between an origin-destination zone pair *r-s* must be represented as a function of the travel time between the zone pair. At network user equilibrium, the travel time on all used paths between any origin-destination zone pair are equal, and are also

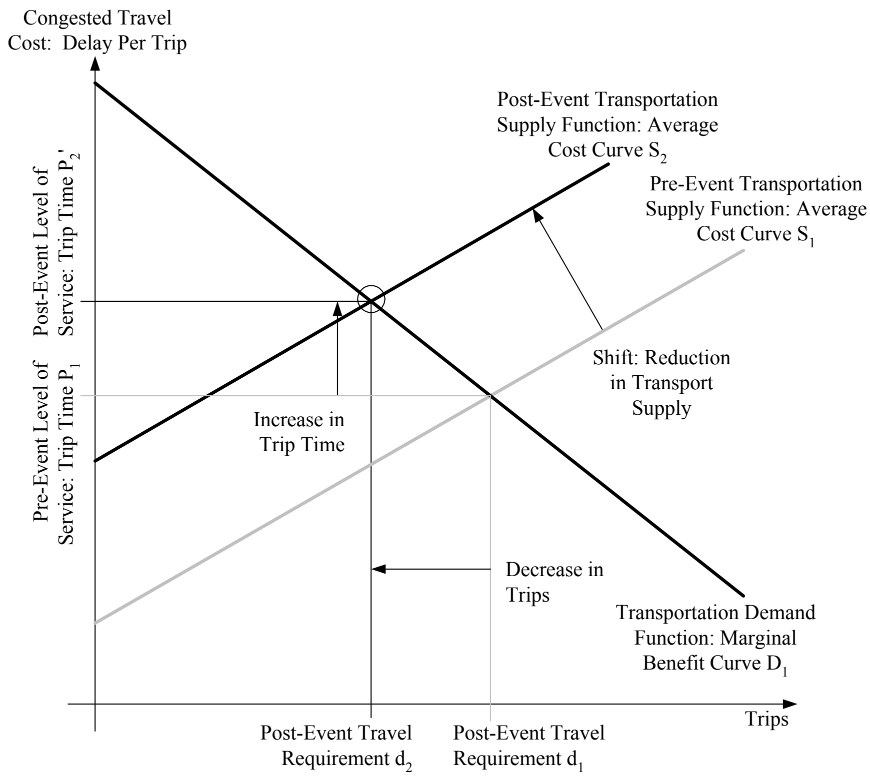

Fig. 2.3 User equilibrium transportation flows given variable travel demand in a network damaged by an earthquake

equal to or less than the travel times on any unused paths. In addition, in the case of a variable-demand formulation, the O-D trip rates must satisfy the travel demand function. These conditions define user equilibrium under conditions of variable demand (Beckmann et al., 1956). The problem can be formulated analytically as

$$\min z(x,q) = \sum_a \int_0^{x_a} t_a(w)dw - \sum_{rs} \int_0^{q_{rs}} D_{rs}^{-1}(w)dw \tag{2.26}$$

subject to

$$\sum_k f_k^{rs} = q_{rs}\,,\ \forall r,s\,, \tag{2.27}$$

$$f_k^{rs} \geq 0\,,\ \forall k, r, s\,, \tag{2.28}$$

$$q_{rs} \geq 0\,,\ \forall r,s\,, \tag{2.29}$$

$$q_{rs} = D_{rs}(u_{rs}),\ \forall r,s\,, \tag{2.30}$$

$$x_a = \sum_{rs}\sum_k f_k^{rs} \cdot \delta_{a,k}^{rs}\,,\ \forall a\,, \tag{2.31}$$

where

t_a	= link performance function of link a,
D	= demand function,
D^{-1}	= inverse of demand function,
f_k^{rs}	= flow on path k connecting O-D pair r-s,
q_{rs}	= trip rate between O-D pair r-s,
u_{rs}	= travel time between O-D pair r-s,
x_a	= flow on link a, and
$\delta_{a,k}^{rs}$	= 1 if link a is on path k between O-D pair r-s, otherwise 0.

The first term on the right-hand side of Equation (2.26) defines link volumes and travel times that the user equilibrium requires. The second term adjusts trip rates between O-D pairs so that the travel demand loaded on to the network corresponds to a defined demand function.

An algorithm based on the secant method was developed to solve this link flow formulation (Press, 1992). This algorithm is an extension of the standard algorithm for solving the user equilibrium problem, except for the requirement of finding auxiliary trip rates in step 2 (Cho, 2002).

- Step 0: Initialization.
  Find an initial feasible flow pattern $\{x_a^n\}$, $\{q_{rs}^n\}$. Set n:=1.
- Step 1: Update link travel times and time associated with trip making.
  Set $t_a^n = t_a(x_a^n)\ \forall a$, and compute $D_{rs}^{-1}(q_{rs}^n)\ \forall r,s$.
- Step 2: Find auxiliary link volumes and trip rates.
  Compute the shortest path, m, between each O-D pair r-s based on link travel time $\{t_a^n\}$ that satisfies the relationship

$$c_m^{rs^n} = \min_{\forall k}\left\{c_k^{rs^n}\left(t_a^n\right)\right\} \tag{2.32}$$

Find auxiliary trip rates based on the following criteria:

If

$$c_m^{rs^n} < D_{rs}^{-1}\left(q_{rs}^n\right) \tag{2.33}$$

then set

$$g_m^{rs^n} = \overline{q_{rs}} \tag{2.34}$$

where m is the shortest path, and $\overline{q_{rs}}$ is the upper bound on trip rate.

If

$$c_m^{rs^n} > D_{rs}^{-1}\left(q_{rs}^n\right) \tag{2.35}$$

then set

$$g_k^{rs^n} = 0 \ \forall k \tag{2.36}$$

If

$$\left| c_m^{rs^n} - D_{rs}^{-1}\left(q_{rs}^n\right)\right| < \varepsilon \tag{2.37}$$

then set

$$g_m^{rs^n} = g_m^{rs^{n-1}} \tag{2.38}$$

The auxiliary link volume

$$y_a^n = \sum_{rs}\sum_k g_k^{rs^n} \cdot \delta_{a,k}^{rs} \ \forall a \tag{2.39}$$

The auxiliary trip rate

$$v_{rs}^n = \sum_k g_k^{rs^n} \ \forall r,s \tag{2.40}$$

- Step 3: Determine the best direction of search.

  Solve the following system for α.

$$\min z(\alpha) = \sum_a \int_0^{x_a^n + \alpha\left(y_a^n - x_a^n\right)} t_a(w)dw - \sum_{rs} \int_0^{q_{rs}^n + \alpha\left(v_{rs}^n - q_{rs}^n\right)} D_{rs}^{-1}(w)dw \tag{2.41}$$

subject to $0 \le \alpha \le 1$.

- Step 4: Flow update

  Set the new link flows to

$$x_a^{n+1} = x_a^n + \alpha_n\left(y_a^n - x_a^n\right) \tag{2.42}$$

and the new trip rates to

$$q_{rs}^{n+1} = q_{rs}^n + \alpha_n\left(v_{rs}^n - q_{rs}^n\right) \tag{2.43}$$

- Step 5: Convergence test

  If the following inequality holds for predefined small number κ,

$$\sum_{rs} \frac{\left| D_{rs}^{-1}\left(q_{rs}^{n}\right) - u_{rs}^{n} \right|}{u_{rs}^{n}} + \sum_{rs} \frac{\left| u_{rs}^{n} - u_{rs}^{n-1} \right|}{u_{rs}^{n}} \leq \kappa \tag{2.44}$$

terminate. Otherwise, set n:=n+1 and go to step 1.

2.2.2 Freight Demand

The Metropolitan Transportation Commission (MTC) has person trip O-D estimates available for 1990 and, recently, for 1998. The MTC provides freight O-D estimates for 1998 but has no freight O-D estimates available for 1990. The standard methods of developing freight O-D estimates rely on collecting survey data. Such data collection is relatively expensive, and freight tables have not generally been available even for large metropolitan areas. They remain unavailable, for example, in Los Angeles.

This study was begun before the 1998 MTC highway network model and associated freight and person-trip O-D estimates were published, which induced us to develop a freight demand model capable of estimate freight O-D tables. A number of disparate and incomplete freight data sources were available at the inception of the project. Consequently, we employ a systematic, non-survey based freight demand model (Gordon and Pan, 2001) that assembles freight data from a number of public sources. Their approach is not based on a freight O-D survey but is instead based on intra- and inter-regional commodity flow data by industrial sector. Systematic data-assembly and reconciliation play an important role in this approach.

Not all industrial sectors are relevant. We consider only sectors for which commodities are mainly transported by truck. Gordon and Pan (2001) identified four aggregate industrial sectors that account for most urban freight movements. These are mining, durable manufacturing, non-durable manufacturing, and transportation utilities. We rely on their classification scheme.

Figure 2.4 summarizes our approach. Data are assembled to provide trip generation estimates for inter-regional and intra-regional freight movements. Network locations where inter-regional freight is transferred to-or-from trucks are identified. Inbound and outbound commodity flows from inter-regional trips are accounted for at each specific site. Intra-regional truck movements are estimated by using employment data for each TAZ, and by accounting for commodity flows between industrial sectors.

After constructing inter- and intra-regional freight trip generation estimates, we execute a verification step to determine whether these trip production and attraction estimates are in reasonable agreement with other data sources. Our procedure also produces an estimate of employment by TAZ, which we compare with actual figures. This verification step should be completed before trip distribution estimates are produced.

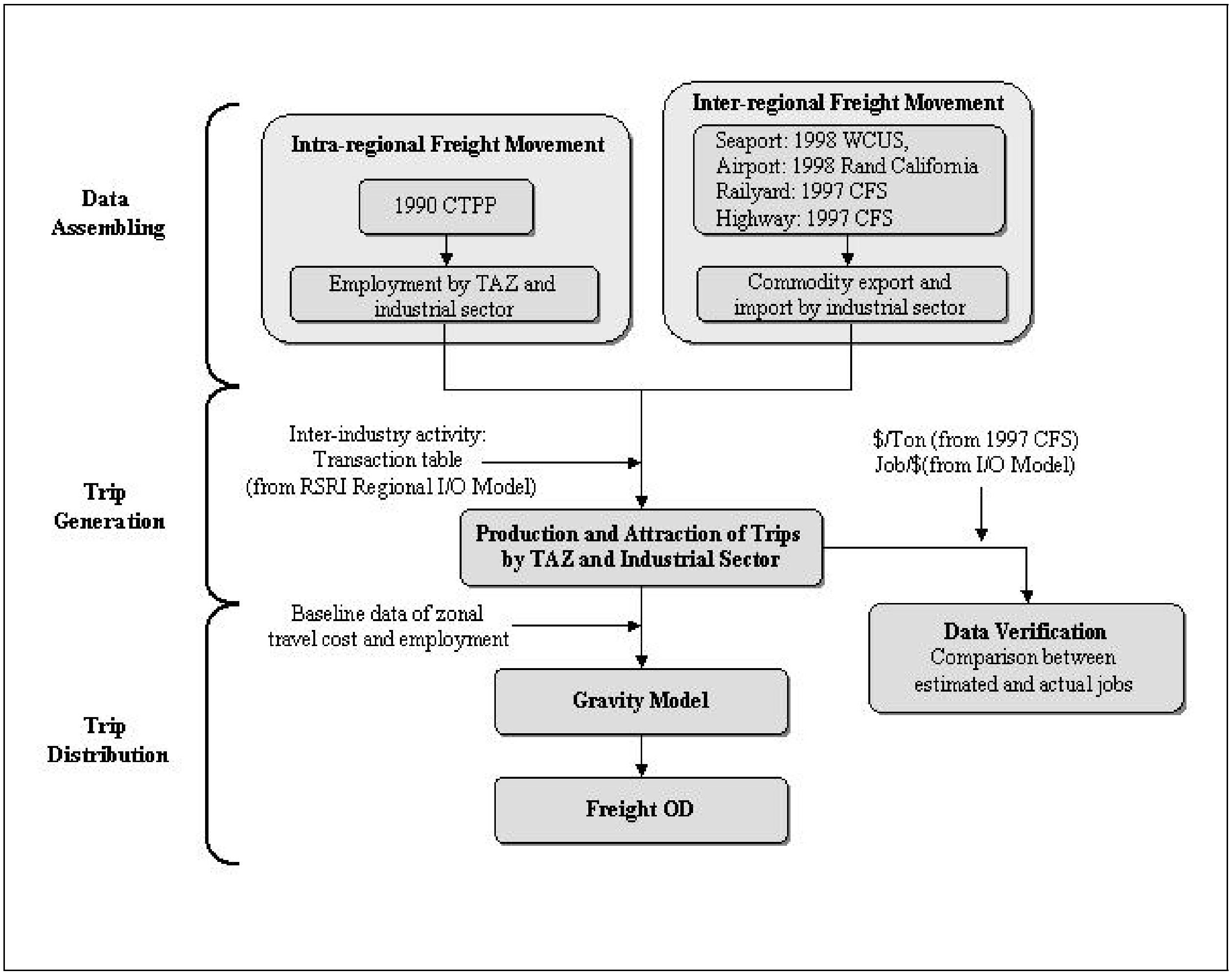

Fig. 2.4 Summary of the freight origin–destination estimation model

The MTC's 1990 highway network model does not account for external zones. Therefore, for consistency with 1990 MTC person O-D data, we treat only the 1,099 TAZs inside the Bay Area, excluding through freight traffic. According to the U.S. DOT's report of truck movements by trip types in the San Francisco Bay Area, the portion of truck through-traffic is less than 1%, a very small portion (U.S. DOT, 2000; U.S. DOC, 2000).

2.2.2.1 Trip Generation

(1) Intra-regional trip generation

We rely heavily on employment data from the 1990 Census Transportation Planning Package (CTPP) for the San Francisco Bay Area to construct intra-regional freight trip generation estimates (BTS, 1990). The CTPP includes employment data by economic sector and by place of employment (TAZs).

We rely on commodity flows between industries to estimate freight trip productions and attractions. In regional economic analysis, a transaction table is often used to depict regional inter-industry activities (Cho et al., 2001). A traditional transaction table indicates shipments from one sector to another. However, It does not specify where the shipments come from and where they terminate. We rely on a transaction table developed from the Regional Science Research Institute's (RSRI) regional input-output model, PC I-O (RSRI, 1996). To convert this aspatial information to spatial flows, we disaggregate and assign these interactions to each TAZ based on 1990 CTPP employment by TAZ and by sector.

The 1990 CTPP employment data are used to generate estimates of freight trip productions and attractions for each TAZ as follows. The total commodity *i* required to support attraction in zone z, D_i^z, is

$$D_i^Z = \sum_j a_{i,j} \cdot X_j^Z \tag{2.45}$$

where

X_j^Z = the total output of commodity *j* in zone *z* given employment in sector j and zone z in baseline year, and

$a_{i,j}$ = the flow from commodity i to commodity j required by unit output of j. This $a_{i,j}$ is the i,j^th element of *A*, the matrix of demand coefficients for the input-output model.

Similarly, the total commodity *j* used to support production in zone *z*, O_j^z, is

$$O_j^Z = \sum_i b_{i,j} \cdot X_i^Z \tag{2.46}$$

where

X_i^Z = the total output of commodity *i* in zone *z* given base year employment in sector *i* and zone *z*, and

$b_{i,j}$ = the flow from commodity *i* to commodity *j* required by per unit output of *i*. This $b_{i,j}$ is the i, j^{th} element of *B*, the matrix of supply coefficients for the input-output model.

(2) Inter-regional freight trip generation

We identified network locations associated with inter-regional freight movement, including seaports, airports, rail yards, and highway network entry points. We assembled freight tonnage data for inbound and outbound freight for each of these sites. We consider only the portion of total inbound and outbound commodity flows that are transferred to trucks at each site. The list of sites and the main data sources used to inventory commodity flows for each site are as follows.

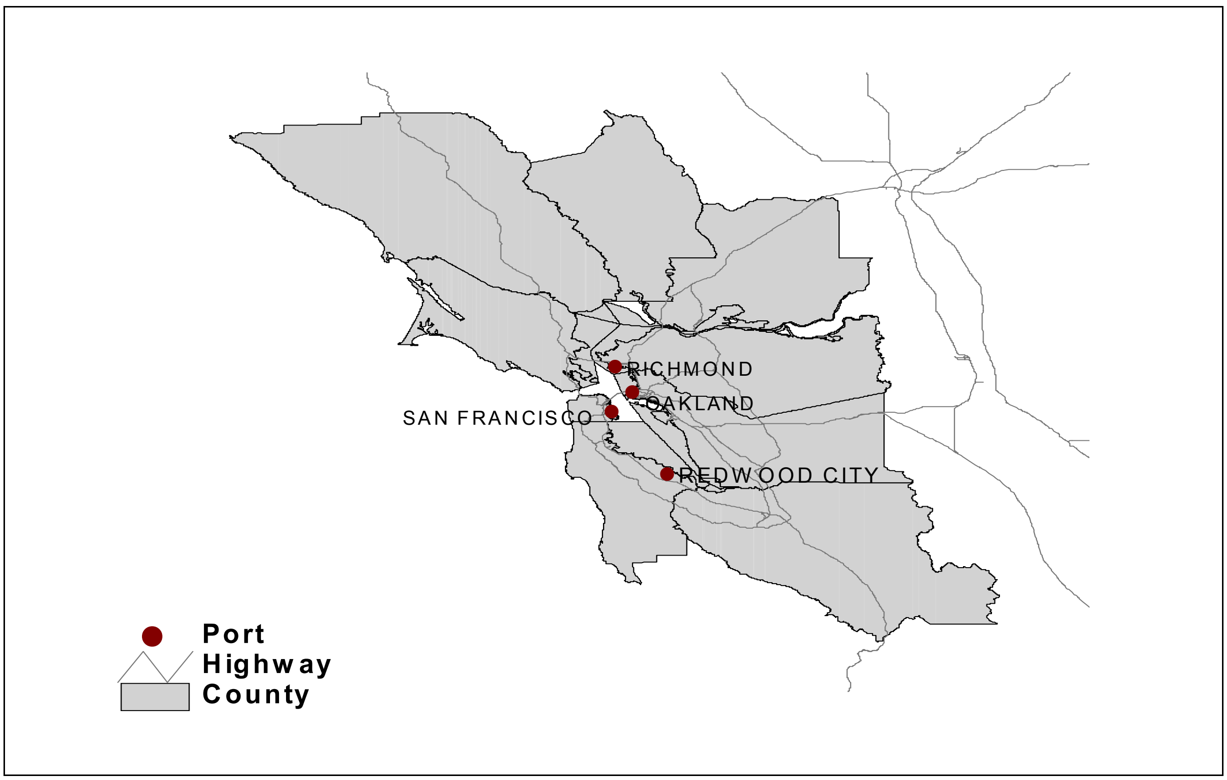

Fig. 2.5 Seaports

Seaports: Four major seaports were included. These are the Port of San Francisco, the Port of Oakland, the Port of Richmond, and the Port of Redwood City (Fig. 2.5). The main data source for ports is the 1998 Waterborne Commerce Statistics of the United States (WCUS). Inbound and outbound commodity flows by sector are available from the WCUS (1998).

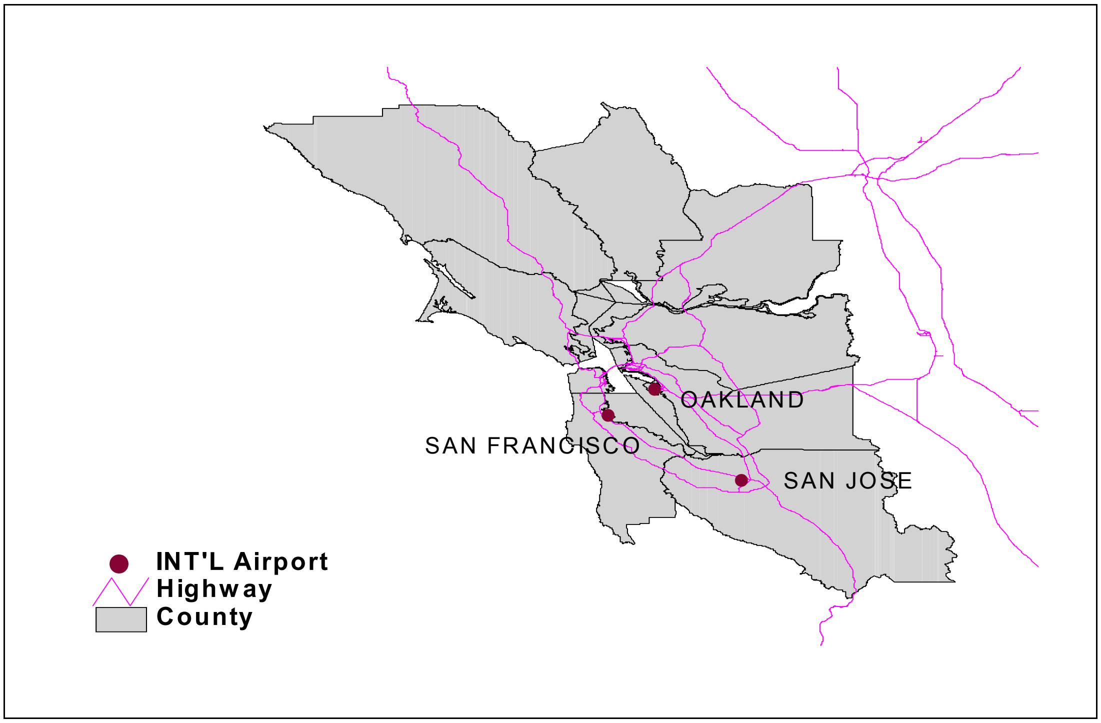

Fig. 2.6 Airports

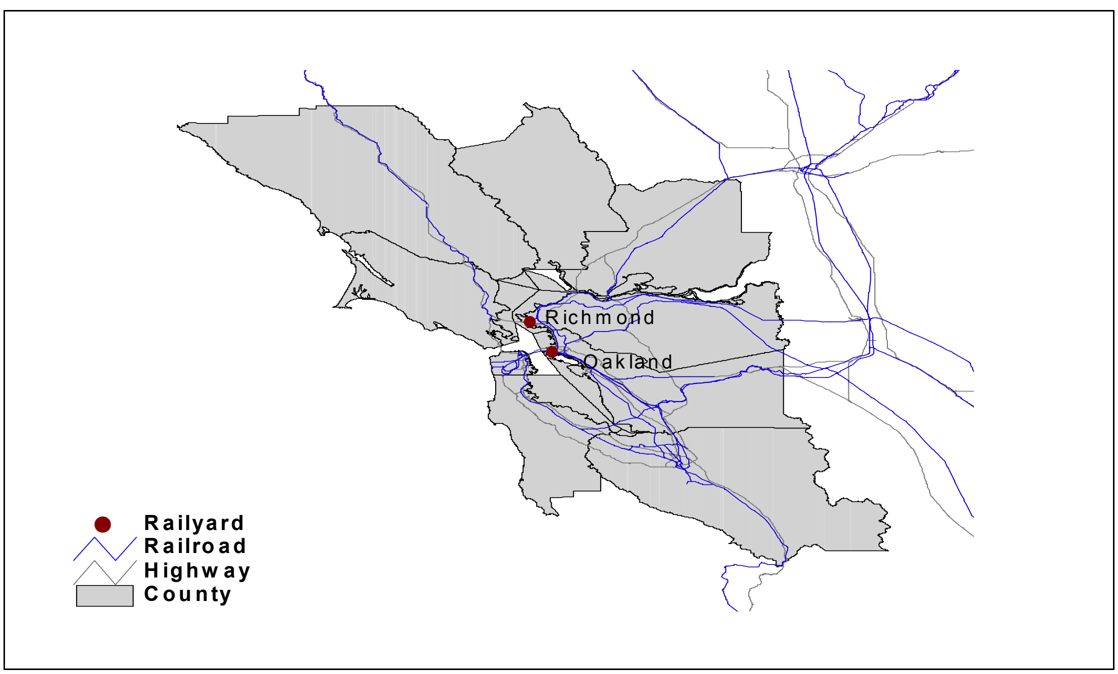

Fig. 2.7 Rail yards

Airports: The three international airports in the Bay Area are included. These are the San Francisco Airport, the Oakland International Airport, and the San Jose International Airport, as shown in Figure 2.6. Rand's 1998 California and International Airport Statistics were used as the main airport data source (RAND, 1998). Unfortunately, economic sector information is not available in the Rand data. We relied instead on the value and tonnage shares of durable and non-durable manufacturing flows listed for air cargo in California in the 1993 Commodity Flow Survey (CFS). We would have preferred to use the sector-specific information from the 1997 CFS, but air and truck flows are combined in the 1997 CFS (U.S. Bureau of Census, 1993 and 1997).

Rail yards: Rail yards supporting freight movement in the Bay Area consist of the Richmond and Oakland rail stations (Fig. 2.7). To estimate rail flows, we combine data from the 1997 CFS for the San Francisco-Oakland-San Jose CMSA with sector-specific information from Caltrans's 1992 Intermodal Transportation Management System (ITMS) (Booz • Allen & Hamilton Inc., 1996).

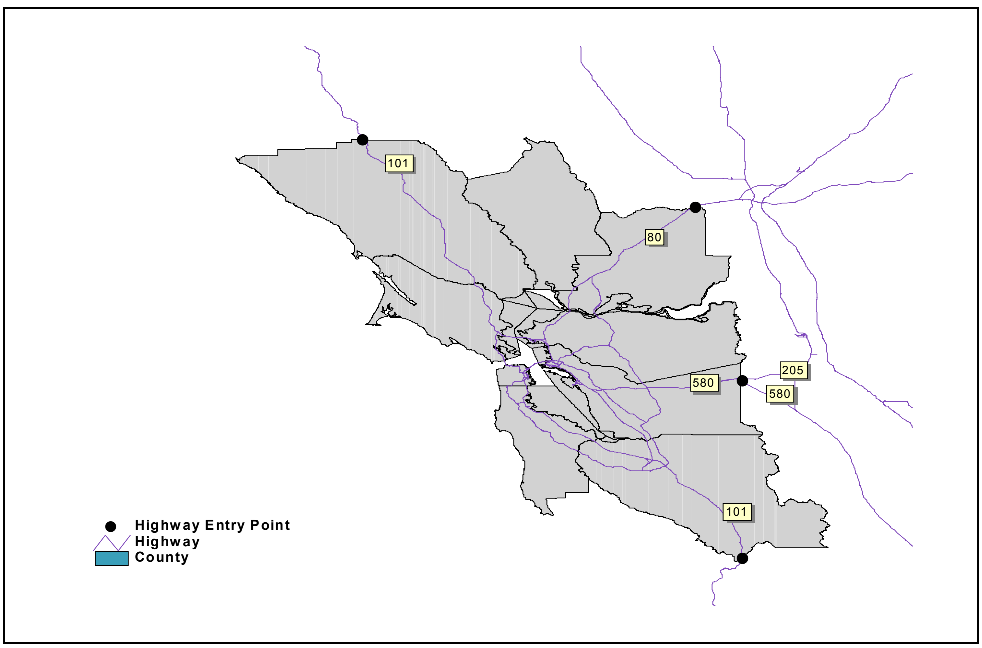

Fig. 2.8 Highway entry and exit points

Highway entry and exit points: Four highway entry and exit points to and from the Bay Area are identified. These are the US 101 North point, the US 101 South point, I-80, and the junction of I-205 and I-580 (Fig. 2.7). As in the case of rail flows, we estimate total inter-regional highway freight flows by combining data from the 1997 CFS for the San Francisco-Oakland-San Jose CMSA with sector-specific information from Caltrans's 1992 Intermodal Transportation Management System (ITMS).

Annual freight tonnage values by sector are converted to Passenger Car Equivalents (PCEs) by calculating tons / PCE by sector as follows;

$$\text{tons / PCE by sector} = A / (B \cdot C) \tag{2.47}$$

where

A = daily tonnage by sector

= annual tonnage by sector / 365,

B = daily trucks by sector

= (total vehicle trips) · (the portion of truck trips relative to total vehicle trips) · (sector share of truck trips), and

C = PCE/truck by sector.

2.2.2.2 Data Verification

Since so many secondary data sources are needed to construct these estimates, it is useful to verify the freight trip production and attraction values. We compare estimated total employment implied by these estimates with the figures reported by the 1990 CTPP for the Bay Area. For this comparison, we convert freight tonnage data to the corresponding number of jobs by referring to dollar-per-ton and dollars-per-job data from the Bay Area input-output model. This estimate of employment in the San Francisco Bay Area employment is in close agreement with census data as shown in Table 2.8.

Table 2.8 Comparison between aggregate estimated employment and actual number of jobs (millions jobs/year)

Estimated Employment Implied by				Actual[a]
Intra-region Freight Flows	Inter-region Freight Flows		Total Freight Flows	
	Inbound	Outbound		
0.84	1.21	0.93	2.98	3.09

Source: a. 1990 CTPP for the San Francisco Bay Area.

2.2.2.3 Trip Distribution

We rely on a conventional gravity model formulation to estimate the intra-regional distribution of freight trips. Before completing the trip distribution estimates, inter-regional freight demands are loaded onto the network at the corresponding TAZs. The total estimated number of freight O-D trips corresponds to 220,757 PCE per day, or 49.17% the MTC's 1998 total transportation demand of 448,989 PCE/day.

2.2.2.4 Comparison with MTC Freight O-D Estimates

As noted above, the MTC provides truck trip O-D matrices for 1998, but not for 1990. It is difficult to compare the quality of the MTC's freight O-D estimates with ours because the details of how the 1998 MTC's freight demands were estimated are unknown. Nevertheless, considering the complexity of estimating intra-regional freight movements, a comparison is a step in the search for methodological improvements.

The MTC's 1998 freight O-D estimates include peak and off-peak daily truck trips for small (2-axle), medium (3-axle) and large (4+ -axle) vehicles. Small trucks account for the largest portion of daily trips, (76.4%), and medium trucks account for the smallest (7.4%). The total number of daily truck trips is 257,585 as shown in Table 2.9.

Table 2.9 Summary of the MTC 1998 freight O-D data (trips / day)

Truck Type	Peak Trips	Off-peak Trips	Total	
Small (2-axle)	63,414	133,396	196,810	(76.4%)
Medium (3-axle)	5,813	13,221	19,034	(7.4%)
Large (4-axle)	12,956	28,785	41,741	(16.2%)
Total	82,183	175,402	257,585	(100.0%)

Our freight O-D estimates and the MTC person trip O-D matrices account for both intra-regional and inter-regional trip. The MTC 1998 freight O-D includes no inter-regional truck trips. Only intra-regional and intra-zonal estimates are provided. We do not estimate intra-zonal flows, which the MTC data indicate account for 3.04% of total daily truck trips (see Table 2.10). The MTC estimates that truck trips account for 3.56% of all daily trips. Our estimate is 1.78% as listed in Table 2.11.

Table 2.10 Intra-zonal freight trip distribution by number of truck axles (trips / day)

Truck Type	Peak	Off-peak	Total	Proportion of total daily truck trips
Small (2-axle)	2,105	4,392	6,497	2.52%
Medium (3-axle)	284	592	876	0.34%
Large (4-axle)	147	307	454	0.18%
Total	2,536	5,291	7,827	3.04%

Source: MTC

Table 2.11 Truck trip proportion of total vehicle (person + freight) trips (PCEs / day): comparison of MTC and PEER estimates

Source	Person Trips[a]	Freight Trips[b]	Total (Person + Freight)	Freight/Total
MTC	12,164,593	448,989	12,613,338	3.56%
PEER	12,164,593	220,757	12,385,350	1.78%

Notes: a. Converted to PCE units from MTC 1998 daily person trips (1 PCE = 1.6 person trips).
b. Converted to PCE units from MTC 1998 daily truck trip by axle category. Small trucks = 1.5 PCE. Medium trucks = 1.5 PCE. Large trucks = 3 PCE, Highway Capacity Manual (TRB 1994), adjusted by Cho (1999).

There are some obvious reasons for some of this difference. First, due to data constraints, we relied on 1990 employment data for freight trip generation. If the more recent employment data from the 2000 CTPP were available, we expect that our trip generation estimates would be higher. Second, our inter-regional freight trip estimates are based on interactions between industrial sectors, which are taken from the transactions table from an economic input-output model. This is a substantive, but incomplete source of information. In reality, there are additional factors affecting freight trip productions and attractions in each TAZ.

To better compare the details of the MTC freight O-D estimates with our own, we computed correlation coefficients between freight and person trip proportions by TAZ. This comparison is limited to the network's 1,099 internal TAZs, because the MTC estimates do not include inter-regional freight truck trips. The correlation between the MTC and PEER shares of freight trip productions and attractions by zone are 0.715 and 0.729, respectively. This high degree of correlation indicates that the patterns in our estimates of freight trip ends and the MTC's values covary closely.

Not surprisingly, this covariance is reduced at the level of intra-regional flows. The system-wide correlation coefficient between our estimates of zone-to-zone freight trip proportions and the MTC's estimates is only 0.318. If the MTC's 1998 freight matrices are survey based, they may present a means of improving the trip-distribution step in our non-survey based freight trip estimates. There is likely more improvement to be gained at our procedure's trip distribution step than at the trip generation step.

2.2.2.5 Limitations of the Freight Demand Model

A systematic, non-survey based freight demand model has considerable utility, since the results of a freight O-D survey cannot normally be expected to be available. The MTC's 1998 freight O-D estimates are a departure from practice, and a likely advance. The comparison between our results and the MTC's estimates suggests some avenues for improvement and additional research with respect to our own approach.

First, our employment data for intra-regional freight trip generation needs be updated to a more recent source, such as 2000 CTPP. Second, our TAZ system should be extended and reconciled with the MTC's 1998 zone system in a way that includes the MTC's external zones. Our freight model considers only 4 external zones, because these are associated with regional highway entry-and-exit points. The MTC's TAZ system has 1,120 TAZs, including 21 new external zones in addition to the 1,099 TAZs associated with their 1990 O-D estimates. And third, our freight trip distribution model has not yet been integrated with the person-trip model. Distribution of person trips and freight trips should occur simultaneously rather than separately. Our trip distribution model relies on a gravity model distance-decay function estimated from 1990 travel times. These travel times are derived from the 1990 person trip O-D requirements. This is a reasonable approximation, but it makes more theoretical sense for the distance decay function to be estimated based on travel times for equilibrium flows that combine person and freight trips. Achieving this will require accounting for the feedback relationship between trip distribution and trip assignment. Modeling trip generation, trip distribution and trip assignment simultaneously for both freight and person trips is computationally challenging, but likely possible. This aspect of the problem needs to be addressed in the future research.

2.2.2.6 Economic Value of Freight Trips

Little research has been done on the value of freight trips. However, assembled commodity value and tonnage data enable us to estimate dollars/PCE for truck trips. We calculated dollars/PCE based on Caltrans District 4's truck traffic volume data, combined with annual tonnage and annual dollar values for commodities by sector derived from the I-O model (Table 2.12). We adopted a method defined and applied by Cho (1999) for the Southern California Association of Governments metropolitan planning area.

Table 2.12 Summary of truck volumes in Caltrans District 4 (1997 trips)

AADT					
Total	Trucks	Axles			
		2	3	4	5+
42,457,395	2,126,498	885,126	249,161	75,067	917,144
	100.00%	41.62%	11.72%	3.53%	43.13%

Source: Caltrans, http://www.dot.ca.gov/hq/traffops/saferesr/trafdata/

According to Caltrans's traffic count data, the total number of 1997 vehicle counts in Caltrans District 4 was 42,457,395, including 2,126,498 truck counts (5.0%) and 40,330,897 non-truck counts (95.0%). Since truck trip distances are usually longer than non-truck truck trip distances, trucks are certainly over-represented in these counts.

We adjust the truck count as follows. Based on data from Caltrans's Intermodal Transportation Management System, the average truck distance in California is 59.82 miles (Cho, 1999). The MTC reports that the average trip length in the Bay Area, excluding truck trips, is 7.03 miles. The truck trip distances are on the order of 8.51 times (59.82 miles/7.03 miles) the non-truck trip distances. Assuming that the probability of a vehicle being observed during a traffic count is linearly proportional to the trip length, trucks are counted approximately 8.51 times more frequently than other vehicles. This reduces the share of trucks otherwise estimated from traffic count data to (2,126,489 / 8.51) / [42,457,395 – 2,126,498 + (2,126,489 / 8.51)], or 0.616%.

According to MTC's 1998 person trip O-D estimates, the total of person trips is 20,239,900 trips / day. At 1.6 person trips / PCE, this is 12,649,938 units of demand / day.

Given the proportion of truck trips estimated from the Caltrans District 4 traffic counts, this implies 78,407 daily truck trips in the Bay Area.

We require the distribution of truck trips by sector expressed as PCE by sector to account for commodity flows by sector. Data from Gordon and Pan (2001) can be used to estimate the proportion of trucks by sector. The distribution of PCE by sector is calculated from the distribution of trucks by axle, and PCE/truck by axle count. See Tables 2.13–2.14.

Table 2.13 PCEs by truck size (number of axles)

Truck Axles	2	3	4	5+
PCE	1.5	1.5	3	3

Sources: Highway Capacity Manual (TRB 1994), as adjusted by Cho (1999).

Table 2.14 The distribution of trucks and PCEs by sector

Sector	California Share (%)[a]	Passenger Car Equivalents[b]
Mining	1.75	2.1999
Durable Manufacturing	6.58	2.1999
Non-durable Manufacturing	6.58	2.1999
Transportation-Utilities	85.09	2.1999
Total	100.00	

Notes: a. Gordon and Pan (2000)
b. Calculated from the proportion of trucks by axle and PCE/truck by axle

An estimate of $/PCE by sector is obtained by combining the commodity flow data by sector with the truck trip data. These values are thus based on the tonnage of commodity flows into and out of the Bay Area, and from actual truck counts. These can be used to estimate the opportunity cost for forgone freight trips resulting from earthquake damage to the transportation system.

3 Application to the San Francisco Bay Area

One of the main objectives of this project is to apply the methodology to an existing highway transportation system. Considering the highly active faults in the San Francisco Bay Area and its very complex transportation network, the participants of the first PEER Transportation Risk Analysis Workshop in 1998 recommended that the application be here. Another rationale for this selection was that part of the complexity of the transportation network is its limited redundancy in some areas. The freeways and state bridges, located in the nine counties of the Bay Area, are under the administration of Caltrans District 4.

According to a recent study by the USGS (1999), it was estimated that the likelihood of at least one earthquake with a moment magnitude of 6.7 or higher in the next 30 years in the San Francisco Bay Area is 62%. Such events are very likely to subject major bridges in the region to severe ground motion due to their proximity to existing faults. In addition to the San Andreas and Hayward faults, the Calaveras and the San Gregorio-Palo Colorado faults are also capable of generating significant earthquakes that can damage the system. However, among the many fault systems in the area, the San Andreas and Hayward faults are reported to have the highest probability of generating a major earthquake. Figure 3.1 shows where these two major faults cross the counties of the San Francisco Bay Area.

The following events are chosen as the scenario earthquakes: events with moment magnitudes of 7.5 and 8.0 on the San Andreas fault, and events with moment magnitudes of 7.0 and 7.5 on the Hayward fault (hereafter referred to as *SA7.5*, *SA8.0*, *HW7.0*, and *HW7.5*). The rupture lengths for magnitudes are estimated, as listed in Table 3.1, using the relationships between earthquake magnitude and rupture length for strike-slip faults developed by Wells and Coppersmith (1994). The distance between bridge sites and the fault for these scenario events is taken as the perpendicular distance from the surface projection of the fault to the bridge site. Both the San Andreas and the Hayward faults have a dip angle of nearly 90^{o}. Thus, this distance definition is appropriate for the attenuation functions considered in the study.

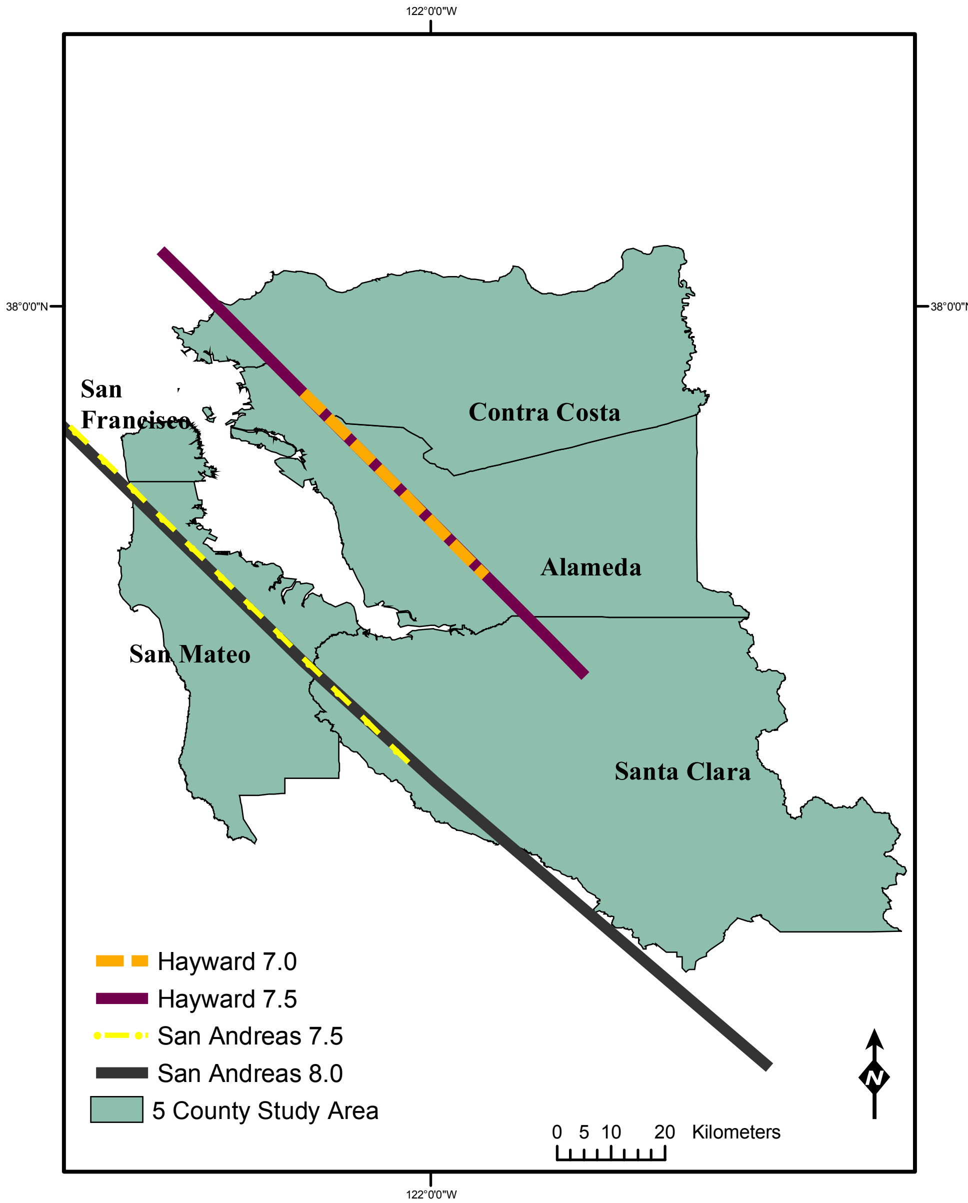

Fig. 3.1 Counties and major faults and scenario events in the San Francisco Bay Area

Table 3.1 Rupture lengths for different scenario events

Moment magnitude	Rupture length (km)
7.0	50
7.5	100
8.0	235

In order to simulate the effects of these scenario events, five of the highly populated counties in the Bay Area are chosen; these are: Alameda, Contra Costa, San Francisco, San Mateo, and Santa Clara. The commercial Geographic Information Systems (GIS) ARC/INFO™, is used for the purpose of data integration and display. Using the GIS software, several different types of information are linked, such as the bridge characteristics, transportation networks, and local soil characteristics.

3.1 DATABASES AND CHARACTERIZATION OF BRIDGES

Data from several databases are used in the study. These are (1) a bridge inventory database obtained from the California Department of Transportation (Caltrans, 1993), (2) a database of the highway transportation network for the Bay Area obtained from the Metropolitan Transportation Commission (MTC), and (3) the soil conditions, and the liquefaction and landslide susceptibility categories of the Bay Area obtained from USGS (1997, 2000). All of these databases are defined as separate layers, and linked to each other using ARC/INFO™. In addition to these data, the county boundaries and the locations of Hayward and San Andreas faults are included as separate layers.

The bridge inventory data used in this project are part of the Structural Maintenance and Inventory System (SMIS) database compiled by Caltrans (1993). Figure 3.2 shows the geographical distribution of the bridges considered in the study. The SMIS database includes information on the bridge locations and the engineering characteristics for all state and local bridges in California. The bridge data are classified according to the HAZUS (1999) scheme, which utilizes the National Bridge Inventory (NBI) physical attributes. The detailed descriptions for each of these attributes can be found in the recording and coding guide for bridges of the Federal Highway Administration (FHWA, 1996). Mainly the following attributes are used in the analyses:

- Year Built
- Seismic design
- Number of spans: single vs. multiple span bridges
- Structure type: concrete, steel, others
- Pier type: multiple column bents, single-column bents, and pier walls

- Abutment type and bearing type: monolithic vs. non-monolithic; high rocker bearings, low steel bearings, and neoprene rubber bearings
- Span continuity: continuous, discontinuous (in-span hinges), and simply supported.

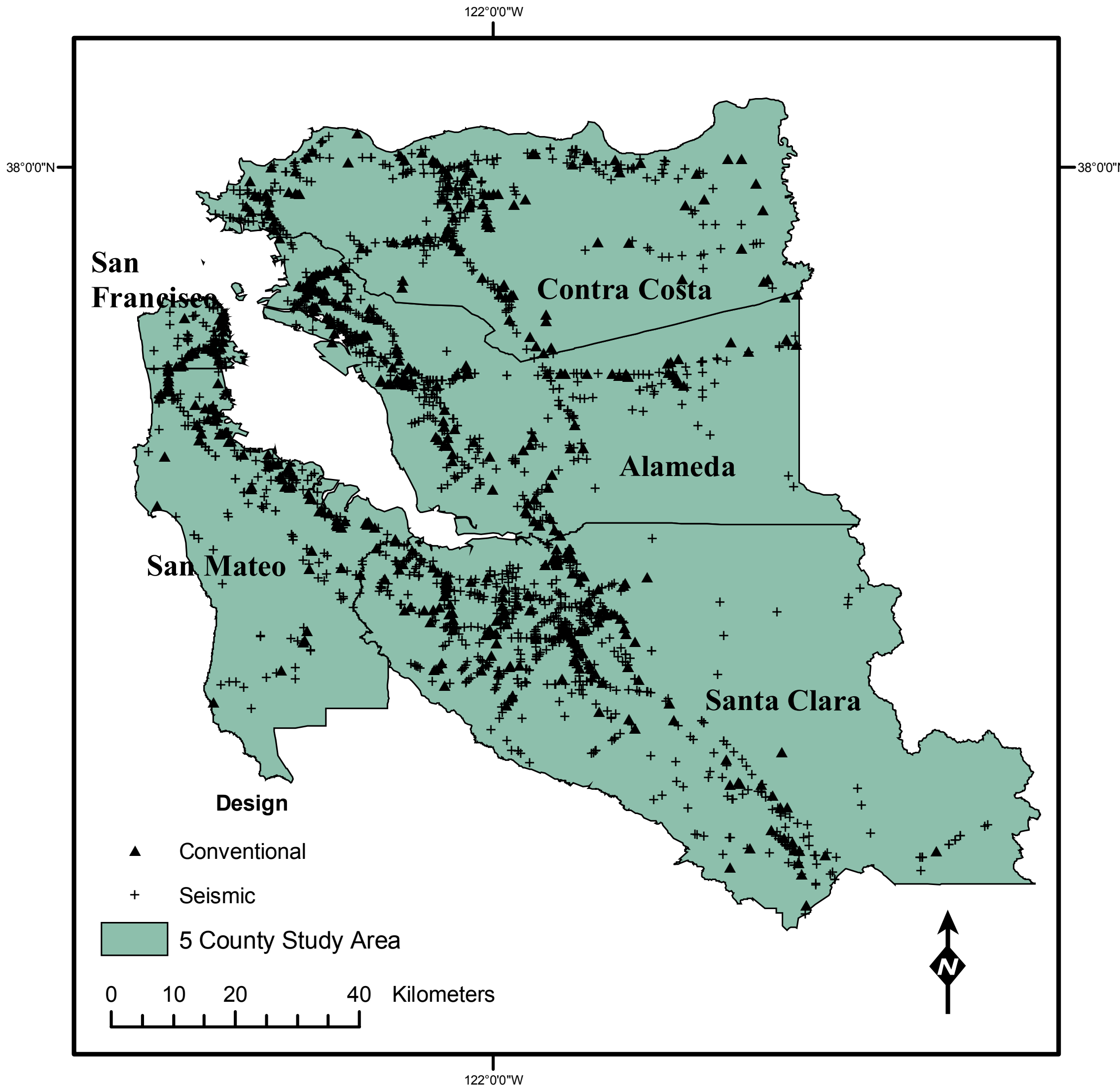

Fig. 3.2 Distribution of bridges by design category in five counties

The bridge database was verified and corrected by Basoz and Kiremidjian (1996). The database contains 2921 state and local bridges in the five counties chosen. Of these, 281 bridges are excluded from the analyses for various reasons (e.g., pedestrian and railroad bridges, and bridges lacking sufficient information). Table 3.2 gives the distribution of the 2640 bridges used in the study by type and by county.

Table 3.2 Number of bridges by category and county

County	State Bridges	Local Bridges	Total Number of Bridges	Number of Bridges Used
Alameda	505	243	748	724
Contra Costa	291	320	611	538
San Francisco	104	53	157	120
San Mateo	234	140	374	336
Santa Clara	552	479	1031	922
Total	1686	1235	2921	2640

The classification of the bridges with respect to their structural properties is based on the bridge classification scheme of HAZUS (1999). There are 28 bridge classes defined in HAZUS. Table 3.3 provides the breakdown of the bridges according to bridge classes and county in which they are located.

Table 3.3 Number of bridges by structural type and county

Bridge Class	Description	NBI Class	Year Built	Design	Contra Costa (28)	Alameda (33)	San Francisco (34)	San Mateo (35)	Santa Clara (37)	All Counties
1	Major Bridge, Length>150m	All	<1975	Conventional	0	1	1	0	0	2
2	Major Bridge, Length>150m	All	≥1975	Seismic	1	0	1	2	0	4
3	Single Span	All	<1975	Conventional	17	29	4	14	24	88
4	Single Span	All	≥1975	Seismic	192	186	30	87	249	744
5*	Multi-Col. Bent, Simple Support, Concrete	101-106	<1990	Conventional	0	0	0	0	0	0
6	Multi-Col. Bent, Simple Support, Concrete	101-106	<1975	Conventional	1	0	0	1	1	3
7	Multi-Col. Bent, Simple Support, Concrete	101-106	≥1975	Seismic	22	7	3	3	20	55
8	Single Col., Box Girder, Continuous Concrete	205-206	<1975	Conventional	20	48	20	19	15	122
9	Single Col., Box Girder, Continuous Concrete	205-206	≥1975	Seismic	53	136	17	50	78	334
10	Continuous Concrete	201-206	<1975	Conventional	5	10	5	3	16	39
11	Continuous Concrete	201-206	≥1975	Seismic	48	70	14	49	164	345

Table 3.3—*continued*

Bridge Class	Description	NBI Class	Year Built	Design	Contra Costa (28)	Alameda (33)	San Francisco (34)	San Mateo (35)	Santa Clara (37)	All Counties
12*	Multi-Col. Bent, Simple Support, Steel	301-306	<1990	Conventional	0	0	0	0	0	0
13	Multi-Col. Bent, Simple Support, Steel	301-306	<1975	Conventional	7	8	5	7	6	33
14	Multi-Col. Bent, Simple Support, Steel	301-306	≥1975	Seismic	18	31	8	7	39	103
15	Continuous Steel	402-410	<1975	Conventional	1	4	0	2	2	9
16	Continuous Steel	402-410	≥1975	Seismic	17	8	3	6	7	41
17*	Multi-Col. Bent, Simple Support, Prestressed Concrete	501-506	<1990	Conventional	0	0	0	0	0	0
18	Multi-Col. Bent, Simple Support, Prestressed Concrete	501-506	<1975	Conventional	2	3	0	1	7	13
19	Multi-Col. Bent, Simple Support, Prestressed Concrete	501-506	≥1975	Seismic	15	42	5	9	34	105
20	Single Col., Box Girder, Prestressed Continuous Concrete	605-606	<1990	Conventional	1	4	0	8	12	25
21	Single Col., Box Girder, Prestressed Continuous Concrete	605-606	≥1975	Seismic	37	69	0	24	152	282
22	Continuous Concrete	601-607	<1975	Conventional	0	2	1	0	1	4
23	Continuous Concrete	601-607	≥1975	Seismic	12	12	0	6	12	42
24	Multi-Col. Bent, Simple Support, Steel	301-306	<1990	Conventional	0	0	0	0	0	0
25	Multi-Col. Bent, Simple Support, Steel	301-306	<1975	Conventional	2	0	1	1	0	4
26	Continuous Steel	402-410	<1990	Conventional	0	0	0	0	0	0
27	Continuous Steel	402-410	<1975	Conventional	0	0	0	0	0	0
28	Bridges that are not classified	-	-	Conventional	67	54	2	37	83	243
Total	-	-	-	-	538	724	120	336	922	2640

*: Non-California Bridges

Bridges are further identified as being designed for *conventional* primarily gravity or *seismic* loads. Seismic design is based on the following properties of the bridges: (1) spectrum modification factor, (2) strength reduction factor due to cyclic motion, (3) drift limits, and (4) longitudinal reinforcement ratio. The distribution of bridges by design criteria is also given in Table 3.4, and is displayed in Figure 3.2. Of 2640 bridges in the study area, 585 are classified as bridges designed for conventional loads. The ratio of conventional to seismic bridges is the highest (39/81 or almost 50%) in San Francisco County, implying a higher earthquake risk for that county. For the remaining counties, the proportion of conventional bridges to seismic bridges is significantly smaller. This is not a surprising observation, since San Francisco County is the oldest of all the counties considered. It should be noted, however, that many of the conventional bridges have undergone either retrofit phase I or retrofit phase II or both.

Table 3.4 Number of bridges by design criteria and county

Design Criteria	Contra Costa	Alameda	San Francisco	San Mateo	Santa Clara	All Counties
Conventional	123	163	39	93	167	585
Seismic	415	561	81	243	755	2055
Total	538	724	120	336	922	2640

Information on the highway transportation network for the study area was obtained from the Metropolitan Transportation Commission. A significant effort was devoted to import the highway network information within ARC/INFO™ and combine it with the bridge inventory database. The bridge data was linked to the highway network and corrected to match bridge locations and network locations. A detailed discussion of the characteristics of the highway transportation network is provided in Section 3.4.

The local soil conditions and the liquefaction susceptibility categories are obtained from the USGS Open File Report 00-444 (USGS, 2000). Figure 3.3 shows the local soil conditions in the study area according to the NEHRP (2000) site classification scheme. Figure 3.4 shows the liquefaction potential of the study area and the locations of the bridges considered in the study (see discussion in Section 2.1.1.1 for the liquefaction susceptibility classification used). In general, the liquefaction susceptibility increases when the bridge site is closer to the Bay.

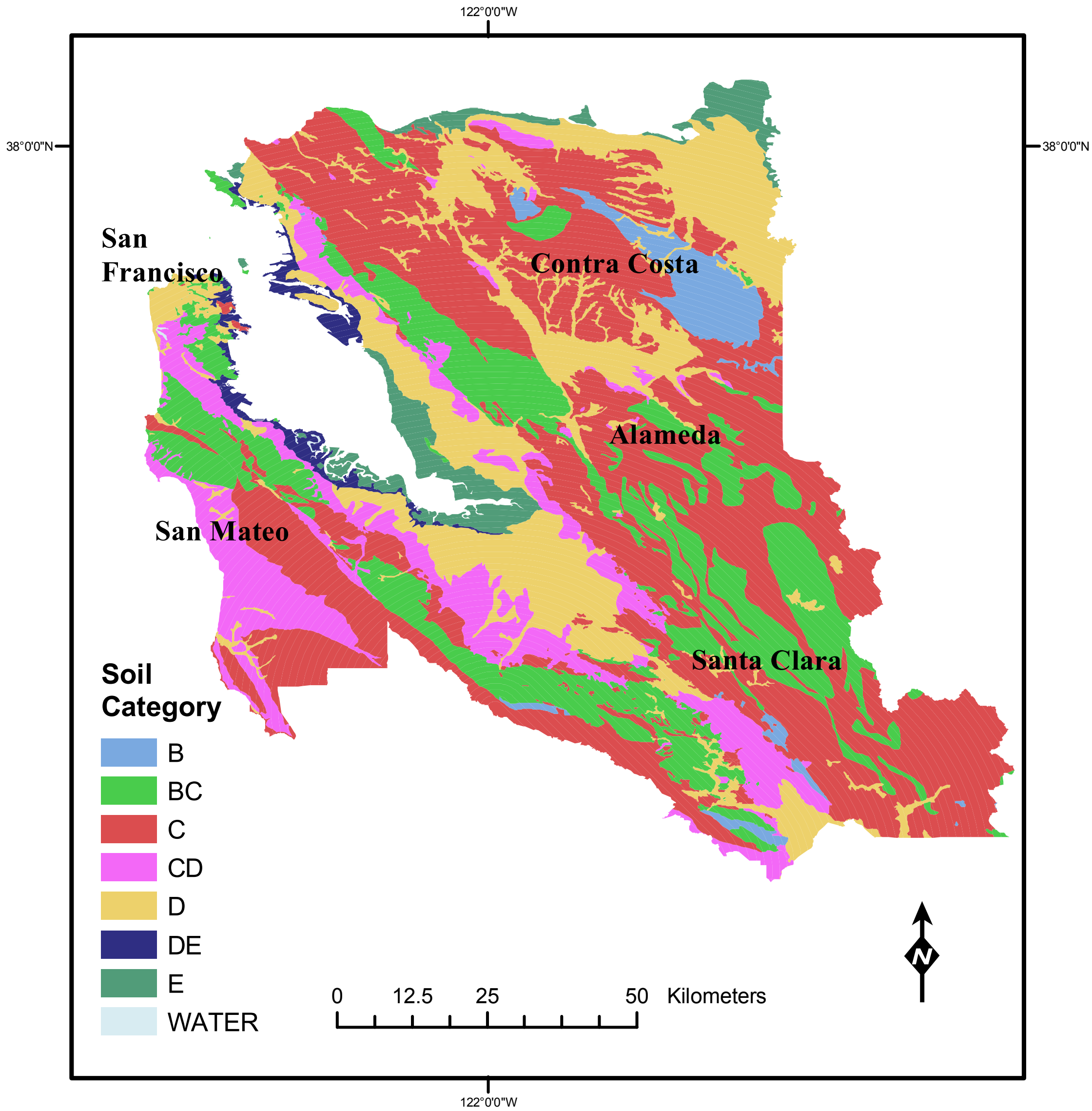

Fig. 3.3 Local soil conditions according to NEHRP site classes

The landslide potential of the study area is shown in Figure 3.5, which is based on the data obtained from USGS Open File Report 97-745 (USGS, 1997). Both of these databases were imported easily because they were provided in GIS-compatible formats from USGS (see the websites referenced). Table 3.5 gives the distribution of soil categories, liquefaction, and landslide susceptibility categories of the bridge sites in the five counties studied.

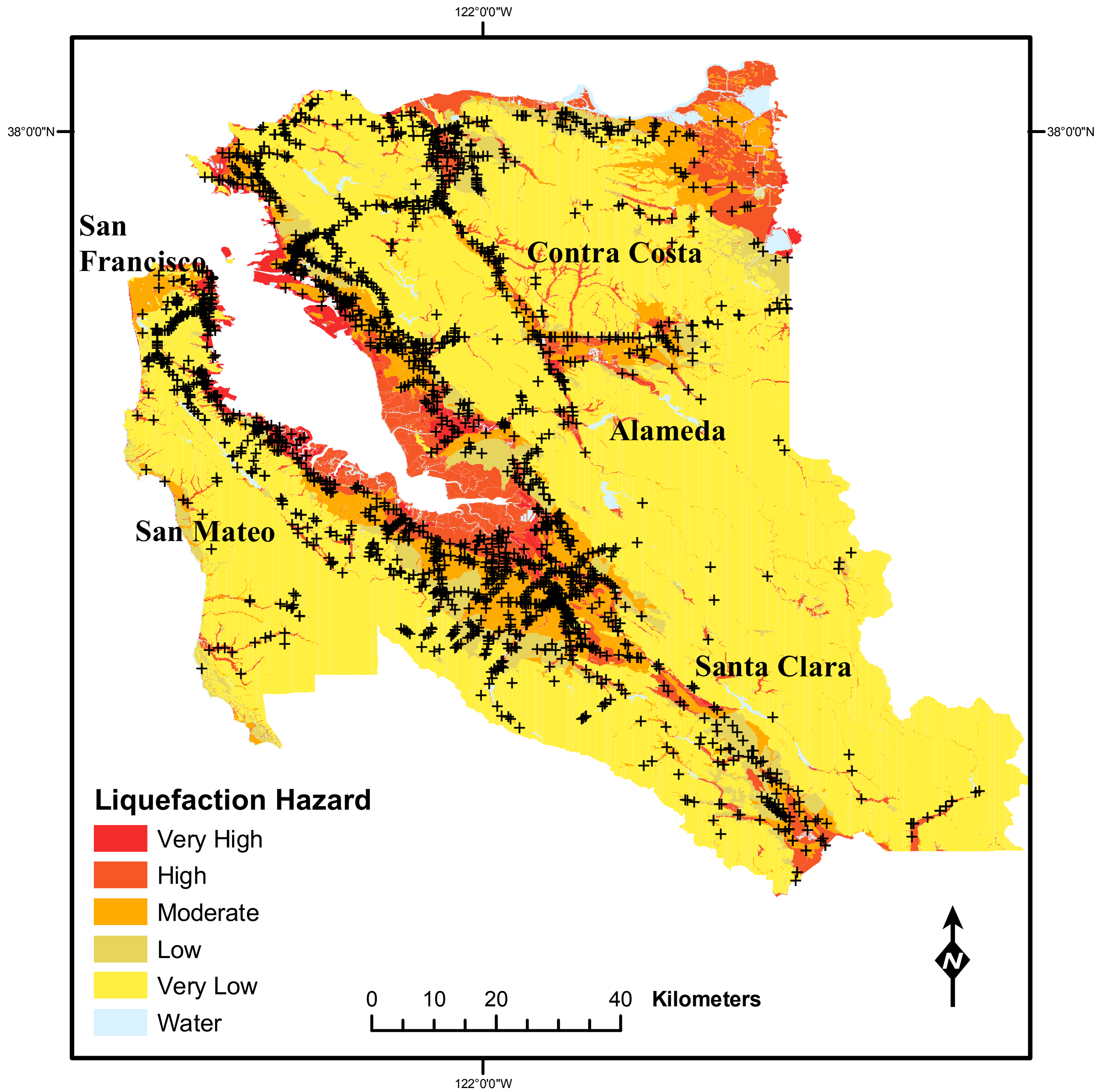

Fig. 3.4 Liquefaction potential for the five counties and bridge locations

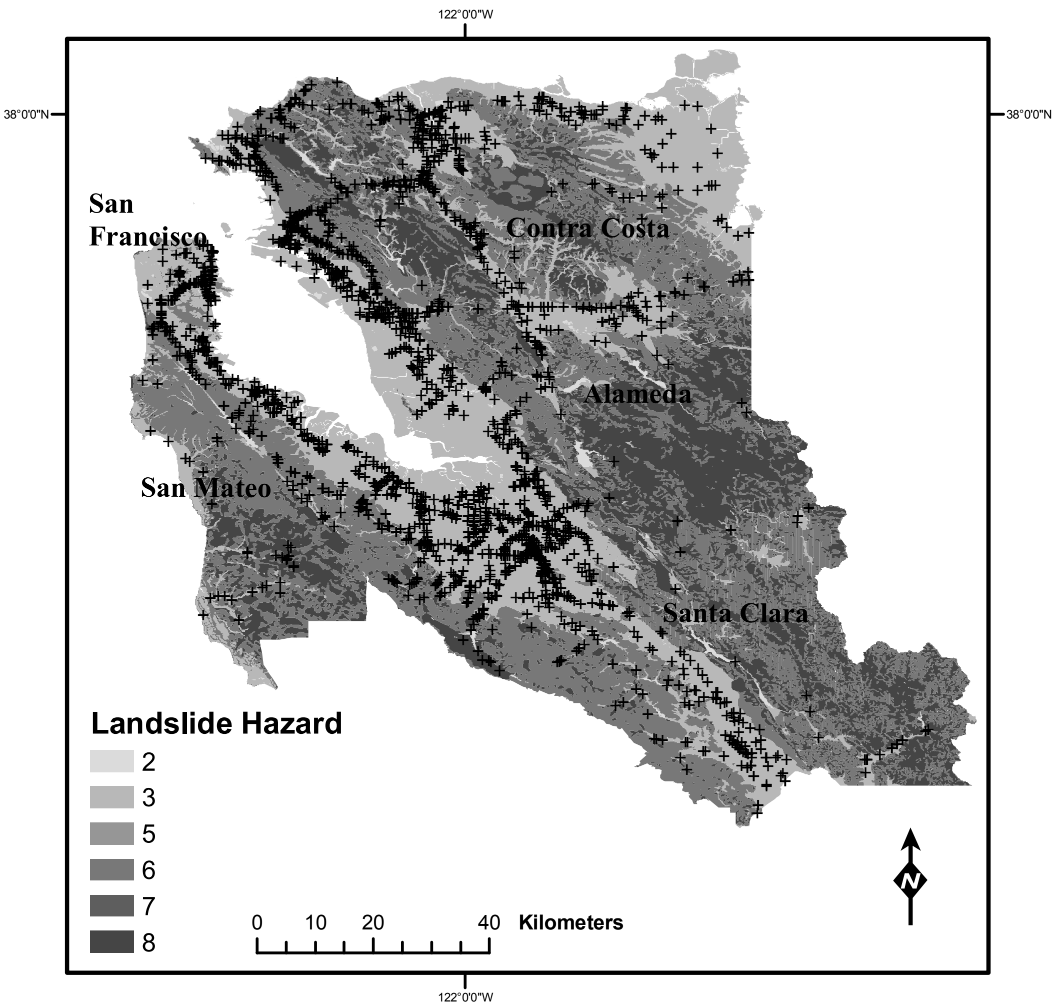

Fig. 3.5 Landslide potential for the five counties and bridge locations

Table 3.5 Number of bridge sites categorized by soil, liquefaction susceptibility, landslide susceptibility, and county

	Categories	Contra Costa	Alameda	San Francisco	San Mateo	Santa Clara	All Counties
Soil Categories	B	1	7	0	0	3	11
	BC	16	83	42	49	33	223
	C	101	68	19	21	76	285
	CD	2	211	16	136	225	590
	D	401	306	27	29	569	1332
	DE	9	48	16	97	11	181
	E	8	1	0	1	5	15
	WATER	0	0	0	3	0	3
	Total	538	724	120	336	922	2640
Liquefaction Susceptibility Categories	very high (VH)	20	79	14	86	63	262
	high (H)	109	80	4	32	197	422
	moderate (M)	144	255	11	41	444	895
	low (L)	109	115	11	35	104	374
	very low (VL)	121	103	77	117	98	516
	water (WATER)	35	92	3	25	16	171
	Total	538	724	120	336	922	2640
Landslide Susceptibility Categories*	VIII	11	7	0	21	29	68
	VI	85	161	28	87	66	427
	III	438	551	91	220	825	2125
	II	4	5	1	8	2	20
	Total	538	724	120	336	922	2640

*: The categories without any bridges are not listed. None is lowest and X is the highest.

3.2 SEISMIC HAZARD OF SAN FRANCISCO BAY AREA

For each scenario event considered, local earthquake ground motion demand is calculated according to the procedures described in Section 2.1.1.1 of the report. Figures 3.7–3.8 show the peak ground acceleration, *PGA*, contours for the scenario events on the Hayward and San Andreas faults. The ground motions are in units of g and have been amplified to reflect the local soil conditions provided by the soil classification map described in Section 2.1.1.1.

Table 3.6 Number of bridge sites by *PGA* category and scenario event from Boore et al. (1997) attenuation function and NEHRP (2000) site classification

***PGA* (in g)**	***HW7.0***	***HW7.5***	***SA7.5***	***SA8.0***
0.0≤ • <0.2	1372	615	934	510
0.2≤ • <0.4	980	1097	1058	1002
0.4≤ • <0.6	288	794	424	578
0.6≤ • <0.8	0	134	215	335
0.8≤ • <1.0	0	0	9	210
1.0≤ • <1.2	0	0	0	5
Total	2640	2640	2640	2640

Table 3.6 summarizes the estimated *PGA* values at the various bridge sites. The second and third columns are for the scenarios on the Hayward fault (*HW7.0* and *HW7.5*), and the last two columns are for the scenarios on the San Andreas fault (*SA7.5* and *SA8.0*). From this table it can be observed that a significant number of bridges will have PGA values larger than 0.4 g. Since most current and recent design criteria are for PGA values of 0.4g, it appears that a large number of bridges will exceed their design acceleration. This does not imply that these bridges will fail, but they are likely to have damage. This observation will be discussed further in Section 3.3.

Table 3.7 provides *PGA* distributions of the bridge sites by county for two of the scenario events considered: *HW7.5* and *SA7.5*. Although the magnitudes of the two events listed in Table 3.6 are the same, as expected the Hayward fault magnitude *7.5* affects Contra Costa and Alameda counties the most. Similarly, the San Andreas fault *7.5* event has the greatest effect on San Francisco and San Mateo counties due to their proximity to the scenario rupture location. Santa Clara County, however, is significantly affected by both scenarios, as it is flanked by both faults. Similar relationships are also observed in the other two scenarios (see Appendix C).

Table 3.7 Number of bridge sites by *PGA* category, scenario event, and county

	PGA (in g)	Contra Costa	Alameda	San Francisco	San Mateo	Santa Clara	All Counties
HW7.5	**0.0≤ • <0.2**	106	21	42	217	229	615
	0.2≤ • <0.4	273	64	78	119	563	1097
	0.4≤ • <0.6	88	576	0	0	130	794
	0.6≤ • <0.8	71	63	0	0	0	134
	0.8≤ • <1.0	0	0	0	0	0	0
	1.0≤ • <1.2	0	0	0	0	0	0
	Total	538	724	120	336	922	2640
SA7.5	**0.0≤ • <0.2**	472	351	0	1	110	934
	0.2≤ • <0.4	65	373	63	33	524	1058
	0.4≤ • <0.6	1	0	55	103	265	424
	0.6≤ • <0.8	0	0	2	190	23	215
	0.8≤ • <1.0	0	0	0	9	0	9
	1.0≤ • <1.2	0	0	0	0	0	0
	Total	538	724	120	336	922	2640

Table 3.8 summarizes the distributions of calculated *PGD* values, as a measure of ground failure demand for the four scenarios. It should be noted that the *PGD* values listed are due to the combined effects of liquefaction and landslide (see Section 2.1.1.1). For example, 11 bridge sites out of 2640 bridge sites have an expected deformation between 150 and 250 inches for the *SA8.0* scenario. As expected, the *PGD* values increase as the magnitudes of the scenarios increase. The difference is obvious when the scenarios *SA7.5* and *SA8.0* are compared; for SA7.5 none of the bridge sites is estimated to sustain a deformation higher than 125 inches, whereas for *SA8.0* a total of 446 (435+11) sites are estimated to be above this level.

Table 3.8 Number of bridge sites by *PGD* category and scenario event

PGD **(in inches)**	***HW7.0***	***HW7.5***	***SA7.5***	***SA8.0***
0≤ • <25	2462	1830	2049	1395
25≤ • <50	73	284	295	397
50≤ • <75	38	107	55	156
75≤ • <100	67	112	45	96
100≤ • <125	0	307	196	150
125≤ • <150	0	0	0	435
150≤ • <250	0	0	0	11
Total	2640	2640	2640	2640

The distribution of *PGD* for bridge sites in the various counties is shown in Table 3.9 for the *HW7.5* and *SA7.5* scenarios. The results are similar to those observed for *PGA*. *PGD* values for all counties and all scenarios are listed in Appendix D.

In order to examine the individual effects of liquefaction and landslide on the ground deformation, different *PGD* values are calculated for the following categories: *liquefaction only*, *landslide only*, and *combined*.

Table 3.9 Number of bridge sites by *PGD* category, two scenario events, and county

	***PGD* (in inches)**	**Contra Costa**	**Alameda**	**San Francisco**	**San Mateo**	**Santa Clara**	**All Counties**
HW7.5	**0≤ • <25**	375	317	110	305	723	1830
	25≤ • <50	68	79	3	31	103	284
	50≤ • <75	6	69	3	0	29	107
	75≤ • <100	7	85	4	0	16	112
	100≤ • <125	82	174	0	0	51	307
	125≤ • <150	0	0	0	0	0	0
	150≤ • <250	0	0	0	0	0	0
	Total	538	724	120	336	922	2640
SA7.5	**0≤ • <25**	531	677	95	126	620	2049
	25≤ • <50	7	47	9	67	165	295
	50≤ • <75	0	0	2	7	46	55
	75≤ • <100	0	0	0	19	26	45
	100≤ • <125	0	0	14	117	65	196
	125≤ • <150	0	0	0	0	0	0
	150≤ • <250	0	0	0	0	0	0
	Total	538	724	120	336	922	2640

Table 3.10 and Figure 3.6 give the distributions of bridges in each *PGD* range of values in these three categories for the *SA8.0* scenario. The vertical axis in Figure 3.6 represents the number of bridges that are exposed to the respective ground displacements, while the horizontal axis represents the *PGD* intervals defined in Table 3.10 by each hazard category. Since Table 3.8 gives the combined effects, the last column of Table 3.10 is equivalent to the last column of Table 3.8.

From Figure 3.6 it can be observed that the number of bridges subjected to large PGD from liquefaction is significantly higher than those from landslides at the same high ranges of PGD. As a result, the combined hazard category is dominated by the liquefaction hazard with only a small contribution from landslides. The distribution of bridges in landslide areas appears to be bi-modal with a peak at the low PGD level and a second peak at the high *PGD* level. This observation is consistent with the large displacements that are computed when using the HAZUS (1999) liquefaction analysis method. It would be interesting to review existing data to verify ground deformation distributions, but such data, even if available, would be very difficult to obtain and the analyses are beyond the scope of this study.

Table 3.10 Number of bridge sites by *PGD* category and ground failure category for the *SA8.0* scenario event

***PGD* (in inches)**	***SA8.0* Landslide**	***SA8.0* Liquefaction**	***SA8.0* Combined**
0≤ • <25	2346	1423	1395
25≤ • <50	152	428	397
50≤ • <75	72	134	156
75≤ • <100	19	109	96
100≤ • <125	35	116	150
125≤ • <150	5	430	435
150≤ • <250	11	0	11
Total	2640	2640	2640

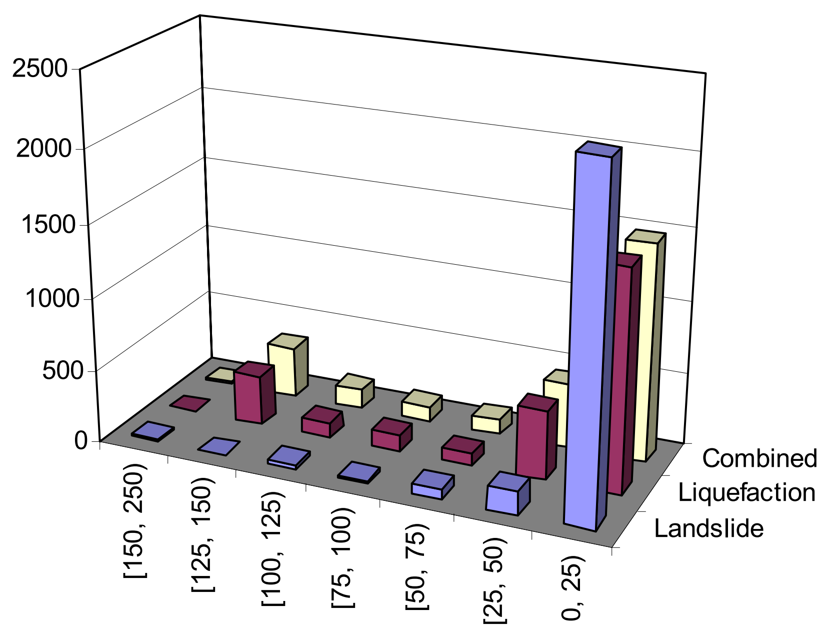

Fig. 3.6 Number of bridges by PGD and ground failure for the scenario SA8.0

3.3 VULNERABILITY ASSESSMENT OF BRIDGES

Using the local earthquake ground motion and deformation demand discussed in the previous section, the expected damage states of bridges are computed according to the procedures described in Section 2.1.3 of the report. This section summarizes the results of these damage estimates.

Table 3.11 presents the distributions of estimated damage states by scenario event for the combined effects of ground-shaking and ground-deformation hazards (Case 4 in Table 2.6). In all of the scenarios there is a substantial amount of damage on the bridge structures. As expected, the distributions of estimated damage states tend to increase (shifts downward) when the moment magnitude increases for events on the same fault (comparison of columns two and three, and columns four and five).

A comparison of the damage state distributions for the scenarios *HW7.5* and *SA7.5* in Table 3.11 demonstrates that, although both events have the same magnitude, the damage due to *HW7.5* is significantly larger than the damage due to *SA7.5*. Appendix E shows that this difference is mainly attributable to the damage in Contra Costa and Alameda counties, where the *HW7.5* scenario is estimated to cause a significant amount of damage. The damage states are determined according to Equation (2.6) and the soil classification shown in Figure 3.3.

Table 3.11 Number of bridges by expected damage state and damage case 6 (see Table 2.6), applying Boore et al. (1997) attenuation function and NEHRP (2000) site classification. (All bridges are in pre-retrofitted state.)

Estimated Damage States	*HW7.0*	*HW7.5*	*SA7.5*	*SA8.0*
none (1)	1734	912	1205	741
slight (2)	165	263	188	134
moderate (3)	75	158	119	69
extensive (4)	333	352	429	350
complete (5)	333	955	699	1346
Total	2,640	2,640	2,640	2,640

Similar trends were found with the Boore et al. (1993) attenuation function default values defined in Equation (2.7), and site conditions given in Table 2.2 of HAZUS (1999). The 1997 NEHRP provisions and the 1997 CDMG (CGS) soil map classifications were used in these computations. This attenuation function and soil classification were used in order to draw comparisons with the results based on the methodology outlined in Section 2.1.1. For the scenario earthquakes from the two different faults (*HW7.0* and *HW7.5*) and (*SA7.5* and *SA8.0*), the total 2640 sites were analyzed and bridges at these sites were categorized by expected damage states ranging from 1 to 5, as listed in Table 2.5. The results of the analysis with the 1994 Boore et al. (1993) attenuation function are given in Table 3.12.

Table 3.12 Number of bridge sites by damage state category and scenario event from Boore et al. (1993) attenuation function. (All bridges are in pre-retrofitted state.)

Estimated Damage State	***HW7.0***	***HW7.5***	***SA7.5***	***SA8.0***
none (1)	1732	1350	1589	1334
slight (2)	575	778	657	634
moderate (3)	221	280	249	413
extensive (4)	91	182	110	201
complete (5)	21	50	35	59
Total	2640	2640	2640	2640

It can be observed that the 1997 attenuation function is significantly more conservative resulting in higher number of damaged bridges. The 1997 attenuation function was developed with more data obtained from near-fault locations which resulted in higher ground motions in the vicinity of the fault rupture. Comparison of Tables 3.11 and 3.12 shows that significantly more bridges are in damage states 4 and 5, resulting in major damage or collapse. While it can be argued that these values may overestimate the potential damage to bridges, it is important to recognize that with recent earthquakes we have observed larger ground motions near faults primarily because more instruments have been placed at such locations providing information previously not available. It should also be observed that if a different attenuation function were used, the damage estimates would again change, pointing to the uncertainty in these analyses.

In order to identify the primary cause for damage to bridges under each scenario for data presented in Table 3.11, the effect of each hazard is examined next. Table 3.13 below summarizes the distribution of estimated damage states for the scenario *SA8.0*, and for the six hazard cases defined in Table 2.6.

Table 3.13 Number of pre-retrofitted bridges by expected damage state and by hazard case for scenario *SA8.0*

Estimated Damage States	Cases					
	Shaking Only (1)	Shaking + Liquefaction (4)	Shaking + Landslide (5)	Shaking + Liquefaction + Landslide (6)	Liquefaction Only (2)	Landslide Only (3)
None(1)	1190	742	1183	741	885	2062
Slight(2)	547	134	521	134	54	36
Moderate(3)	362	73	262	69	54	32
Extensive(4)	323	361	231	350	347	157
Complete(5)	218	1330	443	1346	1300	353
Total	2,640	2,640	2,640	2,640	2,640	2,640

Table 3.13 highlights the fact that liquefaction is the cause for the largest number of bridges in damage state 5. Review of the ground deformation functions and the fragility functions for liquefaction analysis shows that with the large ground displacements estimated using these functions, the damage to bridges is indeed expectedly severe. This raises several issues. The first concerns the accuracy of ground deformation formulations in HAZUS (1999). The second issue relates to the robustness of the fragility functions for liquefaction analysis. It is already widely recognized that more robust methods for ground deformation forecasting and damage assessment are lacking. Improved methods would provide increased reliability in the results.

A review of the geology in the San Francisco Bay Area also shows that most of the liquefiable areas are concentrated around the bay with additional locations of high liquefaction near streams and rivers. The generic liquefaction potential map used in the current analysis, however, is too coarse to capture any remediation that may have been done to decrease the effects of liquefaction. With more recently built bridges, liquefiable sites most likely have been stabilized, decreasing the potential occurrence of liquefaction. This information, however, is not available to the authors and is thus not reflected in the current study. However, will be the subject of subsequent investigations. It is our belief, therefore, that the results from the liquefaction analysis most likely overestimate greatly the damage to bridges.

Figures 3.7 and 3.8 show the geographical distributions of the bridges by estimated damage states when only ground shaking is considered. As these figures suggest, scenarios on the Hayward fault predominantly affect Contra Costa, Alameda, and Santa Clara counties in the

East Bay, whereas scenarios on the San Andreas fault primarily affect San Francisco, San Mateo, and Santa Clara counties.

Using the notation from Section 2.1.1, the *standard normal statistic* for damage state j from hazard k can be defined for each bridge in the study as follows:

$$Z_j^k = \frac{\ln x^k - \ln \alpha_j^k}{\beta^k} \tag{3.1}$$

where

x^k = local earthquake demand at a site (i.e., $S_a(1.0)$) for damage due to ground shaking, and *PGD* for damage due to ground failure);

α_j^k = modified median value; and

β^k = 0.4 or 0.2, when the hazard considered is ground shaking or failure, respectively.

The standard normal statistic Z_j^k allows a direct comparison of damage state distributions (even between two different hazard types).

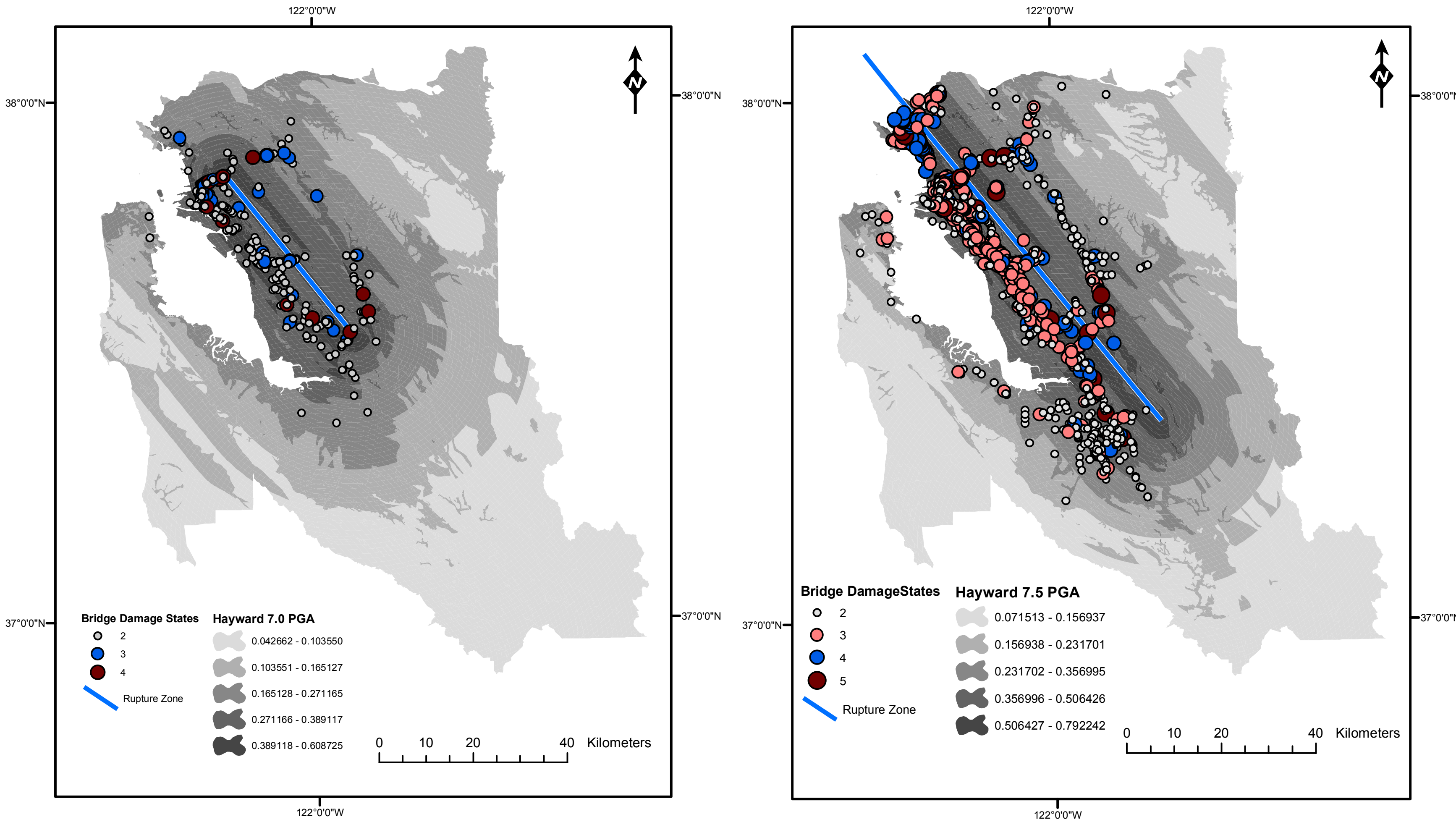

Fig. 3.7 Ground motion contours and distribution of pre-retrofitted bridges by estimated damage state category for *HW7.0* and *HW7.5* scenarios

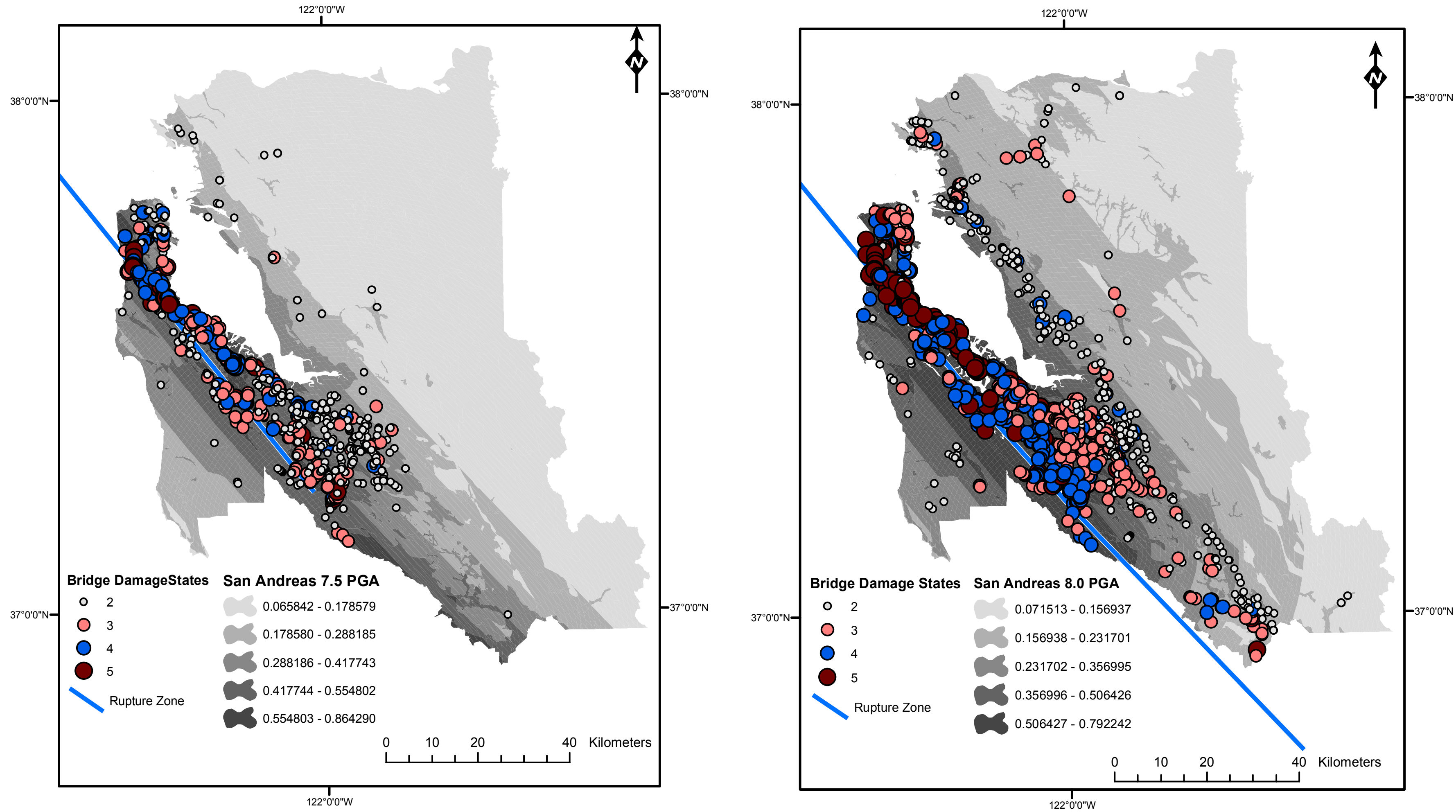

Fig. 3.8 Ground motion contours and distribution of pre-retrofitted bridges by estimated damage state category for *SA7.5* and *HW8.0* scenarios

Table 3.14 and Figure 3.9 show the distributions of standard normal statistic for the scenario *SA8.0* and for damage state 5 (i.e., Z_5^k). In order to examine the individual effects of different hazard components, only hazard cases 1 (ground shaking only), 5 (liquefaction only), and 6 (landslide only) of Table 2.6 are listed.

Table 3.14 Number of bridges by standard normal statistic and damage estimates for damage state 5 and scenario *SA8.0*

Standard Normal Statistic	Hazard Cases		
	Ground Shaking Only (1)	Liquefaction Only (5)	Landslide Only (6)
[-40, -10)	0	94	533
[-10, -8)	0	56	54
[-8, -6)	12	90	75
[-6, -4)	411	125	70
[-4, -2)	1009	179	61
[-2, 0)	881	221	100
[0, 2)	303	194	85
[2, 4)	24	254	76
[4, 6)	0	176	86
[6, 8)	0	250	47
[8, 10)	0	113	23
[10, 40)	0	326	40
N/A*	0	562	1390
Total	2640	2640	2640

*: N/A stands for not applicable, and represents the cases where the corresponding *PGD* is 0

As Figure 3.9 suggests, the only normal-like distribution corresponds to that for ground-shaking demand (second column of Table 3.14), which is nearly symmetric around the mean 0. In contrast, the same statistic for the two cases of ground failure deviates significantly from a normal-like shape. For these two cases, a wide spread of the standard normal statistic implies that a significant proportion of the bridges would almost always fall into damage state 5 (with close to 100% probability). This is best demonstrated by example. Considering the liquefaction case only (column three of Table 3.14), 741 out of a total of 2640 bridges are in damage state 5 (i.e., *128+235+108+270=741*), since they all have a statistic greater than or equal to 4. Similarly, for the same category the table indicates that 451 of the total bridges are not in damage state five almost surely (i.e., *119+72+90+150=451*). For the other scenarios, similar relationships are observed.

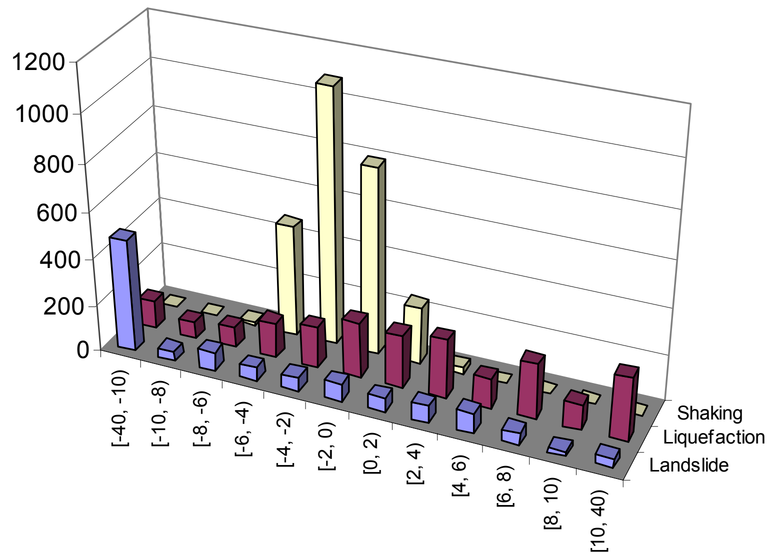

Fig. 3.9 Number of bridges by standard normal statistic (Z) level and damage calculation case for scenario *SA8.0* and damage state 5

A designation of damage state 5 with a probability near 1.0 implies that the probability of being in other damage states is almost zero. Thus, the expected damage state would also be 5. This explains the significantly high damage results summarized in Table 3.11 when liquefaction is considered as a hazard. As discussed earlier, the high estimates of liquefaction damage may be because the fragility functions used in HAZUS (1999) are not representative of the performance of existing bridges or because the data used in the current study consider generic soil conditions and do not account for possible remediation for liquefaction at specific bridge sites. It is beyond the scope of this study, however, to investigate in greater detail the specific reasons for this observation. Further studies should be conducted to determine if indeed the ground deformation values at the median damage state are realistic. Better methods for forecasting ground deformation from liquefaction and landslides are also greatly needed as is bridge-specific soil information.

3.3.1 Results of Retrofit Analysis

As discussed in Section 2.1.4, a retrofit analysis is performed for different retrofit strategies, where bridge capacity is increased by a series of γ values (see Eq. (2.17)). The summary of the results are provided in Table 3.15 for the *SA8.0* scenario for hazard cases 1 (*ground shaking only*) and 4 (*all three hazards together*) of Table 2.6. For the ground shaking only category there is a significant decrease in the damage state distributions. To illustrate, the number of bridges in damage state 5 falls from 218 (no-retrofit case) to 125 (γ = 20%) resulting in almost a 50% reduction. However, when all three hazards are considered for damage calculations, the decrease is not significant even for the case γ = 20%. The number of bridges in damage state 5 drops from 1346 (no-retrofit case) to 1255 (γ = 20%), which implies around 8% improvement. The relatively small decrease in the number of damaged bridges is again due to the damage functions used for the liquefaction analysis. This result, of course is not surprising because changes in the capacity of bridges increase their resistance to ground shaking but not to ground deformation.

Table 3.15 The distribution of expected damage states for the scenario *SA8.0* for hazard cases 1 and 4

	Estimated Damage States	No-Retrofit	γ = 05%	γ = 10%	γ = 20%
Shaking Only (1)	**None (1)**	1,190	1,251	1,293	1,384
	Slight (2)	547	564	559	573
	Moderate (3)	362	339	334	323
	Extensive (4)	323	285	286	235
	Complete (5)	218	201	168	125
	Total	2,640	2,640	2,640	2,640
Shaking + Liquefaction + Landslide (4)	**None (1)**	741	766	783	834
	Slight (2)	134	128	126	114
	Moderate (3)	69	70	68	49
	Extensive (4)	350	349	376	388
	Complete (5)	1,346	1,327	1,287	1,255
	Total	2,640	2,640	2,640	2,640

In order to study the effect of improved local soil conditions it would be necessary to develop a model for reduced ground deformation. Information on the specific soil conditions at the bridge sites, type of foundation, overall structural system, and soil-structure interaction considerations would further improve damage estimates from ground deformation. Such an analysis, however, is beyond the scope of the current study and will be considered in subsequent research.

3.4 HIGHWAY NETWORK CHARACTERISTICS

The Metropolitan Transportation Commission (MTC) Bay Area highway network model consists of 1,120 zones and 26,904 links. These links are defined by 10,647 nodes using geographic coordinates. Each node corresponds to a traffic analysis zone. The links in the Bay Area highway network are coded by the Metropolitan Transportation Commission as follows:

1= Freeway-to-freeway connector,
2= Freeway,
3= Expressway,
4= Collector,
5= Freeway ramp,
6= Dummy link,
7= Major arterial,
8= Metered ramp, and
9= Special (e.g., Golden Gate, TOS, Arterial Signal Coordination).

The free flow speed and traffic capacity for each type of facility are given in Table 3.16. The MTC also provides a 1998 matrix of O-D requirements for this network model. A map of Bay Area traffic analysis zones is shown in Figure 3.10. Part of the street network is shown in Figure 3.11.

Table 3.16 Free-flow speed[a] and capacity[b] by facility and area types[c]

Area Type	Facility											
	Freeway-to-Freeway	Freeway	Expressway	Collector	Freeway Ramp	Centroid Connector	Major Arterial	Metered Ramp	Special		Special	
	(1)	(2)	(3)	(4)	(5)	(6)	(7)	(8)	(9)		(10)	
Core	1,700[a] 40[b]	1,850 55	1,300 40	550 10	1,300 30	2,000 100	800 20	700 25	22,000 65	(A)	1,600 55	(G)
CBD	1,700 40	1,850 55	1,300 40	600 15	1,300 30	2,000 100	850 25	700 25	1,840 50	(B)	850 35	(H)
UBD	1,750 45	1,900 60	1,450 45	650 20	1,400 35	2,000 100	900 30	800 30	1530 55	(C)	860 25	(I)
Urban	1,750 45	1,900 60	1,450 45	650 25	1,400 35	2,000 100	900 30	800 30	11,780 50	(D)	960 35	(J)
Suburb	1,800 50	1,950 65	1,500 50	800 30	1,400 40	2,000 100	950 35	900 35	990 40	(E)		
Rural	1,800 50	1,950 65	1,500 55	850 35	1,400 40	2,000 100	950 40	900 35	1,530 55	(F)		

a: Upper Entry: Capacity at Level of Service "E" in vehicles per hour per lane, i.e., idealized capacity
b: Lower Entry: Free-Flow Speed (miles per hour)
c: (A) Type = Freeway; (B) Type = Freeway-to-Freeway; (C) Type = Expressway; (D) Golden Gate; (E) Major Arterial, signal coordinated; (F) Expressway, signal coordinated; (G) Expressway, signal coordinated; (H) Collector, signal coordinated; (I) Major Arterial, "automatic" signal coordinated. (H) Major Arterial, "automatic" signal coordinated.

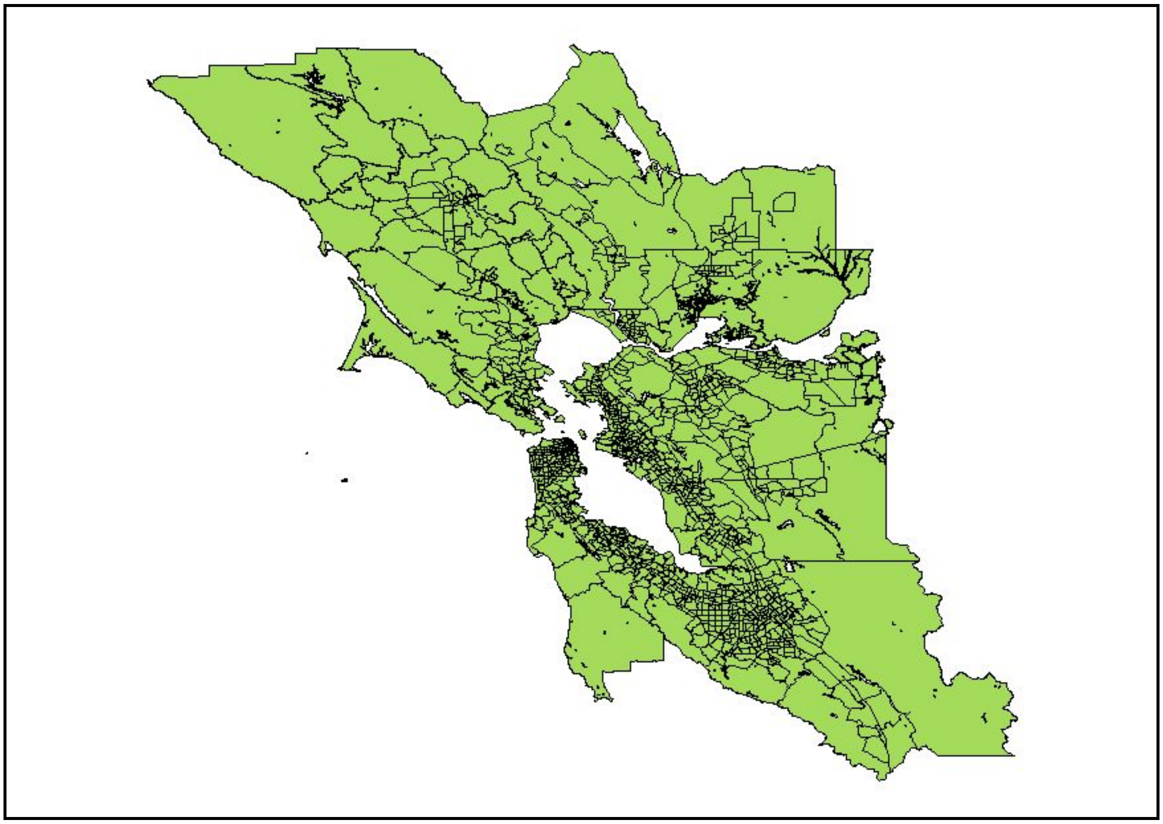

Fig. 3.10 San Francisco Bay Area Traffic Analysis Zones (TAZ)

The Caltrans District 4 bridge database contains data for 4057 state and local bridges. It represents all of the bridges that are a part of the National Bridges Inventory (NBI) in District 4. The bridge map is shown in Figure 3.12. These bridges are combined with the MTC modeling network as part of this project. This permits earthquake damage to the bridges to be translated to loss of network capacities for network performance analysis.

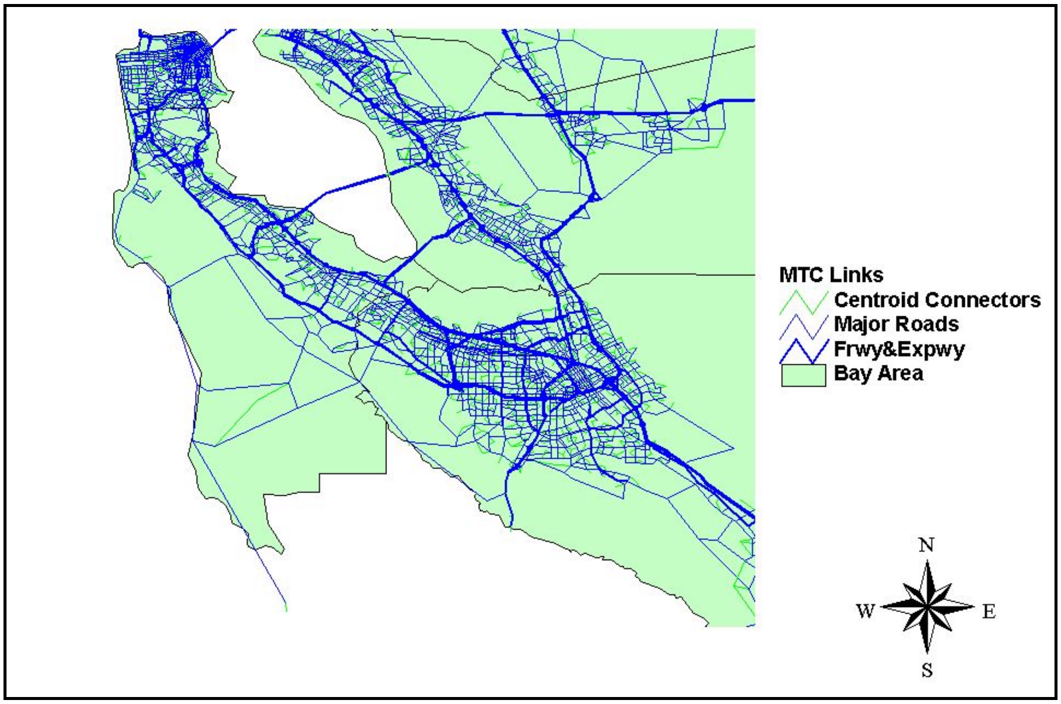

Fig. 3.11 MTC San Francisco Bay Area highway network

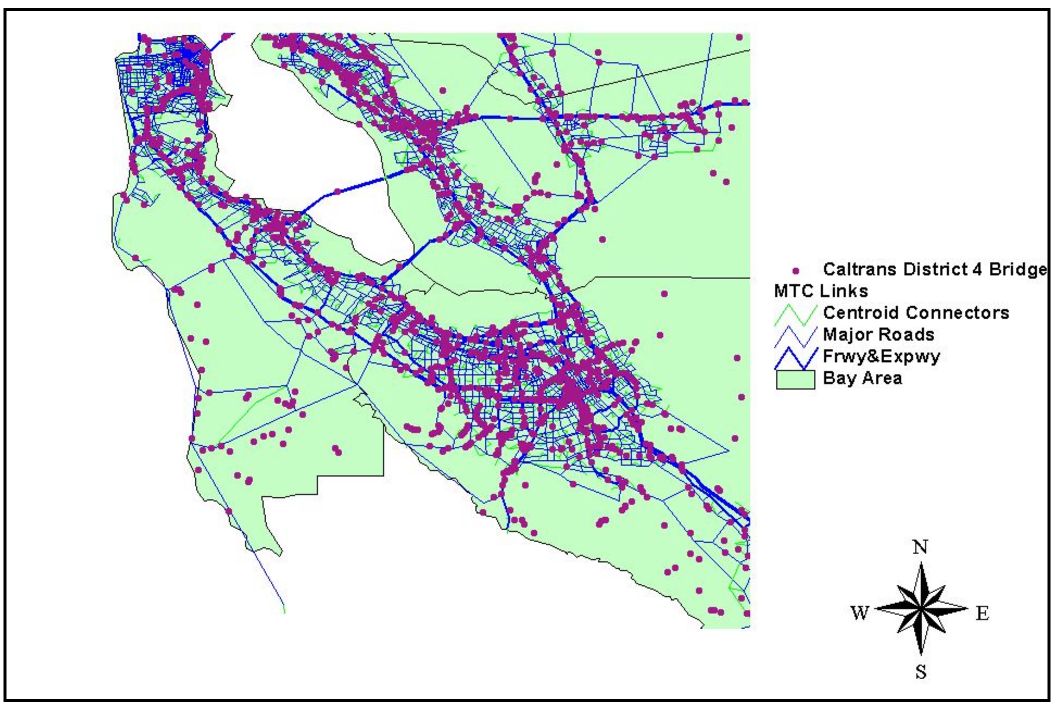

Fig. 3.12 Caltrans District 4 bridges

3.5 PERFORMANCE ASSESSMENT OF NETWORK SYSTEM

3.5.1 Summary of the Application

The change in travel time delays between pre-earthquake and post-earthquake networks was evaluated for defined scenario events. The capacity of each link in the post-earthquake highway network was modified according to the estimated damage to bridges associated with the link. Ideally, post-earthquake transportation flows would be modeled based on estimated damage to both the transportation network and the urban activity system (Cho et al., 2000). This is computationally feasible, but challenging. Furthermore, there is no model available describing the spatial economic activity system of the San Francisco Bay Area. Therefore, travel demands in pre- and post-earthquake scenarios were assumed to be the same in the fixed-demand assignment model, and to be a function of the network level of service in the variable-demand assignment model.

The approach permits the benefits of Caltrans's retrofit program with respect to the transportation network performance to be assessed once fragility curves become available for retrofitted structures. The estimated time delays predicted by models that incorporate fragility curves for retrofitted structures can be compared with the delays estimated given damage to un-retrofitted structures. A flowchart summarizing the procedures for this proposed application is given in Figure 3.13.

3.5.2 Pre-Processing Data Inputs

3.5.2.1 Auto-Merge of Bridges and Links

The MTC planning network is an abstract representation of the real world street network. Caltrans District 4 bridge data are spatial in nature. These two data sets must be merged so that damaged bridges can be allocated to the corresponding network links. This task was completed using an Arcview extension, "geoprocessing." Given a reasonable definition of proximity, bridge data sets were merged with geographically closest highway links. Bridges were classified into two subgroups: highway bridges that carry highway traffic and local bridges that carry only local traffic. MTC network links were also divided into highway links and local links. An auto-merge operation was performed for each subgroup. That is, highway bridges were merged to highway links and local bridges were merged to local links. This subgroup approach improves the quality of auto-merge. Note that the centroid connectors were not considered in this task, since these connectors are virtual links that do not physically exist. After the auto-merge step, a manual check comparing the narrative description of bridge and link location was completed for several dense areas within the network ensure the quality of the auto-merge results.

3.5.2.2 Obtaining Two-Hour Morning Peak Travel Demand

The 1998 person trip demand and the freight trip demand estimates for the Bay Area highway network are provided by the MTC based on a 1990 MTC household survey. Person trip demand data are given for five principal trip purposes (home-based work, home-based shop/other, home-based social/recreation, home-based school, and non-home-based) and five travel modes,

- driving alone
- ridesharing (2 people)
- ridesharing (3 or more people)
- transit
- bicycling
- walking

All these data were combined with the freight trip demand data and converted to passenger car equivalents, a standardized measure of road space demand.

Typically travel cost is examined on a daily base. Therefore the entire time of day profile should be studied thoroughly. However, it is challenging to model simultaneously travelers' trip requirements, choices of route and time-of-day, and the network level of service that results. In this study, the A.M. peak demand is applied in the fixed-demand model, and is treated as the upper bound of the trip requirements in the variable-demand model.

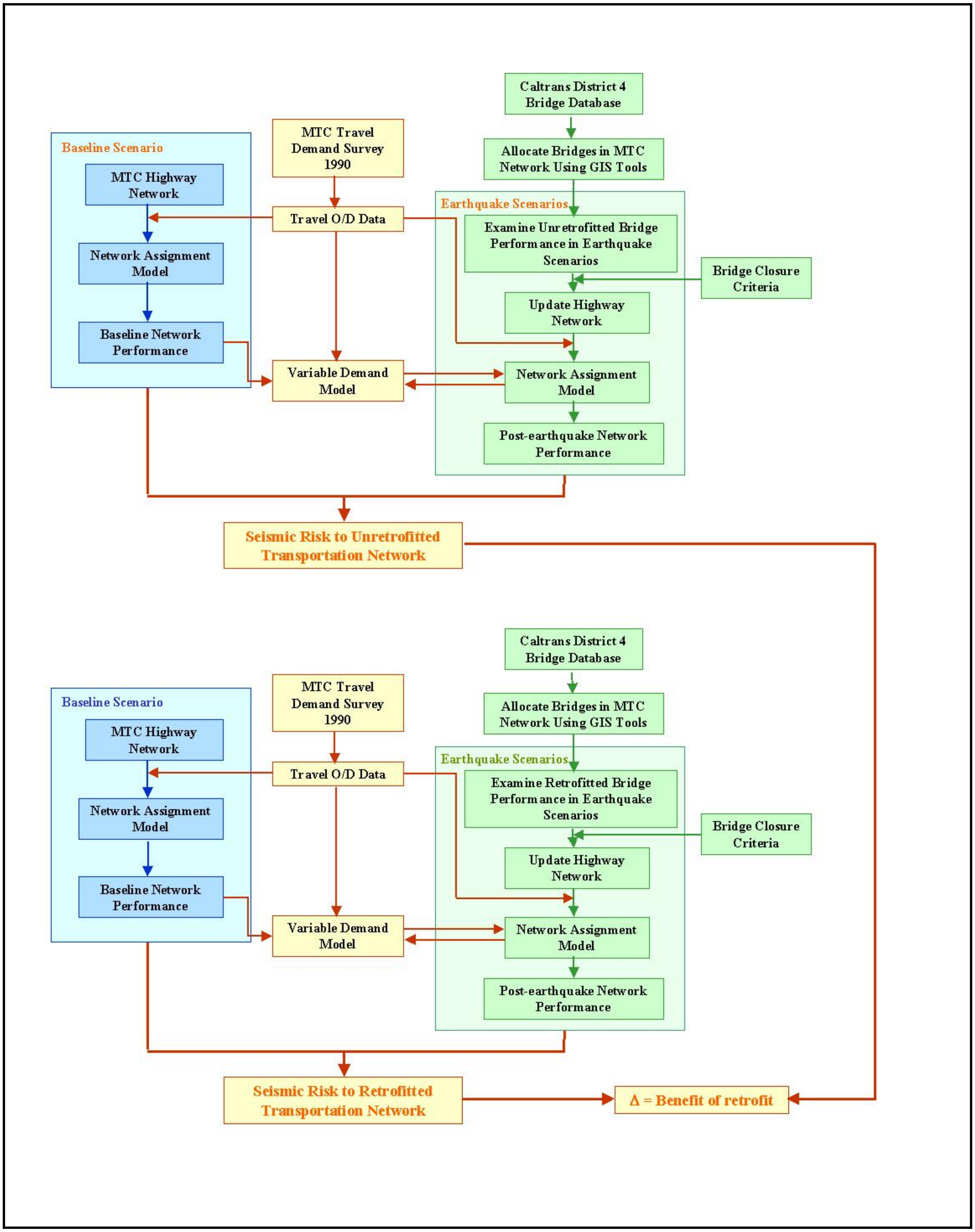

Fig. 3.13 Evaluating the benefits of bridge retrofits based on the impact of an earthquake on the Bay Area transportation network

3.5.3 Damage States and Loss of Functionality

We have searched the literature extensively for empirical or theoretical descriptions of the relationship between physical damage to facilities and the resulting loss of functionality of transportation links (Caltrans, 1999; Robert, 1997; Yee and Leung, 1996). Most studies assume complete closure of facilities when damage is above a certain level. There is very little acknowledgement of the possibility of residual capacity or limited use of damage facilities, and no standard, widely accepted criterion to follow. The decision of whether a facility should be open relies most on the inspector's experience and engineering judgment.

As noted previously in Table 2.5, Caltrans defines five categories of earthquake damage to bridges:

1 = no damage,
2 = minor damage,
3 = moderate damage,
4 = severe damage, and
5 = collapse.

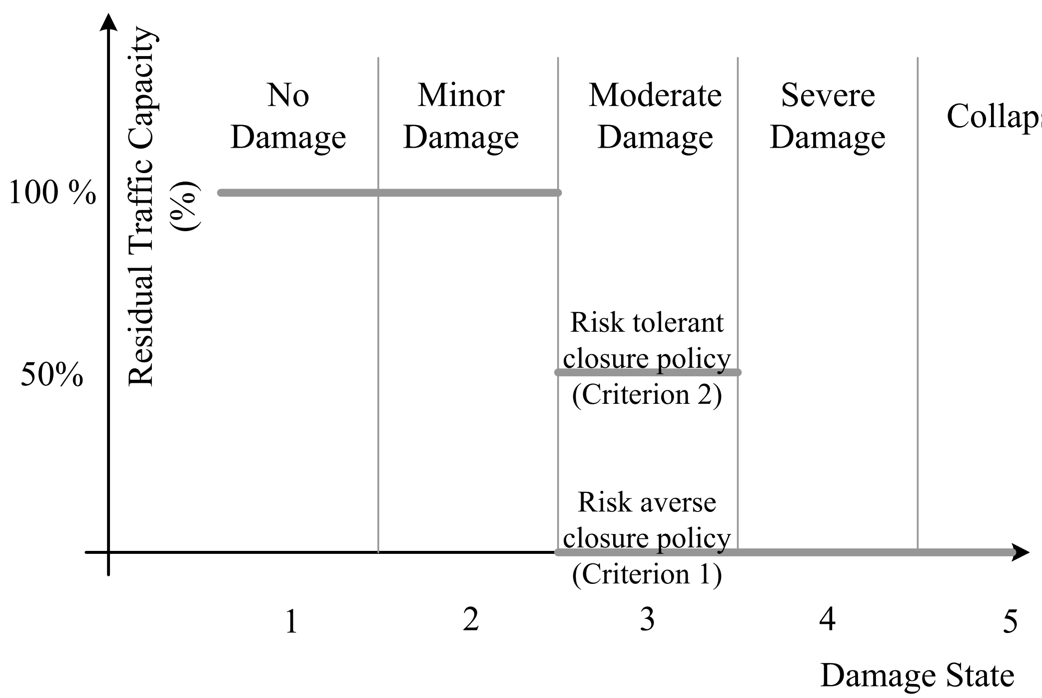

Fig. 3.14 Bridge damage state vs. residual traffic capacity: risk-tolerant and risk-averse bridge closure policies

Practice indicates that moderately damaged bridges are at the boundary of the closure decision. Two bridge closure criteria are applied in this study. The first is a risk-averse policy that calls for closing bridges that are damaged at the moderate level or above. The second is risk-tolerant policy that calls for closing only bridges that are severely damaged, while leaving the moderately damaged bridges open. The traffic capacity on these moderately damaged structures would likely be reduced, and we assume that these moderately damaged bridges can be kept open with half of their pre-event capacity to accommodate traffic. See Figure 3.14. We investigate both bridge closure criteria.

3.5.4 Selected Scenarios

The impact of earthquake damage on network performance was studied for four scenario earthquakes, and one observed, benchmark event. These are magnitude 7.5 and 8.0 earthquakes on the San Andreas fault, magnitude 7.0 and 7.5 earthquakes on the Hayward fault, and the magnitude 6.9, 1989 Loma Prieta earthquake on the San Andreas fault. Three mechanisms that may cause damage to bridges are considered for the network analysis. These were defined in Table 2.6 as:

- ground motion,
- liquefaction, and
- landslide.

Figure 3.15 gives one realization of the estimated share of bridges in each damage category for the four scenario earthquakes. Table 3.16 provides the corresponding estimates for the benchmark Loma Prieta event. Loss of functionality due to damage to components is determined based on these damage data. Combining the five earthquake scenarios with the two bridge closure criteria, there are ten preliminary cases to be studied. These cases are listed in Table 3.17. The resulting shares of closed links in cases associated with bridge closure criterion 1 are summarized in Table 3.18.

Table 3.17 Study case reference list

Bridge Closure Criteria	Hayward 7.0	Hayward 7.5	San Andreas 7.5	San Andreas 8.0	Loma Prieta 6.9
1: Risk Averse	HW701	HW751	SA751	SA801	LP691
2: Risk Tolerant	HW702	HW752	SA752	SA802	LP692

3.5.5 Fixed-Demand Results

This section presents network analysis results generated by applying the fixed-demand trip assignment model for earthquake scenarios HW701 and HW751. There is little to be gained from modeling all four scenarios, because these predictions are problematic under an assumption of fixed demand. A large share of the results corresponds to unfeasible, over-saturated link flows. Figure 3.19 presents details for the earthquake scenario HW751. The black coordinates identify bridges that are severely damaged or collapsed, leading to complete closure of the associated links. The gray coordinates identify moderately damaged bridges, which reduce the traffic capacities of associated links by half. Imposing the pre-event level of transportation demand given this substantial loss of functionality leads to a very large increase in predicted congestion levels throughout the network.

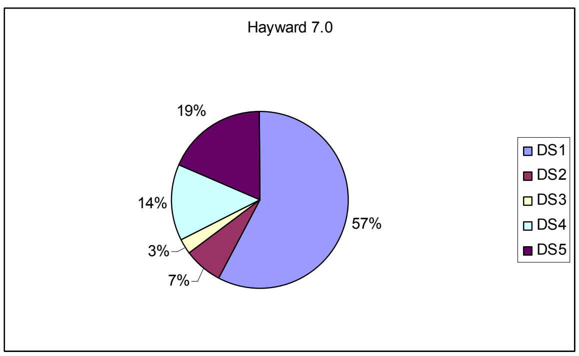

Magnitude 7.0 Scenario Event on the Hayward fault

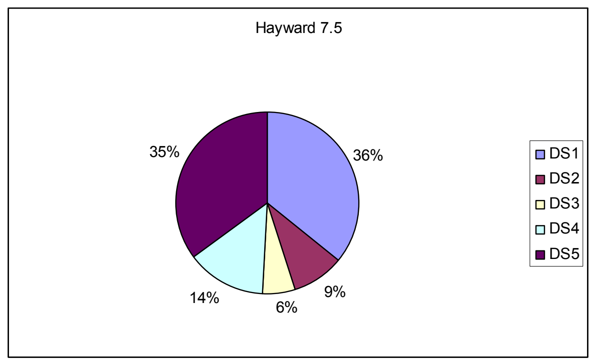

Magnitude 7.5 Scenario Event on the Hayward fault

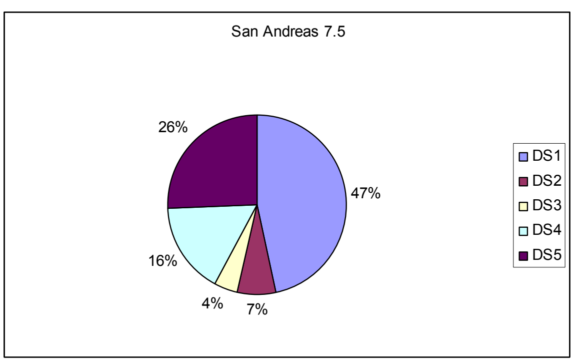

Magnitude 7.5 Scenario Event on the San Andreas fault

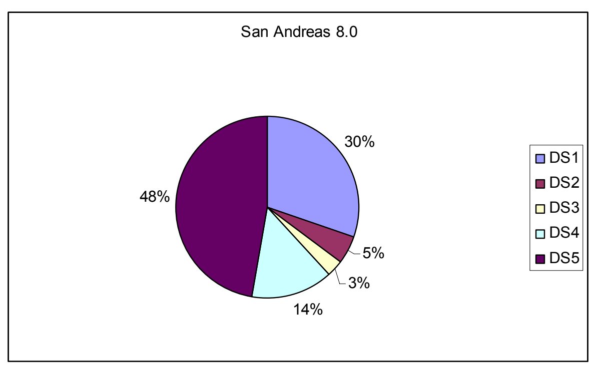

Magnitude 8.0 Scenario Event on the San Andreas fault

Fig. 3.15 Distribution of damage to Caltrans District 4 bridges resulting from scenario events

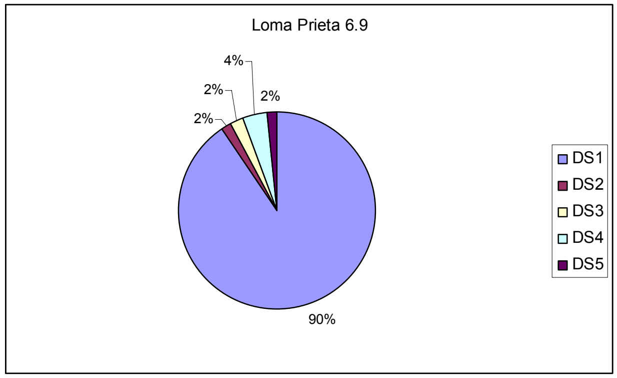

Fig. 3.16 Distribution of damage to Caltrans District 4 bridges resulting from the magnitude 6.9 Loma Prieta event on the San Andreas fault

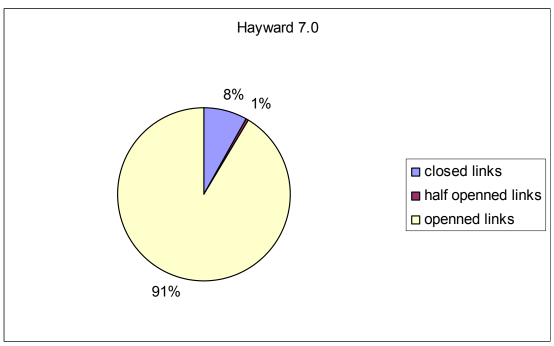

Magnitude 7.0 Scenario Event on the Hayward fault

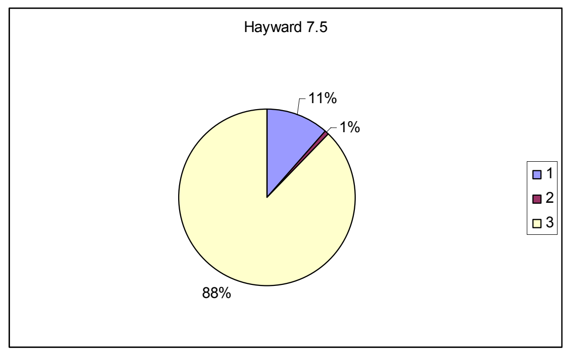

Magnitude 7.5 Scenario Event on the Hayward fault

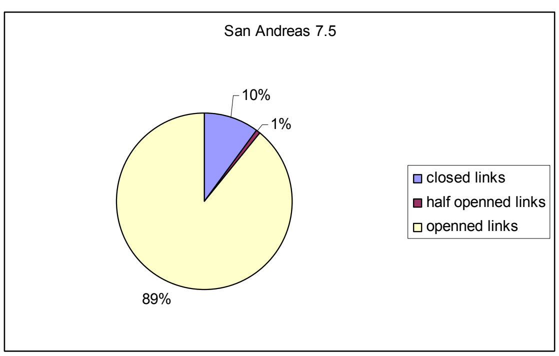

Magnitude 7.5 Scenario Event on the San Andreas fault

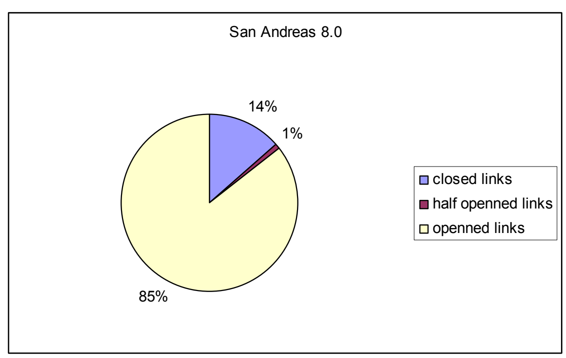

Magnitude 8.0 Scenario Event on the San Andreas fault

Fig. 3.17 Resultant link closures by earthquake scenario: Bridge Closure Criterion 1

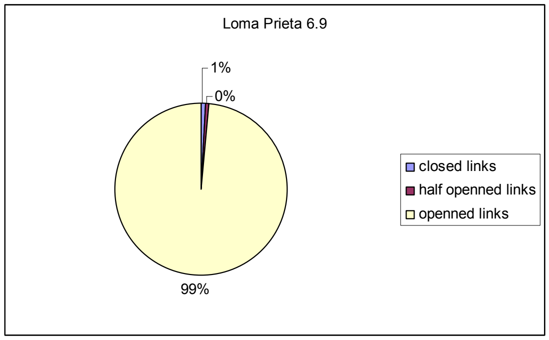

Fig. 3.18 Magnitude 6.9 Loma Prieta event on the San Andreas fault

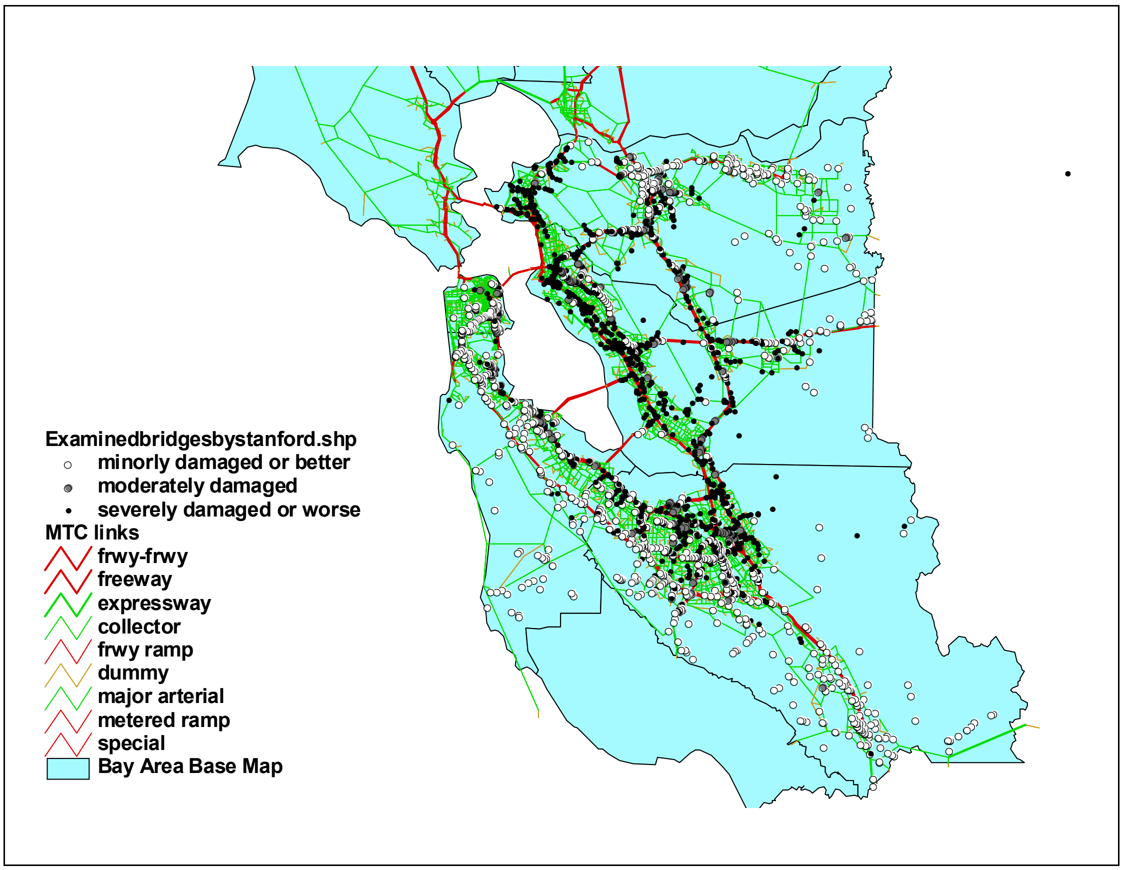

Fig. 3.19 Damaged bridges in scenario Hayward 7.5

The volume-capacity ratios of the network links are the standard index of congestion. A summary of pre- and post-earthquake volume-capacity ratios for different types of links is given in Table 3.18. The significant increase of traffic on local streets is a result of redistribution of competing traffic over the damaged network. This redistribution indicates that the local street network can accommodate considerable additional demand if the highway system loses substantial capacity following an earthquake. Note that even though the closure of damaged links caused a significant increase in traffic congestion over all, the average volume-capacity ratio of freeway links does not change to the same degree. This is due to a large number of freeway links that were isolated from the network. Following an earthquake, freeway links are more likely to become isolated are than local streets. In the scenarios that we have modeled, a substantial number of the bridges were severely damaged, which caused closure of a large number of freeway ramps.

Table 3.18 Summary of volume-capacity ratios by facility type given fixed travel demand

Facility Type	v/c Ratio	Scenario		
		Baseline	HW701	HW751
Freeway to Freeway Ramps	Average v/c	0.43	0.52	0.52
	Max v/c	1.10	3.16	4.81
Freeways	Average v/c	0.64	0.69	0.71
	Max v/c	1.24	3.33	4.94
Expressways	Average v/c	0.50	0.86	1.07
	Max v/c	1.16	4.42	9.29
Collectors	Average v/c	0.18	0.82	0.99
	Max v/c	1.33	12.15	11.81
On/Off Ramps	Average v/c	0.30	0.72	0.81
	Max v/c	1.29	6.52	11.21
Centroid Connectors	Average v/c	0.01	0.01	0.01
	Max v/c	0.13	0.32	0.32
Major Arterials	Average v/c	0.31	0.90	1.04
	Max v/c	1.41	11.24	8.64
Metered Ramps	Average v/c	0.59	1.16	1.58
	Max v/c	1.28	5.22	7.47
Special	Average v/c	0.99	3.70	3.85
	Max v/c	1.21	4.27	4.59
System-wide Average v/c		0.25	0.66	0.77
System-wide Max v/c		1.41	12.15	11.81

As a result, some undamaged freeway links may not be accessible to traffic due to damage to associated ramps, and thus have v/c ratios of zero. These zero values bring down the average v/c ratio of this group of facilities.

The fixed-demand assignment model assigns all pre-earthquake demand to the network. Consequently, following the earthquake, some links were assigned more vehicles than their capacities can accommodate. The logical maximum value for a v/c ratio is 1. A few links have a modeled v/c ratio in the neighborhood of 11, which is a highly unrealistic, unusable result. The share of unrealistically congested links, i.e., links with modeled v/c ratios slightly greater than 1, in the pre-event baseline is around 1%. This is acceptable for standard network modeling applications. However, the shares of unrealistically congested links in the two earthquake scenarios HW701 and HW751 are more than 25% (See Table 3.19). This large share of unrealistically large v/c ratio produces meaninglessly inflated link travel time estimates.

Table 3.19 Post-earthquake share of over-saturated (v/c > 1) links given fixed travel demand

Link Conditions	Scenario		
	Baseline	HW701	HW751
Number of links for which v/c > 1	252	6449	7018
Number of open links	26904	24720	23856
Share of links with v/c > 1	1%	26%	29%

A comparison of total vehicle hours of travel for the pre-event baseline and the two earthquake scenarios is provided in Table 3.20. The predicted total vehicle hours of delay is dramatically larger in the post-earthquake networks relative to the baseline network. However, this increase is exaggerated. In the volume-delay functions used to model congestion costs as a function of link flow, link travel times increase very rapidly as the v/c ratio approaches and exceeds unity. In conventional network applications, this explosive growth in predicted link delay imposes a numerical penalty sufficient to ensure that no further appreciable flow is assigned to the link. Additional flows are redirected to other paths as the nonlinear program used to identify user equilibrium flows is solved. The logic of this approach fails in the earthquake context because capacity losses are system-wide. Predicted link travel times are enormous for those links with unrealistically large v/c ratios. Consequently, these delay estimates are not valid.

In addition to the problem of assigning link flow greatly in excess of capacity, the fixed-demand trip assignment model is not able to treat travel demand between isolated zone pairs. Closure of damaged links may cause a loss of connectivity in the network, and it may become infeasible to travel between some zone pairs. For example, the members of zone pairs 439-330 and 605-611 are isolated from each other in earthquake scenario HW751. Attempting to assign trips between the members of either of these zone pairs of results in a mathematical infeasibility in the nonlinear program used to model these flows. To ensure feasibility, the demand for travel between these two pairs was deleted in this circumstance and not assigned to the network. It would be preferable to assign these flows in a way that accounts for the adjustments travelers make in their choice of destination when some locations become inaccessible.

Table 3.20 Summary of total vehicle hours by link type, fixed travel demand (hours)

Facility Type	Scenario		
	Baseline	HW701	HW751
Freeway to Freeway Connectors	6,668	287,472	22,99,946
Freeways	223,765	6,095,856	20,894,450
Expressways	33,162	15,234,488	107,516,757
Collectors	47,156	Not computable[a]	Not computable
On/off Ramps	14,552	23,684,218	Not computable
Centroid Connectors	107	185	190
Major Roads	149,692	Not computable	16,00,994,720
Metered Ramps	1,805	4,863,005	66,869,964
Golden Gate Bridge	1,959	9,512,223	1,4399,025
Total	478,866	Not computable	Not computable

Note: a. The travel time estimate exceeds the maximum value computable by the software used to estimate user equilibrium flows.

3.5.6 Variable-Demand Model Application

A variable-demand assignment model was formulated and implemented for all the earthquake scenarios in an effort to overcome the limitations of the fixed-demand assignment model. This section presents the methodology and results from the variable-demand traffic assignment model.

A fully specified travel demand function might include origin-destination specific parameters reflecting population size, income distribution, and vehicle ownership for origin zones, as well as employment intensity or retail activity variables for destination zones.

Endogenizing both route choice and travel demand in a single traffic assignment formulation is computationally challenging. Consequently, in an integrated modeling environment, travel time is the only argument of the demand function between a given O-D pair.

3.5.6.1 Estimating Parameters for Distance Decay Function

A distance decay function describes the relationship between the level of travel demand and the travel time (or other generalized measures of cost). This function might be expected to be strictly decreasing with respect to the travel time between zone-pairs. As travel time increases, trip rates logically should decrease, and vice versa. This assumption has the advantage of ensuring that the inverse travel demand function can be defined, which provides analytical convenience. In reality, however, the distribution of trip rates with respect to interzonal travel time is peaked at a small positive value. For the origin-destination matrix for the San Francisco Bay Area, this peak is at travel times of about 8 minutes.

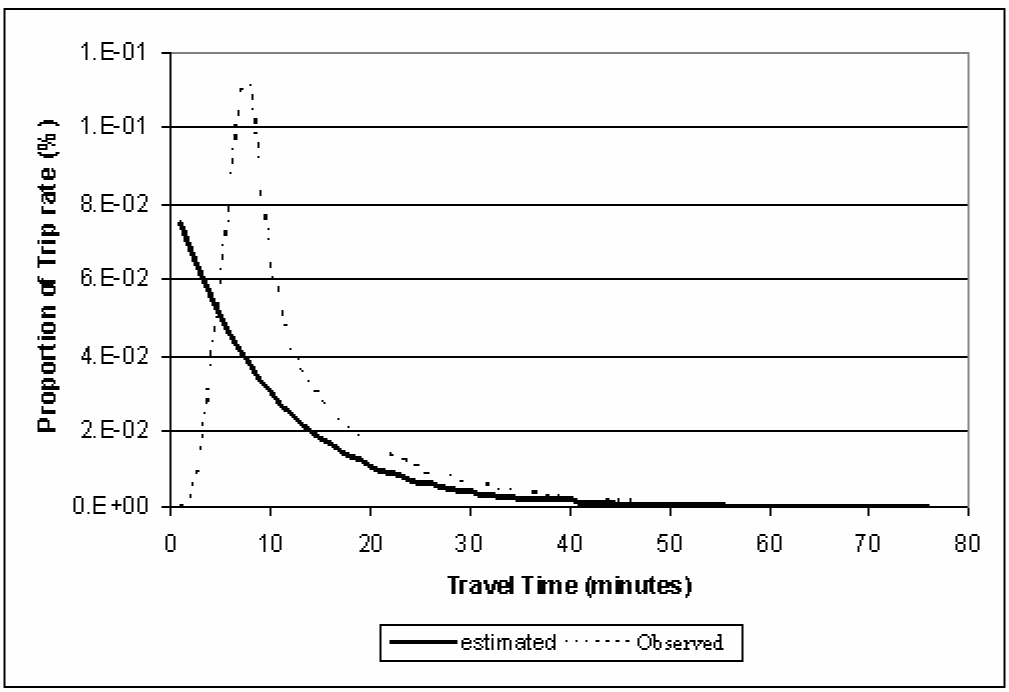

Fig. 3.20 Observed and estimated trip rates as a function of travel time for the San Francisco Bay Area

For modeling purposes, this nonmonotonic relationship must be estimated with a best-fitting monotonic form, as shown in Figure 3.20. This function is also bounded above. For example, the maximum number of vehicle trips generated between a given origin-destination is bounded by the population size at the origin.

The demand function in Equation (3.2) was applied in this analysis. This is a standard gravity model formulation that models the decay of interaction between economic agents distributed over distances.

$$q_{rs} = O_r \cdot D_s \cdot A_r \cdot B_s \, exp(\alpha + \beta \cdot u_{rs}) \tag{3.2}$$

where

q_{rs}	= trip rate between O-D pair *r-s*,
u_{rs}	= travel time between O-D pair *r-s*,
O_r	= trip production from origin zone *r*,
D_s	= trip attraction to destination zone *s*,
A_r	= coefficient to be estimated associated with origin zone *r*,
B_s	= coefficient to be estimated associated with destination zone *s*, and
α, β	= model parameters to be estimated.

The coefficients and parameters in Equation (3.2) were estimated against the San Francisco Bay Area data by implementing an iterative process. The zone-to-zone travel times (u_{rs}) were estimated using a fixed-demand user equilibrium model based on the O-D requirements provided by MTC. A regression model estimated parameters α, β based on the distribution of O-D requirements and the associated zone-to-zone travel times. The final estimations of the two regression coefficients are

$$\alpha = 3.17096517 \tag{3.3}$$

, and

$$\beta = -0.127305279. \tag{3.4}$$

Given travel time and estimated parameters, a gravity model was applied to estimate zone-specific coefficients (A_r, B_s). The detailed procedure for estimating the values of A_r and B_s is described below. Once all unknowns are estimated, a new set of O-D requirement (q_{rs}) can be estimated. These steps must be repeated until the estimated values α and β converge.

Adding both sides of Equation (3.2) over all the destination zones gives

$$\sum_s q_{rs} = O_r A_r \sum_s D_s B_s \exp(\alpha + \beta u_{rs}) . \tag{3.5}$$

Because

$$\sum_s q_{rs} = O_r \ , \tag{3.6}$$

the parameter A_r can be calculated using the relationship

$$A_r = \sum_s \frac{1}{D_s B_s \exp(\alpha + \beta u_{rs})} \ . \tag{3.7}$$

Similarly, adding both sides of Equation (3.2) over all the origin zones gives

$$\sum_r q_{rs} = D_s B_s \sum_r O_r A_r \exp(\alpha + \beta u_{rs}) \ . \tag{3.8}$$

Because

$$\sum_r q_{rs} = D_s \ , \tag{3.9}$$

the parameter B_s can be calculated using the relationship

$$B_r = \sum_r \frac{1}{O_s A_s \exp(\alpha + \beta u_{rs})} \ . \tag{3.10}$$

Data from the baseline model are used as the initial inputs to estimate the parameters A_r and B_s. These include the attraction of zone r (O_r), the production of travel at zone s (D_s), the travel demand, q_{rs}, between the zone pair *r-s*, and the travel time, u_{rs}, between the zone pair *r-s*. The value of B_s is initialized at one. Then, the values of A_r are estimated using Equation (3.7), and the values for B_s are updated using Equation (3.10). Once the values of A_r and B_s are updated, the value of q_{rs} is updated using Equation (3.2). These steps must be repeated for final estimations of A_r and B_s until the values of q_{rs} converge.

However, estimating trip distribution in this fashion for the variable-demand model leads to a mismatch between the total number of baseline trips predicted by the fixed-demand and variable-demand model. The parameters A_r and B_s in the travel demand function were estimated iteratively based on the interzonal travel times derived from the fixed-demand trip assignment model. However, the resultant O-D requirements determined at each iteration generate a variety of different interzonal travel times. Agreement between the total number of baseline trips in the fixed-demand and variable-demand assignment models can be improved by updating the interzonal travel times at each iteration, rather than by relying on the interzonal travel times from the fixed-demand mode. The final procedure for obtaining the coefficients in the variable-demand model is shown in Figure 3.21.

3.5.6.2 Results from Variable-Demand Assignment Model

This section presents the network analysis results for the variable-demand trip assignment model. As noted in above, two bridge closure criteria are considered in this study. The total number of trips to be assigned varies according to network performance. Table 3.21 summarizes the total number of trips assigned to the baseline network and for the earthquake scenarios. These results agree with our expectations. In general, more severe earthquakes result in a lower network level of service, and this suppresses travel demand. Closure criterion 2 is less risk tolerant then closure criterion 1, and results in greater reductions in network capacity than closure criterion 1. This further suppresses level of service, and predicted trip requirements are logically lower under criterion 2 than under criterion 1.

Table 3.21 Summary of total trips assigned to the network in a 2-hour period given variable travel demand and two different bridge closure criteria

	Scenario					
	Baseline	**HW 7.0**	**HW 7.5**	**SA 7.5**	**SA 8.0**	**LP 6.9**
Closure Criteria 1	1,854,997	1,327,970	1,179,735	1,214,400	1,046,474	1,742,334
Closure Criteria 2	1,854,997	1,306,889	1,154,899	1,187,179	1,033,560	1,720,355

Links subjected to increased traffic in earthquake scenario HW751 relative to the baseline scenario are highlighted in Figure 3.22. Links with decreased traffic are highlighted in Figure 3.23. In general, traffic is shifted from damaged freeways and highways to neighboring local streets. This outcome is qualitatively similar to the flow shifts predicted by the fixed-demand model.

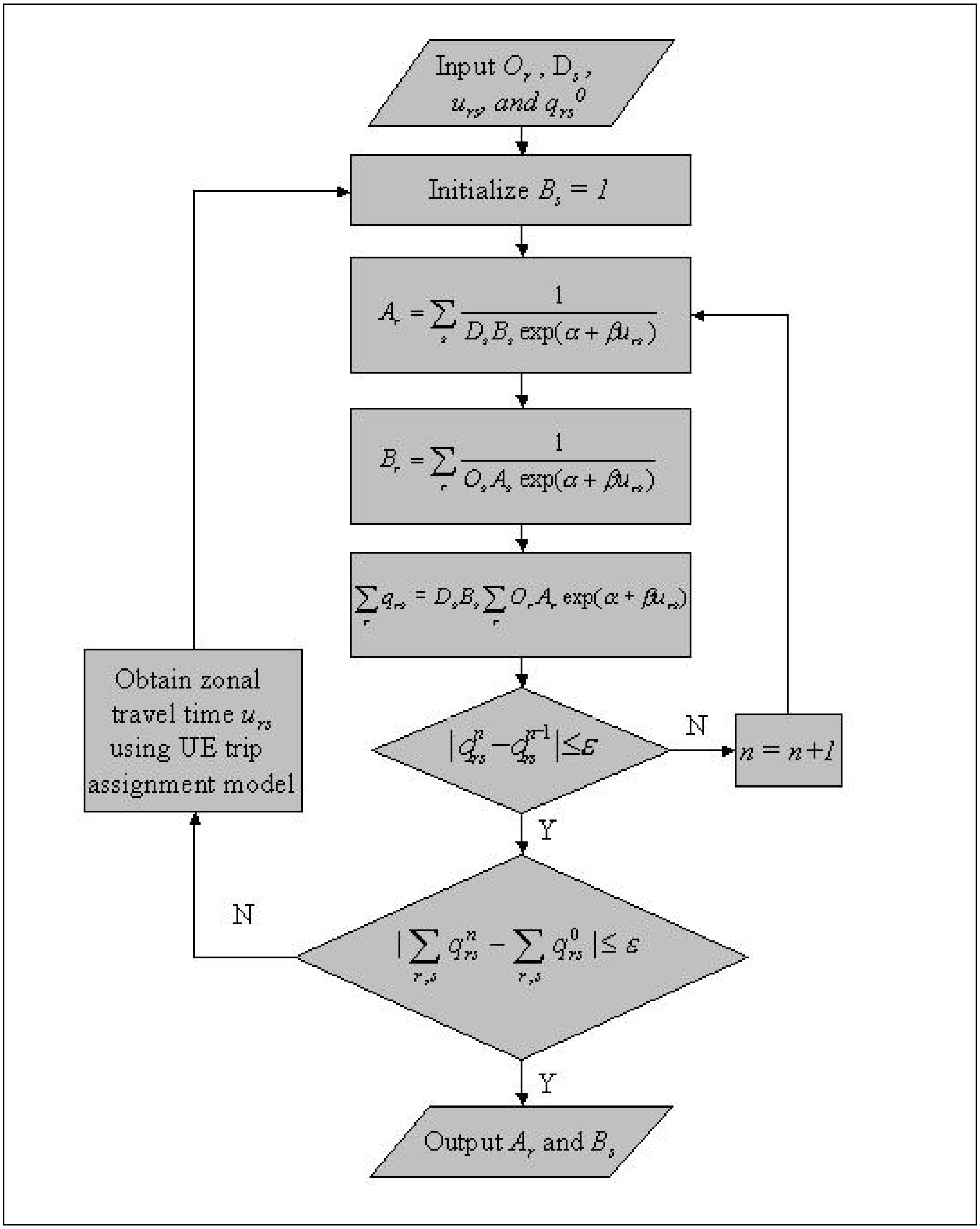

Fig. 3.21 Final procedure for obtaining coefficients in the travel demand function

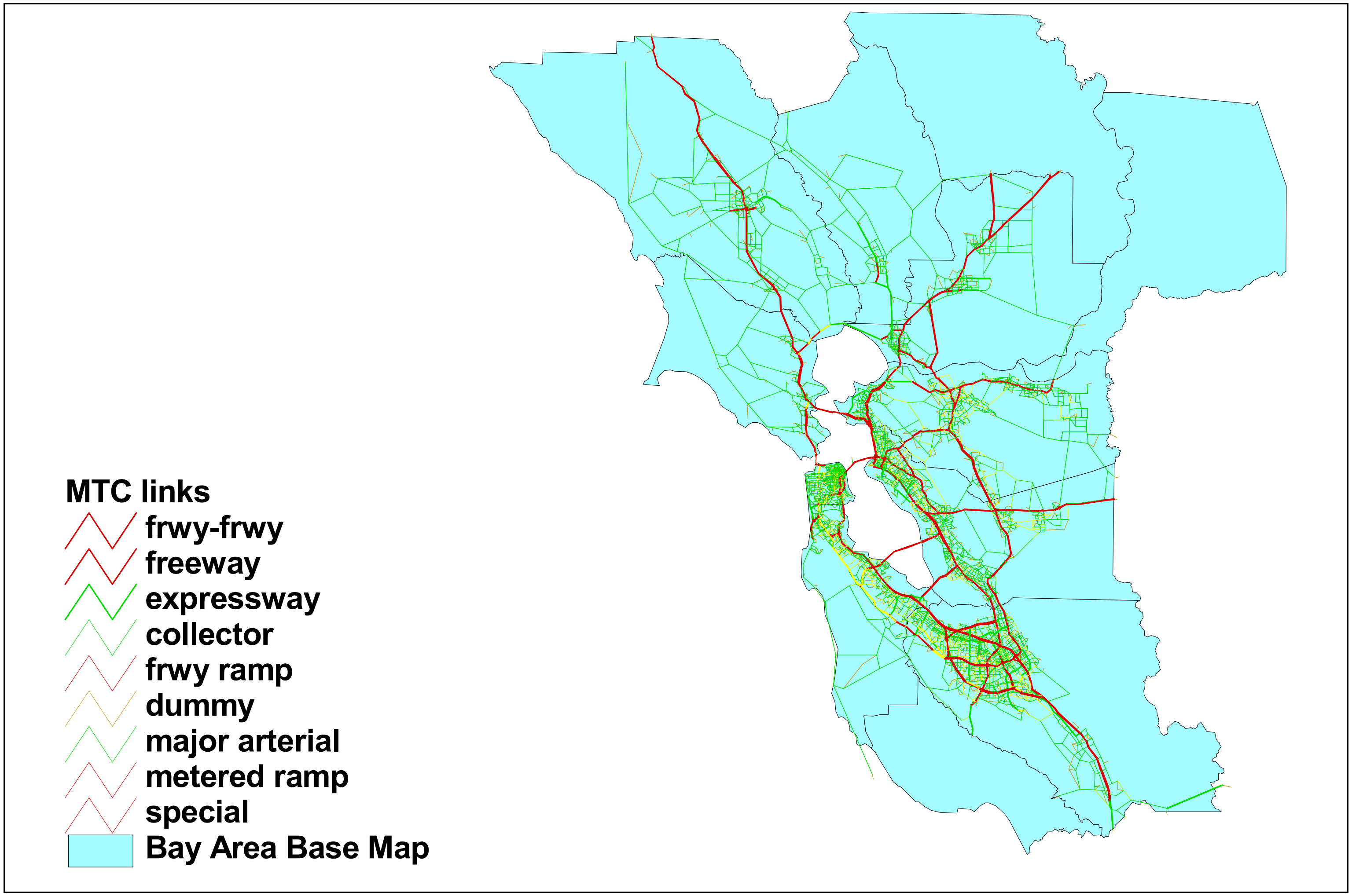

Fig. 3.22 Traffic increases on some local streets in Scenario HW751, variable travel demand

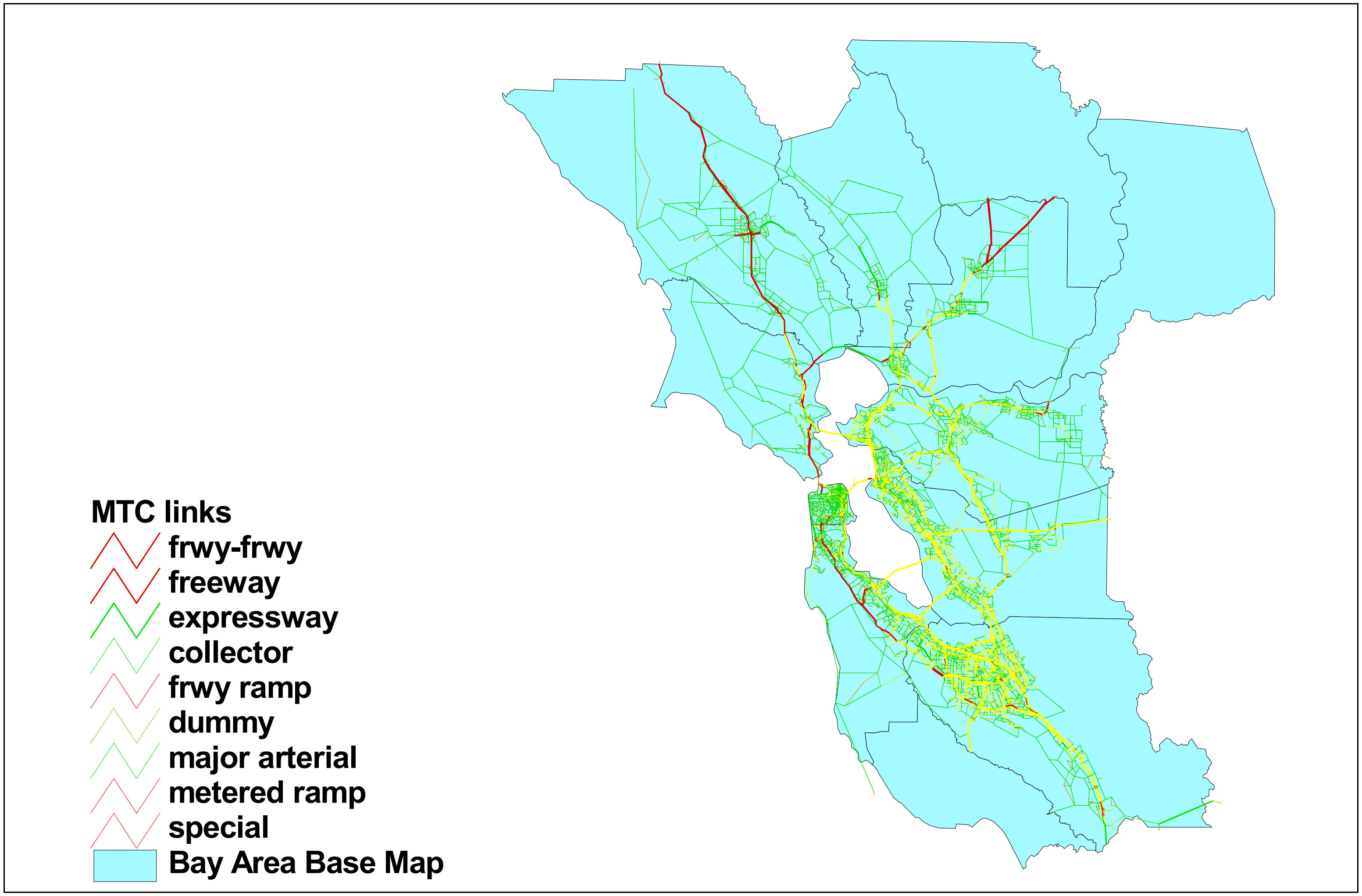

Fig. 3.23 Traffic reductions on freeway links and some local streets in Scenario HW751, variable travel demand

Table 3.22 Summary of volume-capacity ratio by link type, scenario, and bridge closure criterion given variable travel demand

Facility Type	v/c Ratio	Scenario and Bridge Closure Criterion										
		Baseline	HW701	HW702	HW751	HW752	SA751	SA752	SA801	SA802	LP691	LP692
Freeway to Freeway Connectors	Average v/c	0.40	0.23	0.20	0.18	0.15	0.21	0.20	0.14	0.13	0.39	0.39
	Max v/c	1.10	1.26	1.26	1.28	1.28	1.23	1.30	1.05	1.03	1.26	1.22
Freeways	Average v/c	0.53	0.26	0.25	0.22	0.20	0.25	0.24	0.18	0.17	0.47	0.47
	Max v/c	1.18	1.23	1.24	1.28	1.25	1.11	1.11	0.93	0.94	1.29	1.29
Expressways	Average v/c	0.49	0.31	0.30	0.26	0.26	0.23	0.23	0.20	0.20	0.43	0.42
	Max v/c	1.21	1.18	1.24	1.45	1.27	1.24	1.21	1.27	1.26	1.32	1.26
Collectors	Average v/c	0.17	0.17	0.17	0.16	0.16	0.18	0.18	0.17	0.17	0.17	0.17
	Max v/c	1.31	1.36	1.41	1.28	1.31	1.45	1.36	1.52	1.39	1.30	1.30
On/Off Ramps	Average v/c	0.30	0.23	0.22	0.20	0.19	0.22	0.22	0.18	0.18	0.30	0.30
	Max v/c	1.25	1.38	1.39	1.44	1.42	1.38	1.38	1.35	1.36	1.37	1.33
Centroid Connectors	Average v/c	0.01	0.00	0.00	0.00	0.00	0.00	0.00	0.00	0.00	0.01	0.01
	Max v/c	0.13	0.06	0.06	0.06	0.06	0.07	0.07	0.06	0.06	0.13	0.13
Major Arterials	Average v/c	0.29	0.27	0.27	0.25	0.25	0.26	0.26	0.23	0.23	0.29	0.30
	Max v/c	1.40	1.44	1.45	1.46	1.46	1.52	1.54	1.51	1.51	1.42	1.40
Metered Ramps	Average v/c	0.62	0.43	0.42	0.36	0.35	0.39	0.37	0.23	0.23	0.57	0.56
	Max v/c	1.28	1.40	1.40	1.39	1.42	1.55	1.50	1.28	1.24	1.32	1.31
Golden Gate Bridge	Average v/c	0.61	0.60	0.60	0.58	0.58	0.58	0.58	0.56	0.55	0.61	0.61
	Max v/c	0.62	0.60	0.60	0.60	0.60	0.61	0.61	0.57	0.56	0.62	0.62
System-wide Average v/c		0.23	0.19	0.18	0.17	0.17	0.18	0.18	0.16	0.16	0.23	0.23
System-wide Max v/c		1.40	1.44	1.45	1.46	1.46	1.55	1.54	1.52	1.51	1.42	1.40

Table 3.23 Post-earthquake share of over-saturated (v/c > 1) links given variable travel demand

Link Conditions	Scenario					
	Baseline	HW701	HW751	SA751	SA801	LP691
No. of links with v/c > 1	168	212	173	182	157	198
Number of open links	26,904	24,720	23,856	24,224	23,221	26,645
Share of links with v/c > 1	0.62%	0.86%	0.73%	0.75%	0.68%	0.74%

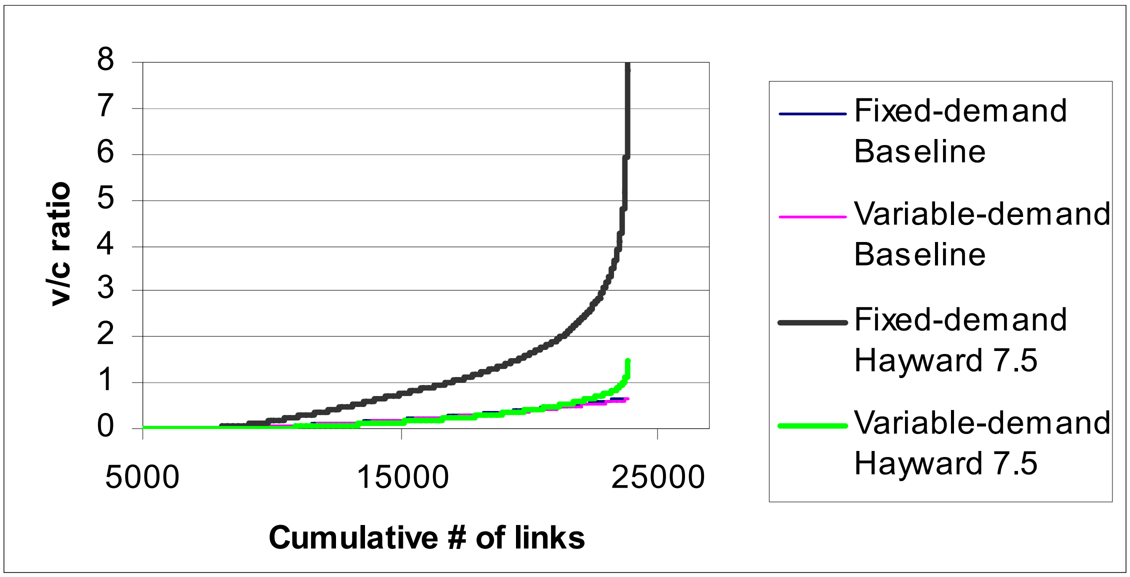

Fig. 3.24 Cumulative distribution of post-earthquake volume/capacity ratios: a comparison of fixed and variable travel demand estimates

A summary of v/c ratios for different link types is given in Table 3.22. The share of links with v/c ratios greater than 1 in each scenario is listed in Table 3.23. Comparing Tables 3.23 and 3.19 shows that the share of these unrealistically congested links is much smaller than in the case of the fixed-demand model. Figure 3.24 shows how the cumulative distribution of v/c ratios changes as the assignment model shifts from the fixed-demand to the variable-demand perspective. The largest v/c ratio drops from 12 in the case fixed-demand model to only about 1.5 for the variable-demand formulation. Even though the variable-demand model still predicts v/c ratios greater than 1 for a few network links, the share of links predicted to have unrealistically large v/c ratio is negligible.

A comparison of total vehicle hours of delay across the baseline and various earthquake scenarios is given in Table 3.24. The total vehicle hours traveled increases in the post-earthquake networks relative to the baseline network, but not as dramatically in the variable-demand case as for the fixed-demand model. The variable-demand model assigns fewer trips to the network. The proportionate difference in trip production and attraction between the fixed-demand and the variable-demand models is shown in Figures 3.25–3.26, respectively. These results are presented at the TAZ level. As in the case of the fixed-demand model, some freeway links are isolated by network damage, even though they are otherwise fully functional. The Golden Gate Bridge is a consistent example of this outcome across all earthquake scenarios.

The reduced travel demand predicted by the variable-demand model results in fewer total vehicle hours of travel. However, less total time delay does not indicate lower costs. The trips being eliminated because of high travel costs have value. These absences impose an opportunity cost. Any measure of total losses should account for both the total observed delay, and the value of the trips forgone.

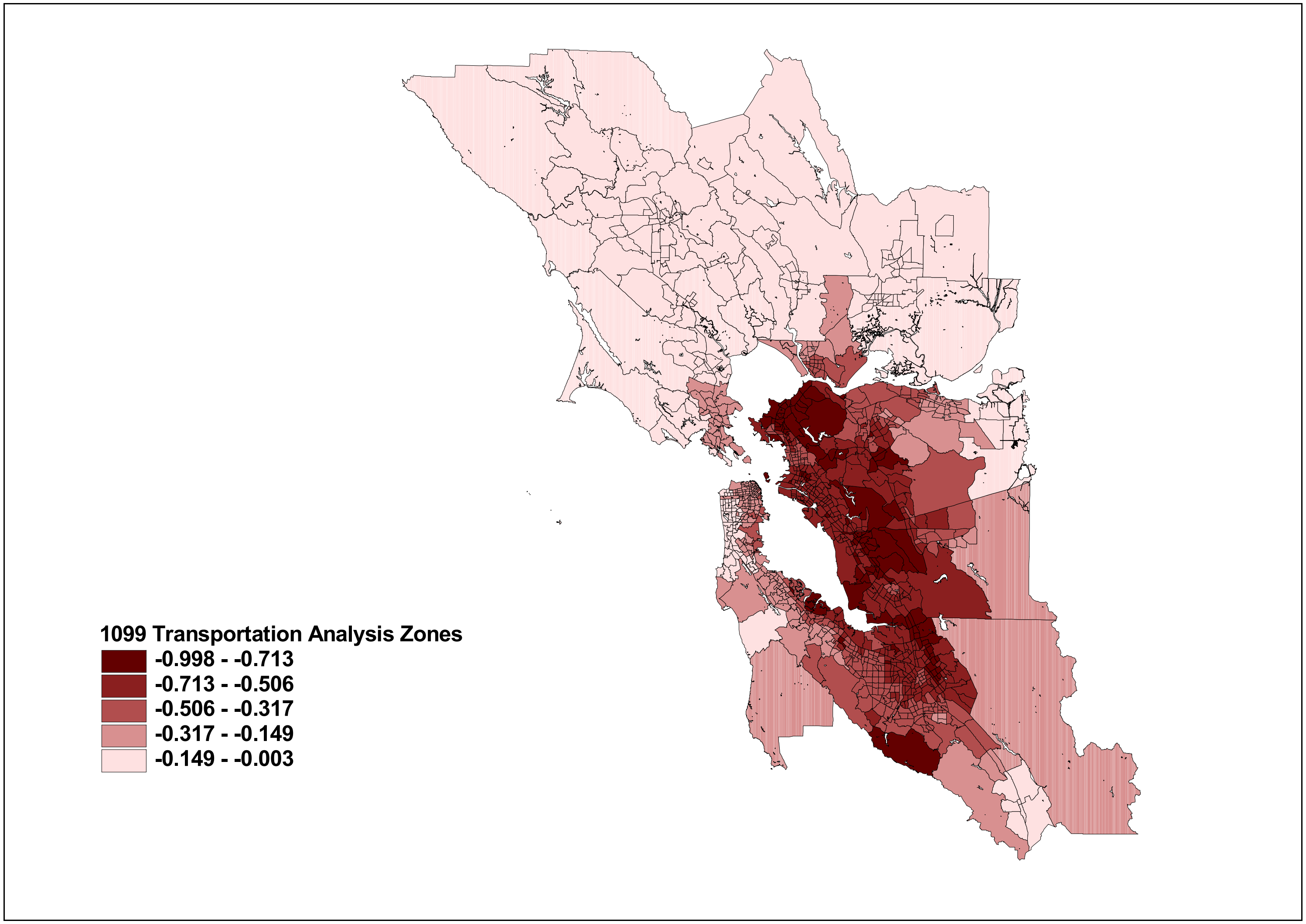

Fig. 3.25 Proportionate differences in trip production estimates, variable- vs. fixed-demand models

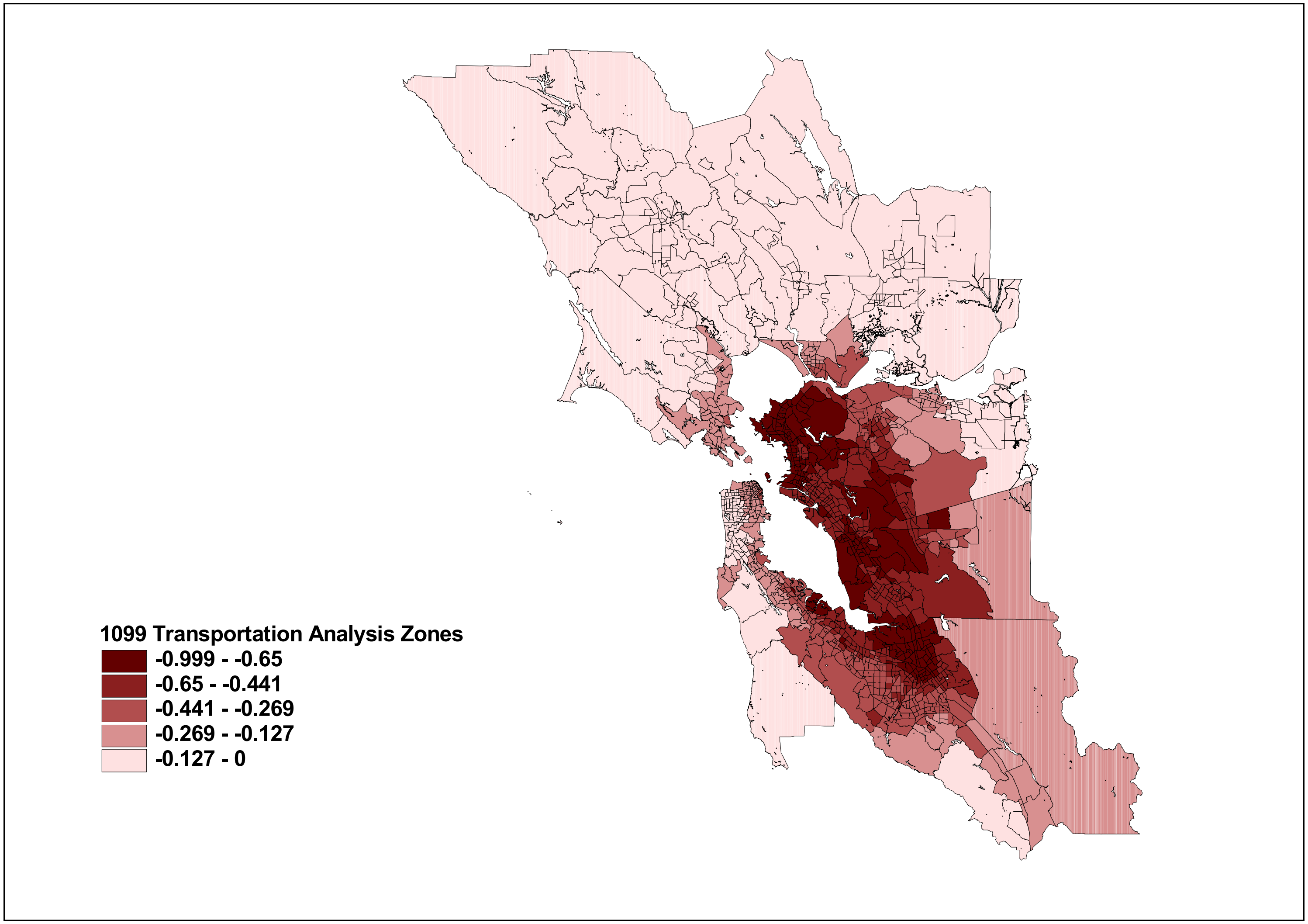

Fig. 3.26 Proportionate differences in trip attraction estimates, variable- vs. fixed-demand models

Table 3.24 Summary of total vehicle hours of travel by link type, variable travel demand model

Facility Type	Scenario and Bridge Closure Criterion										
	Baseline	HW701	HW702	HW751	HW752	SA751	SA752	SA801	SA802	LP691	LP692
Freeway to Freeway Ramps	5,775	3,222	2,884	2,461	2,046	1,961	1,928	982	802	5,615	5,386
Freeways	161,826	62,072	58,872	46,953	43,009	56,568	51,071	34,675	32,720	142,236	137,787
Expressways	30,026	18,092	17,294	14,112	13,693	12,416	12,161	10320	10,184	26,377	25,223
Collectors	41,677	42,483	42,464	40,214	39,933	42,881	43,591	41,628	41,408	41,509	41,879
On/off Ramps	15,256	11,069	10,891	9,710	8,492	10,307	9,525	7,675	7,556	16,499	16,378
Centroid Connectors	105	35	31	27	22	43	42	32	31	104	104
Major Roads	133,471	123,335	122,290	110,821	110,337	113,647	113,310	99,931	98,163	137,074	138,289
Metered Ramps	2,126	1,841	1,897	1,247	1,215	1,944	1,612	570	540	2,175	1,975
Golden Gate Bridge	524	515	514	502	502	506	505	475	466	522	521
System-wide Total	390,788	262,663	257,136	226,048	219,250	240,272	233,747	196,288	191,871	372,111	367,542

3.5.7 Opportunity Costs

The earthquake engineering literature traditionally emphasizes damage to structures and contents. More recently, social science–based research on earthquakes has addressed the measurement of business interruption costs (Gordon, Richardson, and Davis, 1998; Rose and Benavides, 1998; Boarnet, 1998; Cho et al., 2001). In this section, our focus is on estimating the increased travel delay, and the opportunity cost of travel forgone following an earthquake. All of these calculations are based on a morning-peak period of two hours' duration.

Increases in network congestion following an earthquake suppress travel demand, but the total number of vehicle hours of travel may still increase as a result of the earthquake. Slower speeds mean more travel time for those trips that still occur following an earthquake. The difference between system-wide vehicle hours of baseline travel and post-earthquake travel can be calculated from the results from the variable-demand model. Person trips and freight trips should be treated separately in this calculation, since the values of time are different are for these flows. Results are reported here in terms of vehicle hours.

In addition to increased delays, congestion decreases travel demand. A number of the trips that occur in baseline scenario disappear in an earthquake scenario. These trips forgone impose an opportunity cost. In the absence of a model of the metropolitan economy, it is not clear how to compute these opportunity costs, but a lower bound is available. Travel is a derived demand, and the trips occurring in the baseline provide benefits at least as large as the cost of the trip. Thus the opportunity cost of each trip forgone following an earthquake is at least as large as the delay cost associated with this trip in the baseline. Summing across all trips forgone provides a lower bound on system-wide opportunity costs.

Following an earthquake, some new trips occur that were not present in the baseline. The benefits provided by these trips are at least as large as the costs associated with them, otherwise they would not occur. In the interests of conservatism, the aggregate lower bound on the benefits provided by these new trips is netted out of the aggregate opportunity cost of trips forgone.

A number of competing value of time estimates are available in the literature. According to the 2000 Census 2000 County Business Patterns for San Francisco [http://www.census.gov/epcd/cbp/map/00data/06/075.txt], the total annual payroll is $31,060,972,000, and the total number of employees is 555,647. Thus the average annual payroll per employee is $55,901, or

$26.88 per hour. This is higher than the value of time typically assumed for planning purposes by transportation agencies. Travel time is usually accounted for at a value considerably less than the average wage. We rely on the average wage in this case to help improve what would otherwise be a very loose lower-bound calculation. An estimated value of $5,117.27 per PCE for freight trips, averaged across different industrial sectors, is reported in Section 2.3. Table 3.25 combines these values to estimate the delay and opportunity cost for person and freight trips in the HW701 and HW751 earthquake scenarios.

Table 3.25 Delay and opportunity cost in two earthquake scenarios, two-hour A.M. peak period

Scenario	Delay (Vehicle Hours)		Opportunity Cost ($)	
	Auto trips[a]	Freight trips	Auto trips[b]	Freight trips
HW701	240,038	19,463	5,696,653	222,529,873
HW751	207,404	16,817	6,716,551	279,880,290

Note: a. Automobiles account for 92.5% of the total Caltrans District 4 vehicle counts.
b. This assumes an average vehicle occupancy (AVO) of 1.0. This is conservative, because the baseline AVO exceeds 1.0, and would likely increase following and earthquake.

Total delay costs are lower for the more severe earthquake. This does not indicate a better level of service on the network. Rather, it is the result of travel demand reductions resulting from a lower level of service. Logically, opportunity costs move in the opposite direction: Additional opportunity costs accrue as more trips are forgone. Freight trips account for the largest share of opportunity costs because of the relatively high value of commodity flows.

3.5.8 Extensions

3.5.8.1 Relationship between Bridge Damage Status and Functionality

As noted previously, it is mostly unclear whether a moderately damaged bridge should be closed or kept open. We modeled only two bridge closure criteria, one reflecting risk aversion, and one reflecting risk tolerance. Testing two bridge closure criteria provides some insight into the performance implications of the bridge closure decision. Following a severe earthquake, a risk-averse bridge closure criterion would forgo use of residual traffic capacity that would certainly deliver additional transportation benefits but which would also reduce further loss of life from additional structural failures. In practice, the decision is not likely to be binary. Temporary repairs and shoring to reduce the likelihood of collapse are likely to be the order of the day for moderately damaged bridges, mitigating risk while extracting value residual capacity.

From a simulation perspective, it is sensible to consider expected capacity. In future research, the relationship between bridge damage state and functionality will be modified to account for an expected partial loss of functionality. See Figure 3.27.

3.5.8.2 Time Period To Be Modeled

We evaluate network performance with respect to two hours of peak daily transportation demand. A more complete time-of-day representation of travel demand would be needed to evaluate the potential benefits of bridge retrofits. The standard procedure is to model delay in each time period separately to provide an estimation of overall network performance. Post-earthquake time-of-day traffic profiles are speculative. Some of the demand suppressed by reductions in peak period level of service would be shifted to other times of day, and ultimately accommodated. This would require an extension of the variable-demand model to include a temporal dimension.

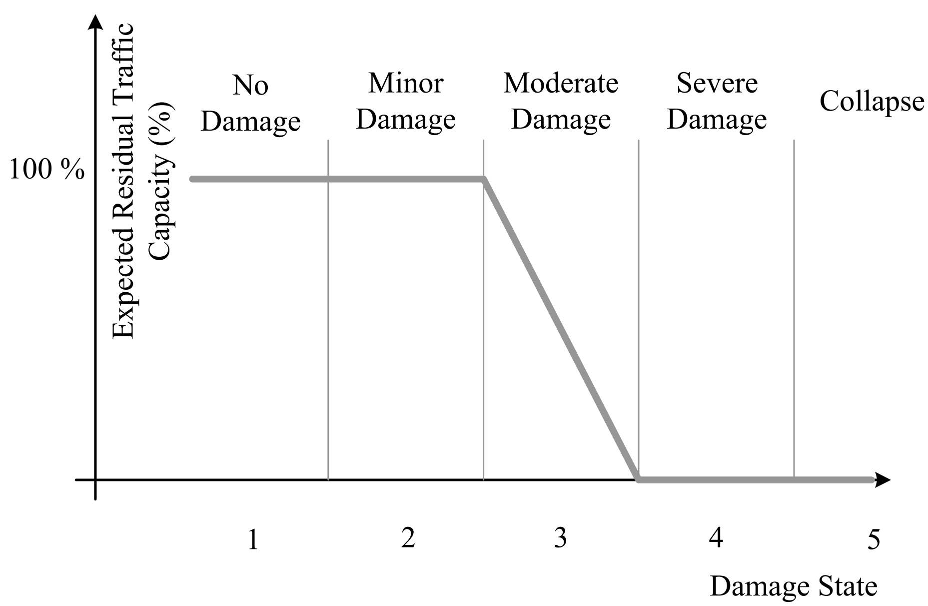

Fig. 3.27 Bridge damage state vs. expected residual traffic capacity

3.6 LOSS ESTIMATION

3.6.1 Direct Loss Estimation

The loss calculations are based on Equation (2.16), which gives the estimated loss of a bridge within a given area and given repair cost per unit area (*Area* and *Cost* parameters respectively, see Section 2.1.3). The information of repair costs per unit area for different NBI bridge classes is obtained from Caltrans, and is listed in Table 3.26 for reference. Due to lack of information for all the corresponding HAZUS bridge classes, an average value of $110/sq ft is assumed for the classes with unknown cost information.

Table 3.26 Repair cost per unit area for NBI bridge classes

NBI Class	Repair Cost ($ per sq ft)
101	117.5
104	115
105	120
901	145
905	110
501	125
504	130
505	165
Other	110

Based on the damage state probabilities obtained in Section 3.1, Table 3.27 below summarizes the results for the six different hazard cases defined in Table 2.6 by cost category (best mean, minimum, and maximum; see Section 2.1.3 for category definitions) and by scenario events. As expected, the loss amount is significant when liquefaction is taken into consideration as a part of hazard components (cases 2, 4, and 5). From the tables for the best mean cost category, and for the scenario *SA8.0*, the expected total repair cost exceeds $1.5 billion, whereas the same loss drops by almost $900 million when liquefaction is not included (cases 1, 3, and 6).

Table 3.27 Expected total repair cost by hazard and cost categories for the four scenario events (costs are in $x1000)

Cost Categories		Scenario	Hazard Cases: Ground Shaking Only (1)	Ground Shaking + Liquefaction (2)	Ground Shaking + Landslide (3)	Ground Shaking + Liquefaction + Landslide (4)	Liquefaction Only (5)	Landslide Only (6)
	Best Mean	***HW7.0***	$77,360	$474,473	$84,201	$475,119	$455,893	$16,162
		HW7.5	$283,150	$1,088,700	$320,862	$1,093,745	$1,039,951	$97,644
		SA7.5	$285,434	$955,696	$340,908	$970,270	$882,901	$139,585
		SA8.0	$634,299	$1,533,934	$763,012	$1,539,517	$1,482,278	$468,547
	Minimum	***HW7.0***	$38,635	$298,383	$42,256	$298,633	$290,516	$7,645
		HW7.5	$155,606	$689,895	$180,663	$692,205	$669,129	$58,963
		SA7.5	$150,900	$581,016	$176,887	$586,573	$547,112	$72,438
		SA8.0	$349,450	$979,684	$434,118	$981,734	$951,747	$263,707
	Maximum	***HW7.0***	$147,174	$1,033,232	$159,331	$1,034,195	$1,003,123	$27,156
		HW7.5	$571,341	$2,337,583	$653,639	$2,345,426	$2,258,896	$205,422
		SA7.5	$550,800	$1,990,711	$637,071	$2,008,119	$1,864,313	$250,281
		SA8.0	$1,247,827	$3,295,373	$1,525,952	$3,301,859	$3,194,121	$917,438

3.6.2 Results of Retrofit Analysis

Similar to the analysis in Section 3.3.1, the expected loss of the scenario events is calculated for all of the four scenarios. Table 3.28 summarizes the loss estimates from the scenario *SA8.0* for the four different retrofitting cases and for the six hazard cases in the three cost categories (best mean, minimum, and maximum). When all three hazard types are considered together (case 4 of Table 3.28) the expected repair cost falls from $1.540–$1.467 billion, which accounts for a 6% reduction in cost. However, the reduction is 24% when the loss estimate is based on ground shaking only. In that case, the total loss of $634 million drops to $483 million (best mean category). Similar relationships are observed for the other cost categories within the same hazard case.

For hazard case 6 (landslide only), provided in the last column of Table 3.28, mean cost reduction is 10% (from \$469 million–\$426 million). The cost reduction is 18% for the minimum and maximum repair cost categories (\$263 million–\$217 million and \$917 million–\$760 million, respectively), where the difference is due to the modification by repair cost ratio with the number of spans of the bridges taken into account. As discussed in Section 2.1.3 the repair cost ratio of the best mean category for damage state five is modified based on the number of spans of a bridge. The main component of the loss term for the *landslide only* category is due to a single bridge (bridge no: 37 0029) which has 37 spans (with a length of 927 ft), and the landslide susceptibility category is found to be 8 (which implies a high landslide susceptibility). When the retrofitting calculations are done, the damage state of the bridge shifts toward the less damaged side; however, the cost of repair increases because of the inconsistencies stated in the definition of repair cost ratios. For that particular bridge it is more "economical" to be in damage state five (complete) rather than damage state four (extensive). This example clearly demonstrates the problem with the fragility functions particularly for ground deformation.

Table 3.28 Expected total repair costs by hazard case and by retrofit category for the scenario event *SA8.0* (Cost in \$x1000)

	Retrofitting Cases	Shaking Only (1)	Shaking + Liquefaction (2)	Shaking + Landslide (3)	Shaking + Liquefaction + Landslide (4)	Liquefaction Only (5)	Landslide Only (6)
Best Mean	**No-Retrofit**	\$634,299	\$1,533,934	\$763,012	\$1,539,517	\$1,482,278	\$468,547
	γ=5%	\$592,014	\$1,513,122	\$733,932	\$1,519,697	\$1,464,717	\$460,476
	γ =10%	\$552,924	\$1,493,543	\$705,958	\$1,501,178	\$1,448,291	\$450,503
	γ =20%	\$483,310	\$1,458,023	\$651,834	\$1,467,954	\$1,418,709	\$425,912
Minimum	**No-Retrofit**	\$349,450	\$979,684	\$434,118	\$981,734	\$951,747	\$263,707
	γ =5%	\$323,613	\$968,288	\$408,282	\$970,623	\$942,461	\$251,017
	γ =10%	\$300,118	\$957,132	\$384,545	\$959,767	\$933,160	\$239,013
	γ =20%	\$259,207	\$934,895	\$342,797	\$938,178	\$914,026	\$217,235
Maximum	**No-Retrofit**	\$1,247,827	\$3,295,374	\$1,525,952	\$3,301,859	\$3,194,121	\$917,438
	γ =5%	\$1,158,730	\$3,257,279	\$1,438,913	\$3,264,662	\$3,163,550	\$875,608
	γ =10%	\$1,077,351	\$3,220,151	\$1,358,543	\$3,228,481	\$3,133,081	\$835,403
	γ =20%	\$934,797	\$3,146,745	\$1,215,774	\$3,157,115	\$3,070,905	\$760,680

3.7 LOMA PRIETA (1989) EARTHQUAKE

The Loma Prieta earthquake of October 17, 1989, occurred near the counties under study. The epicenter was located in a sparsely populated area to the south of the five counties. A 40 km segment of the San Andreas fault ruptured. The earthquake was felt as far south as Los Angeles, and as far to the east as western Nevada. The cost of the earthquake to the transportation system was $1.8 billion. $300 million of this amount was attributed to the damage on bridges and viaducts (including the damage sustained by the Cypress Viaduct and the San Francisco–Oakland Bay Bridge). This was according to the report of the Governor's Board of Inquiry on the 1989 Loma Prieta Earthquake (1990).

Figure 3.28 shows the rupture zone of the earthquake, the ground motion contours according to the ShakeMap by USGS (2003a), and the bridges with actual damage as reported by Caltrans (1989). A significant number of bridges far from the epicenter of the earthquake experienced damage during the earthquake. Some of the major damage occurred around areas of intense liquefaction along highway I-80 (some of those bridges are not in the bridge database used for the analyses, and hence not shown in Fig. 3.28). A number of routes in proximity to the rupture zone also experienced significant damage (on I-280 there were 16 bridges damaged).

A summary of the observed damage from the Loma Prieta Earthquake and the estimated damage states according to the methodology followed in the previous sections, is presented in Table 3.29. The damage classifications used in the damage reports by Caltrans are different from those used in this research. For comparison purposes, the observed bridge damaged data were reclassified as follows. In Table 3.29. *Minor* (actual) damage corresponds to HAZUS damage states 2 and 3, and *Major* (actual) damage corresponds to HAZUS damage states 4 and 5. The damage state estimates listed in Table 2.6 are for hazard cases 1 (*ground shaking only*) and 4 (*ground shaking, liquefaction, and landslide together*) because data were available only for these hazards. From Table 3.29 it can be seen that the estimated number of damaged bridges according to hazard case 1 is 5 and hazard case 4 is 250. The actual damage reported from the earthquake in the study area, however, is only 117 (out of 2640).

Table 3.29 Number of bridges by estimated damage state and actual damage state category for the Loma Prieta 1989 earthquake

HAZUS Damage States	Shaking Only (1)	Shaking + Liquefaction + Landslide (4)	Actual Damage States	Actual Damage
1	2635	2390		
2	4	46	**Minor**	113
3	1	56		
4	0	105	**Major**	4
5	0	43		
Total Damaged Bridges*	5	250	**Total Damaged Bridges**	117
Total Bridges	2640	2640	**Total Bridges**	2640

Figures 3.29–3.30 show the geographical distribution of the bridges in different estimated damage states for the two hazard cases considered. As seen in Figure 3.29, the ground-shaking category estimates only a few damaged bridges (all of them are less than or equal to damage state 3). These are distributed throughout Santa Clara County. The analyses for all three hazards give significantly different results from the previous case (Fig. 3.30). Almost all of the damaged bridges are again estimated to be in Santa Clara County, though there are a few in San Mateo County. For the "all hazards considered" case, no damage was estimated for Contra Costa and Alameda counties. However, this is highly misleading because of the incompleteness of the database. The original database, acquired in the late 1990s, did not include the Cypress structure, which sustained high damages (near collapse). It was speculated that the project methodology overestimated the damage due to liquefaction and landslide when the bridge sites were located close to the rupture zone (and when the ground motion demand is relatively high). The damage was likely to be underestimated due to the same hazards when the bridge sites were located far from the rupture zone.

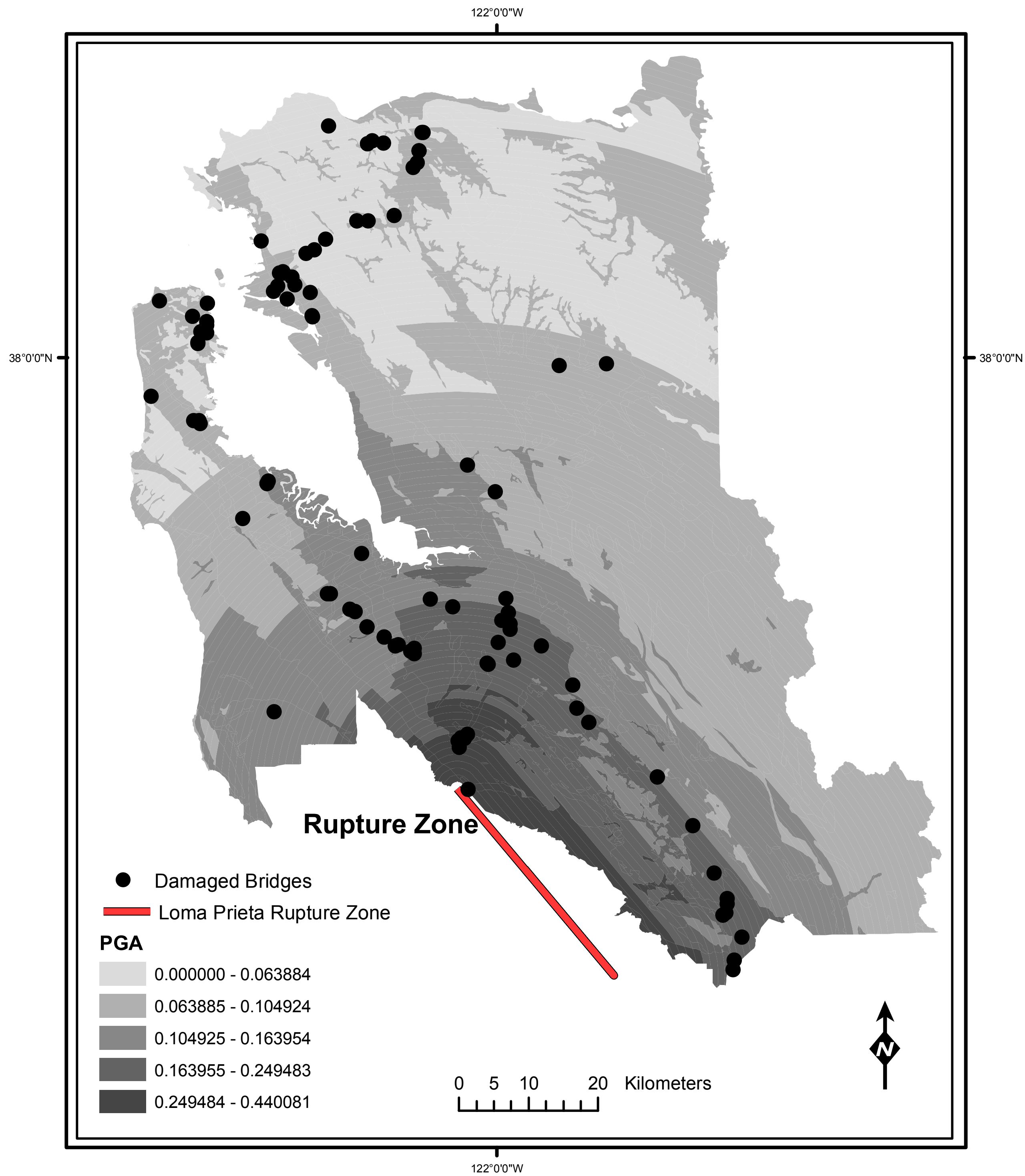

Fig. 3.28 Loma Prieta 1989 earthquake rupture zone, ground motion contours, and damaged bridges in the study area

The damage data obtained from Caltrans did not include cost estimates for all the bridges reported. For the bridges where repair costs were available (83 out of 117), the total loss is about $8.5 million. The analyses performed for all the bridges in Section 3.6 are repeated for the Loma Prieta earthquake and the results are summarized in Table 3.30. These include the three cost categories (best mean, minimum, and maximum — see Table 2.7) and the hazard cases 1 (ground shaking only) and 4 (ground shaking, liquefaction, and landslides). The loss estimates for the "ground shaking only" category is considerably lower than the values obtained from the data. Loss estimates considering all three hazards result in significantly larger values than those obtained from observation. The review of the data did not allow us to distinguish between the repair costs associated with different hazards. A problem that was identified from the data was that the repair costs also included other scheduled bridge modifications and upgrades, such as lane widening, that are not part of the seismic rehabilitation costs.

Table 3.30 Loss estimates of Loma Prieta 1989 earthquake by hazard case and by repair cost category

Repair Cost Category	Ground Shaking Only (1)	Ground Shaking + Liquefaction + Landslide (4)
Best Mean	$2,565,852	$102,430,444
Minimum	$922,283	$44,038,260
Maximum	$3,720,923	$161,708,552

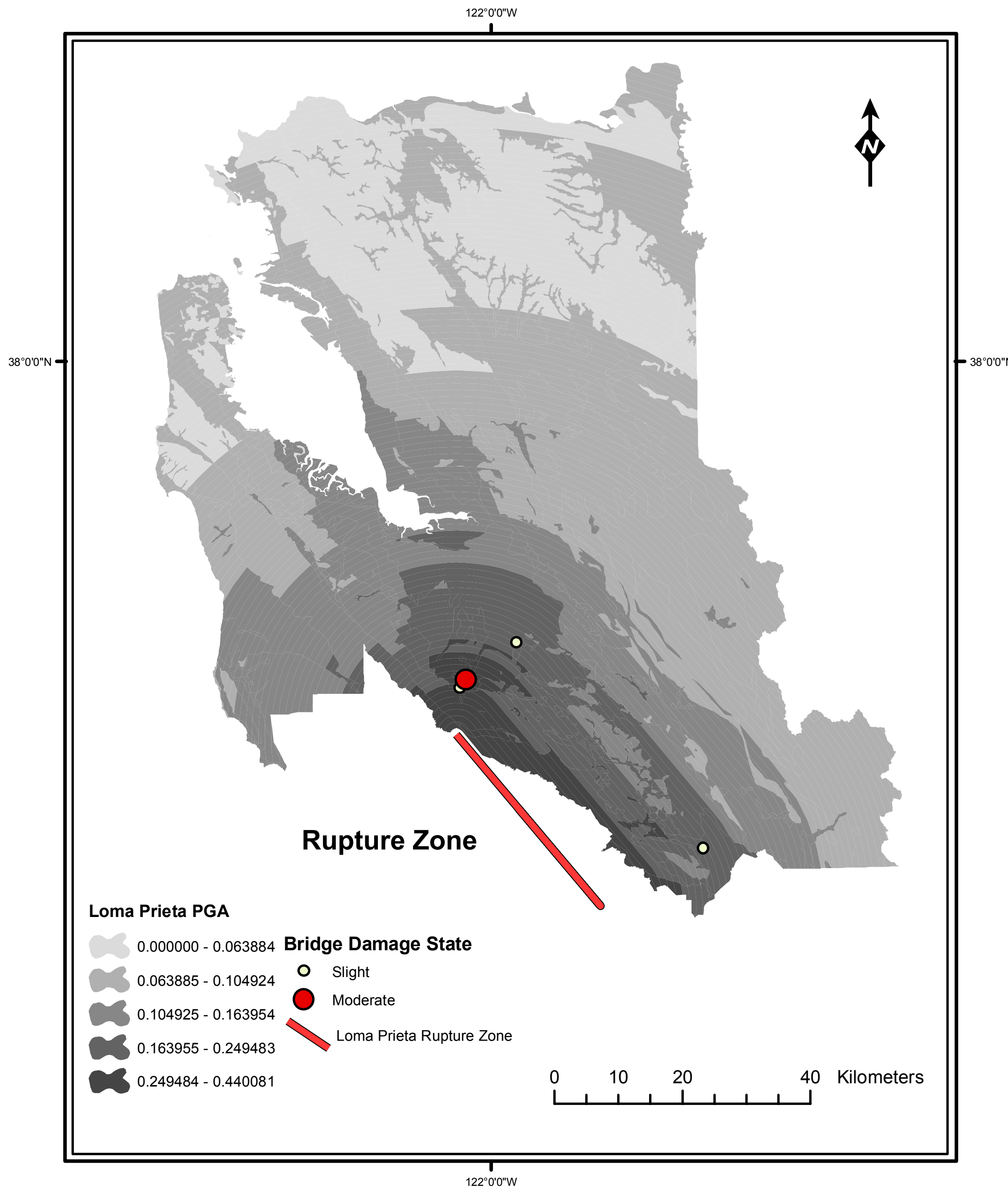

Fig. 3.29 Bridge locations by estimated damage state when only ground shaking is considered

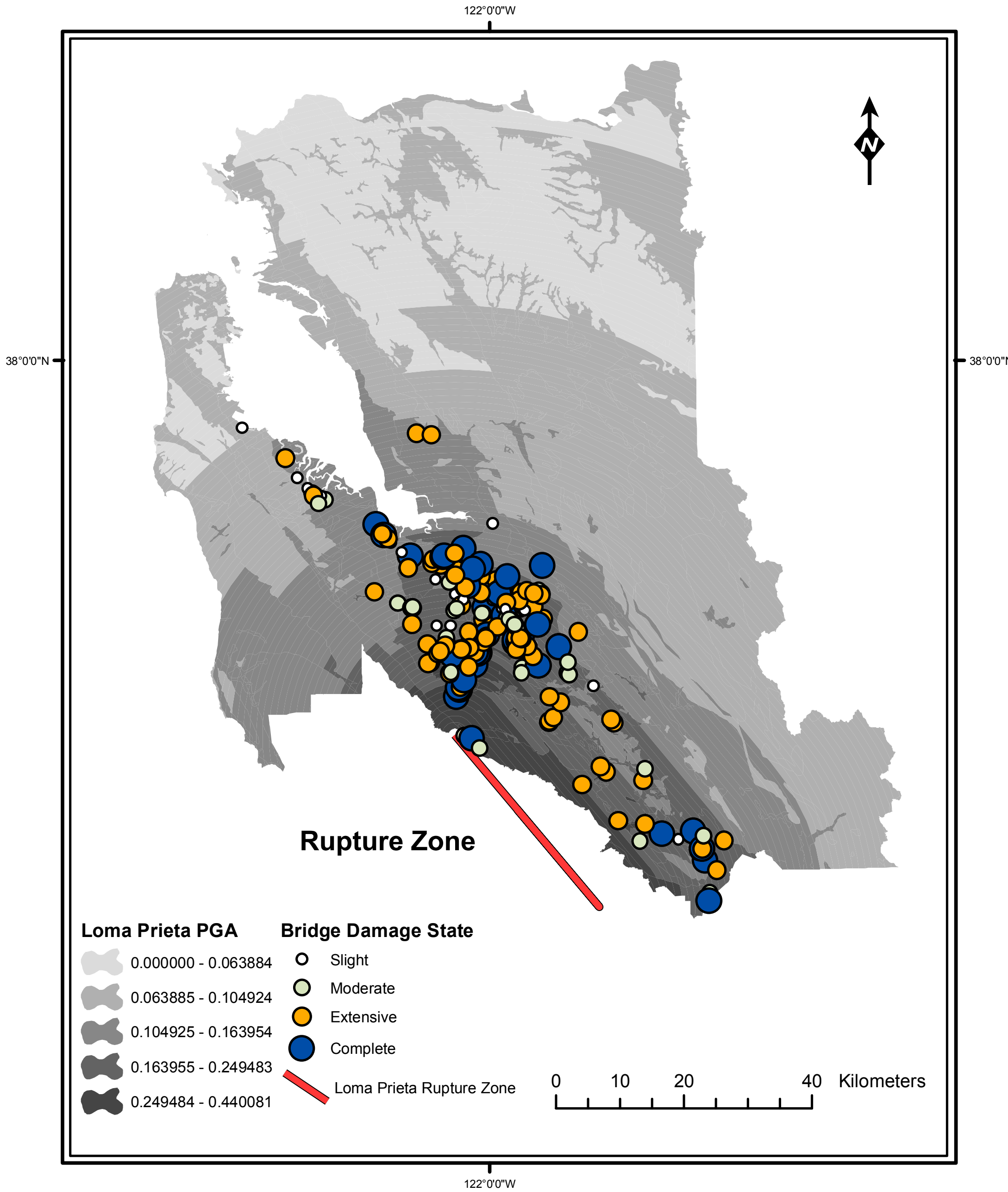

Fig. 3.30 Bridge locations by estimated damage state and when ground shaking, liquefaction, and landslide hazards are considered together

4 Emergency Response Network Analysis within GIS

4.1 BACKGROUND AND PROBLEM DEFINITION

Traffic routing is one of the many activities of emergency response planning and management, used both for purposes of pre-event preparedness and mitigation and post-event response and recovery. Finding the best routes for emergency response vehicles in emergency situations, such as after bridge closures due to damage from an earthquake, is challenging.

Highway network analysis for daily traffic routing, in general, has been intensively researched. Integration of highway network analysis in emergency response planning and management, however, is a more recent research topic. The use of GIS for seismic risk assessment has been widely accepted within the last decade. However, the use of GIS for highway network analysis for post-earthquake emergency response planning and management has been mostly limited to the display of road and bridge closures and alternative routes. Until now, network analysis itself has largely been performed outside of GIS, mainly due to the lack of compatibility between infrastructure inventory and detailed highway network data necessary for GIS-based network analysis. The few GIS applications that are available for post-earthquake traffic routing have been developed for demonstration purposes or are in a prototype stage. Most of these applications, if not all, need to translate a highway network database to a non-GIS platform, in which the graph theory-based operations are performed. Usually the non-GIS platforms require a cumbersome definition of connectivity between network components, such as nodes and arcs (Hobeika, 1987; Werner et al., 2000). The applications have not integrated the automatic creation of the network database. In general, building a highway network suitable for routing applications is very time consuming, and many of the commercially available products, used for daily traffic routing, are created through the labor of an intense and continuous workforce collecting and manipulating data. After a major earthquake, it is almost impossible to create a detailed highway network database fast enough to facilitate emergency response management. Therefore, it is essential to incorporate a value-added highway network database to any practical emergency response application.

This research centered on the development of T-RoutER, a GIS-based traffic-routing application for emergency response planning and management used to determine the best routes for traffic before and after bridge closures due to earthquakes. The application utilizes a commercially available highway network database and can be used after an earthquake (or after any other disaster, such as hurricane, flood, and fire) to assist in determining alternative detours on a near real-time basis.

The following sections present the use of GIS for network analysis, the highway network data necessary for network analysis, and the T-RoutER application developed in this research project. The components of T-RoutER, automation and customization in GIS and the issues related to linking detailed highway network data with Caltrans bridge data are also discussed.

4.2 NETWORK ANALYSIS IN GIS — METHODOLOGY

Earthquake emergency response planning and management requires information on the infrastructure inventory, configuration of the highway network system, and pre-event and post-event status of the network system. These data are usually acquired from a state transportation agency. Especially in recent years, the departments of transportation of many states have recognized the importance of sharing data among different divisions of their departments. These agencies have moved toward a common platform, namely Geographic Information Systems (GIS), for collecting, maintaining and analyzing infrastructure, highway network and traffic data (GIS-T, 2002, TRB, 2002). Employing a common platform, such as GIS, ensures consistency and expedites the process of combining different data sources.

The detail of road network database maintained by different states varies from all public roads to no network database (Fig. 4.1). As a state government agency, the California Department of Transportation (Caltrans) maintains GIS-compatible data for the state's major highways only. The surface streets are considered to be under the jurisdiction of local government agencies. Therefore, the limited traffic-routing information that Caltrans does maintain for surface streets is not integrated with their major highway databases. Without integration of arterial streets, traffic routing will be limited to major highways. Several of the states, including California, are interested in developing surface street layers. In the absence of such a database, a commercially available street-level database can fulfill the need.

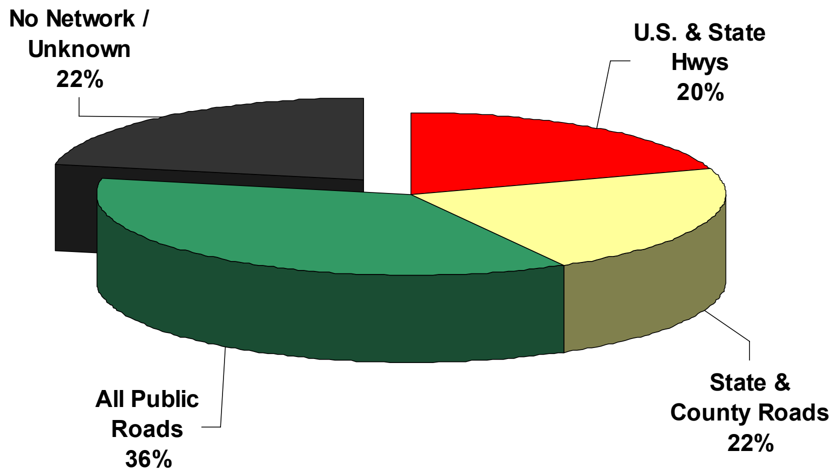

Fig. 4.1 Road network database maintained by state DOTs (GIS-T, 2002)

4.2.1 Defining Fundamental Properties of the Highway Network System in GIS

Traffic models demand large amounts of data, including the configuration of the highway network, zone-data and trip matrices. GIS is a natural tool for handling most of these data, as it can ease the work process by spatially integrating otherwise disparate data. A GIS can incorporate the highway network's descriptive information for nodes and arcs with the information on the topological relationship among the nodes and arcs, based on graph theory (Fig. 4.2). A node describes the location at which two or more lines connect and the endpoints of each line. An arc is a set of ordered coordinates that represent the shape of linear geographic features such as contours, county boundaries, streams, or roads. An arc is synonymous with a line (AGI, 1999). Nodes and arcs can carry information about their position within the topology of a network. The topology defines the spatial relationship (i.e., the connectivity and adjacency) between features, such as roads and travel destination points. For example, the topology of a line includes its from- and to-nodes, and its left and right polygons. Arc-node topology supports the definition of linear features and analysis functions such as network tracing.

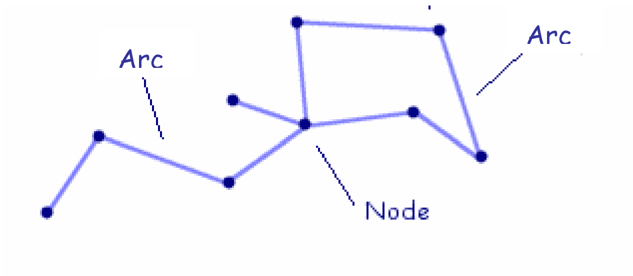

Fig. 4.2 A generic description of highway network in GIS

A GIS-based routing program uses a logical highway network as an index for referencing the actual feature geometry of the roads. A logical network contains information about the topology (connectivity of a network) rather than information about the geometry of the features. A logical network is useful in GIS because many spatial modeling operations do not require geographic co-ordinates; topological information is sufficient. For example, to find an optimal path between two points requires a list of the lines or arcs that connect to each other and the cost to traverse each line in each direction. Geographical coordinates are needed only for drawing the path after it is calculated. Storage of the logical network allows for fast retrieval of features in the GIS (AGI, 1999).

4.2.2 Analyzing the Highway Network in GIS — Shortest Path

Network analysis engines in GIS are available to determine the shortest path, fastest path, or closest facilities to a selected point. These network analysis engines use the well-known Dijkstra's shortest path algorithm (Ahuja et al., 1993), where, in general, the roadways, bridges and tunnels are modeled as arcs, and intersections and origin-destination points are defined as nodes. The shortest path algorithm does not take into account the effects of multiple flows in the network; hence the amount of flow on an arc is not a function of all routes that use that route. The travel time or the distance traveled are used as the impedance factors[1] for the arcs. Miller and Shaw (2001) provide a more detailed discussion on shortest path algorithms for the interested reader.

[1] Impedance is the amount of resistance (or cost) required to traverse a line from its origin node to its destination node or to make a turn (i.e., move from one arc through a node onto another arc). Resistance may be a measure of travel distance, time or speed of travel times the length. Impedance is used in network routing and allocation. An optimum path in a network is the path of least resistance (or lowest impedance).

4.2.3 T-RoutER — Traffic Routing for Emergency Response

T-RoutER is a GIS-based traffic-routing application for emergency response planning and management, used to determine the best routes for traffic before and after bridge closures due to earthquakes. Immediately after an event, the status of the damaged highway network can be estimated either based on predictive risk models (such as the one demonstrated in this project) or from data collected by field specialists, including emergency personnel and Caltrans bridge inspectors. After an event the ground motion levels as reported by the USGS ShakeMap can be used as the input for the damage estimate.

4.2.3.1 Components of T-RoutER — Data and Software

The components of T-RoutER and the underlying GIS environment are discussed below.

Roadway Network Database: T-RoutER uses a commercially available GIS-based highway network database developed by TeleAtlas, formerly known as ETAK (TeleAtlas, 2001). The main reason for using a commercially available highway network database is to include street level network data in order to achieve realistic traffic routing after bridge or roadway closures. When routing emergency vehicles, a detailed and accurate street database including information on the topology of the network and the network flow is necessary to find the shortest and fastest paths. After an earthquake, major highways may not be passable due to bridge and/or roadway damage, and arterial streets become critical to maintaining network flow. Modeling a network with only the interstate and state highways for post-event routing applications does not provide realistic routing information, since more often than not, arterial streets are used in re-routing traffic after a major earthquake.

Other commercial street databases that were considered for this project required constructing the logical network. This time-consuming step would be necessary not only for pre-event highway network configuration but also after any change made to an arc's traffic flow capacity in order to model bridge closures due to earthquake-induced failure. For large networks, such as the nine counties of the San Francisco Bay Area, this process takes longer than would be acceptable for near-real-time applications. However, TeleAtlas street data include a built-in logical network, which speeds up the process of post-event highway network configuration within GIS. TeleAtlas also provides a robust selection of descriptive attributes that facilitate realistic routing solutions (Table 4.1).

Each bridge and road segment is represented as an arc in this database. In order to determine which arc corresponds to a specific bridge from the Caltrans database, it is necessary to develop a tedious matching algorithm (Section 4.2.6 below).

Table 4.1 TeleAtlas database — attributes used for routing

Attribute Name	Full Name
ID	Transportation Element Identification: • Road Element Identification • Ferry Connection Element Identification • Address Area Boundary Element Identification
Name	Official Street Name
RouteNum	Blank: Not applicable (Multiple values are separated by "/.")
Meters	Feature Length (in meters)
FRC	Functional Road Class: -1: Not applicable (FEATTYP 4165) 0: Main Road: Motorways 1: Roads not belonging to "Main Road" major importance 2: Other Major Roads 3: Secondary Roads 4: Local Connecting Roads 5: Local Roads of High Importance 6: Local Roads 7: Local Roads of Minor Importance 8: Others
FOW	Form of Way: -1: Not applicable 1: Part of Motorway 2: Part of Multi Carriageway which is not a Motorway 3: Part of a Single Carriageway – Default 4: Part of a Roundabout 6: Part of an ETA: Parking Place 8: Part of an ETA: Unstructured Traffic Square 10: Part of a Slip Road 11: Part of a Service Road 12: Entrance / Exit to / from a Car Park 14: Part of a Pedestrian Zone 15: Part of a Walkway 17: Special Traffic Figures 20: Road for Authorities
SLIPRD	0: No Slip Road – Default 1: Parallel Road 2: Slip Road of a Grade Separate Crossing 3: Slip Road of a Crossing At Grade

Table 4.1—*continued*

Attribute Name	Full Name
FREEWAY	0: No Part of Freeway – Default 1: Part of Freeway
ONEWAY	Direction of Traffic Flow: Blank: Open in Both Directions – Default TF: Open in Negative Direction FT: Open in positive Direction N: Closed in Both Direction
F_LEVEL	Begin Level: 0: default (Range: -9 to +9)
T_ELEV	End Level: 0: default (Range: -9 to +9)
KPH	Speed Limit
MINUTES	Travel Time
RTEDIR	Route Direction (Multiple values are separated by "/"): Blank: Not applicable Direction + | + Route Directional Text where Direction is: FT: Route Directional in the Positive Direction TF: Route Directional in the Negative Direction

Caltrans Bridge Inventory: Bridges damaged in an earthquake can cause disruptions in the traffic flow and hence are critical components of the highway network system. A bridge database with a comprehensive series of attributes, such as the bridge identification features, latitude and longitude, structural characteristics, and traffic flow is among the key components for post-earthquake traffic routing. The most up-to-date Caltrans bridge database is used in this research project.

GIS Platform: T-RoutER is developed within ArcView 3.2 [2]. ArcView 3.2 has its own integrated object-oriented programming (OOP) language, Avenue, and has a number of built-in tools that allow visualization, and query and analysis of geographic data. ArcView does not have an integrated capability for routing analysis. However, the Network Analyst (NA) extension for ArcView includes advanced tools that can be accessed through Avenue scripts, allowing delivery of sophisticated network analysis applications. The NA extension can find the most direct route between two locations and generate detailed directions across the route. T-RoutER builds on the capabilities of the NA to expand the single-origin single-destination computations to multiple-origin multiple-destination analysis. The ArcView environment was chosen because

[2] ArcView 3.2 is a product of ESRI, Inc.

it is a product of the predominant GIS software manufacturer, ESRI, used by most highway transportation management organizations for other data and operations management.

A Routing Algorithm: The routing module uses the "find closest facility" procedure included in the ArcView Network Analyst, which is based on the Dijkstra's shortest path algorithm (ESRI, 1998). The main benefit of using the procedure included in the ArcView Network Analyst is that updating of the logical network after changing an arc is achieved very quickly, making it possible to use the application for near-real-time situations.

4.2.4 Application in GIS — Automation and Customization

The ArcView application window is customized to accommodate the needs of the project (see Fig. 4.3):

- Application buttons are added to load themes, such as bridge inventory, origin-destination points, ground motion levels experienced from a selected event and damaged bridges (determined either by field inspection or by seismic bridge vulnerability models).
- Pull-down menu for performing pre-event and post-event network analysis. In the post-event network analysis, links that represent damaged bridges are automatically selected and closed to traffic. The logical network is then modified to register the closed links and the network analysis is performed using the modified network.

Fig. 4.3 Customized ArcView application UI

The application buttons and the pull-down menu make T-RoutER very easy to use and allow users to input their own data sources. Step by step instructions to run T-RoutER to determine pre- and post-event routes for a set of origin-destination points are outlined below.

4.2.5 Steps for Using T-RoutER

1. Open the ArcView 3.2 customized project.
2. In the project window, click on the Inventory icon 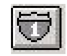 to load bridge inventory shapefile.
3. Click on the “Highway & Bridges” view window.
4. Turn on the origin and destination themes[3].
5. Make the origin theme active and zoom into the active theme .

Pre-event Routing

1. Run pre-event routing analysis (from the Routing pull down menu, select Pre-Event Routing). A series of dialog boxes will appear.
2. Open the attribute table for the street network
3. Select the origin point theme.
4. Select the destination theme.
5. Select a cost unit to use in the shortest path algorithm (select the minutes field to get the fastest path).
6. Select the cost (minutes) used for writing out directions.
7. Select the units (minutes) used for writing out directions.
8. The analyses will produce as many paths as the number of origin-destination pairs. Each origin-destination route combination will appear as a new layer in the table of contents. For example, if the theme includes six hospitals and it is selected both as origin and destination, the routing analyses will produce 30 layers.
9. In order to compile all (or any number of) paths with origin-destination information and the travel time in a single table and GIS layer (shapefile), click on the Combine Tables icon 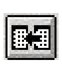 - select all the pertinent paths from the list of shapefiles. You can look at the attribute table that is generated to see a list of the origin-destination IDs, names and travel times.

Post-Event Routing

1. Click on the Load Shaking Map icon  – select the shaking map shapefile. The ground motion levels can be based on either scenario analysis or observed ground-

[3] The point themes representing origin and destination areas is necessary for routing analysis.

shaking levels downloaded in GIS format from the USGS website, ShakeMap. http://www.trinet.org/shake/

2. Click on the Load Damaged Bridges icon  — select the shape file for damaged bridges.
3. Assign bridge damage to the bridge links in the roadway layer.
4. Run post-event routing analysis (from the Routing pull down menu, select Post-Event Routing).
5. Select the origin point theme.
6. Select the destination theme.
7. Select a cost unit to use in the shortest path algorithm (select the minutes field to get the fastest path).
8. Select the cost (minutes) used for writing out directions.
9. Select the units (minutes) used for writing out directions.
10. Each origin destination route combination will appear as a layer in the table of contents.
11. The analyses will produce as many paths as the number of distinct origin-destination pairs. Each origin-destination route combination will appear as a new layer in the table of contents. For example, if the theme includes six hospitals and it is selected both as origin and destination, the routing analyses will produce 30 layers.
12. In order to compile all (or any number of) paths with origin-destination information and the travel time in a single table and GIS layer (shapefile), click on the Combine Tables icon 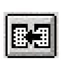 — select all the pertinent paths from the list of shapefiles. You can look at the attribute table that is generated to see a list of the origin-destination ids, names and travel times.

Output

The following are the main output files of the application

- Route lines between selected origin-destination points before and after closure of bridges.
- Directions for each route (pre-event or post-event).
- Time (or distance) to travel for each origin-destination point (also exported as a table).

4.2.6 Connecting the Bridge Database and the Highway Network

The bridge structural information from the Caltrans database and the routing information from TeleAtlas database are both essential for T-RoutER to predict the performance of each bridge during an earthquake, simulate closure of bridges, and create alternate driving routes. Caltrans uses a linear referencing system to identify features along their highways, including bridges. All of the small and large bridges, ramps and connections, as point features, are referenced by their postmiles. In the TeleAtlas highway network, only links representing major bridges, such as the San Francisco-Oakland Bay Bridge, are designated as bridges. Dynamic segmentation, the placement of point and line features along a linear network in GIS, requires a linear referencing system such as Caltrans's postmile method. One can attach descriptive information (such as speed limit and direction) to a road segment, by referencing its beginning and ending distances from the starting point of each highway route. Due to limited routing information in the Caltrans highway network, another network database was needed for TroutER. None of the detailed commercial street databases, including TeleAtlas, use the postmile referencing system. In order to provide access to both databases, bridge point features from one database must be linked to bridge line features from the other. Combining features from these two databases is not a simple, automatic process. In many cases, displaying the bridge coverage upon the highway network demonstrates that the two layers do not overlay (see Fig. 4.4). For routing analysis, the bridges must be a topologically connected part of the street network. Spatially joining (or snapping) the bridge features (as points) to the nearest arcs in the highway network database frequently results in erroneous matches. Using a different approach, matching bridges through a common attribute also proves to be quite challenging, but provides a potentially less error prone method. An algorithm was developed to determine the arcs in the TeleAtlas database that represent the bridges from the Caltrans database.

The algorithm works by comparing attributes such as name, route number, county, and type from each database. The inference rules and the attributes used from each database are listed in Table 4.2. If an inference rule is satisfied, the *bridgeID* from the Caltrans database is assigned to the corresponding TeleAtlas *linkID*. The Caltrans *bridgeID* is then used to determine the network functionality level based on the expected damage state. The expected damage state for a bridge can either be estimated from a vulnerability assessment or based on damage data collected from the field. For emergency response purposes, bridges with moderate damage or worse are closed to traffic. That is, the links corresponding to these bridges are made impassable, and the logical network topology is updated to represent the damaged highway network.

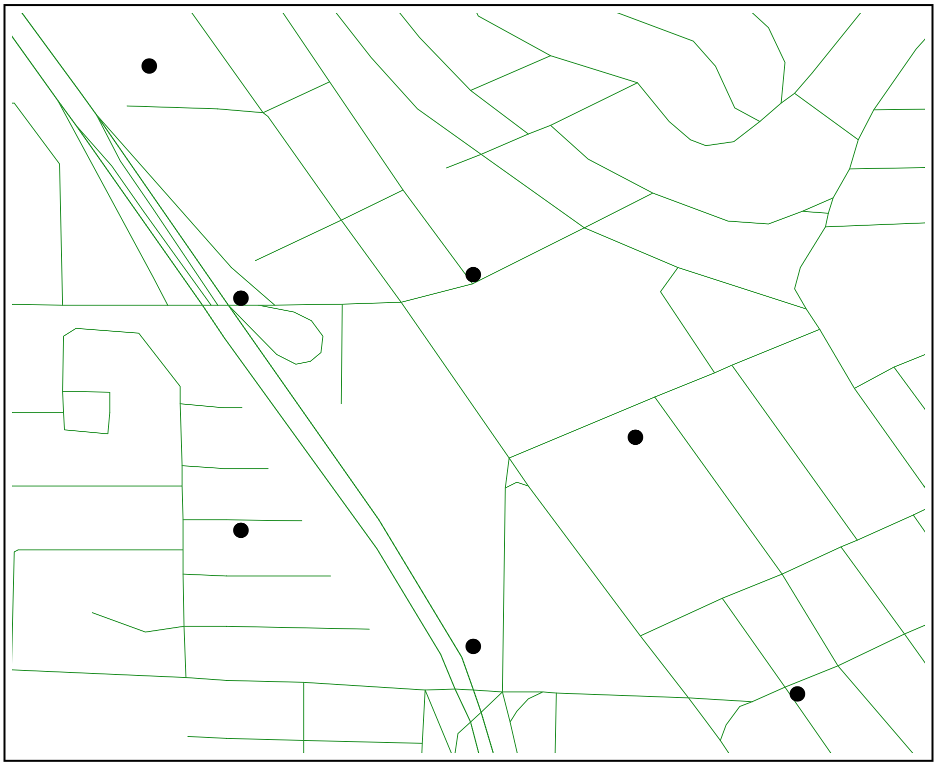

Fig. 4.4 Points do not align with the street segments from the TeleAtlas Highway database

The success of the matching algorithm is highly dependent upon the naming conventions used in the two databases. Sample naming conventions used in the TeleAtlas "Name" field are listed in Table 4.3. In addition, Caltrans uses a standardized naming convention for bridges within its database; for overcrossings, underpasses, and overheads, the abbreviations OC, UP, and OH, respectively, are used. The most challenging items to match from the two databases are separators, ramps, and bridges over creeks. The TeleAtlas database does not include attributes, such as route number or ramp name, to identify the structures designated as ramps in the Caltrans database. Furthermore, the TeleAtlas database does not distinguish bridges over creeks.

With over 4000 bridges in the San Francisco Bay Area, the amount of time required to validate the algorithm for matching the Caltrans database to TeleAtlas network links is extensive. Yet, the process needs to be performed only once for each bridge, and the benefits of having the integrated information outweigh the potential costs. The automation methods developed in this research can be used as a major stepping-stone toward accomplishing this goal.

Table 4.2 Attributes used in matching Caltrans point bridge data to TeleAtlas line data

Attribute in Caltrans Bridge Database	**Attribute in TeleAtlas database**	**Notes**
Latitude, longitude		Used to select a set of links within a given radius – for most cases the bridges are within 0.15 mile of the corresponding link in the TeleAtlas database.
Bridge name	Name	Determine whether a bridge is an over-crossing (OC) an interstate highway, under-crossing (UC) a major interstate highway, separator / connector.
	FRC (functional road class)	Used together with name, determine the road that carries the bridge
Traffic Direction	One way	One-way or two-way traffic carried by the bridge (or the link)
	F_Level, T_level	Used together with one-way to determine the link that carries the bridge. For example, a link corresponding to an over-crossing bridge would need to have F_level = T_level = 1 and most of the time have two-way traffic.
Rte	RouteNum	The route number that the bridge (or the link) carries. Used with the FRC and the OC, UC information. For example if the bridge is UC, then the bridge is carried by a major roadway (hence FRC = 0) and the Rte carried by the bridge should match the Route carried by the link
	FOW, SLPRD	FOW = 10 and SLPRD = 1 or 2 or 3 indicates RAMP

Table 4.3 Abbreviations used in TeleAtlas database

Abbreviation	Description
Ave	Avenue
Blvd	Boulevard
Ct	Court
Dr	Drive
Hwy	Highway
Pkwy	Parkway
Rd	Road
St	Street

4.3 EMERGENCY RESPONSE SCENARIO

4.3.1 Case Study Area

In this case study, T-RoutER is used to determine alternate routes between multiple origins and destinations before and after a scenario event of moment magnitude 7.0 on the Hayward fault. The characteristics of the scenario event and the vulnerability assessment of bridges are discussed in Sections 3.1–3.3.

Alameda County was selected as the study area because the Hayward fault runs beneath several critical highway junctures. Hence, both building damage and bridge damage are expected to be high in this region following a magnitude 7.0 earthquake on the Hayward fault. Figure 4.5 shows the results of a building damage assessment calculated within HAZUS 99 (HAZUS, 1999). The darker colors show higher damage ratios by census block. The prevalence of these darkly colored areas, therefore, highlights the necessity for available and accessible critical facilities (e.g., hospitals) after such an event in this area.

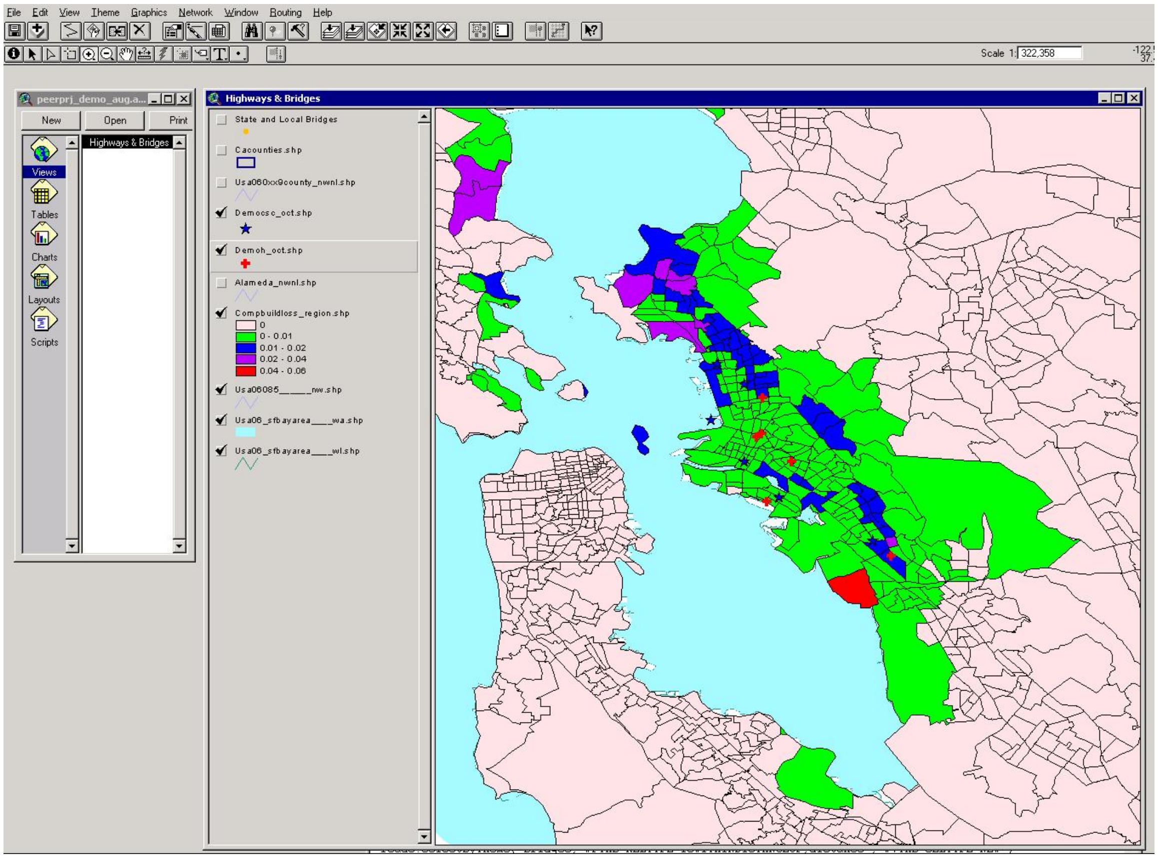

Fig. 4.5 Damage ratio for the default building inventory in Alameda County

4.3.2 T-RoutER in Action

4.3.2.1 Input

The following data sets were used as input for the case study:

Highway Network: TeleAtlas MultiNet Shapefile 4.0 road network data with built-in topology is used as the highway network. The highway network shapefiles for the ten counties of the San Francisco Bay Area were merged: Alameda, Contra Costa, Marin, Mendocino, Napa, San Francisco, San Mateo, Santa Clara, Solano, and Sonoma. The 10 county street-level network database consists of over 360,000 links. Each of these links represents a roadway with one of the functional classes listed in Table 4.4 (excerpted from Table 4.1 in Section 4.2.3.1).

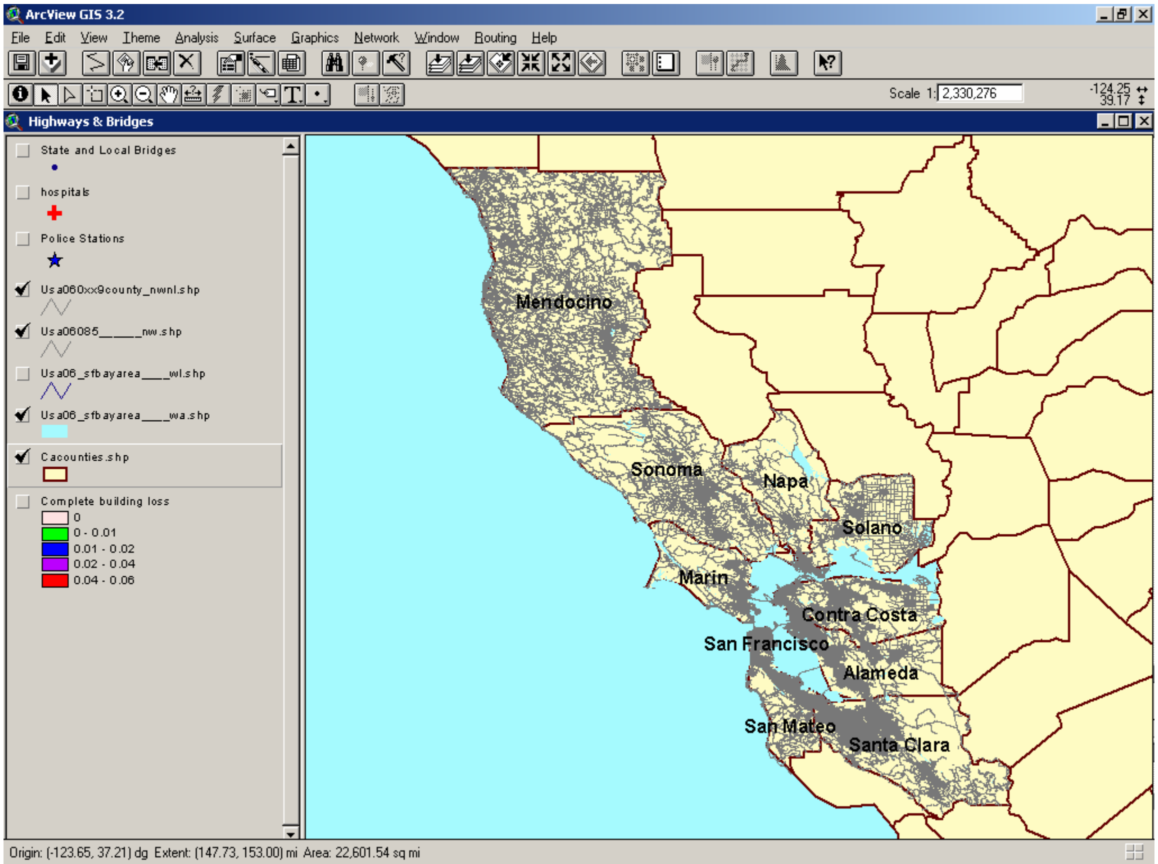

Fig. 4.6 Highway network data for the San Francisco Bay Area

Figure 4.6 shows the network database for the San Francisco Bay Area used in this case study. Traffic-routing analysis can be performed for any origin-destination pairs located in these 10 counties.

Bridge Inventory: Bridges in Alameda County are extracted from the Caltrans bridge inventory for the San Francisco Bay Area (Fig. 4.7). A total of 506 state bridges and 243 local bridges are located in Alameda County, and only the state bridges are considered in this case study.

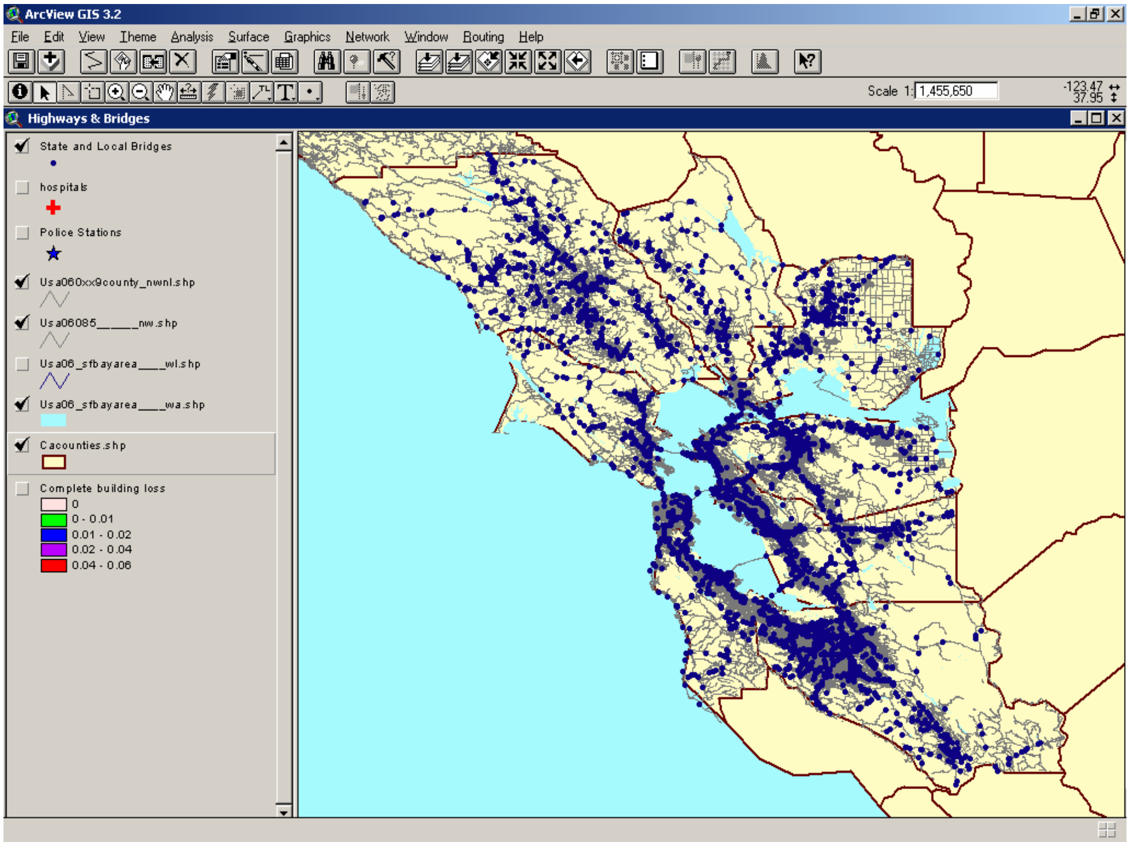

Fig. 4.7 Highway network overlaid with the state and local bridge inventory

Origin-Destination Points: For demonstration purposes, all the hospitals and critical facilities (police stations and city buildings) in Alameda County are selected as potential origin and destination points. Figure 4.8 shows the bridge inventory overlaid upon the highway network. Also shown in this figure are the sets of origin-destination points, i.e., the hospitals in Alameda County. Among these, six hospitals were selected as being in high demand after this event.

Table 4.4 TeleAtlas functional roadway classes

TeleAtlas (Functional Roadway Class)	Examples from the Study Area
Motorways / Main road	I-80
Main road / not major importance	Hwy 92
Other major roads	San Pablo Avenue, Ashby Avenue
Secondary roads	Grizzly Peak Boulevard, Arlington Avenue, Powell Street
Local connecting roads	23rd Avenue, 40th Street, Wild Cat Canyon Road
Local roads of high importance	Manzanita Drive, Oakdale Avenue, Warden Way
Local roads	Commerce Way, Sonoma Way
Local roads with minor importance	E 26th Street Way, Comstock Way

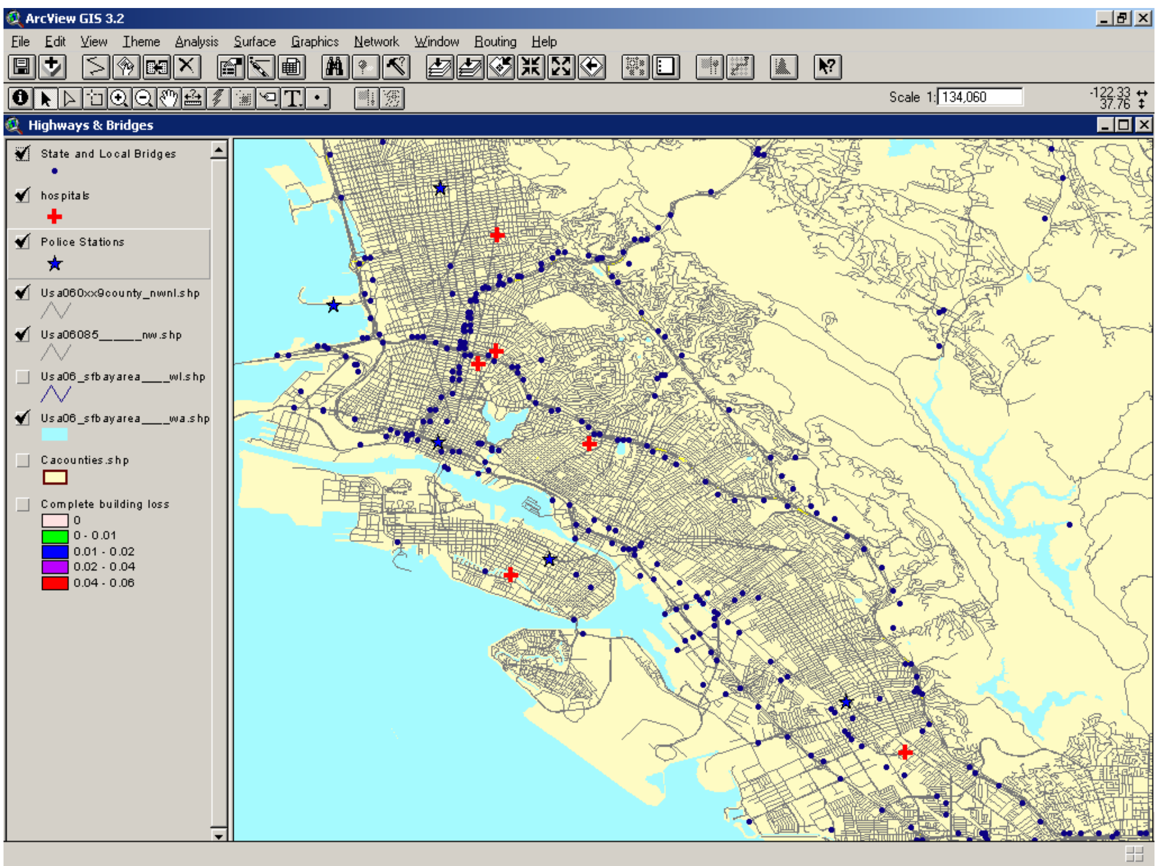

Fig. 4.8 Location of Alameda County hospitals and critical facilities with state and local bridges

Ground Shaking: As discussed in Section 3.1 the ground-shaking levels for all the four scenario events were calculated for each bridge using the Boore et al. (1997) attenuation function[4].

Damaged Bridge Database: Damage calculations are based on ground motion and bridge structural characteristics. The bridge inventory is then grouped by functionality level, and bridges with expected damage state 3 or higher (i.e., moderate damage, major damage and collapse) are assumed to be closed to traffic. As discussed in Sections 3.1–3.3, the seismic hazard analysis and the vulnerability assessment are carried out for the entire San Francisco Bay Area. However, for demonstration purposes, only bridges located in Alameda County are examined.

Waterway: The waterway boundaries (rivers, lakes, and Pacific Ocean) available in the TeleAtlas database are used for spatial reference.

4.3.2.2 Pre-Event Analyses

First, the bridge inventory for the area is loaded to T-RoutER by clicking on the Inventory icon  (Fig. 4.9).

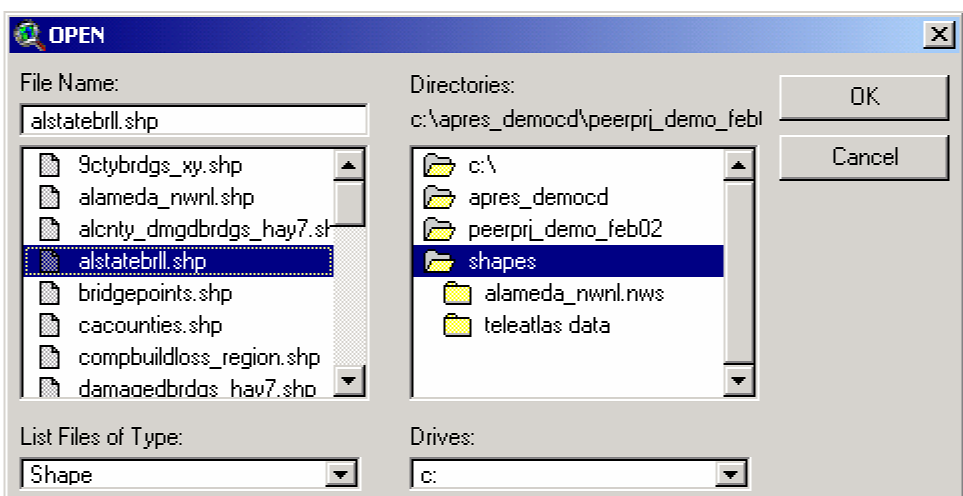

Fig. 4.9 Load inventory open file window

[4] Any other simulated ground shaking map can be used. For post-earthquake applications, ground shaking obtained from USGS ShakeMap can be used (http://www.trinet.org/shake/).

The routes among the selected origin-destinations are computed by selecting the *Pre-Event Routing* option under the Routing pull down menu shown in Figure 4.10. The highway network database, the origin destination sets and the cost unit to be used in the analysis are then selected via dialog boxes (Figs. 4.11–4.13).

Fig. 4.10 Routing pull-down menu

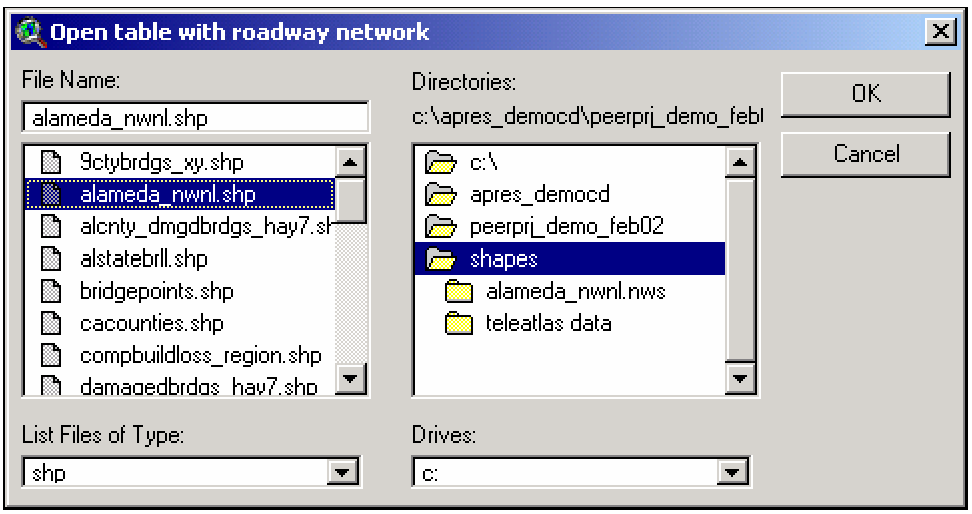

Fig. 4.11 Pop-up window for loading the highway network to be analyzed

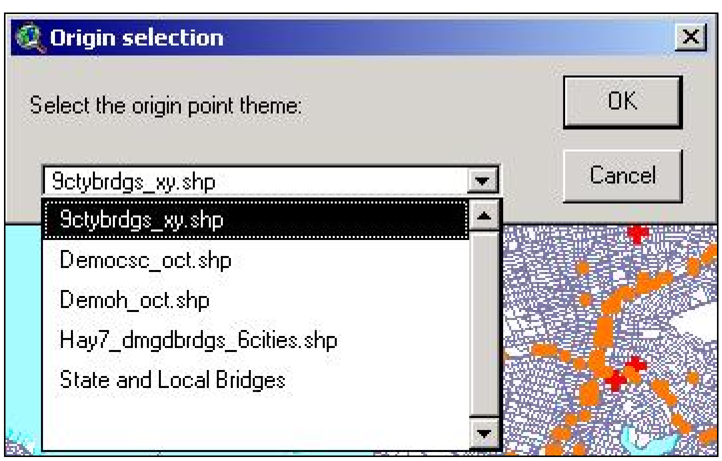

Fig. 4.12 Pop-up window for origin theme selection

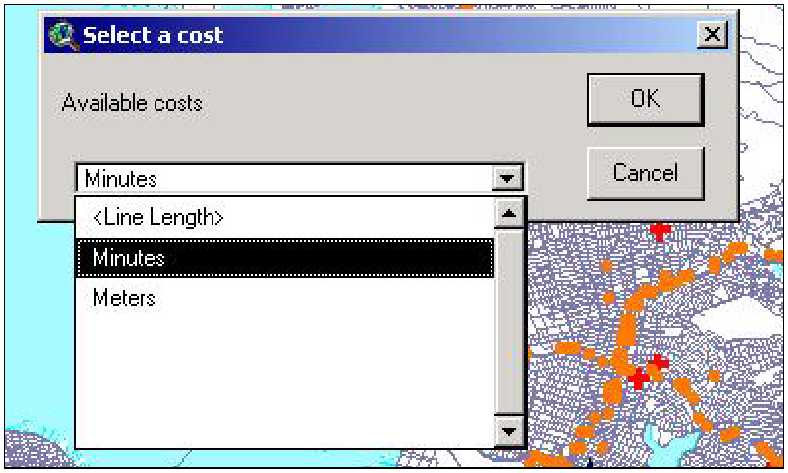

Fig. 4.13 Pop-up window for selecting cost unit for the path calculations

The pre-event routing calculates the fastest (or the shortest) path among all pairs. T-RoutER determines all the shortest paths among all origin-destination combinations in less than a minute (Fig. 4.14). The analyses produce paths for every combination of origin and destination. Each unique origin-destination route appears as a new layer in the table of contents. For example, for the six hospital origin-destination set, the routing analyses produce 30 layers.

The travel times[5] among the selected origin-destination points with no bridge closures are listed in Table 4.5. The table is obtained by clicking on the Combine Tables icon 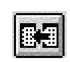 and selecting all the pertinent paths from the list of (new layer routes). The travel times are based on the free volume speed and distance of a link. The free volume speed of each link is based on its functional class as defined in Table 4.4.

[5] The cost of traveling a link can be measured in units of time, distance or even non-time/non-distance units, such as monetary units. In this demonstration project travel time (in minutes) and travel distance (in meters) are used as the cost unit. Each link may carry one-way or two-way traffic. Directional cost units can be used if it takes a different amount of time to travel along some streets in one direction as it does in the opposite direction.

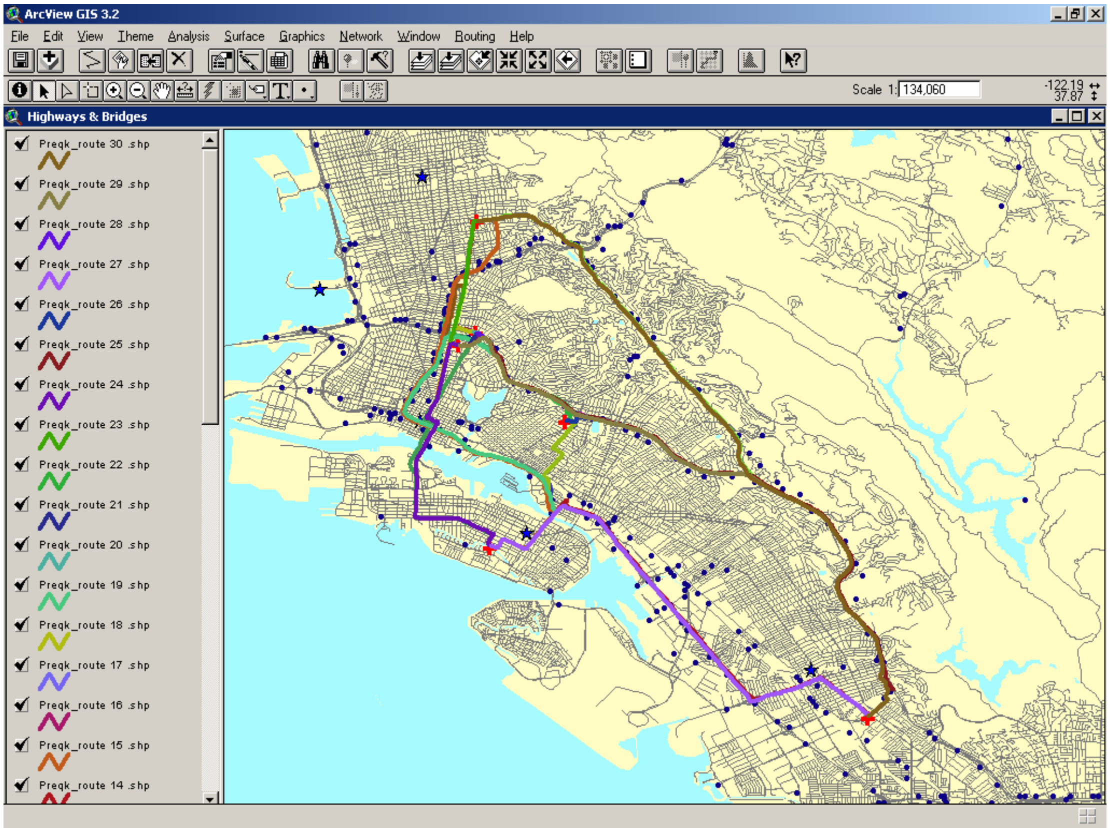

Fig. 4.14 Pre-event routes among selected origins and destinations

Table 4.5 Travel time between selected origins and destinations — pre-earthquake

Origin Label	Destination Label	Travel Time (min)
San Leandro Hospital	Alta Bates Medical Center	17
	Summit Medical Center	15
	Kaiser Permanente-Oakland	14
	Alameda Hospital	13
	Alameda County Med Center-High	12
Summit Medical Center	San Leandro Hospital	15
	Alameda Hospital	11
	Alta Bates Medical Center	6
	Alameda County Med Center-High	5
	Kaiser Permanente-Oakland	1
Kaiser Permanente-Oakland	San Leandro Hospital	14
	Alameda Hospital	11
	Alta Bates Medical Center	5
	Alameda County Med Center-High	5
	Summit Medical Center	1
Alameda Hospital	Alta Bates Medical Center	14
	San Leandro Hospital	13

Table 4.5—*continued*

Origin Label	Destination Label	Travel Time (min)
	Kaiser Permanente-Oakland	11
	Summit Medical Center	11
	Alameda County Med Center-High	9
Alta Bates Medical Center	San Leandro Hospital	16
	Alameda Hospital	14
	Alameda County Med Center-High	8
	Summit Medical Center	5
	Kaiser Permanente-Oakland	5
Alameda County Med Center-High	San Leandro Hospital	12
	Alameda Hospital	9
	Alta Bates Medical Center	8
	Summit Medical Center	5
	Kaiser Permanente-Oakland	4

4.3.2.3 Earthquake Event Simulation

In order to simulate routing traffic during post-earthquake emergency response, the ground motion map is loaded by clicking on the Load Shaking Map icon 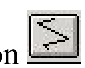 (Figs. 4.15–4.16).

Fig. 4.15 Load ground-shaking map theme

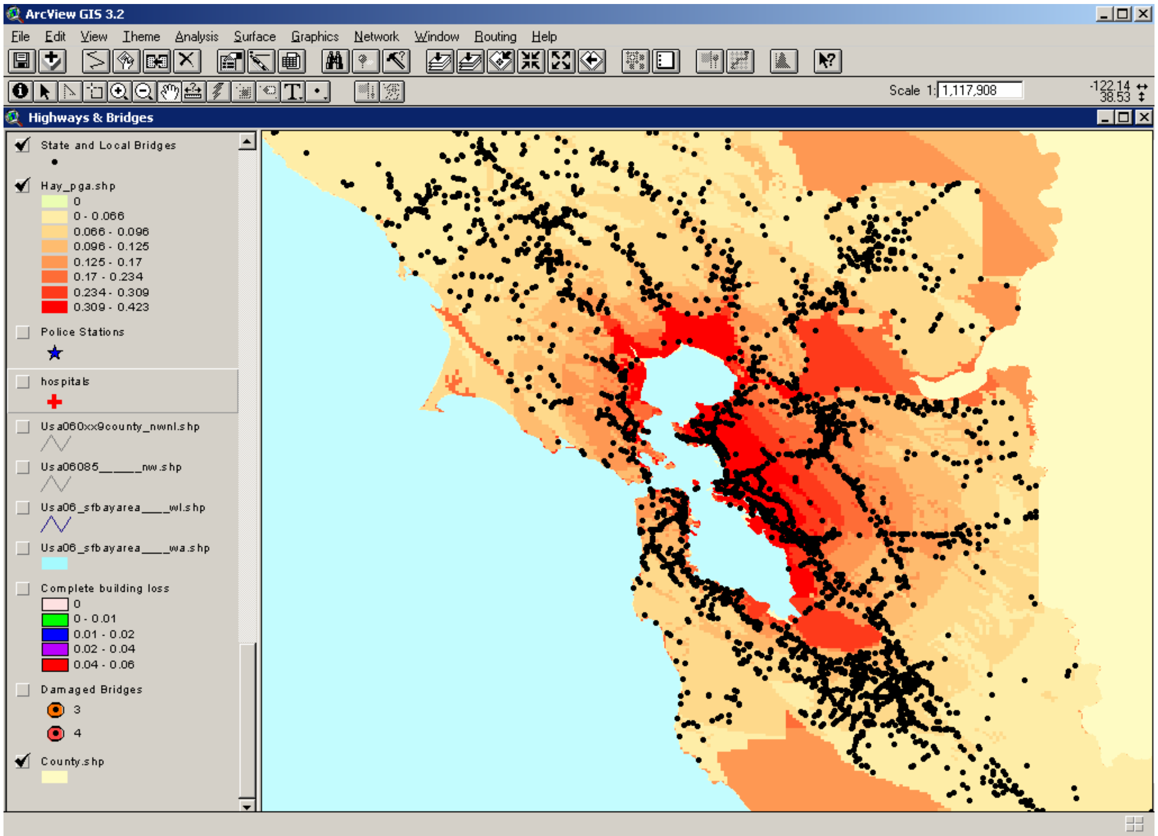

Fig. 4.16 State and local bridges overlaid on ground shaking (PGA) from a magnitude 7 event on the Hayward fault

Next, the damaged bridge map layer is loaded by clicking on the Load Damaged Bridges icon  and selecting the respective shapefile for damaged bridges (Fig. 4.17). Note that the damage calculations are performed outside of GIS but can easily be incorporated within TroutER by script programming. Then all bridges with a damage state of 3 or higher are joined to the corresponding link in the highway network database[6].

[6] For the reasons described in Section 2.4.5, the process of merging the highway network database with the Caltrans bridge database is not fully automated, hence for the study area, the brigdeIDs are manually assigned to links in the network database.

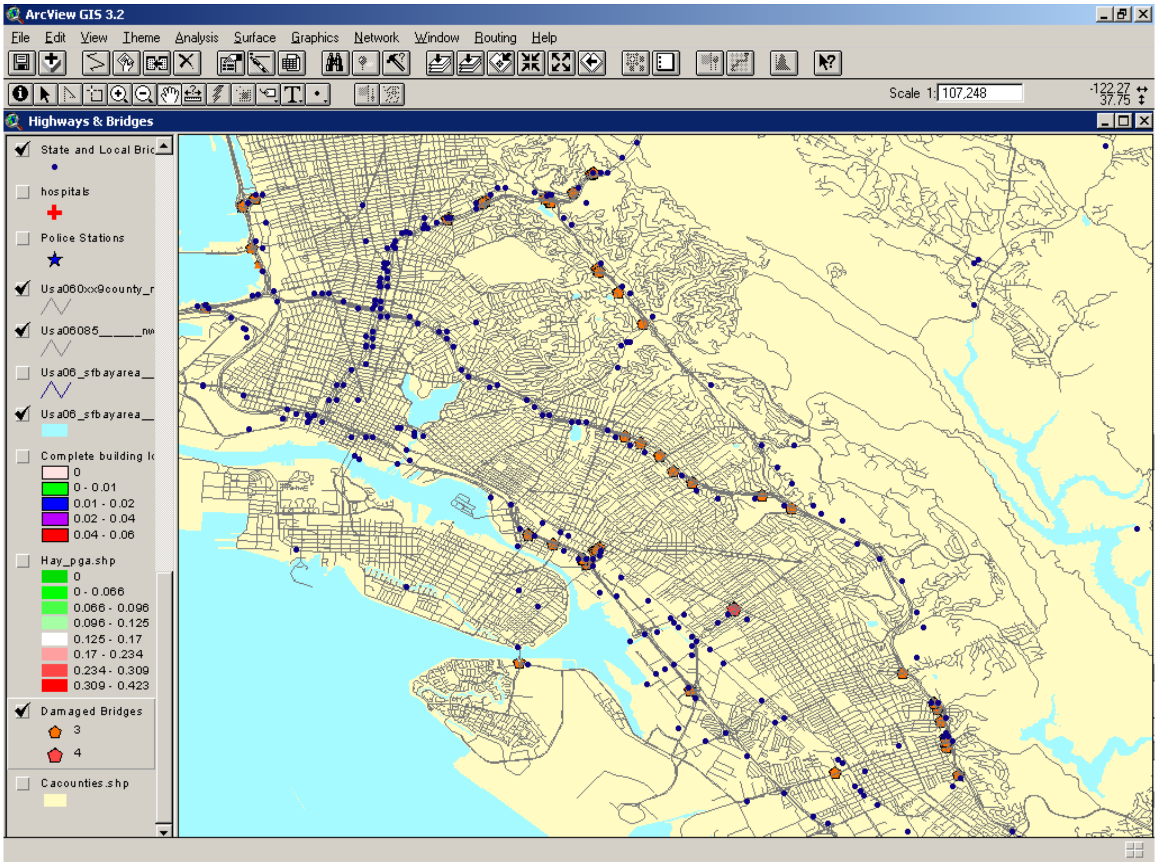

Fig. 4.17 State bridges damaged from a magnitude 7 event on the Hayward fault

4.3.2.4 Post-Event Routing

The routes among the selected origin-destinations are re-computed by selecting the *Post-Event Routing* option under the Routing pull down menu. The highway network database, the origin destination sets and the cost unit to be used in the analysis are then selected via dialog boxes. This process could be fully automated for pre-defined origins and destinations. Bridges that sustain moderate damage or worse are assumed to be inaccessible. The network topology is updated based on the damaged network (Fig. 4.18).

Figure 4.19 shows pre- and post-earthquake routes for two-origin destination pairs. The dashed lines depict the pre-event routes and the solid lines depict the post-event routes. Blue solid and dashed lines show the routes from San Leandro Hospital (SLH) to Alta Bates Medical Center (ABMC). The red solid and dashed lines show the routes from San Leandro Hospital to Summit Medical Center (SMC). Figures 4.20–4.21 show close-up views of the pre- and post-event routes at a location of bridge closures (highlighted in yellow). The areas circled in red delineate the locations of bridge closures. For example, the vehicles traveling on the freeway between SLH and ABMC after the event (shown in blue dashed line) had to take a short detour to bypass the bridge closure on the freeway, merging back with the pre-event route. However, the same bridge closures led to a different post-event route for the vehicles traveling from SLH to SMC.

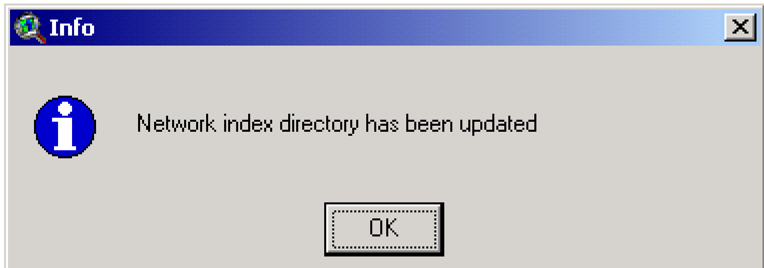

Fig. 4.18 Information dialog box after updating the network due to bridge closures

Table 4.6 lists the pre-event and post-event travel times for the selected origin-destination pairs. The effect of bridge closure is observed in the increased travel times. The origin destination pairs with increased travel time are highlighted in yellow.

Figure 4.22 shows pre- and post-earthquake routes for two-origin destination pairs as calculated based on the shortest distance. In contrast to the pre- and post-event routes calculated based on the fastest path, the shortest paths are not affected from bridge damage, as they mostly follow streets. The dashed blue line depicts the pre-event route from San Leandro Hospital (SLH) to Alta Bates Medical Center, and the dashed red line show the pre-event route from SLH to Summit Medical Center. The post-event route layers, which follow the same paths, are turned off in this scene.

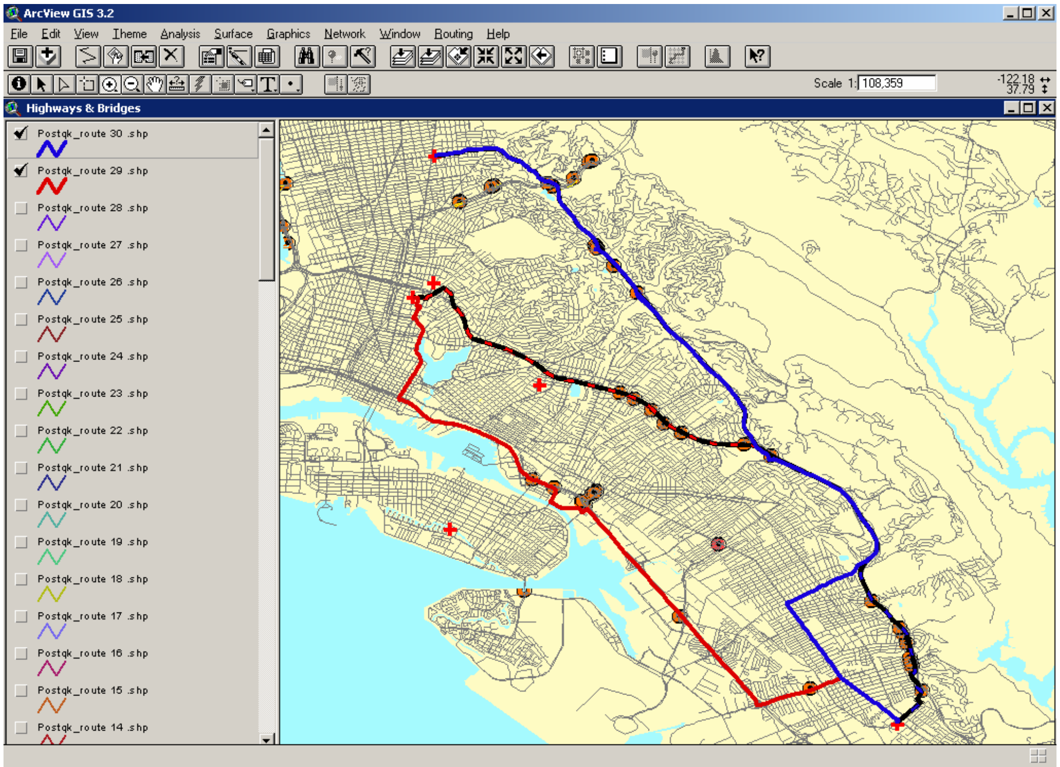

Fig. 4.19 Pre- and post-event routes between two selected origin–destination pairs (fastest path)

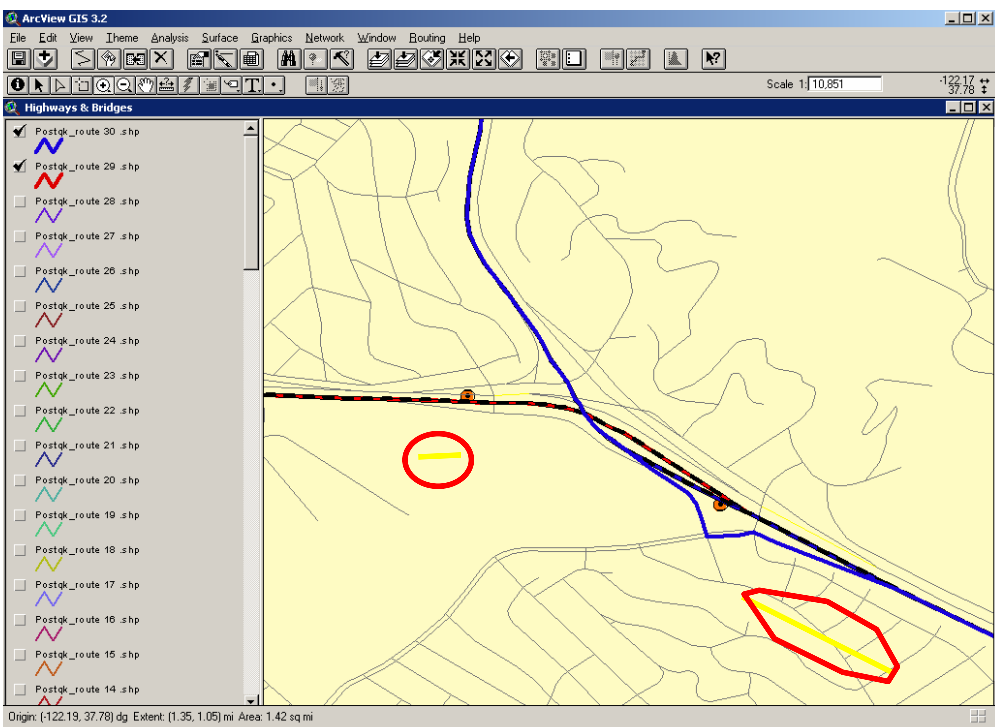

Fig. 4.20 Close-up view of the pre- and post-event routes between two selected origin – destination pairs

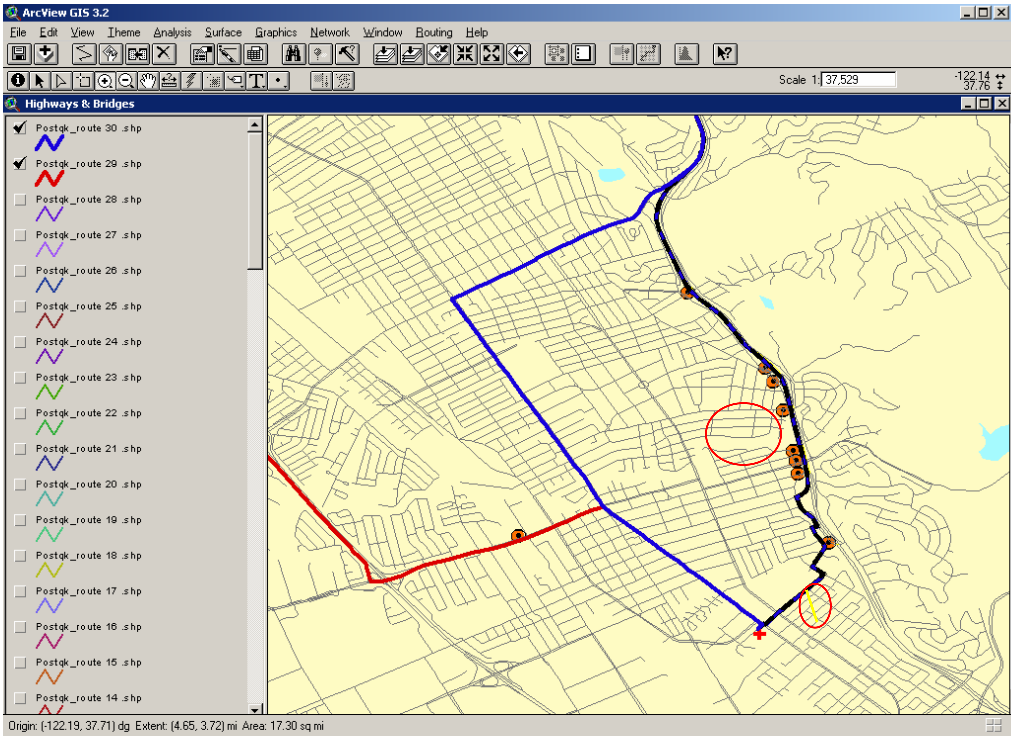

Fig. 4.21 Close-up view of the pre- and post-event routes between two selected origin – destination pairs

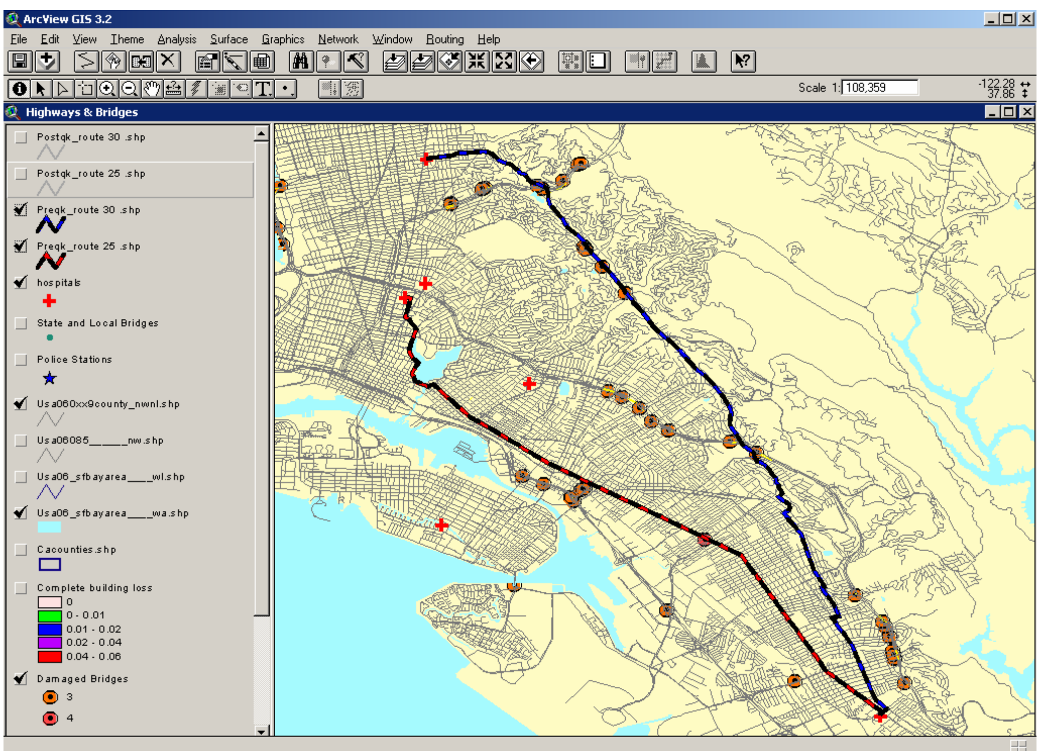

Fig. 4.22 Pre- and post-event routes between two selected origin–destination pairs (shortest path)

Table 4.6 Pre-event and post-event travel times for different origin-destination pairs

Origin Label	Destination Label	Pre-Event Travel Time (min)	Post-Event Travel Time (min)
San Leandro Hospital	Alta Bates Medical Center	17	20
	Summit Medical Center	15	18
	Kaiser Permanente Oakland	14	18
	Alameda Hospital	13	14
	Alameda County Med Center-High	12	15
Summit Medical Center	San Leandro Hospital	15	18
	Alameda Hospital	11	11
	Alta Bates Medical Center	6	6
	Alameda County Med Center-High	5	5
	Kaiser Permanente Oakland	1	1
Kaiser Permanente Oakland	San Leandro Hospital	14	18
	Alameda Hospital	11	11
	Alta Bates Medical Center	5	5
	Alameda County Med Center-High	5	5
	Summit Medical Center	1	1
Alameda Hospital	Alta Bates Medical Center	14	14
	San Leandro Hospital	13	14
	Kaiser Permanente Oakland	11	11
	Summit Medical Center	11	11
	Alameda County Med Center-High	9	9
Alta Bates Medical Center	San Leandro Hospital	16	21
	Alameda Hospital	14	14
	Alameda County Med Center-High	8	8
	Summit Medical Center	5	5
	Kaiser Permanente Oakland	5	5
Alameda County Med Center-High	San Leandro Hospital	12	15
	Alameda Hospital	9	9
	Alta Bates Medical Center	8	8
	Summit Medical Center	5	5
	Kaiser Permanente Oakland	4	4

5 Conclusion

5.1 NETWORK COMPONENT SYSTEMS SEISMIC RISK ASSESSMENT

A general framework for risk assessment of a transportation network was formulated and an example application was presented. It is important to note that although the methodology was developed for earthquake hazards, the same framework can be used for other hazards such as hurricanes, tornadoes, floods, blast, and fires. In such applications, the hazard characterization will change. For earthquake events, the methodology considers ground shaking, liquefaction, and landslide occurrences. Fault displacements that may affect roads or bridges were not included. The hazard assessment components follow well-known hazard analysis methods and rely on application tools developed in HAZUS (1999).

A transportation network analysis method was developed to enable assessment of travel delay times and travel link unavailability under various commuter demand conditions such as fixed- and variable- post-event demands. A non-survey method was developed to estimate freight trips, which is a considerable improvement over the survey approach in that it relies on other regional statistics (e.g., commodity flow, employment, and other statistics) than surveys. Algorithms were developed for trip generation for freight and commuter travel that use inter-regional and intra-regional trip data. A cost model was also developed for freight travel value and was adjusted to MTC truck count, capacity, and commodity flow by economic sectors.

The risk to the transportation system was expressed in terms of loss to physical components of the network, such as bridges, and the loss of functionality of the network. Physical losses represented by repair costs of damaged bridges and functional network losses are expressed in terms of loss of connectivity for specified origin-destination (O-D) paths, travel delay times between O-Ds or reduction in trip making. Network analysis models were developed under the assumption of fixed travel demand and variable travel demand. In the fixed travel demand model, the demand on the system remains constant after an earthquake. With the variable travel demand, demand on the system decreases and the cost of travel increases. Two closure criteria were assumed for the post-event traffic patterns. Closure Criterion 1 corresponds to the risk adverse case where bridges in damage state 3, moderate damage, have zero capacity. Closure Criterion 2 corresponds to the risk tolerant case, where bridges in damage state 3 have their capacity reduced by 50%. Bridges in damage states 4 and 5 are closed in both criteria.

The methodology formulated in this project was applied to five counties in the San Francisco Bay Area. The four scenarios considered include 7.0 and 7.5 earthquakes on the Hayward fault and 8.0 and 8.5 events on the San Andreas fault. These four scenario earthquakes were selected because they correspond to the largest possible events that can occur in the region with significant probabilities of occurrence. For example, the 7.5 Hayward and the 8.0 San Andreas faults earthquakes each have approximately a 10% chance of occurrence in the next 27 years (USGS, 2003b).

- ***Database Generation:*** Several databases were collected for the application and these were integrated in the demonstration of the methodology. The following are the databases used in the study:
  - A bridge inventory database containing information on the location and physical characteristics of bridges in the five study counties; the database was provided by Caltrans and contains 2640 bridges
  - Local soil condition map provided by USGS (2000) that was used to develop soil categories for use in ground motion estimation
  - Liquefaction susceptibility map provided by USGS (2000)
  - Landslide susceptibility map provided by USGS (1997)
  - The San Francisco Bay Area highway network model consisting of 1,120 zones and 26,904 links defined by 10,647 nodes using geographic coordinates. Trip demands are for 1998 based on a 1990 MTC household surveys.
  - Inter-regional and intra-regional freight movement data for trip generation used in freight traffic network analysis. The resulting database is for freight traffic trips in the study region.

A significant component of this project was the verification, cleansing, and merging of these data into coherent, comprehensive databases. Merging the bridge and network link databases posed a particular problem because of their inconsistent formats, and thus a considerable effort was expanded on developing a unified network database that contains both types of information. Other databases, such as soil classification, liquefaction potential and landslide potential were already available in GIS format and were readily utilized. The freight data were tested against other economic indicators for verification purposes. These databases will be used in subsequent studies by PEER researchers and can be made available to other researchers. They have also been made available to Caltrans for future use.

Based on the analysis of the San Francisco Bay Area risk assessment the following observations can be made:

- ***Ground motion effects:*** The ground motions for the different scenario events range from 0g to 1.2g. A significant number of bridges is likely to be subjected to accelerations greater than 0.4g (a value used in most seismic designs). There are 288 bridges for HW7.0, 928 bridges for HW7.5, 648 bridges for SA7.5, and 1,128 bridges for SA8.0 scenarios that fall into that category. In general, more bridges are subjected to higher accelerations with the San Andreas earthquakes than with the Hayward earthquakes.
- ***Ground deformation effects:*** The ground displacements at liquefiable bridge sites are estimated to range from 0″ to 250″. The majority of bridges fall within the category of 0″ to 25″ horizontal displacements; however for scenario earthquakes *HW7.5* and *SA8.0,* more than 1000 bridges are estimated to have ground deformations larger than 25″. Most of the deformations are due to liquefaction. The number of bridges that appear to be subjected to liquefaction appears to be rather excessive, but further investigation was not within the time frame of this project. It would be desirable to review all bridge sites that are currently determined to have liquefied based on our analysis and to confirm that conclusion through independent evaluations. Such an evaluation would require that local soil data be available for examination. At the time of the writing of this report, such data were not available for the large number of bridge sites investigated in this study.
- ***Vulnerability assessment of pre-retrofitted bridges:*** Table 3.11 presents the distribution of damage to bridges to each of the scenario earthquakes when subjected to ground shaking, liquefaction, and landslides. More than half the bridges in the inventory appear to be in moderate to complete damage states (damage states 3–5) for the *HW7.5, SA7.5,* and *SA8.0* scenario earthquakes. This would imply that close to or more than half of the bridges may need to be closed following these events. When only ground shaking is considered in the analysis, the number of bridges in the moderate to complete damage states decrease significantly. For example, the number of bridges in damage state 3 or greater for *SA8.0*

changes from 1,765 to 903 when all site hazards and only ground shaking are included (see Table 3.13). Liquefaction alone causes significant damage (damage state 3 or greater) to 1,764 bridges with the *SA8.0* event.

- ***Loss estimates from bridge damage:*** Loss estimates from *pre-retrofitted bridge* damage were obtained for mean, minimum, and maximum replacement cost estimates. These losses are the main contributors to the direct loss estimates to the system. The losses are largest for the moment magnitude 8.0 scenario earthquake on the San Andreas fault and they range from approximately \$0.6B from ground-shaking hazard alone to a \$1.5B from all hazards when the replacement cost is taken at its best mean value.

Table 5.1 Estimated losses (in \$x1,000) for ground-shaking hazard only; liquefaction hazard only and for ground shaking, liquefaction, and landslide hazards combined*

	Scenario Events	Ground Shaking Only (1)	Liquefaction Only (5)	Ground Shaking + Liquefaction + Landslide (4)
Best Mean	***HW7.0***	\$77,360	\$455,893	\$475,119
	HW7.5	\$283,150	\$1,039,951	\$1,093,745
	SA7.5	\$285,434	\$882,901	\$970,270
	SA8.0	\$634,299	\$1,482,278	\$1,539,517

* From Table 3.27

Table 5.1 summarizes the losses obtained from for the different scenario events, the ground shaking only, liquefaction only, and all hazard computations. The losses are dominated by liquefaction damage. As discussed in Chapter 3, the liquefaction model is rather simplistic and does not account for any soil remediation that may have been performed during the time of construction. Similarly, the liquefaction susceptibility categories are too generic and may not reflect the actual conditions at the site of a bridge. Thus, it is recommended that additional investigations be performed in subsequent studies to develop more realistic estimates.

Repair costs used in the analysis can vary because of the type of bridge, its location and the design characteristics. The mean, minimum and maximum repair costs used represent the range of variability that can be expected with bridge construction. Table 5.2 presents the mean, minimum, and maximum loss estimates for the 8.0 San Andreas scenario earthquake. This corresponds to the worst case scenario for the study region. Again the loss is significantly higher when all hazards are considered than when only ground shaking is used in the analysis, with liquefaction dominating the losses. The loss from all hazards is almost three times higher than the loss from ground shaking.

Clearly, more detailed analysis is required to obtain estimates that are not so highly varied. This will require improved hazard models particularly for liquefaction and landslide potential forecasting, ground deformation estimation, and damage estimation from all ground effects. Similarly more reliable estimates are needed for the replacement costs in order to narrow the range of repair costs.

Table 5.2 Estimated losses for different repair costs for ground shaking and all hazards for the San Andreas scenario 8.0 earthquake (*SA8.0*)*. (Estimates in $x1000)

Repair Cost Category	Ground Shaking Only (1)	Ground Shaking + Liquefaction + Landslide (4)
Best Mean	$634,299	$1,539,517
Minimum	$349,450	$981,734
Maximum	$1,247,827	$3,301,859

*From Table 3.27

- ***Damage and loss estimates for "what-if" retrofit analysis:*** At the time of writing of this report no fragility functions were available for retrofitted bridges. Thus, a simple analysis was performed to estimate the effect of retrofitting on the overall loss estimates. The analysis considers bridges with 5%, 10%, and 20% increases in earthquake resistance capacity. As expected, the loss reduction is most significant for ground shaking, since the resistance capacity is increased only to lateral deformation in the columns of bridges.

  The losses are reduced by about 25% when bridge capacity is increased by 20% uniformly for all bridges in the network. Table 5.3 summarizes the losses for the San Andreas 8.0 scenario for the 20% increase in bridge earthquake lateral displacement capacity. There is only a marginal decrease in the loss when liquefaction and landslides are included. In order to achieve a reduction in loss from liquefaction and landslides, the bridge resistance to lateral spreading and settlement need to be reduced either through site remediation and foundation modifications (e.g., include pile foundation when not present) to resist such movement.

Table 5.3 Loss estimates (in $x1000) for the San Andreas 8.0 (SA8.0) scenario earthquake for increased bridge capacity*

	Retrofitting Cases	Ground Shaking Only (1)	Ground Shaking + Liquefaction + Landslide (4)
Best Mean	No-Retrofit	$634,299	$1,539,517
	γ =20%	$483,310	$1,467,954

*From Table 3.28

- ***Loma Prieta 1989 earthquake comparison results:*** In order to compare the damage and loss estimates to actual observations, damage and loss statistics were obtained from the 1989 Loma Prieta earthquake in the San Francisco Bay Area. The fault rupture for that event was modeled, and damage and loss estimates were obtained using the methodology described in this report. Table 5.4 summarizes the damage estimates from this research and those reported by the post-earthquake investigative teams from Caltrans. It was not possible to make realistic comparisons because the damage state definitions used by Caltrans to gather damage data from the earthquake were different then those used in this study. Furthermore, the damage was not divided by hazard type, and the effort to obtain additional information to identify actual liquefied sites was beyond the scope of this study.

Table 5.4 Comparison of reported and estimated damage for the Loma Prieta 1989 earthquake*

Damage States	Ground Shaking Only (1)	Ground Shaking + Liquefaction + Landslide (4)	Reported Damage States	Reported Damage
1	2635	2390		
2 and 3	5	102	**Minor**	113
4 and 5	0	148	**Major**	4
Total Damaged Bridges*	5	250	**Total Damaged Bridges**	117
Total Bridges	2640	2640	**Total Bridges**	2640

*From Table 3.29

There are more than twice as many bridges predicted damaged than actually observed with the majority of both due to liquefaction. Even if all the bridges reported damaged were damaged from liquefaction, the methodology clearly overestimates the damage, particularly for liquefaction hazard. It is doubtful that a more detailed investigation of the available data will provide more realistic results. However, improvement of the liquefaction methodology presented in this report can certainly provide results that are closer to the observed damage.

- ***Network performance under fixed post-earthquake demand:***

  Under the assumption of fixed post-earthquake demand, analysis of the San Francisco Bay Area network for the scenario earthquakes results in unrealistically congested links. Table 5.5 summarizes the number of links with a v/c ratio greater than 1. This large share of unrealistically large v/c ratio produces meaninglessly inflated link travel time estimates.

Table 5.5 Post-earthquake share of over-saturated (v/c > 1) links given fixed travel demand

Link Conditions	**Scenario**		
	Baseline	**HW701**	**HW751**
Number of links for which v/c > 1	252	6449	7018
Number of open links	26904	24720	23856
Share of links with v/c > 1	1%	26%	29%

A comparison of total vehicle hours of travel for the pre-event baseline and the two earthquake scenarios was provided in Table 3.20 and is given below in Table 5.6. While conventional network analysis can accommodate links with v/c ratios greater than 1, this approach fails in applications of post-earthquake network analysis because capacity losses are system-wide. Predicted link travel times are enormous for those links with unrealistically large v/c ratios. Consequently, these delay estimates are not valid. In addition to the problem of assigning link flow in great excess of capacity, the fixed-demand trip assignment model is not able to treat travel demand between isolated zone pairs. Closure of damaged links may cause a loss of connectivity in the network, and it may become infeasible to travel between some zone pairs. This model was not pursued further because it provides unrealistic results.

Table 5.6 Summary of total vehicle hours by link type, fixed travel demand (hours)*

Facility Type	Scenario		
	Baseline	HW701	HW751
Freeway to Freeway Connectors	6,668	287,472	22,99,946
Freeways	223,765	6,095,856	20,894,450
Expressways	33,162	15,234,488	107,516,757
Collectors	47,156	Not computable[a]	Not computable
On/off Ramps	14,552	23,684,218	Not computable
Centroid Connectors	107	185	190
Major Roads	149,692	Not computable	16,00,994,720
Metered Ramps	1,805	4,863,005	66,869,964
Golden Gate Bridge	1,959	9,512,223	1,4399,025
Total	478,866	Not computable	Not computable

* Extracted from Table 3.20
a. The travel time estimate exceeds the maximum value computable by the software used to estimate user equilibrium flows.

- ***Network performance with variable post earthquake demand:***

  In order to overcome the limitations of the fixed-demand model, a variable-demand assignment model was formulated and implemented in this project. Because of its computational complexity, travel time was the only argument considered in the demand function between a given O-D pair. Application of the variable-demand model resulted in fewer v/c ratios greater than 1 as summarized in Table 5.7. Vehicle travel times, shown in Table 5.8, decreased for both Criterion 1 and 2 for most types of network links and for system-wide travel. However, the decrease, as shown only for the Hayward 7.5, the San Andreas 8.0, and the Loma Prieta 1989 earthquake scenarios, is due to the decrease in available links and fewer trip assignments to the network after an event.

Table 5.7 Summary of v/c-ratios given for variable travel demand and two different bridge closure criteria

Scenario	Baseline	HW751	HW752	SA801	SA802	LP691	LP692
System-wide Average v/c	0.23	0.17	0.17	0.16	0.16	0.23	0.23
System-wide Max v/c	1.40	1.46	1.46	1.52	1.51	1.42	1.40

Table 5.8 Summary of total vehicle hours of travel by link type, variable travel demand model*

Facility Type	Baseline	HW751	HW752	SA801	SA802	LP691	LP692
Freeway to Freeway Ramps	5,775	2,461	2,046	982	802	5,615	5,386
Freeways	161,826	46,953	43,009	34,675	32,720	142,236	137,787
Expressways	30,026	14,112	13,693	10320	10,184	26,377	25,223
Collectors	41,677	40,214	39,933	41,628	41,408	41,509	41,879
On/off Ramps	15,256	9,710	8,492	7,675	7,556	16,499	16,378
Centroid Connectors	105	27	22	32	31	104	104
Major Roads	133,471	110,821	110,337	99,931	98,163	137,074	138,289
Metered Ramps	2,126	1,247	1,215	570	540	2,175	1,975
Golden Gate Bridge	524	502	502	475	466	522	521
System-wide Total	390,788	226,048	219,250	196,288	191,871	372,111	367,542

*From Table 3.24

The cost associated with trips forgone with the reduced travel demand following an earthquake was accounted for through a model that captures the opportunity cost of these trips. The cost for commuter and freight trips were modeled separately and the results are summarized in Table 5.9. These analyses were performed for the two-hour A.M. peak traffic. From this table it can be observed that, although freight traffic has lower vehicle hour delays, the costs associated with them are two orders of magnitude larger than those for commuter traffic. These costs will need to be evaluated over the time that it takes the bridge to be repaired. This will require that the network analysis be performed repeatedly over the repair time of the last bridge in the network. In addition, the network analysis will need to dynamically change the available links as bridges are repaired. Such an analysis is beyond the scope of the current study.

Table 5.9 Delay and opportunity cost in two earthquake scenarios, two-hour A.M. peak period*

Scenario	Delay (Vehicle Hours)		Opportunity Cost ($)	
	Auto trips[a]	Freight trips	Auto trips[b]	Freight trips
HW701	240,038	19,463	5,696,653	222,529,873
HW751	207,404	16,817	6,716,551	279,880,290

Note: a. Automobiles account for 92.5% of the total Caltrans District 4 vehicle counts.
b. This assumes an average vehicle occupancy (AVO) of 1.0. This is conservative because the baseline AVO exceeds 1.0 and would likely increase following an earthquake.
* From Table 3.25

- ***T-RoutER emergency response software and demonstration:*** An algorithm was developed that provides information on the fastest available paths following an earthquake. The fastest path is defined as the path with the shortest travel time. A key feature of the algorithm is that it considers routes between multiple origins and multiple destinations. Furthermore, street level information is included for more realistic routing of emergency vehicles. The software assumes that bridges in damage state 4 or greater are closed, while those in damage states 2 or 3 are still open only for emergency vehicle use. Vehicle routing is made under the assumption that bridges and roads are available and not congested due to traffic. The software is developed with the GIS ARC/INFO to enable easy integration of information from the traffic analysis, earthquake damage scenarios to bridges and other damaged structures, identify locations of critical facilities such as hospitals, fire and police stations. While significant improvements are required to make this software deployable by emergency personnel, it serves an example of potential developments that need to be pursued to facilitate rapid response in major disasters.

6 Extensions

6.1 KEY OUTSTANDING ISSUES

A number of areas, related to this project but beyond its scope, would be of significant value for future investigation. Part of the goal for this project was to carry out seismic hazard and vulnerability estimates and the overall impact of such hazards on transportation systems. In the process, however, key shortcomings were highlighted about the methodology and assumptions used. Further investigation to lessen the limitations described in this section would provide a greater level of accuracy in this type of analysis.

Hazard analysis for various parameters that have not been taken into consideration here would be of value for accuracy in future analysis. Within the context of this project, two of these parameters would include quantitative measures for ground settlement from liquefaction and quantitative measures for lateral spreading. Further study to include consideration of near-field motions (fling effect) and the influence of directivity in hazard analysis would add additional depth to the current scope of earthquake hazard analysis.

For current vulnerability analysis, there are a number of items that when considered or included would provide a more accurate estimate of damage. Damage definitions used in this project are not directly related to physical damage. Damage states that define observable damage for bridge systems, and a more detailed classification methodology for bridges would provide a higher level of accuracy. Additionally, the analysis would benefit from improved definitions of functionality for different damage states, and greater accuracy and level of detail of bridge inventories. From the analytical aspect, a more refined analysis can be achieved by improving fragility functions, applying a unique fragility function for retrofitted bridges, and applying fragility functions that capture the ground deformation from liquefaction, landslides, and fault rupture more adequately. Estimates of repair times, as well as the relationship between bridge repairs and actual loss, would enhance vulnerability analysis. However such information is either assumed or overlooked in the current methodology.

In the aftermath of a major hazard event, a consequence analysis would be of interest to carry out for the sake of defining certain relationships and strategies for the future. Knowing how the costs and travel time delays relate to the travel path would give investigators better ability to develop some functional relationships of how the hazard impacts costs. Further study into a benefit-cost analysis for identifying highest risk links, paths, and other critical junctures would provide information to investigators about user preferences and how to route in order to optimize flows. Related to this would be optimizing retrofit strategies development. The timely completion of repairs under limited resources would pose additional questions about the economic losses incurred in terms of costs and travel time delays.

6.2 DECISION SUPPORT FOR HIGHWAY SYSTEMS

The most important measures of performance in the context of a highway system include total delay, total vehicle miles of travel, and total person miles of travel. The work completed to date links earthquake damage to transportation structures to transportation network performance at a metropolitan scale. This modeling capability is an important step in developing performance-based earthquake engineering procedures for highway systems, but what is most needed now to make seismic risk analysis for highways a more effective tool for decision makers in terms of pre-event planning and post-event response?

The logical first step in using this kind of model to develop new decision support tools is to predict system performance following an earthquake. Post-event, the benefits of any feasible reconstruction sequence can then be computed from the corresponding sequence of improvements in system performance. Total net benefits are determined by comparing the benefits delivered by this sequence of improvements to the cost of reconstruction. In contrast, pre-event decisions, such as evaluating retrofit options, is much more difficult because of the uncertainty of earthquakes.

In any event, it is important to move past a default modeling perspective that relies on trial and error as a means of searching for alternatives. Scenarios are useful, but the real advantage provided by this approach will flow from framing the relevant decisions as an appropriate optimization problem. This is rightfully an optimization context: Retrofit and reconstruction resources are small relative to needs. The costs to be avoided are very large.

6.2.1 Network Design Problem

One way to approach this research challenge is to treat retrofit and reconstruction decisions as a large-scale transportation network design problem. This is a difficult class of problems. Conventional approaches to these problems combine mathematical programming with bi-level control or implicit enumeration techniques. Following a major earthquake, the feasible set of reconstruction sequences is likely to be too large to be tractable. Consequently, even these well-investigated techniques may be difficult to apply to in combination with large, metropolitan area models.

6.2.1.1 Deterministic Network Design

The deterministic transportation network design problem (LeBlanc 1973) focuses on optimal link addition. Subject to budget (and possibly other) constraints, and fixed demand for travel, the objective is to find the transportation network configuration on which user equilibrium flows produce the least total congestion. The fact that travelers compete rather than cooperate in the way they select routes greatly complicates even this deterministic version of the problem, which is typically formulated as an embedded optimization problem with a bi-level structure. The upper level is a decision by the network authority, represented in the standard formulation as the addition of capacity. The lower level, a function of the upper level decision, is the decision by the network user, represented in the standard formulation as a route decision.

Explicit enumeration, i.e., trial and error investigation of all feasible alternatives, would be a prohibitively expensive way to solve even a modestly sized problem. Post-event network reconstruction problems are large-scale network design problems, and there is much to be gained in terms of system performance from prioritizing and sequencing post-event reconstruction projects.

In the case of an implicit enumeration (branch and bound) approach, a nonlinear programming problem is solved at each node in a branch and bound tree. Given link-specific reconstruction or retrofit projects $U = \{u_1, \ldots, u_m\}$, and existing (or remaining) links indexed i =

m+1, …, n, LeBlanc's (1973) standard formulation for the deterministic network design problem is as follows.

$$\text{Min } T(x^*) = \sum_{i=1}^{n} T_i(x_i^*) = T[\arg\min \sum_{i=1}^{n} \int_0^{\sum_{s=1}^{p} x_i^s} t_i(w)\, dw] \tag{6.1}$$

subject to

$$\sum_{i=1}^{m} c_i \cdot u_i \le B \tag{6.2}$$

$$\sum_{s=1}^{p} x_i^s \le M \cdot u_i \qquad \text{for all i = 1, …, m} \tag{6.3}$$

$$\sum_{s=1}^{p} x_k^s \le M \cdot (1 - u_i) \tag{6.4}$$

for all k and i such that project i improves link k

$$D(j,s) + \sum_{\text{links } i \text{ inbound to node } j} x_i^s = \sum_{\text{links } i \text{ outbound from node } j} x_i^s \tag{6.5}$$

for all nodes j and destinations s = 1, …, p

$$x_i^s \ge 0 \tag{6.6}$$

for all links i = 1, …, n and all destinations s = 1, …p

$$u_i = 0,1 \qquad \text{for all i = 1, …m.} \tag{6.7}$$

where

c_i = cost of reconstruction or retrofit project i = 1, …, m;

B = total reconstruction or retrofit budget;

x_i = the flow on link i = 1, …, n;

x_i^s = the flow on link i = 1, …, n to destination s = 1, …p;

$t_i(x_i)$ = the average travel time on link i as function of flow;

$T_i(x_i)$ = the total travel time on link i as a function of flow

= $x_i \cdot t_i(x_i)$;

$D(j,s)$ = the (fixed) demand for travel from node j to destination s; and

M = an arbitrarily large number greater than the capacity of any link i.

The minimization of Equation (6.1) takes place over a choice of discrete projects u_i. The first class of constraints (Eq. 6.2), consists of a single budget constraint. The second class of constraints (Eq. 6.3) ensures that additional capacity from any new project is available to accommodate travel flows. The third class of constraints (Eq. 6.4) removes the capacity that would otherwise be provided by any links replaced by new projects. The fourth class of constraints (Eq. 6.5) ensures that the total demand for travel is accommodated on the network. The remaining constraints (Eqs. 6.6 and 6.7) are standard feasibility constraints.

6.2.1.2 Special Implications of Demand Shifts: Quantifying Welfare Losses

The standard version of the network design problem focuses on the total cost of travel on the network, treating travel demand as exogenous. In an earthquake context, this standard perspective must be extended to accommodate shifts along the travel demand function of the sort accounted for in the variable travel demand formulation. Fortunately, the estimated function used to model changes in travel demand following an earthquake can and should also be used to estimate system-wide changes in the net benefits provided by travel. These changes should enter the objective function of the network design problem along with system-wide travel costs.

This opportunity to estimate changes in the total net benefits provided by travel is perhaps the most useful consequence of the variable-demand perspective. Figure 6.1 modifies Figure 2.3 to include a representation of the total cost of travel on the network. Figure 6.2 depicts the total benefits of travel on the network. Since the travel demand curve D_1 describes the marginal benefit of travel, the area beneath the curve is the total benefit accruing to travelers. Figure 6.3 depicts the net total benefits of travel, i.e., the consumer surplus, that accrues due to travel. Figure 6.4 depicts two kinds of changes in the net benefits of travel associated with a reduction in transportation supply. The area of the gray rectangle is the loss of net benefits that would otherwise accrue to continuing users of the system, who now experience a lower level of service than before the earthquake. The area of the black triangle is the reduction in net benefits to due to trips forgone.

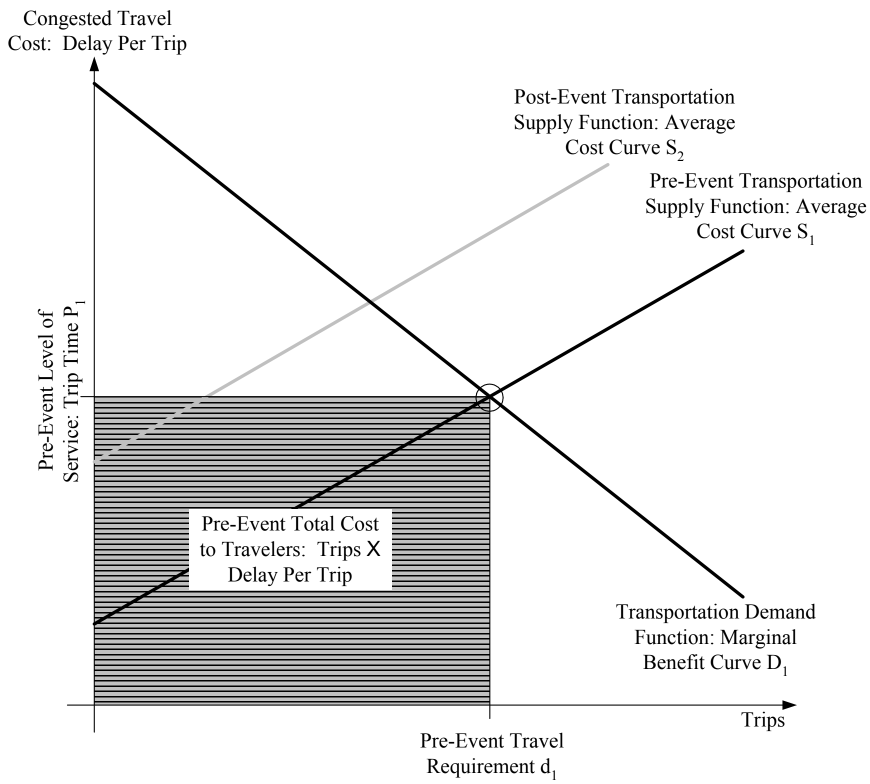

Fig. 6.1 The total cost of pre-event travel

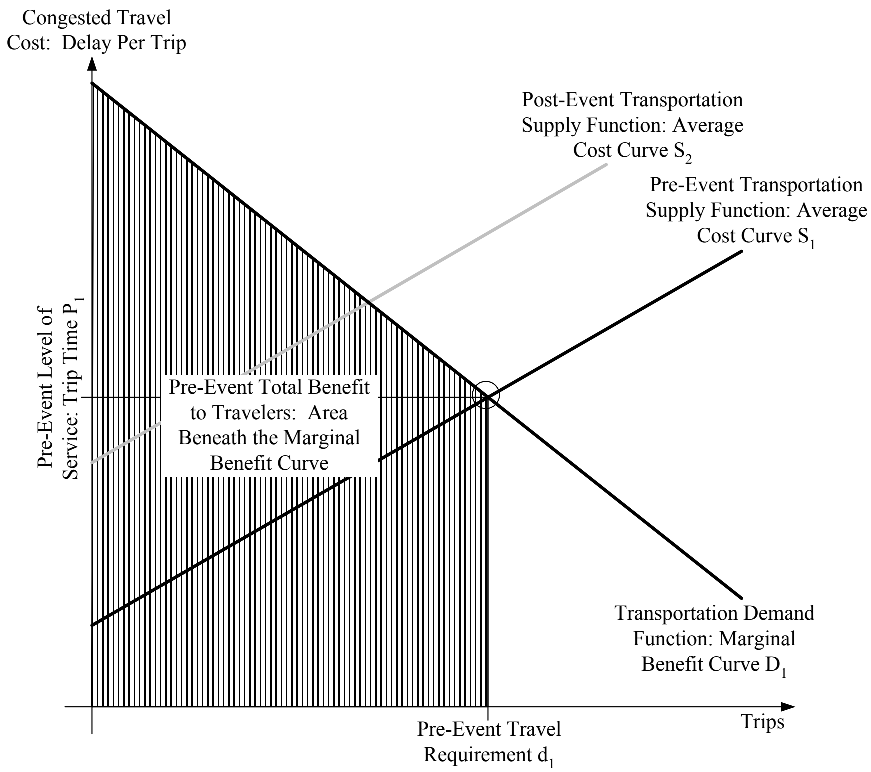

Fig. 6.2 The total benefits of pre-event travel

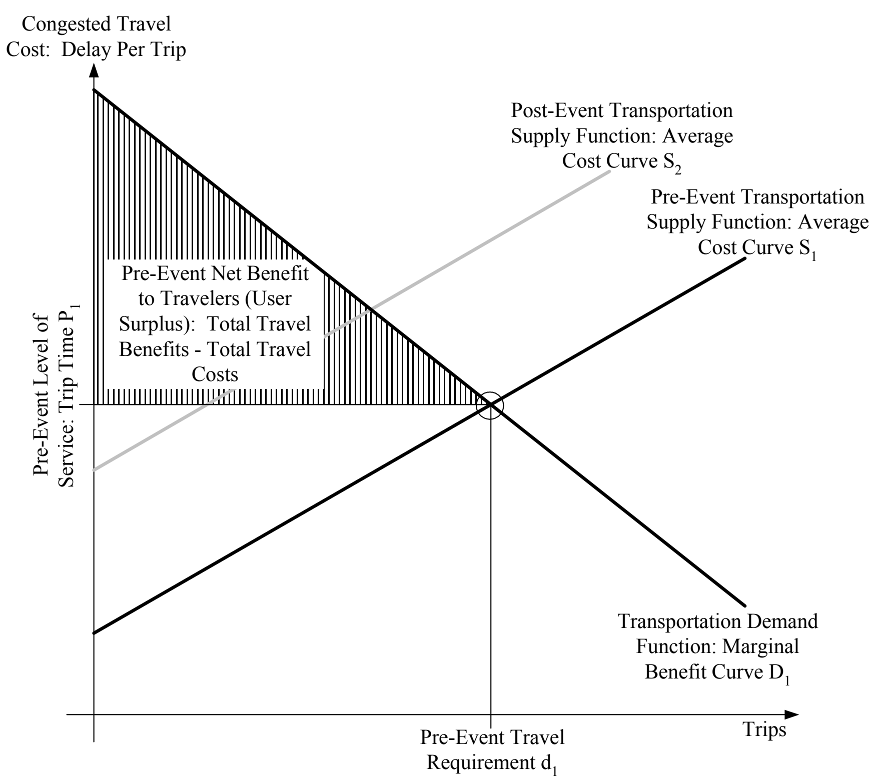

Fig. 6.3 The net benefits of pre-event travel—consumer surplus

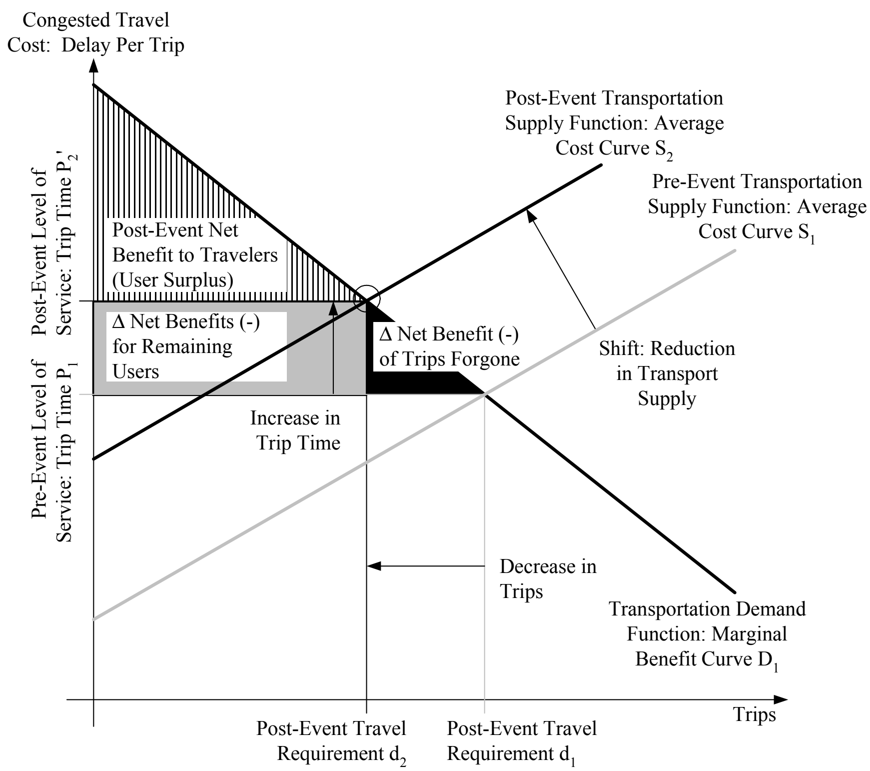

Fig. 6.4 Reductions in the net benefits of travel on a network damaged by an earthquake

Parameterizing the travel demand function to account for reductions in demand as a result of lower levels of service provides the means to compute these net changes in benefits for flows occurring between each origin-destination pair. The upper level of the objective for the deterministic network design problem can then be modified to account for these changes in net travel benefits resulting from variable demand, in addition to the traditional treatment of changes in the total cost of travel on the network. In post-earthquake circumstances, such a formulation would identify how to maximize the benefits from discrete link reconstruction options for any fixed level of expenditure.

In the event of a very large earthquake, the relevant set of relevant post-event questions will include not just which links to reconstruct, but how links should be grouped into construction projects, and in what order the resulting sequence of projects should be executed. Such a time-staged network design problem would logically be formulated as a discrete state dynamic programming problem, with deterministic network design problems, extended to account for net changes in the benefits of travel, solved for each period and state. Unfortunately, the state space for such a formulation would grow quickly with the number of potential repair clusters to be treated (Cho et al., 2000). This constrains the utility of the dynamic programming approach for very large problems.

6.2.1.3 Stochastic Network Design

As noted previously, pre-earthquake facility decisions are more complicated than post-event decisions. These are perhaps best represented as examples of the stochastic transportation network design problem, which focuses on the performance of degraded networks (Bell and Iida, 1997, 2001). As in the standard deterministic formulation, the objective is to find the transportation network configuration on which user equilibrium flows produce the least expected total congestion, subject to retrofit budget (and possibly other) constraints. Unfortunately, the stochastic version of the problem is an embedded optimization problem with a tri-level structure. The upper level is a decision by the network authority, in this case a pre-event retrofit or reconstruction decision. The intermediate level outcome, a function of the upper level decision, is a random result of nature, i.e., the earthquake. The lower level, a function of the upper-level decision and the intermediate outcome, is the decision by the traveler.

As in the deterministic case, explicit enumeration of options is out of the question. The solution space for the stochastic version of the problem is even larger than for the deterministic problem. A transportation network with M links presents 2^M retrofit options. A random act of nature converts the network to a collection of L < M links. Thus the total number of possible networks to be considered is

$$\sum_{L=1}^{M} {}_M C_L \cdot 2^L \tag{6.8}$$

Thus, from a computational perspective, pre-event bridge retrofit decisions are vexingly difficult to optimize in a network context. A way forward, is still required, of course. Public authority has a compelling economic incentive to make rational decisions about the seismic retrofit of transportation structures regardless of how difficult it is do so optimally. Practical alternatives must be identified and evaluated. Further, transportation authorities need to be able to respond quickly and cogently with plans when presented with special budget opportunities to undertake seismic retrofit and reconstruction programs. Since such pre-earthquake decisions cannot yet be treated optimally, they must certainly be handled heuristically.

6.2.2 Role of Heuristics

The nonlinear programming/constrained optimization approach used here to model network flows provides some avenues for developing appropriate heuristics. Mathematical constraints identifying the flows on individual links have dual variables associated with them. If a constrained optimization problem is solved by primal/dual techniques, such as is the case here, then the optimized values of the dual variables describe the instantaneous rates of change in the problem objective function as the corresponding constraints are relaxed. This information is likely relevant to heuristic retrofit decisions, but also presents some limitations. Optimized dual variables describe the implications of incremental changes in the structure of the corresponding constraints. Very dramatic changes in network topology resulting from an earthquake will produce changes in flows with impacts on problem objective functions well outside the range that can be imputed from the instantaneous information included in the optimal values of dual variables. Further, network authorities will logically be interested in impacts on total system costs, not the artifactual objective function used to model user equilibrium flows. This distinction is at the very core of the network design problem. However, further work in this area may provide some useful insight into the development of appropriate heuristics for pre-event retrofit decisions.

6.2.3 Accounting for Activity Shifts

Performance-based earthquake engineering calls for assessing the adequacy of a structure's design in terms of a key vector of decision variables, e.g., the mean average frequency of earthquake loss exceeding a given dollar value. According to Cornell and Krawinkler (2000)

> This building/bridge-specific loss estimation option, …, is very attractive because it permits an evaluation of design (or retrofit) alternatives and provides the owner with the information he/she is most interested in. The question is whether it can be brought to a sufficiently objective level to acquire the confidence of engineers and owners.

In the earthquake context, benefits thus consist of costs avoided. Pre- and post-event earthquake plans, i.e., mitigation and response decisions, should be based on benefit estimates that are as full and comprehensive as possible.

In the urban context, pre- and post-event decisions mitigate several different kinds of costs. These include

- replacement and repair costs associated with structures and building contents (referred to as "replacement and repair costs" in the regional science and economics literatures, and "direct costs" in the earthquake engineering literature);
- the opportunity costs associated with losing productive access to the capital plant when facilities are damaged (referred to as "direct costs" in the regional science and economics literatures, and "indirect costs" in the earthquake engineering literature);
- the secondary costs associated with losses to suppliers when producers stop bidding on production inputs because of damage to capital facilities (referred to as "indirect costs" in the regional science and economics literatures);
- the secondary costs associated with losses to suppliers of labor (households) when producers and their other suppliers stop bidding on labor because of damage to capital facilities (referred to as "induced costs" in the regional science and economics literatures);
- the costs associated with interruptions in services provided by public infrastructure systems (lifelines);
- the costs associated with injury and loss of life;
- the direct costs of productivity losses (administrative costs) associated with financing pre- and post-event decisions;
- the indirect and induced costs of productivity losses (the full economic burden of taxation and code enforcement) associated with financing pre- and post-event decisions.

From a policy-making and political perspective, it is also important to know what income groups, economic sectors, and communities benefit from pre- and post-event decisions, and who pays, i.e., incidence (Gordon et al., 2002).

Transportation systems are but one kind of lifeline system. The advances provided by modeling the reductions in travel demand resulting from post-earthquake changes in transportation supply are in important step in relating transportation and earthquake engineering models in a way that better support decisions intended to reduce seismic risks transportation networks or to help guide reconstruction of damaged networks. However, even the work accomplished to date is deficient with respect to capturing the impact of an earthquake on the urban activity system.

The demand for transportation is derived from the demand for other goods and services. The full impact of an earthquake on transportation system performance requires accounting for the earthquake's impact on transportation demand separate from demand responses to level of service. The latter corresponds to movement along a demand curve, as described in Figure 2.3. The former also involves a shift in the transportation demand curve. See Figure 6.5.

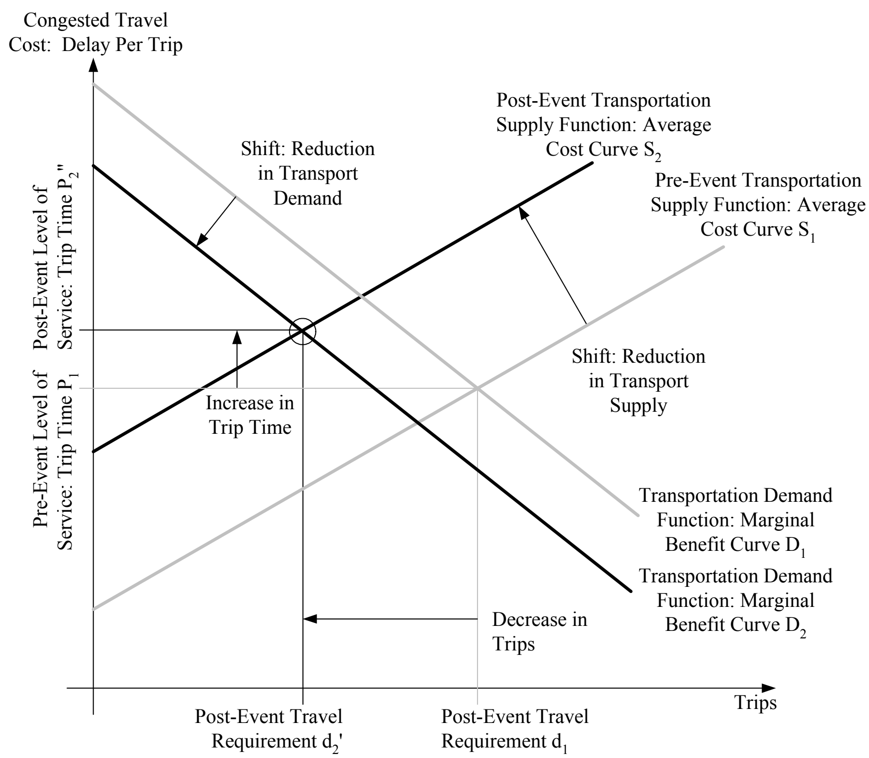

Fig. 6.5 Simultaneous changes in transportation demand and supply in a region damaged by an earthquake

These additional shifts in the derived demand for transportation cannot be modeled without accounting for the earthquake's impact on buildings and production activities (Cho et al., 1999; An et al., 2003). Such exercises are feasible, but computationally too expensive to be folded into the decision support activities described above. Improvements in integrated modeling techniques, algorithms, and computing machinery will likely eventually change this constraint, but until this happens, the variable transportation demand approach summarized here provides the best mechanism available for developing pre- and post-earthquake transportation facility decision support models of sufficient computational tractability to be of use in practice.

REFERENCES

Association for Geographic Information (AGI, 1999), *GIS Dictionary*, http://www.geo.ed.ac.uk/

Ahuja, Ravindra K., Thomas L. Magnanti, and James B. Orlin (1993), *Network flows: theory, algorithms, and applications*, Prentice Hall, Englewood Cliffs, NJ.

An, D.H., Gordon, P., Moore, J.E. II, and Richardson, H. (2003) "Regional Economic Models for Performance Based Earthquake Engineering," forthcoming in the *American Society of Civil Engineers / Natural Hazards Research Applications and Information Center Natural Hazards Review*.

Ang, Alfredo H.S., and Wilson H. Tang (1975), *Probability concepts in engineering planning and design: Volume 1 – Basic principals*, John Wiley & Sons.

Basoz, N., and A. Kiremidjian (1996), *Risk assessment for highway transportation systems*, Report No: 118, J. A. Blume Earthquake Engineering Center, Dept. Civil Eng., Stanford University, Stanford, California.

Basoz, N., and A. Kiremidjian (1997), *Evaluation of bridge damage data from the Loma Prieta and Northridge, CA Earthquakes*, Report No: 127, J. A. Blume Earthquake Engineering Center, Dept. Civil Eng., Stanford University, Stanford, California.

Basoz, N., and J. Mander (1999), *Enhancement of the Highway Transportation Module in HAZUS*, in *Report to National Institute of Building Sciences.* Washington, D.C.

Beckmann, M., MaGuire, C. B., and Winston, C.B. (1956) *Studies in the economics of transportation*, Yale University Press, New Haven.

Bell, Michael G. H. and Yansunori Iida (1997) *Transportation Network Analysis*, Chichester, NY: John Wiley & Sons, Ltd.

Bell, Michael G. H. and Yansunori Iida (2001) "Estimating the Terminal Reliability of Degradable Transport Networks," paper presented at the Triennial Symposium on Transportation Analysis (TRISTAN) IV, San Miguel, Portugal (June 13-19).

Boarnet, M. (1998) "Business Losses, Transportation Damage and the Northridge Earthquake," *Journal of Transportation and Statistics*, 1(2), 49-64.

Booz • Allen & Hamilton Inc. Team (1996) *California Intermodal Transportation Management System (ITMS)*, submitted to California Department of Transportation, Sacramento, CA.

Boore, D., W. Joyner, and T. Fumal (1993), “Estimation of Response Spectra and Peak Ground Acceleration from Western North America Earthquakes: Interim Report”, *Open File Report 93-509,* U.S. Geological Survey, Reston Virginia, 72 p.

Boore, D., W. Joyner, and T. Fumal (1997), “Equations for Estimating Horizontal Response Spectra and Peak Acceleration from North American Earthquakes: A Summary of Recent Work”, *Seismic Research Letters*, 687(1), 128-154.

California Department of Transportation (Caltrans, 1989), *The Loma Prieta Earthquake*, Caltrans PEQIT Report, Division of Structures, Sacramento, CA.

California Department of Transportation (Caltrans, 1993), *OSM&I Coding Guide for SMS*, Division of Structures, Office of Structures Maintenance and Investigations, Sacramento, CA.

California Department of Transportation (Caltrans, 2003) The Truck and Vehicle Data System Unit: 1997 Annual Average Daily Truck Traffic on California State Highways <http://www.dot.ca.gov/hq/traffops/saferesr/trafdata/>.

California Department of Transportation (Caltrans, 1999) *Post-Earthquake Investigation Team Manual*.

Chang, s., Shinozuka, M., and Moore, J. (2000). “Probabilistic Earthquake Scenarios: Extending Risk Analysis Methodologies to Spatially Distributed Systems”, *Earthquake Spectra* 16(3), pp.557-572.

Cho, S., Gordon, P., Moore, J.E. II, Richardson, H.W., Shinozuka, M., and Chang, S.E., (2000) “Analyzing Transportation Network Reconstruction Strategies: A Full Cost Approach,” Review of Urban and Regional Development Studies, 12: 212-227.

Cho, S., Moore, J. E., Richardson, H. W., Shinozuka, M., and Chang, S. (2001) “Integrating Transportation Network and Regional Economic Models to Estimate the Costs of a Large Earthquake,” *Journal of Regional Science*, 41 (1), pp. 39-65.

Cho, S, Fan, Y. Y, and Moore, J. E. (2003) “Modeling Transportation Network Flows as a Simultaneous Function of Travel Demand, Earthquake Damage, and Network Level Service,” paper presented at the ASCE Technical Council on Lifeline Earthquake Engineering’s (TCLEE) 6th U.S. Conference and Workshop, Long Beach, CA .

Cho, S., Gordon, P., Moore, J.E., Richardson, H.W., Shinozuka, M., Chang, S., Cho, S., Lee, K., Lee, K., and Ki, J.H.; with Gang Yu, Shashank Agrawal, Anupam Bordia, Xue Dong, and Yue Yue Fan (1999) “Integrating Transportation Network and Regional Economic Models to Estimate the Costs of a Large Urban Earthquake: Volume II of a Technical Report to the National Science Foundation," Award CMS 9633386 (EHM), School of Policy, Planning & Development, University of Southern California Los Angeles, California 90089-0626 http://www.usc.edu/sppd/research/eqloss/.

Cornell, A. and Krawinkler, H. (2000) "Progress and challenges in seismic performance assessment," *PEER Center News*, 3 (2), Pacific Earthquake Engineering Research Center, University of California, Berkeley.

EERI (1990). "Loma Prieta Earthquake Reconnaissance Report", *Earthquake Spectra*, Supplemental Vol. 6, L. Benushka, Ed., 247p.

Ellen, S.D. (1999). "Differential settlement due to liquefaction caused cracking of paved road on Paul's Island", U.S. Geological Survey: Digital Data Series DDS-29 Version 1.2, http://pubs.usgs.gov/dds/dds-29/

Environmental Systems Research Institute, Inc. (ESRI, 1998), "ArcView Network Analyst, An ESRI White Paper", http://www.esri.com/library/ whitepapers/pdfs/ana0498.pdf.

Environmental Systems Research Institute, Inc. (ESRI, 1999), *Glossary*, http://www.esri.com/ library/glossary/i_l.html.

Federal Highway Administration (FHWA, 1996), *Recording and Coding Guide for the Structural Inventory and Appraisal of the Nation's Bridges*, Report No: FHWA-PD-96-001, Office of Engineering Division, Federal Highway Administration, U.S. Department of Transportation, http://www.fhwa.dot.gov/bridge/bripub.htm.

Ghasemi, H. et al. (1996). "Magnetoreological Dampers"; www.eng.fsu.edu/.../ Fuzzy%20Control%20of%20Magn**et**orheologic**al**%20Dampers%20in%20Civil%20Structures.ppt

GIS for Transportation Symposium (GIS-T, 2002), *GIS-T 2002 State Summary*, Georgia Department of Transportation, Atlanta, Georgia.

Gordon, P and Pan Q, (2001) *Assembling and Processing Freight Shipment Data: Developing a GIS-based Origin-Destination Matrix for Southern California Freight Flows*, report to Metrans, project No. 99-25, the University of Southern California, Los Angeles, CA.

Gordon, P., Richardson, H., and Davis, B. (1998) "Transportation-Related Impacts of the Northridge Earthquake," *Journal of Transportation and Statistics* 1(2): 21-36.

Gordon, P., Moore, J.E. II, and Richardson, H.W. (2002) "Economic-Engineering Integrated Models for Earthquakes: Socioeconomic Impacts," Final Report for Project G4/1031999, Pacific Earthquake Engineering Research (PEER) Center Report 2002/19.

Governor's Board of Inquiry on the 1989 Loma Prieta Earthquake (1990), *Competing Against Time*, State of California, Office of Planning Research.

HAZUS (1999), Earthquake Loss Estimation, Technical Manual, National Institute of Building Sciences, Washington D.C.

Hobeika, A. G., Manchikalapudi, L. N., Kim, S. (1991) *Transportation Problems Faced after Big Earthquakes: a Case Study of the Loma Prieta Earthquake*, NSF report.

INRO Consultants Inc. (1998) *EMME/2 User's Manual Software Release 9*, Montreal, Canada.

Kiremidjian, A.S., J. Moore, N. Basoz, K. Burnell, Y. Fan, and A. Hortacsu (2002), "Earthquake Risk Assessment for Transportation Systems: Analysis of Pre-Retrofitted System", *Proceedings of the 7th National Conference on Earthquake Engineering*, Boston, July.

Kramer, S. L. (1996), *Geotechnical Earthquake Engineering*, Prentice Hall.

LeBlanc, L.J. (1973) "Mathematical Programming Formulations for Large Scale Network Equilibrium and Network Design Problems," Ph.D. Dissertation, Department of Industrial Engineering and Management Science, Northwestern University.

Meyer, C.E. (1999) "Aerial view of roadbed collapse near the interface of the cantilever truss sections of the San Francisco-Oakland Bay Bridge. View northwestward". U.S. Geological Survey; Digital Data Series DDS-29 Version 1.2, http://pubs.usgs.gov/dds/dds-29/

Meyer, C.E. (1999) "Landslide debris blocks both eastbound lanes of Highway 17 near Summit Road. Foreground material is damaged lane separators". U.S. Geological Survey; Digital Data Series DDS-29 Version 1.2, http://pubs.usgs.gov/dds/dds-29/

Press, W. H.; Flannery, B. P.; Teukolsky, S. A.; and Vetterling, W. T (1992) "Secant Method, False Position Method, and Ridders' Method." §9.2 in Numerical Recipes in FORTRAN: The Art of Scientific Computing, 2nd ed. Cambridge, England: Cambridge University Press, pp. 347-352.

Putnam, S. H. (1983) *Integrated urban models: Policy analysis of transportation and land use*, Pion Ltd., London.

Rand California (1998) *RAND California Business and Economic Statistics: Foreign Trade: Exports Imports – California* <http://ca.rand.org/stats/statlist.html>.

Regional Science Research Institute (RSRI) (1996) *PC-IO: A Regional Input-Output Model*, Regional Science Research Institute, New Jersey.

Robert, J.E. (1997) "Implementation Overview: Highway Bridges and Transportation Systems", *Proceedings of the CUREe Northridge Earthquake Conference,* Los Angeles, CA.

Rose, A and Benavides, J. (1998) *Regional Economic Impact of Electricity Lifeline Disruptions Stemming from the Northridge Earthquake*, Final Report to the National Science Foundation, Department of Energy, Environmental, and Mineral Economics, The Pennsylvania State University, University Park, PA.

Sheffi, Y. (1985) *Urban Transportation Networks: Equilibrium Analysis with Mathematical Programming Methods*, Prentice Hall.

TeleAtlas (2001). "Street-Level Digital Transportation Network", personal communications, TeleAtlas Corporation; Boston, MA 02114.

Transportation Research Board (TRB, 2002), TRB 81st Annual Meeting, Washington, D.C., January 13-17.

U.S. Bureau of Census (1993) *1992 Economic Census: Transportation Communication, and utilities – 1993 Commodity Flow Survey – California*, TC92-CF-52, U.S. Department of Transportation and U.S. Department of Commerce, Washington DC.

U.S. Bureau of Census (1997) *1997 Economic Census: Transportation - 1997 Commodity Flow Survey – San Francisco-Oakland-San Jose, CA CMSA*, EC97TCF-MA-CA(4), U.S. Department of Transportation and U.S. Department of Commerce, Washington DC, <http://www.census.gov/prod/ec97/97cfca736.pdf>.

U.S. Bureau of Census (2000) *1997 Economic Census: Transportation – 1997 Commodity Flow Survey – San Francisco-Oakland_San Jose, CA* CMSA, EC97TCF-MA-CA(4), U.S. Department of Transportation and U.S. Department of Commerce, Washington DC, , <http://www.census.gov/prod/ec97/97tcf-ca.pdf>.

U.S. Bureau of Transportation Statistics (1990) *Census Transportation Planning Package CDROM*, U.S. Department of Transportation, Washington DC.

U.S. Department of Transportation - Federal Highway Administration (1996) Quick Response Freight Manual Final Report.

USGS (1997), *San Francisco Bay Region Landslide Folio – Open-File Report 97-745*, http://wrgis.wr.usgs.gov/open-file/of97-745/.

USGS (1999), *Earthquake Probabilities in the San Francisco Bay Region: 2000 to 2030 - A Summary of Findings – Open File Report 99-517*, http://geopubs.wr.usgs.gov/open-file/of99-517/.

USGS (2000), *Preliminary maps of quaternary deposits and liquefaction susceptibility, nine-county San Francisco Bay Region, California: a digital database – Open File Report 00-444*, http://geopubs.wr.usgs.gov/open-file/of00-444/.

USGS (2002), *Peak Ground Acceleration for Loma Prieta Earthquake*, http://quake.wr.usgs.gov/research/strongmotion/effects/shake/216859/pga.html/.

USGS (2003a), Peak Ground Acceleration Map for Loma Prieta Earthquake (1989), http://quake.wr.usgs.gov/research/strongmotion/effects/shake/216859/pga.html.

USGS (2003b), Earthquake Probabilities in the San Francisco Bay Region: 2002–2031, Open File Report 03-214.

Yee, A. and Leung, S. K (1996) "The 1994 Northridge Earthquake – A Transportation Impact Overview", *1994 Northridge Earthquake*, Transportation Research Board / National Research Council, ISSN 0097-8515.

Yee, A. and Leung, S. K (1996) "The 1994 Northridge Earthquake – Traffic Management Strategies", *1994 Northridge Earthquake*, Transportation Research Board / National Research Council, ISSN 0097-8515.

Wells, D.L. and Coppersmith, K.L. (1994), "New Empirical Relationships among Magnitude, Rupture Length, Rupture Width, Rupture Area, and Surface Displacement", *Bulletin of the Seismological Society of America* , 84(4), 974-1002.

Wardrop, J. G (1952) "Some Theoretical Aspects of Road Traffic Research." *Proceedings of the Institute of Civil Engineers*, 1, part II.

Water Resources Support Center of U.S. Army Corps of Engineers (WCUS) (1998) *Waterborne Commerce of the United States: Part 4- Waterway and Harbors Pacific Coast, Alaska and Hawaii*, Waterborne Commerce Statistic Center, Virginia, <http://www.wrsc.usace.army.mil/ndc/wcusnatl96.pdf>.

Werner, S. D., C. E. Taylor, J. E. Moore, J. S. Walton, and S. Choet (2000), "Risk-Based Methodology for Assessing the Seismic Performance of Highway Systems." MCEER-00-0014, SUNY Buffalo, Buffalo, NY.

Wilson, A. G. (1970) *Entropy and regional modeling,* Pion Ltd., London.

Wilson, R. C., and D. K. Keefer (1985), "Predicting real limits of earthquake-induced landsliding" *Geol. Surv. Prof. Pap.*, 317-345.

Wilshire, H.G. (1999) “Bent reinforcement bars in failed support column, Cypress viaduct”. U.S. Geological Survey; Digital Data Series DDS-29 Version 1.2, http://pubs.usgs.gov/dds/dds-29/.

Youd T. Leslie, and David M. Perkins (1978), “Mapping liquefaction-induced ground failure potential”, *ASCE Journal of the Geotechnical Engineering Division*, 104(4), 433-446.

Appendix A: Expected Displacement Factor for Landslide Analysis

Expected displacement factor E[$DF|a_c/a_{is}$] for a given ratio of the critical acceleration (a_c) and the induced acceleration (a_{is}) is approximated with the following data points, which are based on Figure 4.16 of HAZUS Manual (1999).

a_c/a_{is}	E[$DF\|a_c/a_{is}$] (in cm/cycle)	a_c/a_{is}	E[$DF\|a_c/a_{is}$] (in cm/cycle)
0.00	100.000	0.55	1.800
0.05	61.000	0.60	1.300
0.10	40.000	0.65	0.900
0.15	28.000	0.70	0.600
0.20	18.800	0.75	0.350
0.25	14.000	0.80	0.214
0.30	10.600	0.85	0.100
0.35	7.400	0.90	0.049
0.40	5.200	0.95	0.015
0.45	3.600	≥1.00	0.000
0.50	2.600		

Appendix B: Definitions of Damage States

Basoz and Mander (1999) define the five damage states used in HAZUS as follows:

Slight/Minor (damage state 2)
Minor cracking and spalling to the abutment, cracks in shear keys at abutments, minor spalling and cracks at hinges, minor spalling at the column (damage requires no more than cosmetic repair) or minor cracking to the deck.

Moderate (damage state 3)
Any column experiencing moderate (shear cracks) cracking and spalling (column structurally still sound), moderate movement of abutment (less than two inches), extensive cracking and spalling of shear keys or bent bolts, keeper bar failure without unseating, rocker bearing failure or moderate settlement of the approach.

Extensive (damage state 4)
Any column degrading without collapse – shear failure – (column structurally unsafe), significant residual movement at connections, or major settlement approach, vertical offset of the abutment, differential settlement at connections, shear key failure at abutments.

Complete (damage state 5)
Any column collapsing and connection losing all bearing support, which may lead to imminent deck collapse, tilting of substructure due to foundation failure.

Appendix C: *PGA* Distributions by Scenario Event and by County

	PGA (in g)	Hayward 7.0	Hayward 7.5	San Andreas 7.5	San Andreas 8.0			*PGA* (in g)	Hayward 7.0	Hayward 7.5	San Andreas 7.5	San Andreas 8.0
Contra Costa (28)	**1.0≤ • <1.1**	3	0	15	1		**San Mateo (35)**	**1.0≤ • <1.1**	33	1	0	0
	0.9≤ • <1.0	184	106	457	346			**0.9≤ • <1.0**	291	216	1	0
	0.8≤ • <0.9	279	150	65	176			**0.8≤ • <0.9**	12	119	10	2
	0.7≤ • <0.8	66	123	0	14			**0.7≤ • <0.8**	0	0	23	13
	0.6≤ • <0.7	4	46	1	0			**0.6≤ • <0.7**	0	0	45	16
	0.5≤ • <0.6	2	42	0	0			**0.5≤ • <0.6**	0	0	58	16
	0.4≤ • <0.5	0	30	0	1			**0.4≤ • <0.5**	0	0	145	47
	0.3≤ • <0.4	0	41	0	0			**0.3≤ • <0.4**	0	0	45	62
	0.2≤ • <0.3	0	0	0	0			**0.2≤ • <0.3**	0	0	9	132
	0.1≤ • <0.2	0	0	0	0			**0.1≤ • <0.2**	0	0	0	43
	0.0≤ • <0.1	0	0	0	0			**0.0≤ • <0.1**	0	0	0	5
	Total	538	538	538	538			**Total**	336	336	336	336
Alameda (33)	**1.0≤ • <1.1**	5	0	18	7		**Santa Clara (37)**	**1.0≤ • <1.1**	159	0	2	0
	0.9≤ • <1.0	36	21	333	147			**0.9≤ • <1.0**	567	229	108	9
	0.8≤ • <0.9	44	37	373	319			**0.8≤ • <0.9**	191	281	211	46
	0.7≤ • <0.8	357	27	0	251			**0.7≤ • <0.8**	5	282	313	155

	0.6≤ • <0.7	262	201	0	0			**0.6≤ • <0.7**	0	101	124	309
	0.5≤ • <0.6	20	375	0	0			**0.5≤ • <0.6**	0	29	141	174
	0.4≤ • <0.5	0	50	0	0			**0.4≤ • <0.5**	0	0	20	99
	0.3≤ • <0.4	0	13	0	0			**0.3≤ • <0.4**	0	0	3	96
	0.2≤ • <0.3	0	0	0	0			**0.2≤ • <0.3**	0	0	0	31
	0.1≤ • <0.2	0	0	0	0			**0.1≤ • <0.2**	0	0	0	3
	0.0≤ • <0.1	0	0	0	0			**0.0≤ • <0.1**	0	0	0	0
	Total	724	724	724	724			**Total**	922	922	922	922
San Francisco (34)	**1.0≤ • <1.1**	0	0	0	0		**All Five Counties**	**1.0≤ • <1.1**	200	1	35	8
	0.9≤ • <1.0	94	42	0	0			**0.9≤ • <1.0**	1172	614	899	502
	0.8≤ • <0.9	26	73	18	4			**0.8≤ • <0.9**	552	660	677	547
	0.7≤ • <0.8	0	5	45	22			**0.7≤ • <0.8**	428	437	381	455
	0.6≤ • <0.7	0	0	39	36			**0.6≤ • <0.7**	266	348	209	361
	0.5≤ • <0.6	0	0	16	27			**0.5≤ • <0.6**	22	446	215	217
	0.4≤ • <0.5	0	0	2	21			**0.4≤ • <0.5**	0	80	167	168
	0.3≤ • <0.4	0	0	0	9			**0.3≤ • <0.4**	0	54	48	167
	0.2≤ • <0.3	0	0	0	1			**0.2≤ • <0.3**	0	0	9	164
	0.1≤ • <0.2	0	0	0	0			**0.1≤ • <0.2**	0	0	0	46
	0.0≤ • <0.1	0	0	0	0			**0.0≤ • <0.1**	0	0	0	5
	Total	120	120	120	120			**Total**	2640	2640	2640	2640

Appendix D: *PGD* Distributions by Hazard Category, by Scenario, and by County

	PGD (in inches)	HW7.0 Liq. Only	HW7.0 Land Only	HW7.0 Comb	HW7.5 Liq. Only	HW7.5 Land Only	HW7.5 Comb	SA7.5 Liq. Only	SA7.5 Land Only	SA7.5 Comb	SA8.0 Liq. Only	SA8.0 Land Only	SA8.0 Comb
Contra Costa (28)	150≤ • <250	0	0	0	0	0	0	0	0	0	0	0	0
	125≤ • <150	0	0	0	0	0	0	0	0	0	1	0	1
	100≤ • <125	0	0	0	82	0	82	0	0	0	6	0	6
	75≤ • <100	3	0	3	6	2	7	0	0	0	2	0	2
	50≤ • <75	5	0	5	5	2	6	0	0	0	1	0	1
	25≤ • <50	2	2	3	66	16	68	7	0	7	4	0	4
	10≤ • <25	73	1	74	102	41	105	9	0	9	96	0	96
	5≤ • <10	132	3	132	60	29	57	63	0	63	104	1	104
	0< • <5	111	56	113	98	108	105	136	5	139	39	25	47
	• = 0	212	476	208	119	340	108	323	533	320	285	512	277
	Total	538	538	538	538	538	538	538	538	538	538	538	538
Alameda (33)	150≤ • <250	0	0	0	0	0	0	0	0	0	0	0	0
	125≤ • <150	0	0	0	0	0	0	0	0	0	6	0	6
	100≤ • <125	0	0	0	174	0	174	0	0	0	35	0	35
	75≤ • <100	64	0	64	85	0	85	0	0	0	7	0	7

	50≤ • <75	33	0	33	67	2	69	0	0	0	5	0	5
	25≤ • <50	68	0	68	76	8	79	47	0	47	51	0	51
	10≤ • <25	234	4	238	167	100	168	58	0	58	248	0	248
	5≤ • <10	107	10	105	33	74	38	134	0	134	49	0	49
	0< • <5	98	411	144	7	465	86	162	4	165	101	58	109
	• = 0	120	299	72	115	75	25	323	720	320	222	666	214
	Total	724	724	724	724	724	724	724	724	724	724	724	724
San Francisco (34)	**150≤ • <250**	0	0	0	0	0	0	0	0	0	0	0	0
	125≤ • <150	0	0	0	0	0	0	0	0	0	18	0	18
	100≤ • <125	0	0	0	0	0	0	14	0	14	1	0	1
	75≤ • <100	0	0	0	4	0	4	0	0	0	6	0	6
	50≤ • <75	0	0	0	3	0	3	2	0	2	3	3	6
	25≤ • <50	0	0	0	3	0	3	9	0	9	23	8	21
	10≤ • <25	10	0	10	12	0	12	35	5	35	32	6	31
	5≤ • <10	7	0	7	6	0	6	13	6	13	29	34	29
	0< • <5	14	0	14	22	7	23	39	63	40	5	52	7
	• = 0	89	120	89	70	113	69	8	46	7	3	17	1
	Total	120	120	120	120	120	120	120	120	120	120	120	120

	PGD (in inches)	HW7.0 Liq. Only	HW7.0 Land Only	HW7.0 Comb	HW7.5 Liq. Only	HW7.5 Land Only	HW7.5 Comb	SA7.5 Liq. Only	SA7.5 Land Only	SA7.5 Comb	SA8.0 Liq. Only	SA8.0 Land Only	SA8.0 Comb
San Mateo (35)	**150≤ • <250**	0	0	0	0	0	0	0	0	0	0	7	7
	125≤ • <150	0	0	0	0	0	0	0	0	0	150	1	151
	100≤ • <125	0	0	0	0	0	0	117	0	117	10	31	40
	75≤ • <100	0	0	0	0	0	0	16	3	19	45	13	26
	50≤ • <75	0	0	0	0	0	0	3	4	7	20	42	21
	25≤ • <50	0	0	0	31	0	31	30	40	67	71	117	66
	10≤ • <25	31	0	31	62	0	62	130	105	95	12	76	14
	5≤ • <10	56	0	56	18	0	18	6	75	13	1	16	3
	0< • <5	30	2	32	44	7	51	7	87	13	2	24	5
	• = 0	219	334	217	181	329	174	27	22	5	25	9	3
	Total	336	336	336	336	336	336	336	336	336	336	336	336
Santa Clara (37)	**150≤ • <250**	0	0	0	0	0	0	0	0	0	0	4	4
	125≤ • <150	0	0	0	0	0	0	0	0	0	255	4	259
	100≤ • <125	0	0	0	51	0	51	65	0	65	64	4	68
	75≤ • <100	0	0	0	16	0	16	26	0	26	49	6	55
	50≤ • <75	0	0	0	29	0	29	38	8	46	105	27	123
	25≤ • <50	2	0	2	100	4	103	157	8	165	279	27	255
	10≤ • <25	51	0	51	308	2	307	391	35	380	124	95	115

	5≤ • <10	122	0	122	121	2	120	78	15	76	12	103	13
	0< • <5	380	3	382	112	151	127	98	244	107	7	466	22
	• = 0	367	919	365	185	763	169	69	612	57	27	186	8
	Total	922	922	922	922	922	922	922	922	922	922	922	922
All Five Counties	**150≤ • <250**	0	0	0	0	0	0	0	0	0	0	11	11
	125≤ • <150	0	0	0	0	0	0	0	0	0	430	5	435
	100≤ • <125	0	0	0	307	0	307	196	0	196	116	35	150
	75≤ • <100	67	0	67	111	2	112	42	3	45	109	19	96
	50≤ • <75	38	0	38	104	4	107	43	12	55	134	72	156
	25≤ • <50	72	2	73	276	28	284	250	48	295	428	152	397
	10≤ • <25	399	5	404	651	143	654	623	145	577	512	177	504
	5≤ • <10	424	13	422	238	105	239	294	96	299	195	154	198
	0< • <5	633	472	685	283	738	392	442	403	464	154	625	190
	• = 0	1007	2148	951	670	1620	545	750	1933	709	562	1390	503
	Total	2640	2640	2640	2640	2640	2640	2640	2640	2640	2640	2640	2640

Appendix E: Expected Damage--State Distributions by County and Scenario Event (No Retrofit Case $\gamma = 0\%$)

(No retrofit $\gamma = 0\%$)	Damage State	Hayward 7.0						Hayward 7.5						San Andreas 7.5						San Andreas 8.0					
		1	**2**	**3**	**4**	**5**	**6**	**1**	**2**	**3**	**4**	**5**	**6**	**1**	**2**	**3**	**4**	**5**	**6**	**1**	**2**	**3**	**4**	**5**	**6**
Contra Costa (28)	**1**	511	349	507	347	357	531	339	185	332	183	221	461	529	452	529	452	456	538	483	348	482	348	369	537
	2	18	16	17	18	13	2	87	49	85	48	35	9	9	18	9	18	14	0	43	19	44	19	4	1
	3	7	12	7	12	10	0	39	29	29	31	15	5	0	12	0	12	12	0	11	11	11	11	6	0
	4	2	121	5	120	118	3	62	82	44	80	75	32	0	45	0	45	45	0	1	116	1	116	115	0
	5	0	40	2	41	40	2	11	193	48	196	192	31	0	11	0	11	11	0	0	44	0	44	44	0
	Total	538	538	538	538	538	538	538	538	538	538	538	538	538	538	538	538	538	538	538	538	538	538	538	538
Alameda (33)	**1**	466	218	450	217	314	688	81	46	80	46	198	536	708	485	708	485	494	724	556	348	556	348	394	724
	2	199	121	203	119	43	19	310	104	274	104	36	28	15	27	15	27	24	0	143	70	143	70	35	0
	3	40	38	43	40	24	1	237	70	181	59	7	43	1	30	1	30	24	0	18	27	18	27	18	0
	4	19	105	23	106	101	14	74	71	131	75	55	71	0	132	0	132	132	0	7	114	7	114	115	0
	5	0	242	5	242	242	2	22	433	58	440	428	46	0	50	0	50	50	0	0	165	0	165	162	0
	Total	724	724	724	724	724	724	724	724	724	724	724	724	724	724	724	724	724	724	724	724	724	724	724	724
San Francisco (34)	**1**	118	101	118	101	103	120	110	91	110	91	95	120	49	31	49	31	51	111	28	6	24	6	19	75
	2	2	3	2	3	1	0	7	3	7	3	2	0	45	23	40	23	7	1	21	13	20	13	7	3
	3	0	1	0	1	1	0	3	5	3	5	2	0	10	2	10	2	2	1	33	3	19	3	5	5
	4	0	8	0	8	8	0	0	7	0	7	7	0	15	22	19	22	19	5	22	34	28	32	29	16
	5	0	7	0	7	7	0				14	14	0	1	42	2	42	41	2	16	64	29	66	60	21

	Total	120	120	120	120	120	120	120	120	120	120	120	120	120	120	120	120	120	120	120	120	120	120	120	120
San Mateo (35)	**1**	336	284	336	284	284	336	326	213	326	213	218	335	37	18	29	17	53	146	11	1	11	1	28	48
	2	0	4	0	4	4	0	9	32	8	31	27	0	55	9	28	8	30	18	26	7	13	7	1	7
	3	0	3	0	3	3	0	1	21	1	21	21	0	87	24	56	21	4	2	28	3	8	2	1	11
	4	0	33	0	33	33	0	0	31	1	32	31	1	119	71	117	46	40	89	104	21	27	12	14	48
	5	0	12	0	12	12	0	0	39	0	39	39	0	38	214	106	244	209	81	167	304	277	314	292	222
	Total	336	336	336	336	336	336	336	336	336	336	336	336	336	336	336	336	336	336	336	336	336	336	336	336
Santa Clara (37)	**1**	917	785	917	785	786	922	668	379	666	379	444	912	493	220	490	220	313	848	112	39	110	38	75	678
	2	5	21	5	21	21	0	216	77	211	77	24	1	321	116	292	112	56	13	314	25	301	25	7	25
	3	0	19	0	19	18	0	28	42	27	42	35	1	90	57	66	54	37	3	272	29	206	26	24	16
	4	0	66	0	66	66	0	7	161	11	158	157	4	15	189	50	184	176	36	189	76	168	76	74	93
	5	0	31	0	31	31	0	3	263	7	266	262	4	3	340	24	352	340	22	35	753	137	757	742	110
	Total	922	922	922	922	922	922	922	922	922	922	922	922	922	922	922	922	922	922	922	922	922	922	922	922
All Five Counties	**1**	2348	1737	2328	1734	1844	2597	1524	914	1514	912	1176	2364	1816	1206	1805	1205	1367	2367	1190	742	1183	741	885	2062
	2	224	165	227	165	82	21	629	265	585	263	124	38	445	193	384	188	131	32	547	134	521	134	54	36
	3	47	73	50	75	56	1	308	167	241	158	80	49	188	125	133	119	79	6	362	73	262	69	54	32
	4	21	333	28	333	326	17	143	352	187	352	325	108	149	459	186	429	412	130	323	361	231	350	347	157
	5	0	332	7	333	332	4	36	942	113	955	935	81	42	657	132	699	651	105	218	1330	443	1346	1300	353
	Total	2640	2640	2640	2640	2640	2640	2640	2640	2640	2640	2640	2640	2640	2640	2640	2640	2640	2640	2640	2640	2640	2640	2640	2640
	Hazard Cases:	1: Groundshaking only							4: GS + Liq + Land																
		2: GS + Liquefaction							5: Liq only																
		3: GS + Landslide							6: Land only																

Appendix F: Expected Damage-State Distributions by Scenario Event and by Retrofit Category

	Damage	Hayward 7.0						Hayward 7.5						San Andreas 7.5						San Andreas 8.0					
	State	1	2	3	4	5	6	1	2	3	4	5	6	1	2	3	4	5	6	1	2	3	4	5	6
No-Retrofit	1	2,348	1,737	2,328	1,734	1,844	2,597	1,524	914	1,514	912	1,176	2,364	1,816	1,206	1,805	1,205	1,367	2,367	1,190	742	1,183	741	885	2,062
	2	224	165	227	165	82	21	629	265	585	263	124	38	445	193	384	188	131	32	547	134	521	134	54	36
	3	47	73	50	75	56	1	308	167	241	158	80	49	188	125	133	119	79	6	362	73	262	69	54	32
	4	21	333	28	333	326	17	143	352	187	352	325	108	149	459	186	429	412	130	323	361	231	350	347	157
	5	0	332	7	333	332	4	36	942	113	955	935	81	42	657	132	699	651	105	218	1,330	443	1,346	1,300	353
	Total	2,640	2,640	2,640	2,640	2,640	2,640	2,640	2,640	2,640	2,640	2,640	2,640	2,640	2,640	2,640	2,640	2,640	2,640	2,640	2,640	2,640	2,640	2,640	2,640
5 % Retrofit	1	2,369	1,770	2,349	1,767	1,856	2,609	1,586	956	1,573	954	1,198	2,382	1,857	1,243	1,843	1,241	1,387	2,395	1,251	767	1,243	766	892	2,069
	2	218	153	223	154	87	9	634	266	586	264	124	58	443	186	367	182	131	6	564	128	536	128	66	38
	3	38	64	40	64	51	5	257	141	200	131	78	19	166	145	125	138	116	19	339	75	215	70	52	29
	4	15	334	21	335	327	14	131	349	178	354	319	104	135	424	184	396	377	131	285	365	216	349	353	169
	5	0	319	7	320	319	3	32	928	103	937	921	77	39	642	121	683	629	89	201	1,305	430	1,327	1,277	335
	Total	2,640	2,640	2,640	2,640	2,640	2,640	2,640	2,640	2,640	2,640	2,640	2,640	2,640	2,640	2,640	2,640	2,640	2,640	2,640	2,640	2,640	2,640	2,640	2,640
10 % Retrofit	1	2,414	1,812	2,400	1,809	1,887	2,614	1,642	998	1,627	996	1,225	2,396	1,917	1,282	1,898	1,280	1,415	2,398	1,293	784	1,284	783	919	2,072
	2	183	129	183	131	75	4	645	271	568	260	124	49	421	179	351	171	121	4	559	126	529	126	49	52
	3	31	75	33	73	58	8	205	121	175	120	77	14	152	160	94	154	127	21	334	73	203	68	58	24
	4	12	312	19	314	308	12	125	347	175	351	315	106	120	404	184	371	370	141	286	397	222	376	371	162
	5	0	312	5	313	312	2	23	903	95	913	899	75	30	615	113	664	607	76	168	1,260	402	1,287	1,243	330
	Total	2,640	2,640	2,640	2,640	2,640	2,640	2,640	2,640	2,640	2,640	2,640	2,640	2,640	2,640	2,640	2,640	2,640	2,640	2,640	2,640	2,640	2,640	2,640	2,640
20 % Retrofit	1	2,461	1,864	2,450	1,863	1,926	2,618	1,756	1,086	1,732	1,084	1,296	2,401	2,013	1,350	1,982	1,345	1,472	2,399	1,384	835	1,370	834	939	2,099
	2	147	107	144	107	56	1	606	249	524	235	87	50	372	165	301	160	107	6	573	114	527	114	57	30
	3	25	63	27	61	54	9	176	101	146	101	68	22	153	158	95	142	116	24	323	57	157	49	48	40

	4	7	334	16	336	332	10	85	331	160	338	323	98	73	380	180	381	361	143	235	406	214	388	379	157
	5	0	272	3	273	272	2	17	873	78	882	866	69	29	587	82	612	584	68	125	1,228	372	1,255	1,217	314
	Total	2,640	2,640	2,640	2,640	2,640	2,640	2,640	2,640	2,640	2,640	2,640	2,640	2,640	2,640	2,640	2,640	2,640	2,640	2,640	2,640	2,640	2,640	2,640	2,640

Hazard	1: Groundshaking only	4: GS + Liq + Land
	2: GS + Liquefaction	5: Liq only
	3: GS + Landslide	6: Land only

PEER REPORTS

PEER reports are available from the National Information Service for Earthquake Engineering (NISEE). To order PEER reports, please contact the Pacific Earthquake Engineering Research Center, 1301 South 46th Street, Richmond, California 94804-4698. Tel.: (510) 665-3405; Fax: (510) 665-3420.

PEER 2006/04 *Probabilistic Seismic Evaluation of Reinforced Concrete Structural Components and Systems.* Tae Hyung Lee and Khalid M. Mosalam. August 2006.

PEER 2006/02 *Pacific Earthquake Engineering Research Center Highway Demonstration Project.* Anne Kiremidjian, James Moore, Yue Yue Fan, Nesrin Basoz, Ozgur Yazali, and Meredith Williams. April 2006.

PEER 2006/01 *Bracing Berkeley. A Guide to Seismic Safety on the UC Berkeley Campus.* Mary C. Comerio, Stephen Tobriner, and Ariane Fehrenkamp. January 2006.

PEER 2005/15 *CPT-Based Probabilistic Assessment of Seismic Soil Liquefaction Initiation.* R. E. S. Moss, R. B. Seed, R. E. Kayen, J. P. Stewart, and A. Der Kiureghian. April 2006.

PEER 2005/14 *Workshop on Modeling of Nonlinear Cyclic Load-Deformation Behavior of Shallow Foundations.* Bruce L. Kutter, Geoffrey Martin, Tara Hutchinson, Chad Harden, Sivapalan Gajan, and Justin Phalen. March 2006.

PEER 2005/13 *Stochastic Characterization and Decision Bases under Time-Dependent Aftershock Risk in Performance-Based Earthquake Engineering.* Gee Liek Yeo and C. Allin Cornell. July 2005.

PEER 2005/12 *PEER Testbed Study on a Laboratory Building: Exercising Seismic Performance Assessment.* Mary C. Comerio, editor. November 2005.

PEER 2005/11 *Van Nuys Hotel Building Testbed Report: Exercising Seismic Performance Assessment.* Helmut Krawinkler, editor. October 2005.

PEER 2005/10 *First NEES/E-Defense Workshop on Collapse Simulation of Reinforced Concrete Building Structures.* September 2005.

PEER 2005/08 *Damage Accumulation in Lightly Confined Reinforced Concrete Bridge Columns.* R. Tyler Ranf, Jared M. Nelson, Zach Price, Marc O. Eberhard, and John F. Stanton. April 2006.

PEER 2005/07 *Experimental and Analytical Studies on the Seismic Response of Freestanding and Anchored Laboratory Equipment.* Dimitrios Konstantinidis and Nicos Makris. January 2005.

PEER 2005/06 *Global Collapse of Frame Structures under Seismic Excitations*. Luis F. Ibarra and Helmut Krawinkler. September 2005.

PEER 2005//05 *Performance Characterization of Bench- and Shelf-Mounted Equipment.* Samit Ray Chaudhuri and Tara C. Hutchinson. May 2006.

PEER 2005/04 *Numerical Modeling of the Nonlinear Cyclic Response of Shallow Foundations.* Chad Harden, Tara Hutchinson, Geoffrey R. Martin, and Bruce L. Kutter. August 2005.

PEER 2005/03 *A Taxonomy of Building Components for Performance-Based Earthquake Engineering.* Keith A. Porter. September 2005.

PEER 2005/02 *Fragility Basis for California Highway Overpass Bridge Seismic Decision Making*. Kevin R. Mackie and Bozidar Stojadinovic. June 2005.

PEER 2005/01 *Empirical Characterization of Site Conditions on Strong Ground Motion.* Jonathan P. Stewart, Yoojoong Choi, and Robert W. Graves. June 2005.

PEER 2004/09 *Electrical Substation Equipment Interaction: Experimental Rigid Conductor Studies.* Christopher Stearns and André Filiatrault. February 2005.

PEER 2004/08 *Seismic Qualification and Fragility Testing of Line Break 550-kV Disconnect Switches.* Shakhzod M. Takhirov, Gregory L. Fenves, and Eric Fujisaki. January 2005.

PEER 2004/07 *Ground Motions for Earthquake Simulator Qualification of Electrical Substation Equipment.* Shakhzod M. Takhirov, Gregory L. Fenves, Eric Fujisaki, and Don Clyde. January 2005.

PEER 2004/06 *Performance-Based Regulation and Regulatory Regimes.* Peter J. May and Chris Koski. September 2004.

PEER 2004/05 *Performance-Based Seismic Design Concepts and Implementation: Proceedings of an International Workshop.* Peter Fajfar and Helmut Krawinkler, editors. September 2004.

PEER 2004/04 *Seismic Performance of an Instrumented Tilt-up Wall Building.* James C. Anderson and Vitelmo V. Bertero. July 2004.

PEER 2004/03 *Evaluation and Application of Concrete Tilt-up Assessment Methodologies.* Timothy Graf and James O. Malley. October 2004.

PEER 2004/02 *Analytical Investigations of New Methods for Reducing Residual Displacements of Reinforced Concrete Bridge Columns.* Junichi Sakai and Stephen A. Mahin. August 2004.

PEER 2004/01 *Seismic Performance of Masonry Buildings and Design Implications.* Kerri Anne Taeko Tokoro, James C. Anderson, and Vitelmo V. Bertero. February 2004.

PEER 2003/18 *Performance Models for Flexural Damage in Reinforced Concrete Columns.* Michael Berry and Marc Eberhard. August 2003.

PEER 2003/17 *Predicting Earthquake Damage in Older Reinforced Concrete Beam-Column Joints.* Catherine Pagni and Laura Lowes. October 2004.

PEER 2003/16 *Seismic Demands for Performance-Based Design of Bridges.* Kevin Mackie and Božidar Stojadinovic. August 2003.

PEER 2003/15 *Seismic Demands for Nondeteriorating Frame Structures and Their Dependence on Ground Motions.* Ricardo Antonio Medina and Helmut Krawinkler. May 2004.

PEER 2003/14 *Finite Element Reliability and Sensitivity Methods for Performance-Based Earthquake Engineering.* Terje Haukaas and Armen Der Kiureghian. April 2004.

PEER 2003/13 *Effects of Connection Hysteretic Degradation on the Seismic Behavior of Steel Moment-Resisting Frames.* Janise E. Rodgers and Stephen A. Mahin. March 2004.

PEER 2003/12 *Implementation Manual for the Seismic Protection of Laboratory Contents: Format and Case Studies.* William T. Holmes and Mary C. Comerio. October 2003.

PEER 2003/11 *Fifth U.S.-Japan Workshop on Performance-Based Earthquake Engineering Methodology for Reinforced Concrete Building Structures.* February 2004.

PEER 2003/10 *A Beam-Column Joint Model for Simulating the Earthquake Response of Reinforced Concrete Frames.* Laura N. Lowes, Nilanjan Mitra, and Arash Altoontash. February 2004.

PEER 2003/09 *Sequencing Repairs after an Earthquake: An Economic Approach.* Marco Casari and Simon J. Wilkie. April 2004.

PEER 2003/08 *A Technical Framework for Probability-Based Demand and Capacity Factor Design (DCFD) Seismic Formats.* Fatemeh Jalayer and C. Allin Cornell. November 2003.

PEER 2003/07 *Uncertainty Specification and Propagation for Loss Estimation Using FOSM Methods.* Jack W. Baker and C. Allin Cornell. September 2003.

PEER 2003/06 *Performance of Circular Reinforced Concrete Bridge Columns under Bidirectional Earthquake Loading*. Mahmoud M. Hachem, Stephen A. Mahin, and Jack P. Moehle. February 2003.

PEER 2003/05 *Response Assessment for Building-Specific Loss Estimation.* Eduardo Miranda and Shahram Taghavi. September 2003.

PEER 2003/04 *Experimental Assessment of Columns with Short Lap Splices Subjected to Cyclic Loads*. Murat Melek, John W. Wallace, and Joel Conte. April 2003.

PEER 2003/03 *Probabilistic Response Assessment for Building-Specific Loss Estimation.* Eduardo Miranda and Hesameddin Aslani. September 2003.

PEER 2003/02 *Software Framework for Collaborative Development of Nonlinear Dynamic Analysis Program.* Jun Peng and Kincho H. Law. September 2003.

PEER 2003/01 *Shake Table Tests and Analytical Studies on the Gravity Load Collapse of Reinforced Concrete Frames.* Kenneth John Elwood and Jack P. Moehle. November 2003.

PEER 2002/24 *Performance of Beam to Column Bridge Joints Subjected to a Large Velocity Pulse.* Natalie Gibson, André Filiatrault, and Scott A. Ashford. April 2002.

PEER 2002/23 *Effects of Large Velocity Pulses on Reinforced Concrete Bridge Columns.* Greg L. Orozco and Scott A. Ashford. April 2002.

PEER 2002/22 *Characterization of Large Velocity Pulses for Laboratory Testing.* Kenneth E. Cox and Scott A. Ashford. April 2002.

PEER 2002/21 *Fourth U.S.-Japan Workshop on Performance-Based Earthquake Engineering Methodology for Reinforced Concrete Building Structures*. December 2002.

PEER 2002/20 *Barriers to Adoption and Implementation of PBEE Innovations.* Peter J. May. August 2002.

PEER 2002/19 *Economic-Engineered Integrated Models for Earthquakes: Socioeconomic Impacts.* Peter Gordon, James E. Moore II, and Harry W. Richardson. July 2002.

PEER 2002/18 *Assessment of Reinforced Concrete Building Exterior Joints with Substandard Details.* Chris P. Pantelides, Jon Hansen, Justin Nadauld, and Lawrence D. Reaveley. May 2002.

PEER 2002/17 *Structural Characterization and Seismic Response Analysis of a Highway Overcrossing Equipped with Elastomeric Bearings and Fluid Dampers: A Case Study.* Nicos Makris and Jian Zhang. November 2002.

PEER 2002/16 *Estimation of Uncertainty in Geotechnical Properties for Performance-Based Earthquake Engineering.* Allen L. Jones, Steven L. Kramer, and Pedro Arduino. December 2002.

PEER 2002/15 *Seismic Behavior of Bridge Columns Subjected to Various Loading Patterns.* Asadollah Esmaeily-Gh. and Yan Xiao. December 2002.

PEER 2002/14 *Inelastic Seismic Response of Extended Pile Shaft Supported Bridge Structures.* T.C. Hutchinson, R.W. Boulanger, Y.H. Chai, and I.M. Idriss. December 2002.

PEER 2002/13 *Probabilistic Models and Fragility Estimates for Bridge Components and Systems.* Paolo Gardoni, Armen Der Kiureghian, and Khalid M. Mosalam. June 2002.

PEER 2002/12 *Effects of Fault Dip and Slip Rake on Near-Source Ground Motions: Why Chi-Chi Was a Relatively Mild M7.6 Earthquake.* Brad T. Aagaard, John F. Hall, and Thomas H. Heaton. December 2002.

PEER 2002/11 *Analytical and Experimental Study of Fiber-Reinforced Strip Isolators*. James M. Kelly and Shakhzod M. Takhirov. September 2002.

PEER 2002/10 *Centrifuge Modeling of Settlement and Lateral Spreading with Comparisons to Numerical Analyses***.** Sivapalan Gajan and Bruce L. Kutter. January 2003.

PEER 2002/09 *Documentation and Analysis of Field Case Histories of Seismic Compression during the 1994 Northridge, California, Earthquake.* Jonathan P. Stewart, Patrick M. Smith, Daniel H. Whang, and Jonathan D. Bray. October 2002.

PEER 2002/08 *Component Testing, Stability Analysis and Characterization of Buckling-Restrained Unbonded Braces™.* Cameron Black, Nicos Makris, and Ian Aiken. September 2002.

PEER 2002/07 *Seismic Performance of Pile-Wharf Connections.* Charles W. Roeder, Robert Graff, Jennifer Soderstrom, and Jun Han Yoo. December 2001.

PEER 2002/06 *The Use of Benefit-Cost Analysis for Evaluation of Performance-Based Earthquake Engineering Decisions*. Richard O. Zerbe and Anthony Falit-Baiamonte. September 2001.

PEER 2002/05 *Guidelines, Specifications, and Seismic Performance Characterization of Nonstructural Building Components and Equipment*. André Filiatrault, Constantin Christopoulos, and Christopher Stearns. September 2001.

PEER 2002/04 *Consortium of Organizations for Strong-Motion Observation Systems and the Pacific Earthquake Engineering Research Center Lifelines Program: Invited Workshop on Archiving and Web Dissemination of Geotechnical Data, 4–5 October 2001*. September 2002.

PEER 2002/03 *Investigation of Sensitivity of Building Loss Estimates to Major Uncertain Variables for the Van Nuys Testbed.* Keith A. Porter, James L. Beck, and Rustem V. Shaikhutdinov. August 2002.

PEER 2002/02 *The Third U.S.-Japan Workshop on Performance-Based Earthquake Engineering Methodology for Reinforced Concrete Building Structures*. July 2002.

PEER 2002/01 *Nonstructural Loss Estimation: The UC Berkeley Case Study.* Mary C. Comerio and John C. Stallmeyer. December 2001.

PEER 2001/16 *Statistics of SDF-System Estimate of Roof Displacement for Pushover Analysis of Buildings.* Anil K. Chopra, Rakesh K. Goel, and Chatpan Chintanapakdee. December 2001.

PEER 2001/15 *Damage to Bridges during the 2001 Nisqually Earthquake.* R. Tyler Ranf, Marc O. Eberhard, and Michael P. Berry. November 2001.

PEER 2001/14 *Rocking Response of Equipment Anchored to a Base Foundation.* Nicos Makris and Cameron J. Black. September 2001.

PEER 2001/13 *Modeling Soil Liquefaction Hazards for Performance-Based Earthquake Engineering.* Steven L. Kramer and Ahmed-W. Elgamal. February 2001.

PEER 2001/12 *Development of Geotechnical Capabilities in OpenSees.* Boris Jeremi . September 2001.

PEER 2001/11 *Analytical and Experimental Study of Fiber-Reinforced Elastomeric Isolators*. James M. Kelly and Shakhzod M. Takhirov. September 2001.

PEER 2001/10 *Amplification Factors for Spectral Acceleration in Active Regions.* Jonathan P. Stewart, Andrew H. Liu, Yoojoong Choi, and Mehmet B. Baturay. December 2001.

PEER 2001/09 *Ground Motion Evaluation Procedures for Performance-Based Design.* Jonathan P. Stewart, Shyh-Jeng Chiou, Jonathan D. Bray, Robert W. Graves, Paul G. Somerville, and Norman A. Abrahamson. September 2001.

PEER 2001/08 *Experimental and Computational Evaluation of Reinforced Concrete Bridge Beam-Column Connections for Seismic Performance*. Clay J. Naito, Jack P. Moehle, and Khalid M. Mosalam. November 2001.

PEER 2001/07 *The Rocking Spectrum and the Shortcomings of Design Guidelines.* Nicos Makris and Dimitrios Konstantinidis. August 2001.

PEER 2001/06 *Development of an Electrical Substation Equipment Performance Database for Evaluation of Equipment Fragilities*. Thalia Agnanos. April 1999.

PEER 2001/05 *Stiffness Analysis of Fiber-Reinforced Elastomeric Isolators.* Hsiang-Chuan Tsai and James M. Kelly. May 2001.

PEER 2001/04 *Organizational and Societal Considerations for Performance-Based Earthquake Engineering.* Peter J. May. April 2001.

PEER 2001/03 *A Modal Pushover Analysis Procedure to Estimate Seismic Demands for Buildings: Theory and Preliminary Evaluation.* Anil K. Chopra and Rakesh K. Goel. January 2001.

PEER 2001/02 *Seismic Response Analysis of Highway Overcrossings Including Soil-Structure Interaction.* Jian Zhang and Nicos Makris. March 2001.

PEER 2001/01 *Experimental Study of Large Seismic Steel Beam-to-Column Connections.* Egor P. Popov and Shakhzod M. Takhirov. November 2000.

PEER 2000/10 *The Second U.S.-Japan Workshop on Performance-Based Earthquake Engineering Methodology for Reinforced Concrete Building Structures.* March 2000.

PEER 2000/09 *Structural Engineering Reconnaissance of the August 17, 1999 Earthquake: Kocaeli (Izmit), Turkey.* Halil Sezen, Kenneth J. Elwood, Andrew S. Whittaker, Khalid Mosalam, John J. Wallace, and John F. Stanton. December 2000.

PEER 2000/08 *Behavior of Reinforced Concrete Bridge Columns Having Varying Aspect Ratios and Varying Lengths of Confinement.* Anthony J. Calderone, Dawn E. Lehman, and Jack P. Moehle. January 2001.

PEER 2000/07 *Cover-Plate and Flange-Plate Reinforced Steel Moment-Resisting Connections.* Taejin Kim, Andrew S. Whittaker, Amir S. Gilani, Vitelmo V. Bertero, and Shakhzod M. Takhirov. September 2000.

PEER 2000/06 *Seismic Evaluation and Analysis of 230-kV Disconnect Switches.* Amir S. J. Gilani, Andrew S. Whittaker, Gregory L. Fenves, Chun-Hao Chen, Henry Ho, and Eric Fujisaki. July 2000.

PEER 2000/05 *Performance-Based Evaluation of Exterior Reinforced Concrete Building Joints for Seismic Excitation.* Chandra Clyde, Chris P. Pantelides, and Lawrence D. Reaveley. July 2000.

PEER 2000/04 *An Evaluation of Seismic Energy Demand: An Attenuation Approach.* Chung-Che Chou and Chia-Ming Uang. July 1999.

PEER 2000/03 *Framing Earthquake Retrofitting Decisions: The Case of Hillside Homes in Los Angeles.* Detlof von Winterfeldt, Nels Roselund, and Alicia Kitsuse. March 2000.

PEER 2000/02 *U.S.-Japan Workshop on the Effects of Near-Field Earthquake Shaking.* Andrew Whittaker, ed. July 2000.

PEER 2000/01 *Further Studies on Seismic Interaction in Interconnected Electrical Substation Equipment.* Armen Der Kiureghian, Kee-Jeung Hong, and Jerome L. Sackman. November 1999.

PEER 1999/14 *Seismic Evaluation and Retrofit of 230-kV Porcelain Transformer Bushings*. Amir S. Gilani, Andrew S. Whittaker, Gregory L. Fenves, and Eric Fujisaki. December 1999.

PEER 1999/13 *Building Vulnerability Studies: Modeling and Evaluation of Tilt-up and Steel Reinforced Concrete Buildings.* John W. Wallace, Jonathan P. Stewart, and Andrew S. Whittaker, editors. December 1999.

PEER 1999/12 *Rehabilitation of Nonductile RC Frame Building Using Encasement Plates and Energy-Dissipating Devices.* Mehrdad Sasani, Vitelmo V. Bertero, James C. Anderson. December 1999.

PEER 1999/11 *Performance Evaluation Database for Concrete Bridge Components and Systems under Simulated Seismic Loads.* Yael D. Hose and Frieder Seible. November 1999.

PEER 1999/10 *U.S.-Japan Workshop on Performance-Based Earthquake Engineering Methodology for Reinforced Concrete Building Structures.* December 1999.

PEER 1999/09 *Performance Improvement of Long Period Building Structures Subjected to Severe Pulse-Type Ground Motions*. James C. Anderson, Vitelmo V. Bertero, and Raul Bertero. October 1999.

PEER 1999/08 *Envelopes for Seismic Response Vectors.* Charles Menun and Armen Der Kiureghian. July 1999.

PEER 1999/07 *Documentation of Strengths and Weaknesses of Current Computer Analysis Methods for Seismic Performance of Reinforced Concrete Members.* William F. Cofer. November 1999.

PEER 1999/06 *Rocking Response and Overturning of Anchored Equipment under Seismic Excitations.* Nicos Makris and Jian Zhang. November 1999.

PEER 1999/05 *Seismic Evaluation of 550 kV Porcelain Transformer Bushings.* Amir S. Gilani, Andrew S. Whittaker, Gregory L. Fenves, and Eric Fujisaki. October 1999.

PEER 1999/04 *Adoption and Enforcement of Earthquake Risk-Reduction Measures.* Peter J. May, Raymond J. Burby, T. Jens Feeley, and Robert Wood.

PEER 1999/03 *Task 3 Characterization of Site Response General Site Categories*. Adrian Rodriguez-Marek, Jonathan D. Bray, and Norman Abrahamson. February 1999.

PEER 1999/02 *Capacity-Demand-Diagram Methods for Estimating Seismic Deformation of Inelastic Structures: SDF Systems*. Anil K. Chopra and Rakesh Goel. April 1999.

PEER 1999/01 *Interaction in Interconnected Electrical Substation Equipment Subjected to Earthquake Ground Motions.* Armen Der Kiureghian, Jerome L. Sackman, and Kee-Jeung Hong. February 1999.

PEER 1998/08 *Behavior and Failure Analysis of a Multiple-Frame Highway Bridge in the 1994 Northridge Earthquake.* Gregory L. Fenves and Michael Ellery. December 1998.

PEER 1998/07 *Empirical Evaluation of Inertial Soil-Structure Interaction Effects.* Jonathan P. Stewart, Raymond B. Seed, and Gregory L. Fenves. November 1998.

PEER 1998/06 *Effect of Damping Mechanisms on the Response of Seismic Isolated Structures.* Nicos Makris and Shih-Po Chang. November 1998.

PEER 1998/05 *Rocking Response and Overturning of Equipment under Horizontal Pulse-Type Motions.* Nicos Makris and Yiannis Roussos. October 1998.

PEER 1998/04 *Pacific Earthquake Engineering Research Invitational Workshop Proceedings, May 14–15, 1998: Defining the Links between Planning, Policy Analysis, Economics and Earthquake Engineering.* Mary Comerio and Peter Gordon. September 1998.

PEER 1998/03 *Repair/Upgrade Procedures for Welded Beam to Column Connections.* James C. Anderson and Xiaojing Duan. May 1998.

PEER 1998/02 *Seismic Evaluation of 196 kV Porcelain Transformer Bushings.* Amir S. Gilani, Juan W. Chavez, Gregory L. Fenves, and Andrew S. Whittaker. May 1998.

PEER 1998/01 *Seismic Performance of Well-Confined Concrete Bridge Columns.* Dawn E. Lehman and Jack P. Moehle. December 2000.